UNIVERSIDAD DE CHILE
FACULTAD DE CIENCIAS FÍSICAS Y MATEMÁTICAS
DEPARTAMENTO DE INGENIERIA DE MINAS

PLURIGAUSSIAN SIMULATION OF NON-STATIONARY CATEGORICAL VARIABLES AND ITS APPLICATION TO ORE BODY MODELING

TESIS PARA OPTAR AL GRADO DE DOCTOR EN INGENIERÍA DE MINAS

NASSER MADANIESFAHANI

PROFESOR GUÍA:
XAVIER EMERY

MIEMBROS DE LA COMISIÓN
BRIAN TOWNLEY CALLEJAS
MARGARET ARMSTRONG
GRÉGOIRE MARIETHOZ

SANTIAGO DE CHILE
2016

Resumen

La simulación condicional de dominios geológicos, codificados por variables regionalizadas categóricas, permite construir escenarios (realizaciones) de la geometría de estos dominios que reproducen su continuidad espacial y sus relaciones de dependencia. Las realizaciones pueden ser procesadas para cuantificar la incertidumbre geológica y determinar la probabilidad que un dominio prevalece en un sitio no muestreado del espacio o conjuntamente en varios sitios. Esta información es útil para el control geológico en la toma de decisiones al explotar un yacimiento.

Entre los enfoques existentes para simular dominios geológicos, el modelo plurigaussiano ha ganado popularidad en la industria petrolera y minera. En este modelo, los dominios se obtienen al truncar uno o más campos aleatorios Gaussianos. Aun así, el modelo está bien establecido solamente en el caso estacionario, cuando la distribución espacial de los dominios es homogénea en el espacio, y sufre de problemas teóricos y prácticos en el caso no estacionario.

Para superar estas limitaciones, esta tesis propone varias mejoras del modelo plurigaussiano. La principal es la extensión del modelo al truncamiento de campos aleatorios intrínsecos de orden k con incrementos generalizados Gaussianos, en lugar de campos aleatorios Gaussianos estacionarios, que permite la reproducción de tendencias espaciales y patrones zonales en la distribución de los dominios geológicos, una característica que, en la práctica, se encuentra comúnmente con los dominios litológicos, mineralógicos y de alteración.

Para eso, se hace propuestas metodológicas en relación con la definición de herramientas y algoritmos geoestadísticos para inferir los parámetros del modelo (regla de truncamiento basada en consideraciones de las relaciones cronológicas y de contacto de los dominios, umbrales de truncamiento, y funciones de covarianzas generalizadas de los campos aleatorios intrínsecos de orden k) y para construir realizaciones condicionadas a datos existentes. Además, las propuestas se ponen en práctica a través de casos sintéticos y un caso real (yacimiento Río Blanco) para demostrar su aplicabilidad.

Los beneficios del modelo plurigaussiano no estacionario propuesto son de dos tipos: (i) permite la reproducción de tendencias en la distribución espacial de los dominios geológicos, y (ii) el proceso de simulación no necesita conocer las proporciones locales de los dominios, de modo que el modelo no se ve afectado por posibles equivocaciones en la especificación de estas proporciones. A pesar del número muy limitado de datos condicionantes, el estudio de caso del yacimiento Río Blanco muestra un notable acuerdo entre los dominios litológicos simulados y el modelo litológico interpretado por los geólogos, y demuestra ser mucho más exitoso que el modelo plurigaussiano estacionario convencional.

La propuesta se presenta así como una alternativa atractiva para construir modelos estocásticos de dominios geológicos, fundada en una base teórica sólida y en la incorporación de conocimientos geológicos cualitativos, como la cronología, las relaciones de contacto o las tendencias espaciales de los dominios a ser simulados, lo cual es útil para guiar el proceso de modelamiento y la validación del mismo.

Abstract

The conditional simulation of geological domains, coded through categorical regionalized variables, allows constructing outcomes (realizations) of the layout of these domains that reproduce their spatial continuity and dependence relationships. These realizations can be further processed to quantify geological uncertainty and to determine the probability that a given domain prevails at any unsampled location or jointly over several locations. This information is essential to geological control in order to take proper decisions when mining an ore deposit.

Among the existing approaches for simulating geological domains, the plurigaussian model has become popular in the petroleum and mining industries. In this model, the domains are obtained by truncating one or more Gaussian random fields. Even so, the model is well-established only in the stationary case, when the spatial distribution of the domains is homogeneous in space, and suffers from theoretical and practical impediments in the non-stationary case.

To overcome these limitations, this thesis proposes several improvements in plurigaussian modeling. The main one is the extension of the model to the truncation of intrinsic random fields of order k with Gaussian generalized increments, instead of stationary Gaussian random fields, which allows reproducing spatial trends and zonal patterns in the distribution of the geological domains, a feature commonly met in practice with lithological, mineralogical and alteration domains.

To this end, methodological proposals are made in relation to the definition of geostatistical tools and algorithms for inferring the model parameters (truncation rule based on considerations of the domain chronology and contact relationships, truncation thresholds, and generalized covariance functions of the underlying intrinsic random fields of order k) and for the construction of realizations conditioned to existing data. Also, the proposals are put in practice through synthetic case studies and a real case study (Río Blanco ore deposit) to demonstrate their applicability.

The benefits of the proposed non-stationary plurigaussian model are twofold: (i) it allows reproducing trends in the spatial distribution of the geological domains, and (ii) the local proportions of the domains are not needed in the simulation process, thus the model is not affected by possible misspecifications of these proportions. Despite the very limited number of conditioning data, the Río Blanco case study shows a remarkable agreement between the simulated rock type domains and the lithological model interpreted by geologists, and proves to be much more successful than the conventional stationary plurigaussian model.

The proposal thus appears as an attractive alternative for stochastic geological domaining, based on a sound theoretical background and on the incorporation of qualitative geological knowledge, such as the chronology, contact relationships or spatial trends of the domains to be simulated, which is helpful for guiding the modeling process and validating it.

Acknowledgments

First and foremost, I want to express my sincere gratitude to my advisor Prof. Xavier Emery for the continuous support in my Ph.D. studies and related research, for his patience, motivation, and immense knowledge. His guidance helped me in all the time of research and writing of this dissertation. I could not have imagined having a better advisor and mentor for my Ph.D. studies.

My sincere thanks also go to the members of the thesis commission, prof. Brian Townley, prof. Margaret Armstrong and prof. Grégoire Mariethoz, for their comments that helped to improve this thesis dissertation, and to the Mining Engineering Department at University of Chile, which provided me an opportunity to join its Ph.D. program and gave me access to its laboratories and research facilities by its esteemed academic professionalism.

I gratefully acknowledge the funding sources that made my Ph.D. work possible. I was funded by the Advanced Mining Technology Center (AMTC) at University of Chile for the duration of my studies, and was honored to be an in-kind researcher of the CSIRO-Chile International Center of Excellence in Mining and Mineral Processing. My work was also partly supported by the Chilean Commission for Scientific and Technological Research CONICYT, through Projects CONICYT/ FONDECYT / REGULAR / N°1130085 and CONICYT PIA Anillo ACT1407.

I furthermore thank the International Association for Mathematical Geosciences (IAMG) for the Mathematical Geosciences Student Award that I was granted in the second year of my studies, providing funding for Ph.D. students who are about to start their careers in geomathematics and geoinformatics.

I have appreciated Mr. Claudio Martínez from Codelco-Chile (Andina Division), who provided me the dataset used in this dissertation.

Last but not least, I would like to thank my family for supporting me spiritually while living and studying in a Ph.D. program overseas.

Contents

Chapter 1: Introduction 1
1 Problem setting 1
2 Key idea of the thesis 4
3 Objectives 4
4 Hypotheses 6
Chapter 2: Literature review 7
1 Simulation of geological domains 7
1.1 Object based models 7
1.1.1 Boolean model 7
1.1.2 Dead leaves model 8
1.2 Simulated annealing 8
1.3 Sequential indicator simulation 9
1.4 Simulation based on multiple-point statistics 9
1.5 Truncated Gaussian model 10
2 Stationarity hypotheses 11
2.1 Full stationarity 11
2.2 Second-order stationarity 11
2.3 Intrinsic stationarity 11
3 Non-stationary models 13
3.1 Piecewise stationary models 13
3.2 Locally stationary models 13
3.3 Conditioned stationary models 13
3.4 Models with non-stationary first or second-order moments 14
3.5 Universal kriging model 14
3.5.1 Model presentation 15
3.5.2 Universal kriging equations 16
4 Intrinsic random fields of order *k* 18

4.1 Introduction 18
4.2 Generalized increments 19
4.3 Definition of an intrinsic random field of order *k* (IRF- *k*) 21
4.4 Generalized covariance 23
4.5 Generalized variogram 25
4.6 Internal representations 26
4.7 Intrinsic kriging 27
4.8 Non-conditional simulation 29
4.9 Conditional simulation 32
Chapter 3: Plurigaussian model 33
1 Conventional stationary model 33
1.1 Model parameters 34
1.1.1 Truncation rule 34
1.1.2 Truncation thresholds 35
1.1.3 Variograms of the underlying Gaussian random fields 36
1.2 Conditional simulation 36
1.3 Discussion 38
1.3.1 Truncation rule 38
1.3.2 Convergence of the Gibbs sampler 42
1.3.3 Domain proportions 42
2 Proposal for non-stationary plurigaussian modeling 44
2.1 Truncation rule 44
2.2 Truncation thresholds 44
2.3 Structural analysis 45
2.4 Conditional simulation 48
Chapter 4: Synthetic case studies 50
1 Step-by-step description of the numerical experiments 50
2 Case 1: linear variograms and truncation rule with three categories 53
3 Case 2: power variograms and truncation rule with three categories 56
4 Case 3: power variograms and truncation rule with six categories 58
5 Sensitivity to the number of conditioning data 62
6 Model validation 63

Chapter 5: Real case study: Geological modeling of the Río Blanco – Los Bronces deposit 69
1 Geological setting 69
2 Lithology 70
3 Data and region of interest 72
4 Exploratory Data Analysis 72
5 Stationary plurigaussian model 76
5.1 Definition of the truncation rule 76
5.2 Definition of the truncation thresholds 77
5.3 Variogram analysis 78
5.4 Construction of realizations of rock domains 80
5.5 Post-processing the realizations 81
6 Non-stationary plurigaussian model 87
6.1 Model presentation 87
6.2 Generalized covariance analysis 88
6.3 Conditional simulation and post-processing of the realizations 89
Chapter 6: Discussion and conclusions 97
1 General discussion 97
2 Conclusions 98
3 Perspectives 99
Bibliography 100
Appendix 116

Chapter 1: Introduction

1 Problem setting

This thesis is concerned with the spatial modeling of geological domains in ore deposits, which may be defined on the basis of lithology, mineralogy or alteration, although the tools and models developed hereafter can also be applied to other fields, such as the modeling of lithofacies in oil and gas reservoirs or hydrofacies in aquifers. Geological domaining is useful by itself in order to plan which material to extract, when and how it should be extracted, to determine the requirements for mining operations, such as drilling, blasting, hauling and crushing, and to forecast the destination of the extracted material (dump, heap leaching, flotation plant, stock pile, etc.). It is also critical for modeling the mineral resources and ore reserves, insofar as the spatial behavior of geological, geotechnical and geo-metallurgical variables, such as the grades of the elements of interest and contaminants, rock density, granulometry, fracturation intensity, work index, solubility ratio, acid consumption or metal recovery, are often controlled by the lithology, mineralogy or alteration. In such a case, a two-stage or cascade approach is frequently used to model the resources and reserves (Chilès and Delfiner, 2012):

(1) Modeling the spatial layout of the geological domains, defined by the characteristics that control the mineralization, such as rock types, mineral types or alterations;

(2) Modeling the geological, geotechnical and geo-metallurgical variables of interest within each domain.

The second stage can be achieved through spatial interpolation methods (such as inverse distance weighting, kriging, simulation, etc.) and is not of direct interest in this thesis. With respect to the first stage, the problem is twofold. The first problem relates to spatial prediction, which aims at determining which geological domain is likely to prevail at locations where direct information is not available. The second problem relates to uncertainty quantification, in order to determine whether or not the spatial layout of the geological domains is accurately predicted and what is the risk of a misclassification.

There exist many options for geological domaining, including:

- *Deterministic modeling***,** based on a geological interpretation or on a model interpolated from the available data on the deposit, typically exploration drill hole samples. It provides a unique model to describe the layout of the geological domains within the deposit. The most common methods of this type are hand contouring and wire framing (Vistelius, 1989; Houlding, 1994; Mallet, 1992, 2002), digitization of the geological domain boundaries (Cáceres et al., 2011), computer graphics techniques for implicit boundary modeling (Carr et al., 2001; McLennan and Deutsch, 2007) and indicator kriging (Deutsch and Journel, 1992; Krige, 1997).

- *Stochastic modeling* or *stochastic simulation*, consisting in constructing multiple realizations of the domains, represented by random sets (indicators) or categorical random fields, i.e., random fields that take nominal values or categories. This approach provides a probabilistic description of the geological domains and, in contrast to deterministic approaches, contributes to uncertainty quantification and to enhanced geological control for the quantitative variables of interest when these variables are homogeneously distributed in each geological domain but the layout of the domain boundaries is uncertain (Dowd, 1994; Dubrule, 1993; Emery and González, 2007a, 2007b).

In turn, simulation approaches can be classified in two main families. One corresponds to object-based models such as the Boolean or dead leaves models (Lantuéjoul, 2002; Stoyan et al., 1996). One problem of this approach is the difficulty in conditioning the realizations to observed data, which often requires the use of iterative algorithms whose rate of convergence may be slow. A second approach corresponds to the so-called pixel-based simulation methods, in which a grid is introduced to discretize the ore deposit into a set of regularly-spaced locations or blocks. Among these methods, sequential indicator simulation (Journel, 1983; Journel and Isaaks, 1984; Alabert, 1987; Journel and Alabert, 1988) and transition probability-based indicator simulation (Carle and Fogg, 1996) offer a flexible framework, but the realizations are often unable to reproduce contact constraints on the simulated domains, therefore lack realism from a geological point of view (Deutsch, 2006). In the past decades, Gaussian-based models have emerged as an alternative to indicator-based approaches. In particular, truncated Gaussian simulation is suited to cases when the geological domains follow an ordered sequence, such as strata in sedimentary deposits, while plurigaussian simulation is more versatile as it allows reproducing more complex transitions between the geological domains. The latter approach has found wide acceptance for modeling petroleum reservoirs and ore deposits (see Armstrong et al., 2011 and references therein, for a thorough review of applications).

However, as most of the geostatistical approaches used in the mining and petroleum industries, the current design of the plurigaussian model is based on an assumption of *stationarity*, through the use of Gaussian random fields whose distributions are invariant by a translation in space. In a nutshell, such an assumption is applicable for regionalized variables that behave homogeneously throughout the region of interest (Matheron, 1971). Specifically, first-order stationarity assumes that the mean of the variable is constant throughout the domain, while second-order stationarity assumes that, in addition to the existence of a constant mean, the covariance or the variogram between the data observed at two locations only depends on the geographical separation of these locations. Nonetheless, the geological domains, represented by indicator variables, often have a spatially varying mean and spatial continuity (covariance). For instance, mineralogical domains exhibit a vertical zonation, where some domains are likely to be found near the surface (gossan cap, leached zone, oxidized zone), while others are present only in depth (supergene sulfide enrichment zone and hypogene or primary sulfide-bearing zone) (Guilbert and Park, 1986). Lateral variations are also often observed in the distributions of rock types or alterations. As an

example, porphyry copper deposits often present inner potassic and phyllic alteration domains, surrounded by a sericitic alteration domain, in turn surrounded by an argillic alteration domain and an outer propylitic alteration domain (Figure 1.1). An assumption of stationarity, implying that the occurrence of every alteration domain is constant in space, is clearly inadequate in such a case. Stationary models may also be inadequate to describe phenomena for which a spatial trend is present due to physical reasons, e.g. folded structures (domes, anticlines or synclines) in geological formations such as petroleum reservoirs and ore deposits.

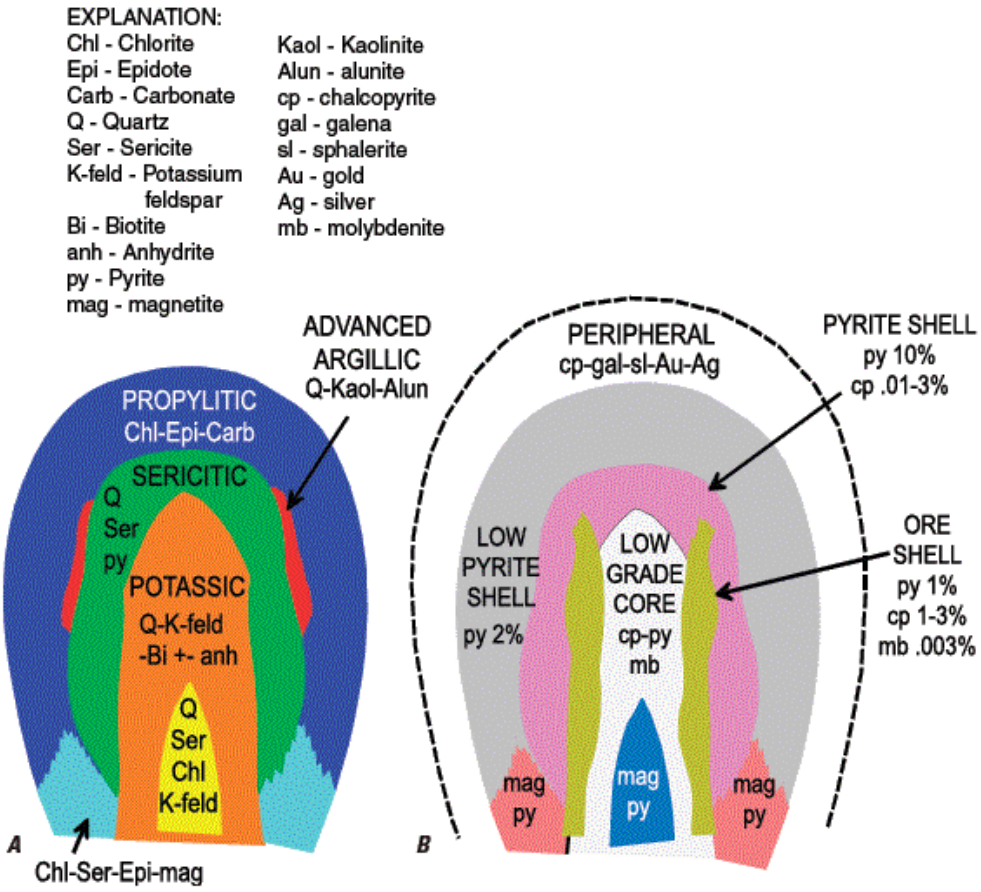

Figure 1.1: Conceptual model of a porphyry copper deposit (modified from Lowell and Guilbert, 1970)

Most of the aforementioned stochastic simulation approaches can be adapted to non-stationary cases by considering spatially varying parameters (indicator mean values for sequential indicator simulation, truncation thresholds for truncated Gaussian and plurigaussian simulation) (Beucher et al., 1993; Deutsch and Journel, 1992; Ravenne et al., 2002). In general, this procedure does not allow managing the uncertainty on the true parameters, as one considers the domain proportions as if they were perfectly known, which is not the case in reality (Biver et al., 2002), therefore an important source of uncertainty may be omitted. Also, handling spatial changes in the model parameters becomes cumbersome in what refers to the inference of spatial continuity (covariance or variogram analysis) and, so far, the formalism is not clearly laid out.

2 Key idea of the thesis

To overcome these difficulties, the idea explored in this thesis is the extension of plurigaussian simulation to non-stationary random fields, by considering categorical random fields obtained through the truncation of one or several intrinsic random fields of order *k* (for short, IRF-*k*) with Gaussian generalized increments (Matheron, 1973; Dimitrakopoulos, 1990; Chilès and Delfiner, 2012). The rationale is that the use of IRF-*k* will allow the reproduction of spatial trends (such as mineral domains that are present near the surface and absent at depth, or alteration domains that are present in the inner part of an ore body and absent in outer parts).

To illustrate this idea, Figure 1.2 displays isopleth maps of realizations of intrinsic random fields on the two-dimensional plane, with increasing orders (left side, from top to bottom). As the order increases, the intrinsic random field shows a greater short-scale regularity and, above all, clearer large-scale trends. In each case, two geological domains can be defined by truncating the intrinsic random field at a given level curve (Figure 1.2 right): the trending behavior in the distribution of the domains so obtained gets more pronounced as the order increases.

3 Objectives

The main objective of this thesis is to enhance the versatility of the conventional plurigaussian model, with a special emphasis in the ability to reproduce trends in the spatial distribution of the geological domains to be simulated. To this end, a generalization of the model will be proposed, based on the truncation of intrinsic random fields of order *k* instead of stationary random fields.

Specific objectives are twofold. From a methodological point of view, they include the design of tools and algorithms for inferring the model parameters (in particular, in respect to the definition of the contact relationships between geological domains and to the so-called structural analysis, i.e., the identification of the spatial correlation structure of the underlying random fields) and for constructing realizations of the geological domains conditioned to existing data. From a practical point of view, the application and validation of the proposed model, tools and algorithms will be sought through synthetic and real case studies.

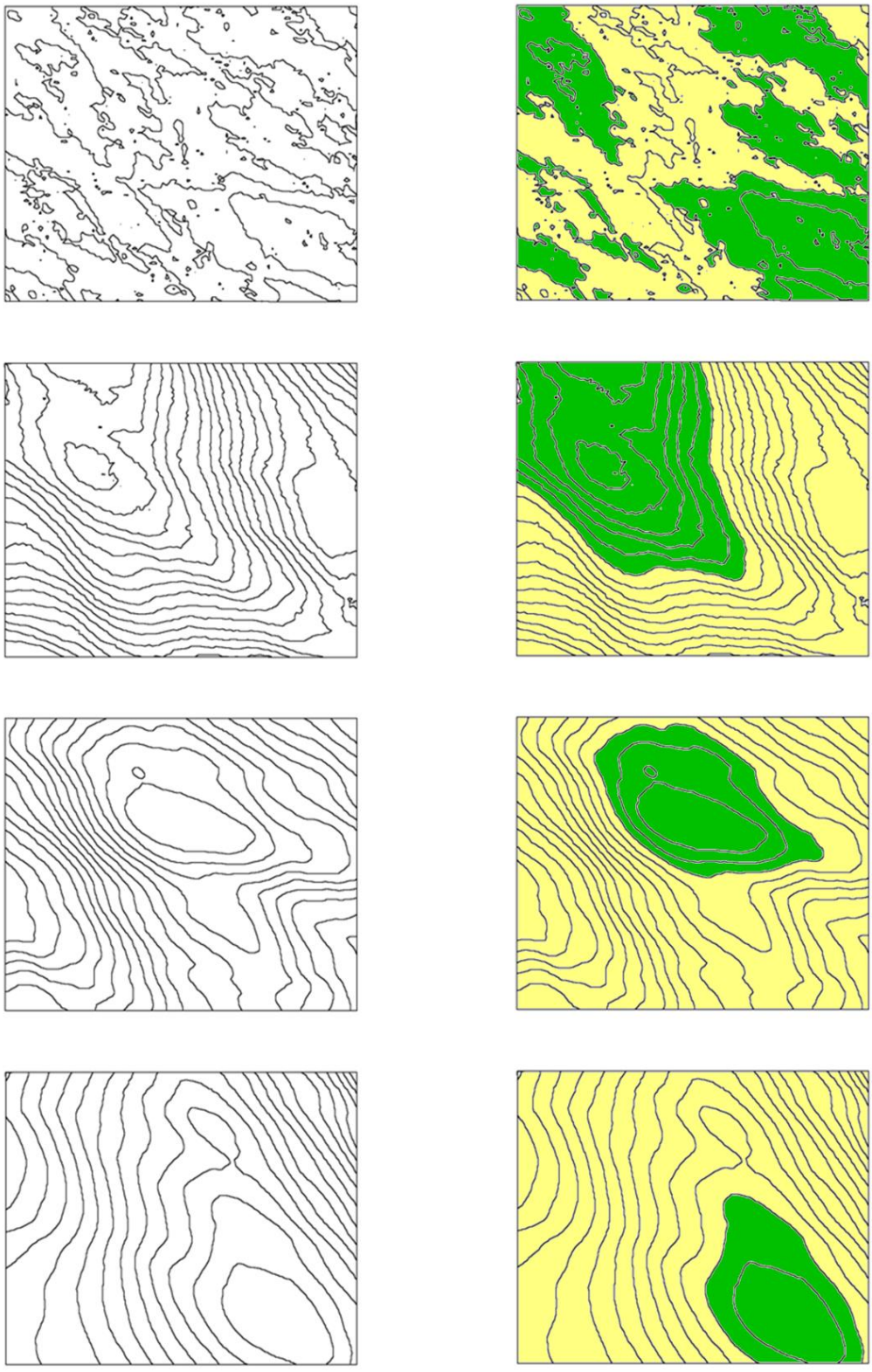

Figure 1.2: Isopleth maps of intrinsic random fields of order k (left) and two geological domains (green and yellow) obtained by truncation at a specific threshold

4 Hypotheses

The proposed research relies on the following hypotheses:

1) In ore deposits, geological domains can be coded by categorical (nominal) variables or by indicator (binary) variables that exhibit a structured behavior at a global scale, but a more irregular behavior at a local scale. The formalism of spatial random fields, associated with the concepts of randomness and of spatial correlation, is suitable to account for such a behavior.

2) Geological domains such as lithological, mineralogical or alteration domains often exhibit spatial trends and changes in their spatial continuity, so that a representation in terms of stationary random fields is questionable. Put another way, the probability of finding a particular domain is not constant in space and depends on the genesis, paragenesis and geological setting of the ore deposit.

3) The domains form a partition of the ore deposit and do not overlap in space. In the case of overprinting processes, each spatial location should be assigned to the dominant process (e.g., the dominant rock type, dominant mineralogical assemblage or dominant alteration type, depending on whether one is interested in lithological, mineralogical or alteration domains).

4) The domains are known at a set of samples for which direct observations (loggings) have been made. The observations are assumed error-free and statistically representative of the deposit. In contrast, interpreted geological models provide more qualitative information, consistent with the genesis, paragenesis and general understanding of the deposit, but that may locally be inaccurate.

5) Conditional simulation techniques allow constructing outcomes (called *realizations*) that reproduce the variability of the geological domains at all spatial scales, and assessing the uncertainty in the domains that are present at unsampled locations.

In the following chapter, the theory of the involved material is presented and discussed.

Chapter 2: Literature review

1 Simulation of geological domains

The geostatistical simulation of categorical random fields representing geological domains can be performed in many ways. In the following, some models and methods for stochastic geological modeling are briefly presented and discussed.

1.1 Object based models

Object-based techniques essentially consist of placing objects (bounded random sets) on a given background. The resulting simulation depends on the input parameters, including the orientation, size and shape distribution of the objects, the hierarchy of the objects and their spatial interaction (repulsion, independence, or clustering). Each object is assigned a constant value that stands for a given category (Chilès and Delfiner, 2012; Stoyan et al., 1996).

1.1.1 Boolean model

A Boolean random set corresponds to the intuitive idea of the union of randomly located objects. The main theoretical results are due to Matheron (1975), although special forms have been used earlier. The stationary Boolean model is defined on the basis of two "ingredients":

1) A homogeneous Poisson point process $\{\mathbf{x}_i: i \in \mathbb{N}\}$ with intensity θ

2) A family of independent and identically distributed random objects $\{A_i: i \in \mathbb{N}\}$, with the same distribution as a "typical" object A.

At each point $\mathbf{x}_i$ of the Poisson process, object A_i is placed. The Boolean model is obtained by considering the union of all the objects so placed. This model has been used to describe reservoirs in fluvial depositional environments (Chessa and Martinius, 1992; Viseur, 1999).

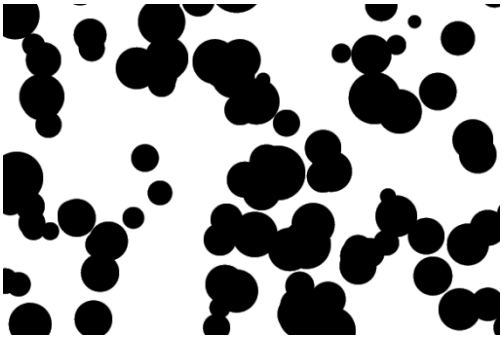

Figure 2.1: Two-dimensional Boolean model using a disc with random diameter as the typical object

1.1.2 Dead leaves model

The dead leaves model has been introduced first by Matheron (1968). This model results from the sequential superimposition of random sets (Serra, 1982, Lantuéjoul, 2002). As such, it provides a tool for studying occlusion phenomena, which are of importance in image modeling and image processing. However, to the best of our knowledge, this model has not been applied to geological and mining case studies.

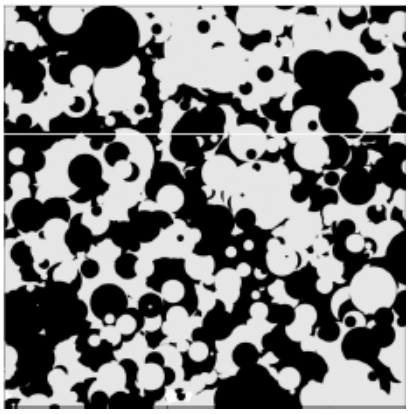

Figure 2.2: Dead leaves model, with discs valued by 0 (white) or 1 (black).

1.2 Simulated annealing

Simulated annealing is a class of algorithms searching for an optimal solution of an optimization problem (Almeida, 2010; Besag, 1986; Farmer, 1992; Geman and Geman, 1984; Kirkpatrick et al., 1983; Rothman, 1985), consisting in minimizing an *objective function* that describes the desired state. The algorithms are iterative, progressively perturbing the current state and assessing whether or not the perturbation decreases the objective function. The perturbation is accepted or rejected, depending on its impact on the objective function and on a scalar parameter called temperature, which decreases when simulation progresses.

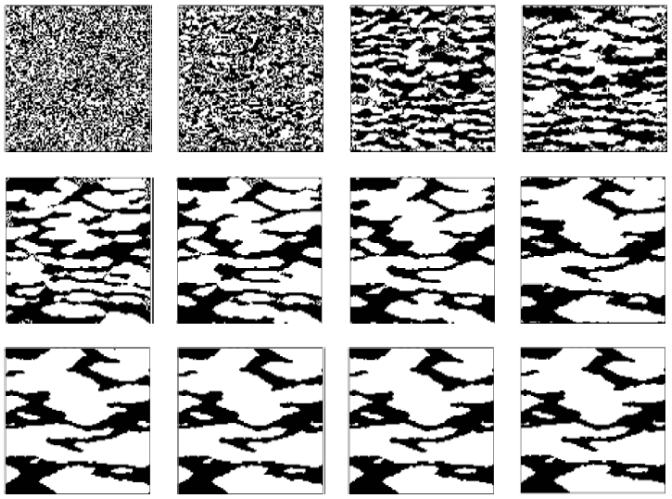

Figure 2.3: The process of producing structured realizations from an initial noisy image

1.3 Sequential indicator simulation

In this approach, the locations targeted for simulation are visited sequentially. The value at each location is obtained by applying Monte Carlo simulation to a distribution function estimated by means of indicator kriging (Journel, 1983; Journel and Isaaks, 1984; Alabert, 1987; Journel and Alabert, 1988; Journel, 1989). This approach requires inferring the proportions and the spatial correlation structure of indicator variables that codify the categories or domains to be simulated. Although it provides a straightforward way to construct numerical models, these models can appear very patchy and unstructured and often fail at representing complex geological structures (Deutsch, 2006). Furthermore, the contact relationships and cross dependence between domains are not explicitly controlled, yielding geologically unrealistic transitions, and the properties of the outcomes are implementation-dependent (Emery, 2004).

1.4 Simulation based on multiple-point statistics

Multiple-point statistics can be defined from a pattern, constituted by a configuration (template) of points with given values, relative to a reference point with an unknown value, and the probability distribution in the reference point conditional to the values of the other points (event) (Guardiano and Srivastava, 1993; Strebelle and Journel, 2000; Ortiz, 2003; Ortiz and Deutsch, 2004; Daly and Caers, 2010). For lack of an explicit random field model, the inference of multiple-point statistics is problematic, as it requires a considerable number of data in identical configurations up to a spatial translation. To circumvent this problem, one often uses a *training image* that allows calculating the frequencies of occurrence of the events related with a given pattern (Chilès and Delfiner, 2012).

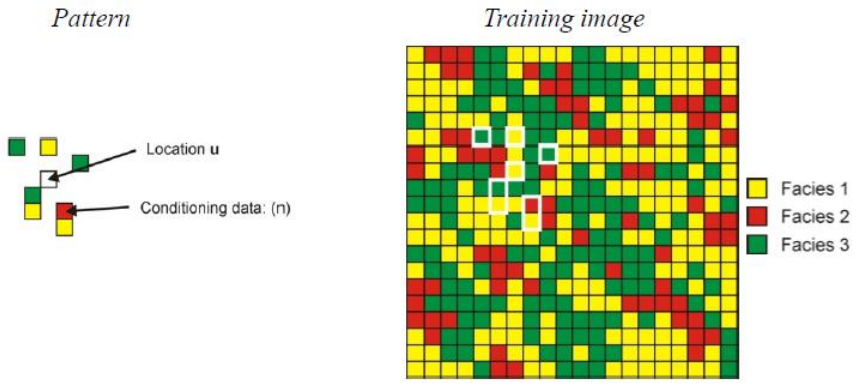

Figure 2.4: Pattern ad training image for simulation based on multiple-point statistics

The training image has to be representative of the geological domains of interest and consistent with the conditioning data, in particular, in relation to the proportions of the different categories. Several simulation techniques based on multiple-point statistics can deal with the case of spatially variable proportions (Chugunova and Hu, 2008; Mariethoz and Caers, 2014).

1.5 Truncated Gaussian model

The truncated Gaussian model was introduced by Matheron et al. (1987, 1988) for simulating the lithofacies found in oil reservoirs, in an attempt to model the internal architecture of the reservoir first, then to generate suitable values of porosity and permeability once the lithofacies is known. The model is designed for reservoirs where the lithofacies occur in a sequential order. The basic idea is to simulate a Gaussian random field over the region of interest and then use one or several thresholds to convert the Gaussian values into lithofacies.

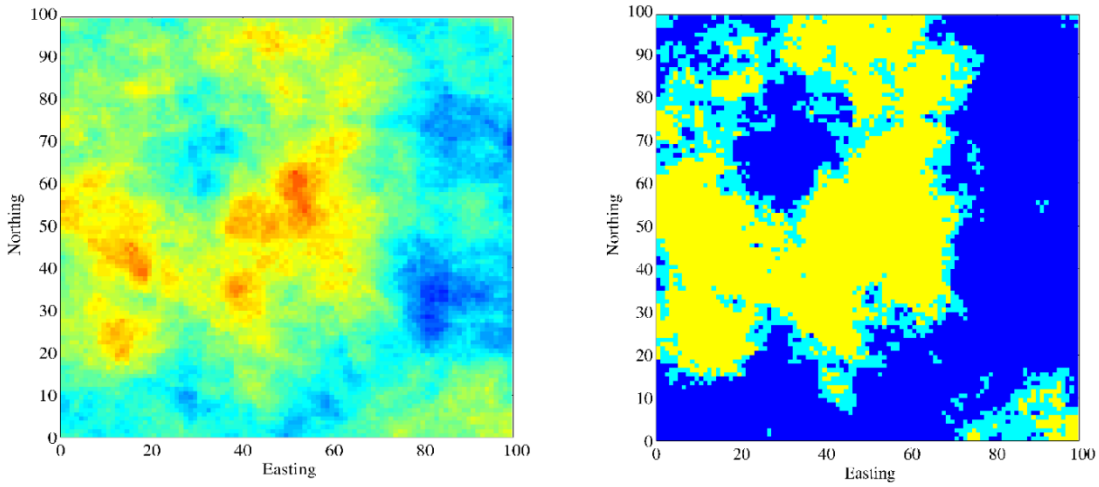

Figure 2.5: Simulated Gaussian random field (left) and truncated field with three lithofacies: yellow, cyan and blue (right)

The plurigaussian model, which generalizes the truncated Gaussian model, will be detailed in the following chapter.

2 Stationarity hypotheses

2.1 Full stationarity

A random field is said to be fully or strictly stationary when its finite-dimensional distributions are invariant under a translation in space (Cox and Miller, 1977; Myers, 1989). Intuitively speaking, the field is homogeneous in the region under study and tends to repeat itself similarly over the space (Chilès and Delfiner, 2012).

2.2 Second-order stationarity

This is a weaker form of stationarity, as it only involves the first two moments (mean value and covariance function) of the random field. A random field is said to be second-order stationary, if its first and second-order moments exist and are invariant under spatial translation. In particular, the first order moment (mean) is constant and the random field therefore fluctuates around this mean value, while the covariance function between the values observed at two locations only depends on the separation of the locations (Cox and Miller, 1977) (Figure 2.6).

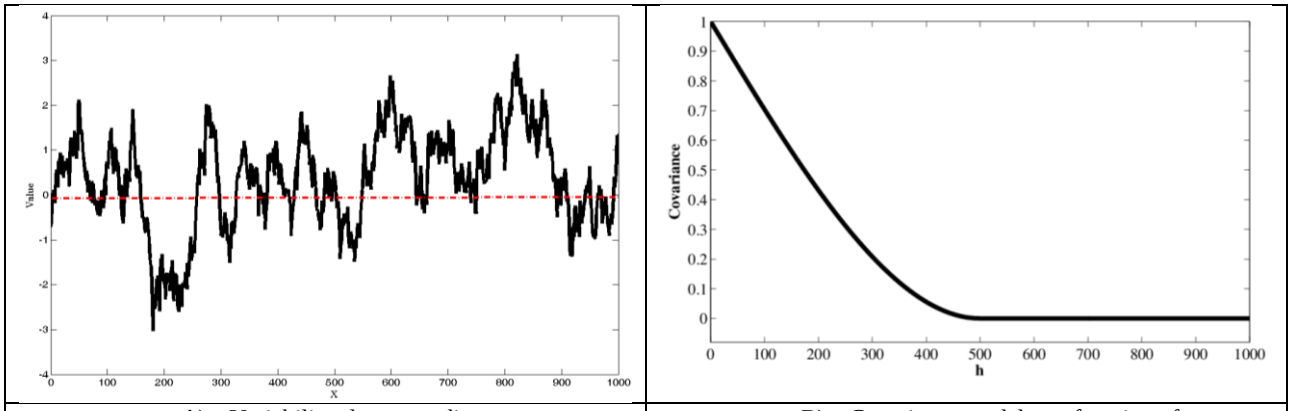

A) Variability along coordinate *x*

B) Covariance model as a function of the separation distance *h*.

Figure 2.6: Realization of a second-order stationary random field (left) and associated covariance function (right)

2.3 Intrinsic stationarity

A more general form of stationarity is the hypothesis of intrinsic stationarity, which states that the *increments* of the random field are second-order stationary (Matheron, 1971). Consequently, a random field $Z = \{Z(\mathbf{x}): \mathbf{x} \in \mathbb{R}^d\}$ is intrinsic if:

$$\forall \mathbf{x}, \mathbf{x}+\mathbf{h} \in \mathbb{R}^d, \begin{cases} E\{Z(\mathbf{x}+\mathbf{h}) - Z(\mathbf{x})\} = <\mathbf{a} \mid \mathbf{h}> \\ \text{var}\{Z(\mathbf{x}+\mathbf{h}) - Z(\mathbf{x})\} = 2\gamma(\mathbf{h}) \end{cases} \quad (2.1)$$

where **a** is a vector in $\mathbb{R}^d$, while < | > represents the usual inner product. If **a** = **0**, the random field is said to be intrinsic without drift. The function $\gamma(\mathbf{h})$ is known as the variogram of the intrinsic random field.

A well-known example is the fractional Brownian surface, for which the variogram is a power function of the separation distance. In Figure 2.7, one can see how the increments of the random field are stationary, while the original random field is not.

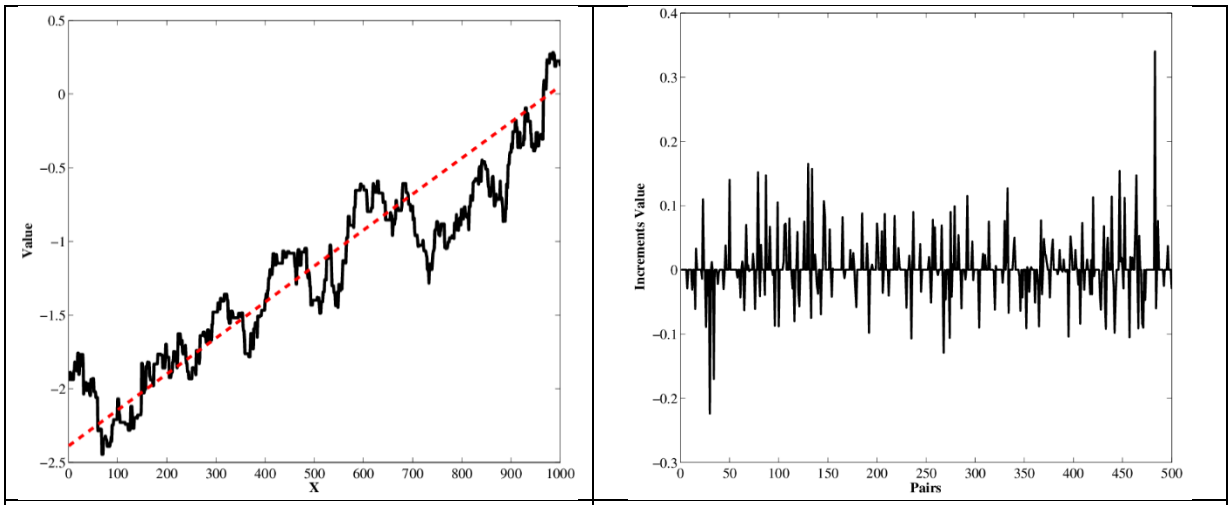

A) Linear drift over along coordinate *x*

B) Stationary increments over the pairs for *h* = 1

Figure 2.7: Realization of an intrinsic random field (left) and of its increments for lag *h* = 1 (right)

3 Non-stationary models

In the stationary case, it is supposed that the mean and variance are constant in the region. These properties are often questionable with geological variables, when experimental data exhibit local variations in their mean values (trends) or in their dispersion (proportional effects) (Myers, 1989). Several approaches have therefore been proposed to avoid or, at least, to alleviate the stationarity requirements.

3.1 Piecewise stationary models

This approach consists in delineating sub-regions on which a stationarity assumption is plausible and assuming that the data are independent across these sub-regions (Kim et al., 2005). In the geosciences context, this approach makes sense when the sub-regions correspond to different geological domains, such as rock types or mineral types, in which it is known that the variable of interest behaves differently (Deustch, 2002). However, it may be problematical when the boundaries between sub-regions are not "hard", i.e. if the transition when crossing a boundary is gradual (in which case the assumption of independence across sub-regions is violated), or when their exact position is uncertain (Larrondo et al., 2004; Ortiz and Emery, 2006; Vargas-Guzman, 2008). Hard transitions may occur when there is a break in the sedimentary geologic record (unconformity or hiatus) or in the presence of structural controls such as a fault, fold or layering (Fossen, 2013).

3.2 Locally stationary models

This approach consists in assuming that the stationarity assumption (either strict, second-order or intrinsic stationarity) is valid only at a local scale. A simple example corresponds to the ordinary kriging model within a moving neighborhood, where one assumes that the first-order moment of the random field is constant at the neighborhood scale, but may vary from one neighborhood to another (Journel and Huijbregts, 1978). This concept can be extended to second-order moments, by defining a locally stationary covariance or variogram (Xu, 1996; Stroet and Snepvangers, 2005; Sullivan et al., 2007). The inference of these moments can be realized by using a moving window centered at the target location (Haas, 1990, 1995; Alfaro, 1994) or by using distance-weighted statistics (Brunsdon et al., 2002; Machuca-Mory and Deutsch, 2008; Machuca-Mory, 2013).

3.3 Conditioned stationary models

Another way to deal with the presence of spatial trends is to incorporate conditioning data. These can be *hard* data (directly measured data) or *soft* data (e.g., rock type information) that account for expert knowledge and supply the lack of hard data in scarcely sampled areas. Although the random field is stationary (thus, with a constant prior mean), the prediction or simulation process is forced to reproduce the conditioning data and, therefore, to reproduce their local properties, in

particular, the local mean and local dispersion (Journel and Rossi, 1989; Journel and Huijbregts, 1978; Robles et al., 2007; Emery and Robles, 2009).

3.4 Models with non-stationary first or second-order moments

In the case of regionalized variables exhibiting a spatial trend, non-stationarity often concerns the first-order moment of the underlying random field, i.e., its expected value at each location. For instance, simple kriging and Gaussian simulation with a locally-varying mean (Deutsch and Journel, 1992) assume that the second-order moments (variance, covariance and/or variogram) are stationary, i.e. invariant under a spatial translation, while the first-order moment explicitly depends on the spatial position and can be modeled (supposedly, without uncertainty) by expert knowledge or by fitting a trend model to the data (Goovaerts, 1997; Costa, 2009; Chilès and Delfiner, 2012).

In such a case, attention must be taken to understand why the trend exists, based on the nature of the data, to use a simple form of the trend if possible, and to avoid extrapolation beyond the available data. Once one decides about which trend to use, one can subtract this trend from the observed data to obtain residuals that can be assumed stationary. One then uses the residuals to compute the experimental variogram, fit a model to it, predict the values at unsampled locations, and finally add the predicted residual back to the trend.

In some occasions the second-order moments are also assumed non-stationary. A few approaches for inferring and modeling non-stationary covariance functions have been proposed, based on spatial deformations (Monestiez and Switzer, 1991; Sampson and Guttorp, 1992; Guttorp and Sampson, 1994; Mardia and Goodall, 1993; Smith, 1996; Damian et al., 2000; Boisvert et al., 2009; Boisvert and Deutsch, 2011), expansions of the covariance into orthogonal functions (Nychka et al., 2002; Pintore and Holmes, 2005), Fourier transformation of the covariance function (Stephenson et al., 2005), convolution models (Higdon et al., 1999; Higdon, 2002) and kernel smoothing (Fuentes, 2001, 2002), among others (see also Sampson et al., 2001). Some of these approaches are suitable for space-time processes for which one has replications of the data at the same locations, but are not applicable when one only avails a limited set of data scattered in space.

3.5 Universal kriging model

An alternative to explicitly modeling a locally varying mean value is to assume that this mean value (also called “drift” or “trend”) is a linear combination of known basis functions, but with unknown coefficients. The random field can then be separated into a deterministic (although unknown) drift and a random residual, which is assumed stationary. This approach has been widely used in kriging applications under the generic name of “kriging with a trend model” (Deutsch and Journel, 1992; Goovaerts, 1997). Specific cases include universal kriging, for which the trend is a polynomial function of the coordinates (Matheron, 1971), trigonometric

kriging, for which the trend is an expansion into sine and cosine functions of the coordinates (Séguret and Huchon, 1990), or external drift kriging, for which the trend is given by one or several auxiliary variables that are exhaustively known (Hudson and Wackernagel, 1994; Rivoirard, 2002; Rivest et al., 2008).

3.5.1 Model presentation

In the presence of a spatial trend, it is questionable to use a stationary model, as the mean value varies in space. A natural approach therefore consists in splitting the variable under study into two components:

• A deterministic drift $m(\mathbf{x})$ that accounts for the spatial trend

• A random residual $R(\mathbf{x})$ that is assumed second-order stationary or intrinsic.

One therefore has:

$$\forall \mathbf{x} \in \mathbb{R}^d, Z(\mathbf{x}) = m(\mathbf{x}) + R(\mathbf{x}) \tag{2.2}$$

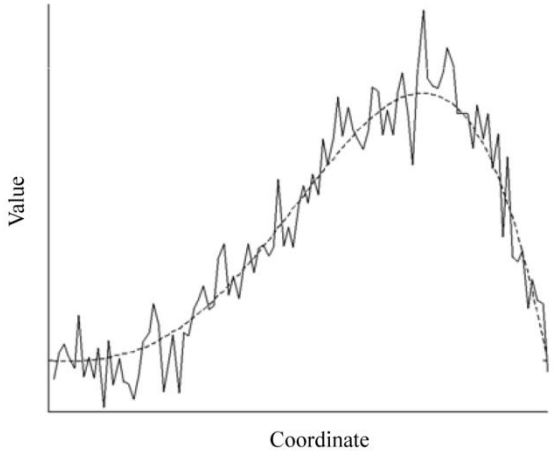

Figure 2.8: Separation into drift and residual

Because the drift is deterministic, the residual R has the same covariance function or variogram as the original random field Z.

Furthermore, the drift is usually taken up as an expansion of known basic functions:

$$\forall \mathbf{x} \in \mathbb{R}^d, m(\mathbf{x}) = \sum_l a_l \, f^l(\mathbf{x}) \tag{2.3}$$

where f^l are polynomials or, more simply, monomials of the coordinates of $\mathbf{x}$. Unlike the non-stationary model presented in Section 3.4, here the exact value of the trend is uncertain, i.e., the coefficients a_l are assumed unknown.

The decomposition into drift and residual is expected to separate two components of the original variable: the drift or trend that varies at a large scale, and the residual that varies at a smaller scale and reflects local anomalies. The decomposition may however be purely algebraic, with no particular meaning for the drift.

3.5.2 Universal kriging equations

Universal kriging was proposed first by Matheron (1969, 1971), who introduced the so-called universality conditions in the kriging system, hence the name universal kriging. There are two variants of universal kriging: with second-order stationary residual and with intrinsic residual. These two predictors should fulfill the following four restrictions (Matheron, 1971; Chilès and Delfiner, 2012):

- *Linearity*. The predictor at the given location is a linear combination of the data values. The data can consist of all the available data (unique neighborhood implementation) or, when they are too many, a subset of these data (moving neighborhood implementation).

- *Authorization*. One has to ensure that the prediction error has a finite expectation and a finite variance.

- *Unbiasedness (universality)*. The expectation of the prediction error should be zero.

- *Optimality*. One wants the prediction error to have a minimal variance.

Finally, the predictor at a given location $\mathbf{x}_0$, from data at locations $\mathbf{x}_1,\ldots,\mathbf{x}_n$, is as follows:

$$Z^*(\mathbf{x}_0) = \sum_{\alpha=1}^{n} \lambda_\alpha Z(\mathbf{x}_\alpha) \tag{2.4}$$

with

- For stationary residual with covariance $C(\mathbf{h})$

$$\begin{pmatrix} C(\mathbf{x}_\alpha - \mathbf{x}_\beta) & f^l(\mathbf{x}_\alpha) \\ f^l(\mathbf{x}_\beta) & 0 \end{pmatrix} \begin{pmatrix} \lambda_\beta \\ \eta_l \end{pmatrix} = \begin{pmatrix} C(\mathbf{x}_\alpha - \mathbf{x}_0) \\ f^l(\mathbf{x}_0) \end{pmatrix} \tag{2.5}$$

- For intrinsic residual with variogram $\gamma(\mathbf{h})$

$$\begin{pmatrix} \gamma(\mathbf{x}_\alpha - \mathbf{x}_\beta) & f^l(\mathbf{x}_\alpha) \\ f^l(\mathbf{x}_\beta) & 0 \end{pmatrix} \begin{pmatrix} \lambda_\beta \\ -\eta_l \end{pmatrix} = \begin{pmatrix} \gamma(\mathbf{x}_\alpha - \mathbf{x}_0) \\ f^l(\mathbf{x}_0) \end{pmatrix} \tag{2.6}$$

These systems appear as a generalization of the ordinary kriging system, for which only one basic function ($f^0 = 1$) and one Lagrange multiplier (η_0) are considered. The properties of universal kriging include:

(1) Exact interpolation at data locations: the data values are reproduced at the data locations.

(2) Smoothing effect: the dispersion of the predicted values tends to be smaller than that of the true values.

(3) Possibility to predict the drift at any location. This can be done to predict the residual at the data locations, thanks to which one can perform variogram analysis and determine the covariance function or the variogram of the residual, as indicated next. The prediction of the drift can also be performed via traditional interpolation techniques, such as moving averages, least squares fitting or smoothing splines.

To implement universal kriging, it only remains to determine the covariance or the variogram of the raw variable (Z) or, equivalently, of the residual (R) (since the drift is deterministic, it has no influence on the covariance or the variogram). One option is to calculate the experimental variogram of the Z-data, but it can be shown (Chilès and Delfiner, 2012) that this experimental variogram tends to overestimate the true variogram of the residual. A second option is to predict the residual (R) at the data locations, then calculate the experimental variogram of the R-data so obtained. However, this experimental variogram is biased with respect to the variogram of the true residual: it is smaller and has a shorter range, making believe that the raw variable Z is the sum of a drift and a residual with poor spatial correlation (Matheron, 1971; Cressie, 1987; Chilès and Delfiner, 2012).

So, as a conclusion for universal kriging, both the experimental variograms of the original data and of the predicted residuals are biased estimators of the true underlying variogram. The bias is small at small distances, but becomes considerable at larger distances. Variogram analysis is therefore the crux for the implementation of universal kriging.

4 Intrinsic random fields of order *k*

4.1 Introduction

The theory of intrinsic random fields of order *k* (Matheron, 1973) was developed in order to circumvent the problem of variogram analysis and, also, to widen the set of phenomena that can be described in the universal kriging model. Broadly speaking, an intrinsic random field of order *k* or IRF-*k* (with $k \in \mathbb{N}$), also known as an integrated process in times series analysis (Box and Jenkins, 1970), is such that its generalized increments, or increments of high order, are stationary.

The case $k = 0$ corresponds to intrinsic stationary random fields, for which the increments are stationary and the spatial correlation structure is described by the variogram. The cases with $k \geq 1$ are suitable for modeling regionalized variables that exhibit trends (drifts) that can be represented as polynomial functions of the spatial coordinates (Chauvet, 1999; Chilès and Delfiner, 2012; Wackernagel, 2003). Here are a few examples of application in the geosciences, for which stationary models are inadequate:

- In geothermal reservoir modeling, temperature and pressure increase with depth, whereas porosity and permibility decrease (Chilès and Gable, 1984; Suárez-Arriaga and Samaniego, 1998).

- In petroleum reservoir modeling, structural characteristics (e.g., depth of the top of a dome-shaped structure or anticline trap) or petrophysical properties such as rock porosity (Delfiner and Chilès, 1977; Dimitrakopoulos, 1990) can be represented by IRF-*k*.

- In groundwater hydrogeology, the hydraulic gradient is often responsible for a trend in the parameters that characterize an aquifer system (hydraulic head, hydraulic conductivity, transmisivity, total discharge, etc.). The use of intrinsic random fields of order *k* is all the more satisfactory because these random fields provide the solution of the partial differential equations linking the hydrogeologic parameters (De Marsily, 1986; Dong, 1990; Kitanidis, 1983, 1999; Le Cointe, 2006).

To date, IRF-*k* have also been applied to model soil properties (Buttafuoco and Castrignano, 2005), mineral grades (David, 1988), pollutant concentrations (Chilès and Gable, 1984) and seefloor depth (Chauvet, 1993; David et al., 1986).

4.2 Generalized increments

Under the intrinsic stationary hypothesis, one actually does not work with the random field of interest, but with its *increments*. This procedure filters out the constant values and the modeling is done with the variogram instead of the covariance function. The intrinsic random fields of order *k* generalize this idea, by working on higher-order increments that filter out not only the constants but also the monomials of degree 1, 2…, i.e., all the components of an eventual drift.

To this end, it is of interest to work on non-stationary random fields such that there exist second-order stationary linear combinations, as stationarity is convenient for the inference of the spatial correlation structure. One thus defines a *generalized increment of order k*, or an *authorized linear combination of order k* (for short, ALC-*k*), as a system of weights and locations $\{\lambda_i,\mathbf{x}_i\}_i$ such that, for any monomial f^l of degree less than or equal to *k*, one has:

$$\sum_i \lambda_i \, f^l(\mathbf{x}_i) = 0 \qquad (2.7)$$

Furthermore, one imposes that the first basic function is constant: $f^0(\mathbf{x}) = 1$. Accordingly, for the one-dimensional space ($d = 1$) the conditions are as follows for $k = 0$, 1 and 2:

For $k = 0$

$$\sum_i \lambda_i = 0$$

For $k = 1$

$$\sum_i \lambda_i = 0 \qquad \sum_i \lambda_i \, x_i = 0$$

For $k = 2$

$$\sum_i \lambda_i = 0 \qquad \sum_i \lambda_i \, x_i = 0 \qquad \sum_i \lambda_i \, x_i^2 = 0$$

In the two-dimensional space ($d = 2$), denoting by (x,y) the coordinates of a generic location, the conditions for $k = 0$, 1 and 2 become

For $k = 0$

$$\sum_i \lambda_i = 0$$

For $k = 1$

$$\sum_i \lambda_i = 0 \qquad \sum_i \lambda_i \, x_i = 0 \qquad \sum_i \lambda_i \, y_i = 0$$

For $k = 2$

$$\sum_i \lambda_i = 0 \qquad \sum_i \lambda_i x_i = 0 \qquad \sum_i \lambda_i y_i = 0$$
$$\sum_i \lambda_i x_i^2 = 0 \qquad \sum_i \lambda_i y_i^2 = 0 \qquad \sum_i \lambda_i x_i y_i = 0$$

The extension to higher-dimensional spaces ($d \geq 3$) and higher orders ($k \geq 3$) is straightforward. A simple way to define a generalized increment of order k based on a set of locations $\{\mathbf{x}_i\}_i$ is to predict one of these locations from the remaining ones by universal kriging, using an arbitrary covariance or variogram model. The universal kriging error fulfills the constraint of a generalized increment of order k (Eq. 2.7), as this is the same as the unbiasedness constraint of universal kriging. An example is shown below, with twenty locations in the two-dimensional space (Figure 2.9 and Table 2.1). The weight assigned to each location varies from order to order, but the sum of the weights is zero for each order.

The minimal number of locations needed to construct an ALC-k is $1+\frac{(k+d)!}{k!d!}$ and depends on both the order k and on the workspace dimension d (Chilès and Delfiner, 2012). For instance for k = 1, one needs 4 locations in the two-dimensional space and 5 locations in the three-dimensional space, while for k = 2, these figures increase to 7 and 11, respectively.

In the following, the set of generalized increments of order k will be denoted by Λ_k.

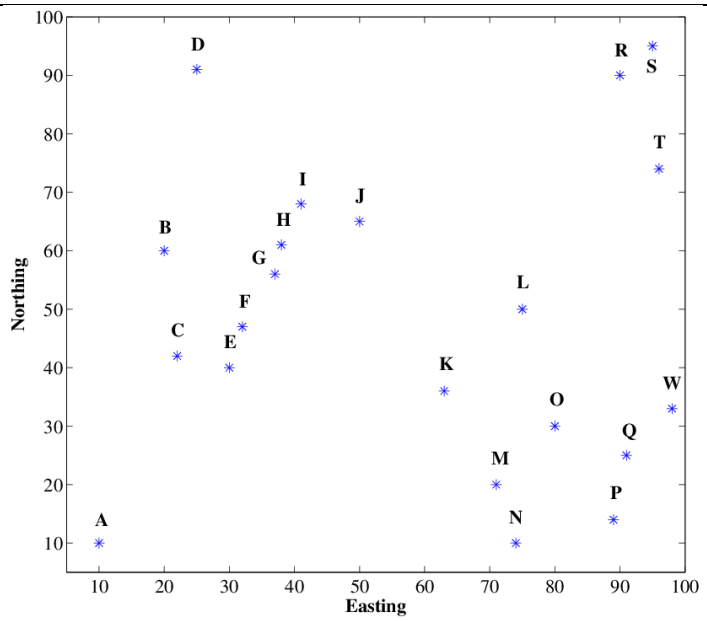

Figure 2.9: Twenty locations in the plane

Weights	Order-0	Order-1	Order-2	Order-3
A	-1	0.8711	8.9047	0.5713
B	0.1014	-1	10.7913	0.2238
C	0.2529	0.4777	-1	1.1941
D	0.2860	0.0687	-37.0268	-1
E	0.6176	-0.2060	-1.9080	-0.1829
F	-0.3549	-0.2543	37.5910	5.6820
G	0.1229	0.2697	-19.6542	-0.9507
H	-0.1925	-0.1152	2.3049	-13.2633
I	0.2386	-0.1384	-5.2096	-0.7176
J	-0.0533	-0.0149	4.4584	-2.0892
K	0.0165	-0.0466	4.9391	6.6205
L	-0.0011	0.0947	-3.3795	-0.0885
M	-0.0049	-0.1733	-0.5011	2.3959
N	0.0164	0.0259	-0.2793	2.6112
O	-0.0183	0.0888	-3.1768	0.9350
P	-0.0183	0.0793	0.1359	-0.6129
Q	0.0090	-0.0214	3.1122	0.4691
R	0.0014	0.0200	-0.1141	-1.0128
S	-0.0009	-0.0238	-0.0670	-0.1398
T	-0.0181	-0.0013	0.4257	-0.6661
W	-0.0004	-0.0009	-0.3468	0.0207
Sum of weights	0	0	0	0

Table 2.1: Weights assigned to the twenty locations

4.3 Definition of an intrinsic random field of order *k* (IRF-*k*)

An IRF-*k* can be defined in two different ways (Chilès and Delfiner, 2012):

First definition

A random field $Z = \{Z(\mathbf{x}): \mathbf{x} \in \mathbb{R}^d\}$ is an intrinsic random field of order k if all its generalized increments of order k have a zero expectation and a variance that is invariant under a spatial translation. In other words, if $\lambda = \{\lambda_i, \mathbf{x}_i\}_i \in \Lambda_k$, then

$$\forall \mathbf{h}, \begin{cases} E\{\sum_i \lambda_i Z(\mathbf{x}_i + \mathbf{h})\} = 0 \\ \text{var}\{\sum_i \lambda_i Z(\mathbf{x}_i + \mathbf{h})\} \text{ does not depend on } \mathbf{h} \end{cases} \tag{2.8}$$

One more property of this first definition is that, if Z_1 is an IRF-k, then for each random field Z_2 that differs by a polynomial of degree less than or equal to k and for each generalized increment $\lambda = \{\lambda_i, \mathbf{x}_i\}_i \in \Lambda_k$, one has:

$$\sum_i \lambda_i Z_1(\mathbf{x}_i) = \sum_i \lambda_i Z_2(\mathbf{x}_i) \tag{2.9}$$

This identity is due to the fact that the generalized increments of order *k* filter out the polynomials of degree less than or equal to *k* (Eq. 2.7), therefore the two random fields Z_1 and Z_2 are indistinguishable if one only works with ALC-*k*. For example, consider an intrinsic random field of order *k* (Z_1) fluctuating along the *x* coordinate in $\mathbb{R}$ (Figure 2.10). The random field Z_2 differs from Z_1 by just one constant, hence both random fields have the same generalized increments.

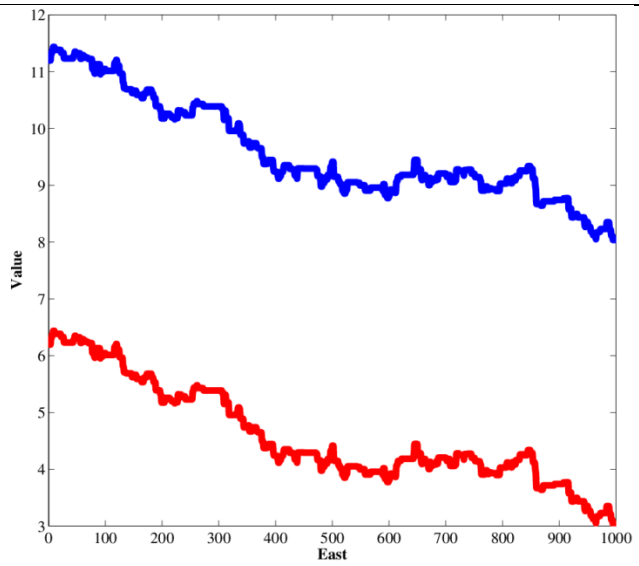

Figure 2.10: Two random fields that differ by a constant. Red line: Z_1, Blue line: Z_2

Second definition

One can extend the definition of an IRF-*k* to an equivalence class of random fields that differ by a (deterministic or random) polynomial of degree less than or equal to *k*, and from which one member of the class is an IRF-*k* in the sense of the first definition. This amounts to defining an IRF-*k* as an application *Z* on the class of ALC-*k* such that:

$$\forall \lambda \in \Lambda_k, Z(\lambda) = \sum_i \lambda_i Z(\mathbf{x}_i) \tag{2.10}$$

Therefore, we will slightly change the first definition and say that:

- $\{Z(\lambda) : \lambda \in \Lambda_k\}$ is an intrinsic random field of order *k*
- $\{Z(\mathbf{x}) : \mathbf{x} \in \mathbb{R}^d\}$ is a *representation* of this intrinsic random field.

In summary, the regionalized variable is viewed as one realization of one representation of an intrinsic random field, which is a class of random fields defined up to a polynomial of degree less than or equal to *k*. Each element of the class generates the same generalized increments or authorized linear combinations of order *k*.

4.4 Generalized covariance

The spatial correlation structure of a second-order stationary random field $Z = \{Z(\mathbf{x}): \mathbf{x} \in \mathbb{R}^d\}$ is defined by its ordinary covariance function $C(\mathbf{h})$. For an intrinsic stationary random field, only the increments are assumed second-order stationary and the variogram $\gamma(\mathbf{h})$ is the structural tool, which allows calculating the variances and covariances of linear combinations whose weights add to zero (Matheron, 1971).

In the same manner, when $Z = \{Z(\mathbf{x}): \mathbf{x} \in \mathbb{R}^d\}$ is an IRF-k, the stationarity assumption is limited to the generalized increments of order k and the spatial correlation structure of Z is characterized by a new function, called a generalized covariance function and denoted by $K(\mathbf{h})$, such that

$$\begin{aligned} &\forall \lambda = \{\lambda_i, \mathbf{x}_i\}_i \in \Lambda_k, \forall \mu = \{\mu_j, \mathbf{x}'_j\}_j \in \Lambda_k, \\ &\operatorname{cov}\{\textstyle\sum_i \lambda_i Z(\mathbf{x}_i), \sum_j \mu_j Z(\mathbf{x}'_j)\} = \sum_i \sum_j \lambda_i \mu_j K(\mathbf{x}_i - \mathbf{x}'_j) \end{aligned} \tag{2.11}$$

In particular, the variance of any ALC-k is:

$$\operatorname{var}\{\textstyle\sum_i \lambda_i Z(\mathbf{x}_i)\} = \sum_i \sum_j \lambda_i \lambda_j K(\mathbf{x}_i - \mathbf{x}_j) \tag{2.12}$$

In other words, one can calculate the variances and covariances of the generalized increments of order k as if there were a covariance function, but replacing this hypothetical covariance function by the generalized covariance. For a second-order stationary random field, the generalized covariance is the usual covariance. For an intrinsic stationary random field, it is the opposite of the variogram up to an arbitrary constant. For an IRF-k, the class of generalized covariance functions becomes broader and broader when k increases. As for the usual covariance or for the variogram, the regularity of the generalized covariance function near the origin reflects the short-scale regularity of the intrinsic random field. The generalized covariance function is defined up to an even polynomial of degree less than or equal to $2k$.

An important example of generalized covariance is the power model, defined as:

$$K(\mathbf{h}) = (-1)^{1+\lceil \alpha/2 \rceil} \|\mathbf{h}\|^{\alpha} \tag{2.13}$$

for any real-valued α different from an even integer such that $0 < \alpha < 2k+2$ (in the above formula $\lceil . \rceil$ represents the integer part). The sign of $K(\mathbf{h})$ alternates with the value of α: it is negative for $0 < \alpha < 2$, positive for $2 < \alpha < 4$, negative for $4 < \alpha < 6$, and so on. When α is an even integer, $K(\mathbf{h})$ is an even degree polynomial and thus equivalent to the nil covariance $K(\mathbf{h}) = 0$. Some realizations are provided in Figure 2.11, in which one sees different types of generalized power covariance functions and their related realizations.

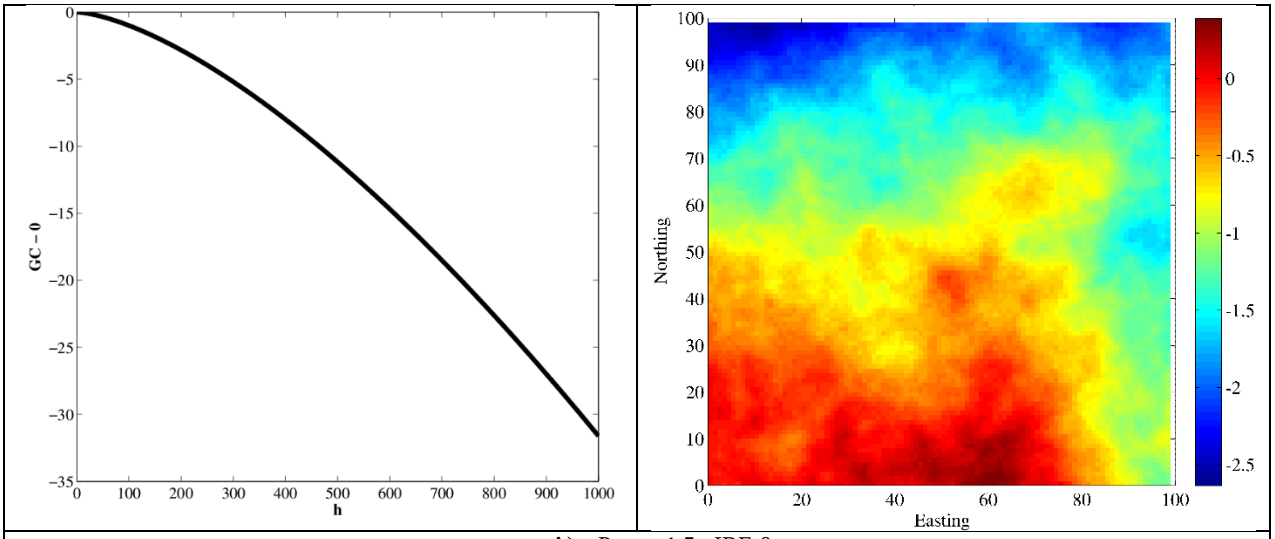

A) Power 1.5; IRF-0

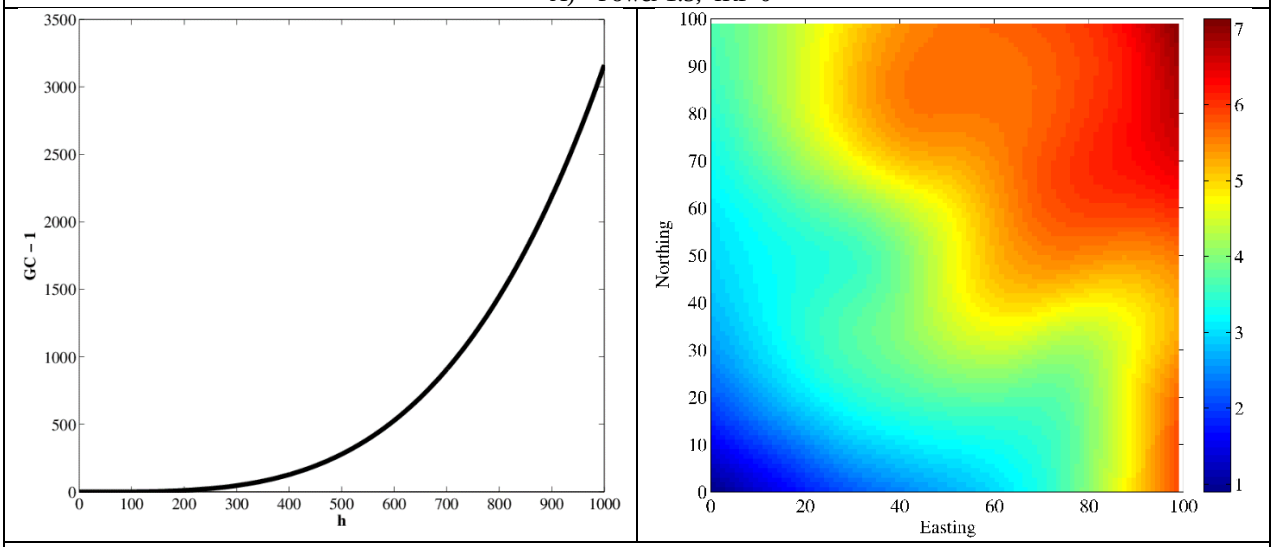

B) Power 3.5; IRF-1

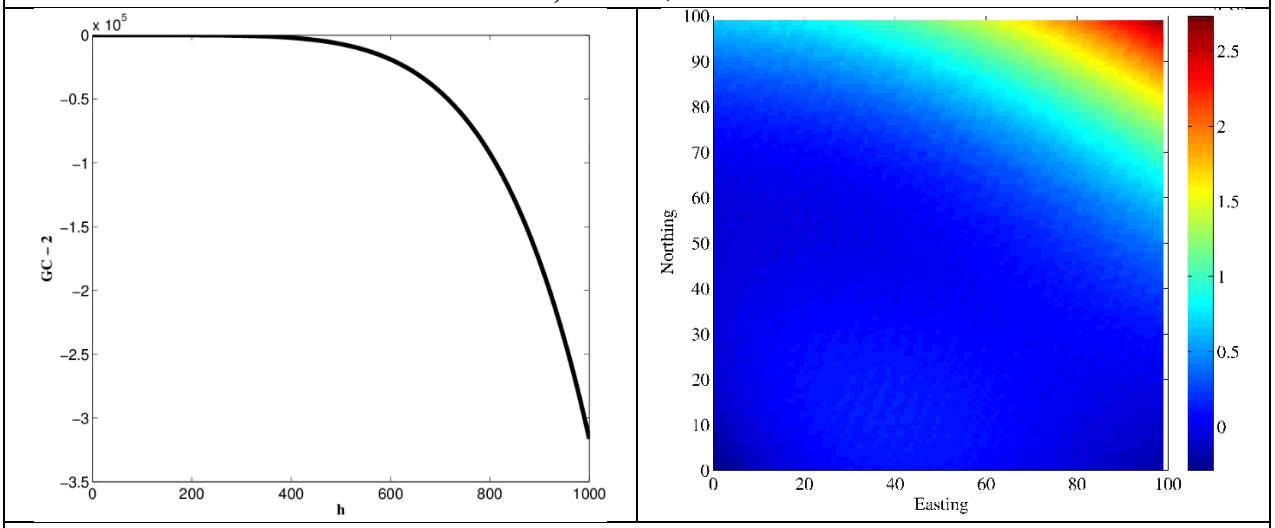

B) Power 5.5; IRF-2

Figure 2.11: Examples of realizations of intrinsic random fields with power generalized covariance

Several approaches have been proposed for identifying the generalized covariance function from a set of data on the intrinsic random fields. Some of these approaches are non-parametric, i.e., do not presume that the generalized covariance belongs to a parametric family of functions (Cressie, 1987; Chilès and Gentier, 1993; Chiasson and Soulie, 1997; Huang et al., 2009), while others are essentially parametric and are often applicable only within the scope of automatic or semi-automatic structure identification (Delfiner, 1976; Kitanidis, 1983, 1985; Marshall and Mardia, 1985; Stein, 1986; Renard, 1989; Zimmerman, 1989; Bruno and Raspa, 1993; Pardo-Igúzquiza, 1997; Kunsch et al., 1997; Cassiani and Christakos, 1998).

As an example of parametric approach, let us consider that the generalized covariance is of the following form:

$$K(\mathbf{h}) = \sum_p b_p \, K_p(\mathbf{h}) \tag{2.14}$$

where $\{K_p(\mathbf{h})\}_p$ are known basic structures (nugget, spline, power model, etc.), while $\{b_p\}_p$ are unknown coefficients. For any ALC-k $\{\lambda_i,\mathbf{x}_i\}_i$ such that the $\mathbf{x}_i$ are data locations, one should have

$$\mathrm{var}\{\sum_i \lambda_i \, Z(\mathbf{x}_i)\} = \sum_p b_p \sum_i \sum_j \lambda_i \, \lambda_j \, K(\mathbf{x}_i - \mathbf{x}_j) \tag{2.15}$$

The left hand expression can be experimentally estimated by $[\sum_i \lambda_i \, Z(\mathbf{x}_i)]^2$, i.e., one should have:

$$[\sum_i \lambda_i \, Z(\mathbf{x}_i)]^2 \approx \sum_p b_p \sum_i \sum_j \lambda_i \, \lambda_j \, K(\mathbf{x}_i - \mathbf{x}_j) \tag{2.16}$$

These equations can be written for many ALC-k, then a least-square fitting algorithm can be used to determine the best set of coefficients $\{b_p\}_p$.

4.5 Generalized variogram

An inconvenient of the generalized covariance is that one cannot calculate an experimental estimate of it and then graphically fit a model. The generalized variogram (Chilès and Delfiner, 2012) is a complementary tool that overcomes this limitation. It is defined, up to a multiplicative factor, as the variance of increments of order k+1:

$$g(\mathbf{h}) = \frac{\Gamma^2(k+2)}{\Gamma(2k+3)} \mathrm{var}\{\Delta_{\mathbf{h}}^{k+1} Z(\mathbf{x})\} \tag{2.17}$$

with Γ the gamma function and

$$\Delta_{\mathbf{h}}^{k+1} Z(\mathbf{x}) = (-1)^{k+1} \sum_{p=0}^{k+1} (-1)^p \, \frac{\Gamma(k+2)}{\Gamma(p+1)\Gamma(k-p+2)} \, Z(\mathbf{x}+p\mathbf{h}) \tag{2.18}$$

Such an increment is an ALC-k, therefore its variance is finite. Some particular cases include:

For $k = 0$: $g(\mathbf{h}) = \frac{1}{2}\operatorname{var}\{Z(\mathbf{x}+\mathbf{h}) - Z(\mathbf{x})\}$ (ordinary variogram) (2.19)

For $k = 1$: $g(\mathbf{h}) = \frac{1}{6}\operatorname{var}\{Z(\mathbf{x}+2\mathbf{h}) - 2Z(\mathbf{x}+\mathbf{h}) + Z(\mathbf{x})\}$ (2.20)

For $k = 2$: $g(\mathbf{h}) = \frac{1}{20}\operatorname{var}\{Z(\mathbf{x}+3\mathbf{h}) - 3Z(\mathbf{x}+2\mathbf{h}) + 3Z(\mathbf{x}+\mathbf{h}) - Z(\mathbf{x})\}$ (2.21)

These formulae can be estimated experimentally without bias, by considering the increments of order $k + 1$ on a set of data and calculating their average squared values. One therefore obtains an experimental generalized variogram, just as one could define an experimental covariance or an experimental variogram in the cases of second-order and intrinsic stationary random fields.

The generalized variogram is related to the generalized covariance through the formula

$$g(\mathbf{h}) = \frac{\Gamma^2(k+2)}{\Gamma(2k+3)} \sum_{p=-(k+1)}^{k+1} (-1)^p \frac{\Gamma(2k+2)}{\Gamma(k+p+2)\Gamma(k-p+2)} K(p\mathbf{h}) \quad (2.22)$$

In particular:

For $k = 0$: $g(\mathbf{h}) = K(\mathbf{0}) - K(\mathbf{h})$ (2.23)

For $k = 1$: $g(\mathbf{h}) = K(\mathbf{0}) - \frac{4}{3}K(\mathbf{h}) + \frac{1}{3}K(2\mathbf{h})$ (2.24)

For $k = 2$: $g(\mathbf{h}) = K(\mathbf{0}) - \frac{3}{2}K(\mathbf{h}) + \frac{3}{5}K(2\mathbf{h}) - \frac{1}{10}K(3\mathbf{h})$ (2.25)

4.6 Internal representations

Some representations of an IRF-*k* may be written as authorized linear combinations of order *k*, therefore they have finite expectation, variance and covariance function. This covariance is, in general, not stationary and is a function of the two locations under consideration, say $C(\mathbf{x},\mathbf{x}')$, rather than $C(\mathbf{x} - \mathbf{x}')$. Such representations are called *internal representations*.

For example, if $Z = \{Z(\mathbf{x}): \mathbf{x} \in \mathbb{R}^d\}$ is a representation of an IRF-0, then one can define another representation that differs by a constant value, by putting:

$$Y(\mathbf{x}) = Z(\mathbf{x}) - Z(\mathbf{x}_0) \quad (2.26)$$

where $\mathbf{x}_0$ is a pre-specified location. This second representation Y is an increment, therefore it has a finite expectation and a finite variance. More generally, if Z is a representation of an IRF-k and $\lambda = \{\{\lambda_i,\mathbf{x}_i\}_i\,;\,(-1,\mathbf{x})\} \in \Lambda_k$, then an internal representation can be defined by putting:

$$Y(\mathbf{x}) = Z(\mathbf{x}) - \sum_i \lambda_i\, Z(\mathbf{x}_i) \tag{2.27}$$

The covariance function of the internal representation $Y = \{Y(\mathbf{x}): \mathbf{x} \in \mathbb{R}^d\}$ can be expressed as if Z had a stationary covariance function, but replacing this covariance by the generalized covariance. One finds:

$$\operatorname{cov}\{Y(\mathbf{x}),Y(\mathbf{x}')\} = K(\mathbf{x}-\mathbf{x}') - \sum_i \lambda_i\, K(\mathbf{x}_i-\mathbf{x}) - \sum_i \lambda_i\, K(\mathbf{x}_i-\mathbf{x}') + \sum_i \sum_j \lambda_i\, \lambda_j\, K(\mathbf{x}_i-\mathbf{x}_j) \tag{2.28}$$

4.7 Intrinsic kriging

A common problem in geostatistics is the prediction of a random field over a domain on the basis of values observed at a limited number of locations. To this end, the random field under study $Z = \{Z(\mathbf{x}): \mathbf{x} \in \mathbb{R}^d\}$ is viewed as a representation of an IRF-k with known order (k) and known generalized covariance $K(\mathbf{h})$. Let us denote by $\{f^l(\mathbf{x})\}_l$ the set of basic drift functions (monomials of the coordinates of degree less than or equal to k), by $\mathbf{x}_0$ the location targeted for prediction and by $\mathbf{x}_1,\ldots, \mathbf{x}_n$ the data locations considered for kriging. These can be all the available data (unique neighborhood implementation) or, if they are too many, a subset of the available data (moving neighborhood implementation).

According to the rules of kriging, four restrictions should be fullfilled in order to deduce the final kriging system: linearity, authorization, unbiasedness and optimality.

Linearity

The predictor at a location $\mathbf{x}_0$ is of the form:

$$Z^*(\mathbf{x}_0) = \sum_{\alpha=1}^{n} \lambda_\alpha Z(\mathbf{x}_\alpha) \tag{2.29}$$

where $\{\lambda_\alpha: \alpha = 1\ldots n\}$ are weights to be defined later.

Authorization

As the allowable linear combinations (ALC-k) are the only ones to have computable expectations and variances, one has to be sure that the prediction error is an ALC-k. This entails the following conditions:

$$\forall l, \sum_{\alpha=1}^{n} \lambda_\alpha f^l(\mathbf{x}_\alpha) = f^l(\mathbf{x}_0) \tag{2.30}$$

Unbiasedness

One wants the prediction error to have a zero expectation. As any ALC-*k* has a zero expectation (Eq. 2.8), this constraint is automatically fulfilled.

Optimality

One wants the prediction error to have a minimal variance. Because the variance of an ALC-*k* can be calculated as if there were a covariance function, by replacing this hypothetical covariance by the generalized covariance, one has:

$$\text{var}\{Z(\mathbf{x}_0) - Z^*(\mathbf{x}_0)\} = K(\mathbf{0}) + \sum_{\alpha=1}^{n} \sum_{\beta=1}^{n} \lambda_\alpha \lambda_\beta K(\mathbf{x}_\alpha - \mathbf{x}_\beta) - 2\sum_{\alpha=1}^{n} \lambda_\alpha K(\mathbf{x}_\alpha - \mathbf{x}_0) \tag{2.31}$$

To minimize this variance subject to the authorization constraint, one has to introduce additional unknowns (Lagrange multipliers) and to cancel out the partial derivatives with respect to the unknowns. One finds:

$$\forall \alpha = 1...n, \sum_{\beta=1}^{n} \lambda_\beta K(\mathbf{x}_\alpha - \mathbf{x}_\beta) + \sum_l \eta_l f^l(\mathbf{x}_\alpha) = K(\mathbf{x}_\alpha - \mathbf{x}_0) \tag{2.32}$$

Therefore, the system of equations to determine the kriging weights is as follows (Chilès and Delfiner, 2012; Chauvet, 1999; Wackernagel, 2003):

$$\begin{pmatrix} K(\mathbf{x}_\alpha - \mathbf{x}_\beta) & f^l(\mathbf{x}_\alpha) \\ f^l(\mathbf{x}_\beta) & 0 \end{pmatrix} \begin{pmatrix} \lambda_\beta \\ \eta_l \end{pmatrix} = \begin{pmatrix} K(\mathbf{x}_\alpha - \mathbf{x}_0) \\ f^l(\mathbf{x}_0) \end{pmatrix} \tag{2.33}$$

where η_l are Lagrange multipliers.This system is formally the same as for universal kriging (Eqs. 2.5-2.6), except that the covariance or the variogram is replaced by the generalized covariance.

The kriging error has the following variance, called the “intrinsic kriging variance”:

$$\text{var}\{Z(\mathbf{x}_0) - Z^*(\mathbf{x}_0)\} = K(\mathbf{0}) - \sum_{\alpha=1}^{n} \lambda_\alpha K(\mathbf{x}_\alpha - \mathbf{x}_0) - \sum_l \eta_l f^l(\mathbf{x}_0) \tag{2.34}$$

Since the generalized covariance is defined up to an even polynomial of degree less than or equal to 2*k*, it can be shown that the results (kriging weights and kriging variance) do not depend on the particular choice of the generalized covariance function. The conditions for having a regular system are the same as in universal kriging, namely, that the basic drift functions at the data locations are linearly independent.

4.8 Non-conditional simulation

The simplest case of an intrinsic random field of order *k* is the fractional Brownian surface, which is an IRF-0 with multivariate Gaussian increments and power variogram. Over the past decades, a few exact algorithms have been proposed to simulate such a random field, such as the Cholesky factorization, as well as circulant-embedding and discrete spectral representations (Chilès and Delfiner, 2012; Stein, 2001, 2002). Since these algorithms are restricted in number of locations targeted for simulation or in their spatial configuration, approximate algorithms have also been designed, in particular, midpoint displacement approaches (Fournier et al., 1982; Voss, 1985), wavelet representations (Flandrin, 1992; Sellan, 1995; Zeldin and Spanos, 1996), Gibbs sampling (Arroyo and Emery, 2015) and turning bands (Yin, 1996; Gneiting et al., 2001; Emery and Lantuéjoul, 2006, 2008).

The turning-bands algorithm is particularly attractive, as it can be extended to the simulation of an IRF-*k* with multivariate Gaussian generalized increments, of any order and any generalized covariance. This algorithm consists in performing a set of independent one-dimensional simulations along lines that span the *d*-dimensional space, and then combining them to produce a *d*-dimensional simulation. For the one-dimensional simulation, Emery and Lantuéjoul (2006, 2008) and Arroyo and Emery (2016) propose the use of piecewise linear functions, piecewise quadratic functions, or weighted cosine functions associated with random frequencies and phases (spectral-turning bands algorithm), depending on the target generalized covariance model, which is extremely efficient in terms of time and memory requirements and allows accurately reproducing the (generalized) covariance, without restriction on the workspace dimension, nor on the number and spatial configuration of the locations where the intrinsic random field has to be simulated (Figures 2.12 and 2.13).

With respect to the line directions, Freulon and Fouquet (1991) showed that the properties of the simulation substantially improve by choosing equi-distributed directions, for instance from a Van der Corput sequence, instead of uniformly distributed directions (Figure 2.14). When the number of lines increases infinitely, the finite-dimensional distributions of the generalized increments tend to multivariate Gaussian, by virtue of the central limit theorem. However, in practice, a finite number of lines has to be used. In two dimensions, Mantoglou and Wilson (1982) suggest using 4 to 16 lines, Chilès (1977) recommends 180 lines (one per degree of angle), while Gneiting (1999) found that 64 lines lead to an excellent reproduction of the target covariance. In three dimensions, several hundreds or thousands of lines should be used (e.g., Tompson et al., 1989; Freulon and Fouquet, 1991; Lantuéjoul, 2002; Emery and Lantuéjoul, 2006). Actually, the number of lines is not the limiting factor of the turning bands algorithm, as the simulation along the lines is very fast. In general, a greater CPU time is developed to post-process the realizations, in particular concerning the conditioning to a set of existing data (see next subsection).

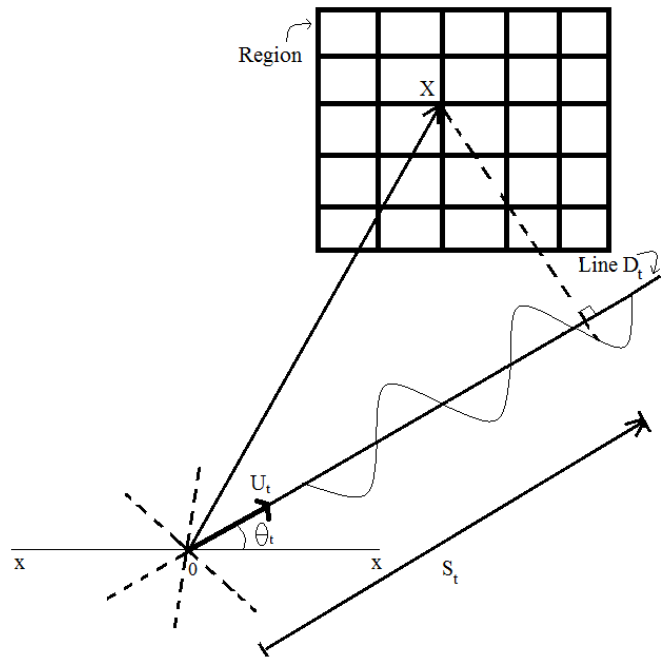

Figure 2.12 : Schematic representation of the turning bands algorithm
(spanning of a cosine wave drawn along a random direction of space)

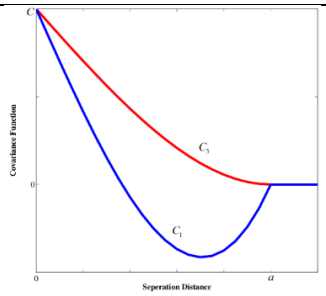

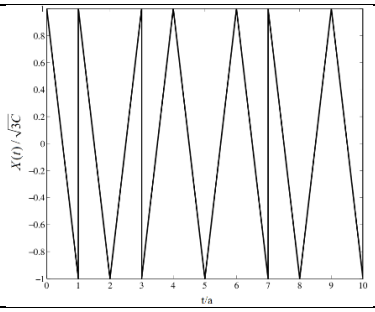

A) Spherical

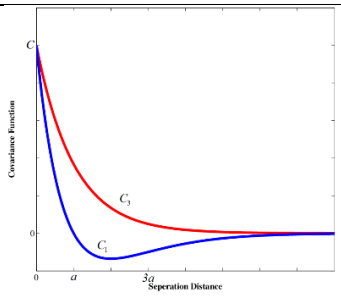

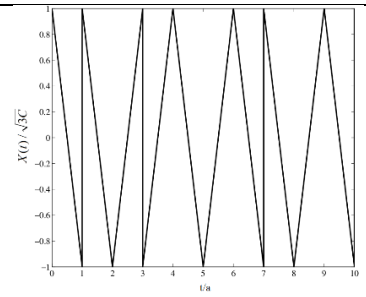

B) Exponential

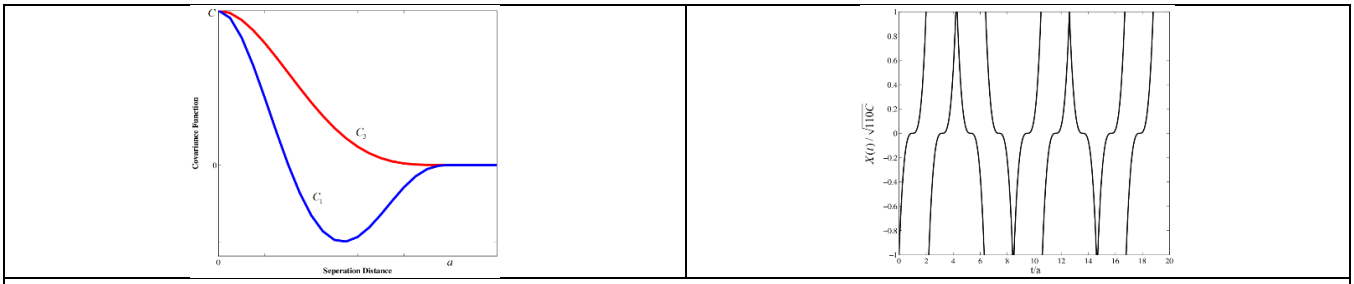

C) Cubic

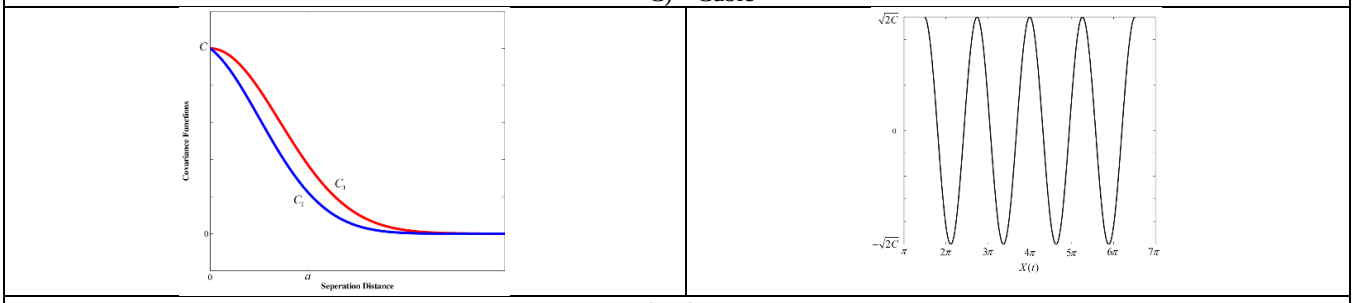

D) Gaussian

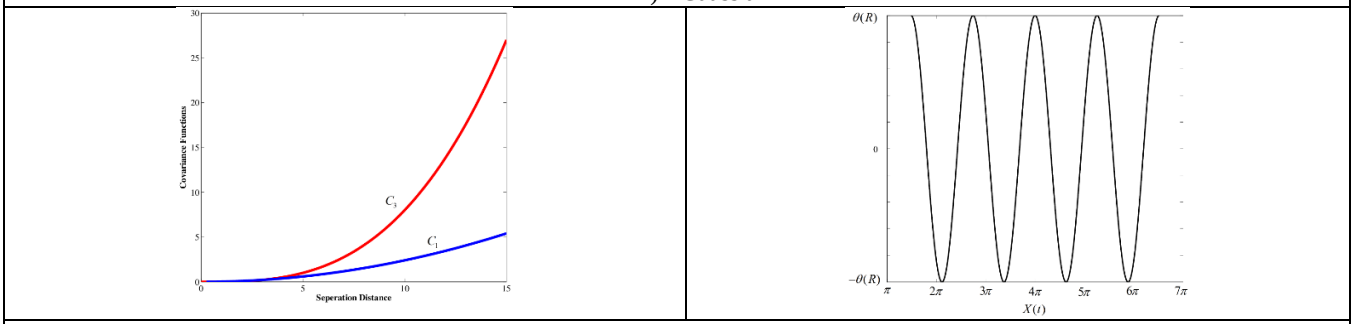

E) Power

Figure 2.13: Left: covariance functions in 1D (blue) and 3D (red). Right: basic random field simulated along a line

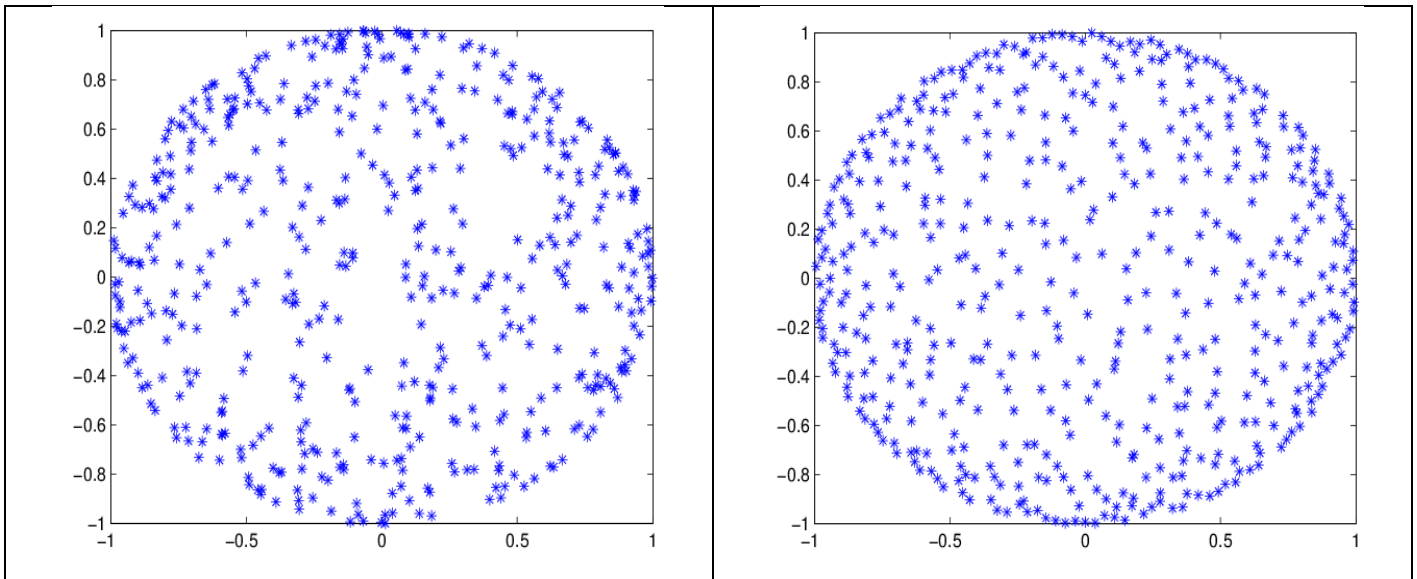

A) Uniform points

B) Van der Corput sequence

Figure 2.14: Projections of 500 points of the unit half-sphere, representing 500 directions in the 3D space

4.9 Conditional simulation

Conditional simulation allows restituting the data values observed at sampling locations by post-processing the non-conditional simulation results.

In the case of a stationary Gaussian random field, it is known (Chilès and Delfiner, 2012) that the distribution at a given location conditional to observations at surrounding locations is Gaussian, with mean value equal to the simple kriging prediction and variance equal to the simple kriging variance. In the case of an IRF-*k* with Gaussian generalized increments, a similar result holds, but simple kriging has to be replaced by intrinsic kriging of order *k* (Emery, 2008a).

Based on this result, it is possible to convert a non-conditional simulation into a conditional one, by (1) calculating the residual between the data values and simulated values at the data locations, (2) kriging this residual from the data locations to the locations targeted for simulation, and (3) adding the kriged residual to the non-conditional simulation (Journel and Huijbregts, 1978). The type of kriging depends on the random field of interest: simple kriging for a stationary random field, ordinary kriging for an IRF-0 and intrinsic kriging of order *k* for an IRF-*k*. Note that, for a given target location, a single kriging system has to be solved for conditioning as many realizations as desired, because the kriging weights are the same for all the realizations.

In Figure 2.15, five conditioning data (magenta circles) have been selected from a reality (black line). The red and blue lines show the conditional simulation and the kriging results, respectively. Both reproduce the conditioning data, but the former also reproduces the spatial variability of the real random field, while the latter gives a smoothed image of it.

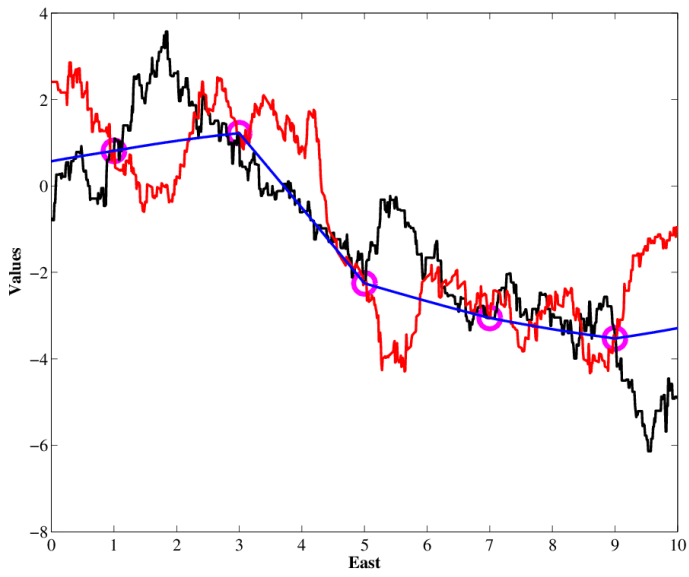

Figure 2.15: Real (black), simulated (red) and kriged (blue) profiles. Magenta circles: conditioning data

Chapter 3: Plurigaussian model

1 Conventional stationary model

The plurigaussian model (Galli et al., 1994) is an extension of the truncated Gaussian model. It is designed to adapt to a wider range of phenomena, by allowing for more complicated types of contacts between the geological domains under consideration, and is currently used in both the petroleum and mining industries (Armstrong et al., 2011). In particular, it has been applied to the modeling of granite-hosted uranium deposits (Skvortsova et al. 2001, 2002), roll front uranium deposits (Fontaine and Beucher, 2006), diamond pipes (Deraisme and Field, 2006), porphyry copper deposits (Carrasco et al., 2007; Emery and González, 2007a, 2007b; Emery et al., 2008), nickel laterite deposits (Rondon, 2009), gold deposits (Yunsel and Ersoy, 2011) and epithermal lead-zinc deposits (Yunsel and Ersoy, 2013). There have been also applications to other fields in the geosciences, such as hydrogeology (Mariethoz et al., 2009).

The basic idea of the plurigaussian model is to consider two or more Gaussian random fields, which are simulated at every location in the region under study, and then use a truncation rule to convert these Gaussian values into geological domains (Figure 3.1). Accordingly, the practical implementation of the model requires defining:

(1) a truncation rule: it has an impact on the contacts between domains;

(2) truncation thresholds: they have an impact on the proportion of space covered by each simulated geological domain;

(3) the covariances or variograms of the underlying Gaussian random fields: they characterize the spatial continuity of these fields, hence, of the geological domains that will be obtained after applying the truncation rule.

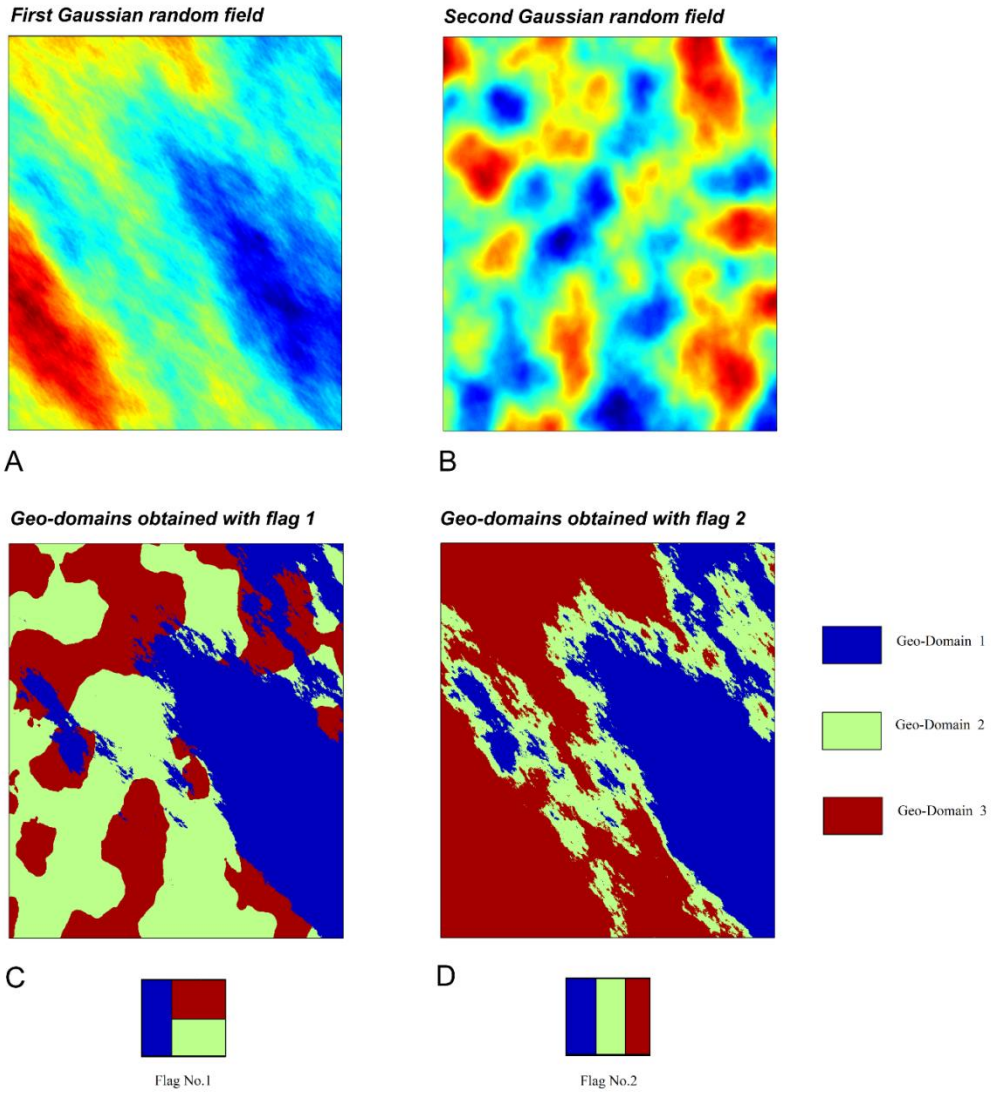

Figure 3.1: Examples of realizations of geological domains (bottom) obtained by truncating two independent Gaussian random fields (top). The truncation rule is represented by a flag below each realization, in which the abscissa axis represents the first Gaussian random field, the ordinate axis represents the second Gaussian random field, and the horizontal and vertical lines represent the truncation thresholds that define the partition of the bi-Gaussian space into geological domains.

1.1 Model parameters

1.1.1 Truncation rule

The truncation rule consists in defining a partition of the Gaussian space, which associates the values of the Gaussian random fields with the geological domains (Armstrong et al., 2011; Lantuéjoul, 2002; Le Loc'h et al., 1994).

Figure 3.1 shows that the domains that touch each other in the truncation rule are also in contact in space. In the absence of contact, the truncation rule can represent sequential contacts between domains, as illustrated in Figure 3.1D with domains 1 and 3. Chronological relationships can also

be accounted for: in Figure 3.1C, the first domain is seen to cross-cut the other two, therefore, from a geological point of view, it should represent a younger domain, while domains 2 and 3 are older. In conclusion, the layout of the truncation rule has implications on the spatial relationships between the geological domains, via the permissible and forbidden contacts between domains, and on their chronological ordering.

1.1.2 Truncation thresholds

Given the geometry of the truncation rule, one has to specify the numerical values (thresholds) that delimit the different domains of the partition in the Gaussian space.

For N underlying Gaussian random fields, grouped into a vector random field $\mathbf{Z} = \{\mathbf{Z}(\mathbf{x}): \mathbf{x} \in \mathbb{R}^d\}$ with N components, and M geological domains, one may, for instance, define $M - 1$ thresholds. Let us suppose that $g(.)$ is the joint probability density function of the Gaussian random fields. In order to calculate the probability of occurrence of the i-th geological domain at a given location $\mathbf{x}$, one needs to solve the following equation:

$$P_i(\mathbf{x}) = \int_{D_i} g(z_1,..., z_N)\, dz_1 ... dz_N \qquad (3.1)$$

where D_i is the region of the partition associated with the i-th geological domain (a subset of $\mathbb{R}^N$ delimited by the thresholds). This equation can sometimes be solved analytically or, most often, numerically by trial and error. Calculations may be speeded up by grouping the domains, as in Figure 3.2: the desired partition is shown on the top line, while the second line shows the order in which the thresholds are evaluated, starting from the top block.

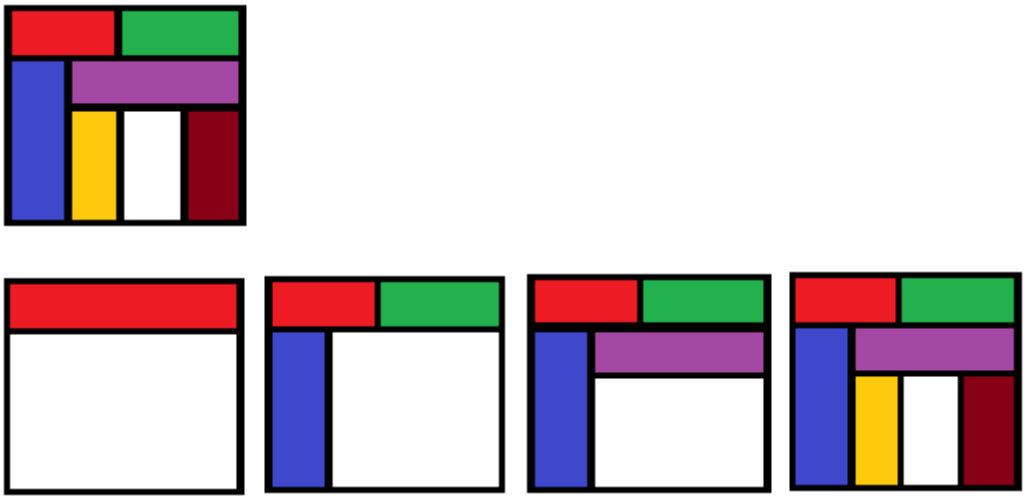

Figure 3.2: Successive groupings to obtain the truncation thresholds (modified from Armstrong et al., 2011)

1.1.3 Variograms of the underlying Gaussian random fields

For any separation vector **h**, the indicator cross variogram between two geological domains (with indices *i* and *j*) is derived from the corresponding non-centered covariance

$$\gamma_{ij}(\mathbf{h}) = C_{ij}(\mathbf{0}) - \frac{1}{2}[C_{ij}(\mathbf{h}) + C_{ij}(-\mathbf{h})] \tag{3.2}$$

with (Armstrong et al., 2011)

$$C_{ij}(\mathbf{h}) = \text{prob}\{\mathbf{Z}(\mathbf{x}) \in D_i, \mathbf{Z}(\mathbf{x}+\mathbf{h}) \in D_j\}$$
(3.3)

If D_i and D_j are rectangular parallelepipeds of $\mathbb{R}^N$ and the components of the vector random field **Z** are independent, the second member of Equation (3.3) is a function of the direct covariances or variograms of the components of **Z** and can be calculated by numerical integration (Dowd et al., 2003) or by using expansions into Hermite polynomials (Emery, 2007b). This establishes a link between the variograms of the underlying Gaussian random fields and the indicator variograms, which are accessible experimentally from the observed geological domains at sampling locations. The former can therefore be determined according to the fitting of the latter, quite often, through a trial-and-error procedure (Le Loc'h and Galli, 1997; Emery, 2007b; Armstrong et al., 2011).

1.2 Conditional simulation

Once the parameters of the plurigaussian model are specified, the simulation can be performed in three main steps (Lantuéjoul, 2002; Emery, 2007b; Dowd, 2003, Armstrong et al., 2011):

(1) Simulate the underlying Gaussian random fields at the data locations, conditionally to the categorical data.

(2) Simulate the Gaussian random fields at the target locations, conditionally to the values obtained in the previous step.

(3) Apply the truncation rule to obtain the simulated domains.

The third step is straightforward, while the second step can be performed by any algorithm for simulating stationary Gaussian random fields: Cholesky decomposition of the covariance matrix (Davis, 1987), sequential Gaussian simulation (Ripley, 1987; Deutsch and Journel, 1992; Gómez–Hernández and Journel, 1993), discrete spectral simulation (Chilès and Delfiner, 1997), continuous spectral simulation (Shinozuka, 1971; Mejia and Rodríguez-Iturbe, 1974; Lantuéjoul, 2002) and turning bands (Matheron, 1973; Lantuéjoul, 1994; Emery and Lantuéjoul, 2006), to name a few (see also Chilès and Delfiner, 2012, and references therein).

The first step can be realized by an iterative algorithm known as the *Gibbs sampler* (Geman and Geman, 1984; Casella and George, 1992), which belongs to the family of Monte Carlo Markov Chain (MCMC) approaches (Ripley, 1987; Gentle, 2009; Chilès and Delfiner, 2012). The general procedure is as follows:

Initialization

For each data location $\mathbf{x}_\alpha$, generate a vector with N components $\mathbf{z}_\alpha$ in $D_{i(\alpha)}$, where $i(\alpha)$ is the index of the geological domain present at $\mathbf{x}_\alpha$.

Iteration

a) Select a data location $\mathbf{x}_\alpha$, regularly or randomly.
b) Calculate the distribution of $\mathbf{Z}(\mathbf{x}_\alpha)$ conditional to the other data $\{\mathbf{Z}(\mathbf{x}_\beta): \beta \neq \alpha\}$. In the stationary case, this is a Gaussian distribution, with mean equal to the simple kriging prediction of $\mathbf{Z}(\mathbf{x}_\alpha)$ and covariance matrix equal to the covariance matrix of the simple kriging errors.
c) Simulate a vector $\mathbf{z}_\alpha$ according to the previous conditional distribution.
d) If $\mathbf{z}_\alpha$ is compatible with the domain prevailing at $\mathbf{x}_\alpha$ (i.e., $\mathbf{z}_\alpha \in D_{i(\alpha)}$), replace the current value of $\mathbf{Z}(\mathbf{x}_\alpha)$ by $\mathbf{z}_\alpha$.
e) Go back to a) and loop many times.

The Gibbs sampler so presented is irreducible, aperiodic and reversible, with the target Gaussian distribution as its ergodic limit. In other words, if the number of iterations increases infinitely, the distribution of the simulated vectors at the data locations converges to the conditional distribution of the desired Gaussian random fields.

Concerning step a), there are some common strategies to select the data (Robert and Sahu, 1997; Galli and Gao, 2001):

- Random sweep: the index of the data is chosen uniformly in $\{1,\ldots, n\}$.
- Deterministic updating: the index of the data is increased by one unit at each iteration.
- Reverse updating: the index of the data is increased by one unit at the first iterations, then decreased by one unit at the next iterations, and so on.
- Random permutation: the index of the data follows a random permutation of $\{1,\ldots, n\}$ for the each group of n successive iterations.

Arroyo et al. (2012) showed that the last strategy (random permutation) is getting much faster to convergence. In this thesis, this strategy will be applied for the Gibbs sampler.

1.3 Discussion

1.3.1 Truncation rule

In practice, to restrict the number of parameters and to ease their inference, one usually considers two independent Gaussian random fields ($N = 2$). Although this simplifies the implementation of the model, it implies severe limitations on the spatial relationships between geological domains, in particular, with respect to permissible and forbidden contacts. For instance, Figure 3.1C shows that three geological domains can touch each other, whereas Figure 3.1D shows two domains that cannot have contact together. Most often the truncation rule consists of a partition of the two-dimensional space into rectangles (Armstrong et al., 2011) or unions of rectangles (Emery, 2007b), although more general designs can be considered (Allard et al., 2012; Deutsch and Deutsch, 2014).

Defining a two-dimensional truncation rule offers the following advantages:

(1) One visually controls the contact relationships between geological domains: two domains are in contact in space if they are in contact on the representation of the truncation rule.

(2) One can also control the chronology relationships between geological domains. In Figure 3.1C, the first domain appears in the foreground (first layer) and can then be interpreted as a younger domain that cross-cuts the other two older domains (2 and 3), which appear in the background (second layer).

However, by restricting to a two-dimensional truncation rule (as in most applications), one is often limited in the number of geological domains that can be modeled, especially when all these domains are mutually in contact, a situation that often arises in practice. For instance, Figure 3.3 presents examples of truncation rules with four geological domains (modified from Armstrong et al., 2011): none of them allows each domain to be in contact with each other, as there is always some prohibited contact between domains.

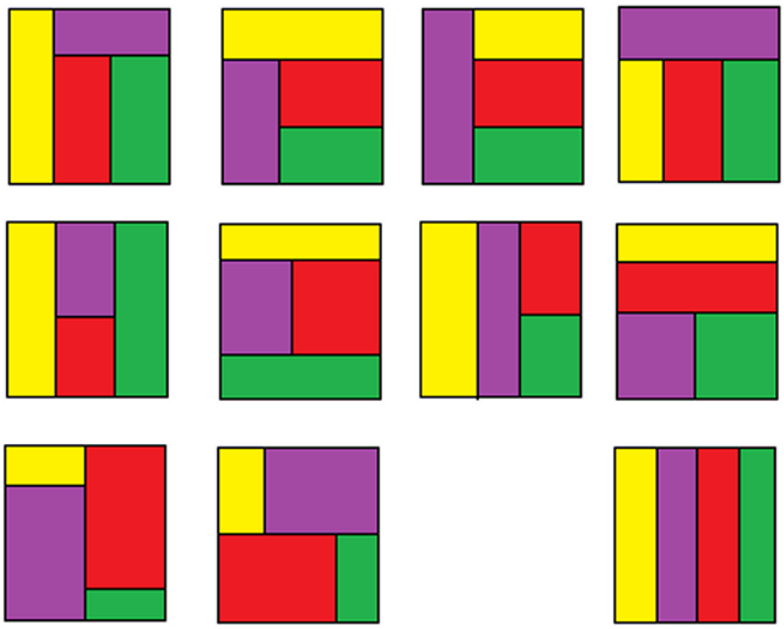

Figure 3.3: Examples of truncation rules with four geological domains (modified from Armstrong et al., 2011). The domains represented in yellow and green are never in contact

To overcome this limitation, following Xu et al. (2006) and Emery (2007b), one idea of this thesis is to increase the number of Gaussian random fields, so as to increase the dimensionality of the truncation rule and to allow the geological domains to be in contact altogether. As an example, consider the following four-domain truncation rule, based on three underlying Gaussian random fields $\{Z_1, Z_2, Z_3\}$ and three truncation thresholds $\{t_1, t_2, t_3\}$, which can be represented by a three-dimensional flag (Figure 3.4):

$$\text{Domain at location } \mathbf{x} = \begin{cases} 1 \text{ if } Z_1(\mathbf{x}) \le t_1 \\ 2 \text{ if } Z_1(\mathbf{x}) > t_1 \text{ and } Z_2(\mathbf{x}) \le t_2 \\ 3 \text{ if } Z_1(\mathbf{x}) > t_1, Z_2(\mathbf{x}) > t_2 \text{ and } Z_3(\mathbf{x}) \le t_3 \\ 4 \text{ if } Z_1(\mathbf{x}) > t_1, Z_2(\mathbf{x}) > t_2 \text{ and } Z_3(\mathbf{x}) > t_3 \end{cases} \tag{3.4}$$

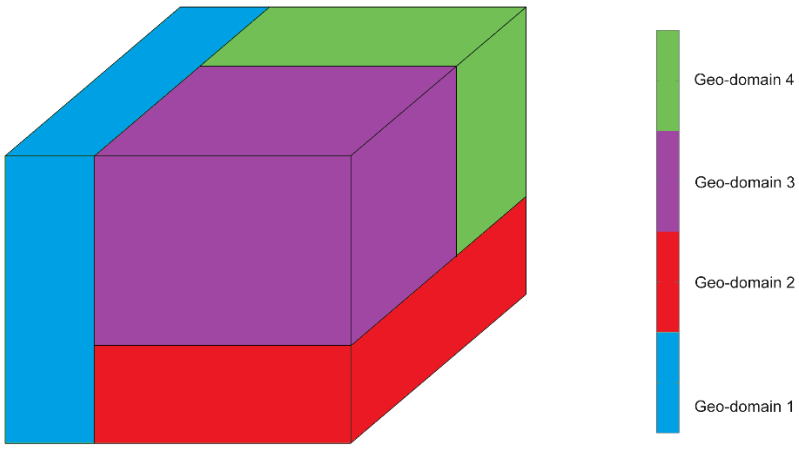

Figure 3.4: Three-dimensional truncation rule with four geological domains that are mutually in contact. Each axis of this flag corresponds to an underlying Gaussian random field

A realization of this model is shown in Figure 3.5. The first geological domain (painted in blue) appears in the foreground or first "layer" (it may represent a younger domain that cross-cuts the other ones). The second domain (red) is in a second layer, while domains 3 and 4 (purple and green) are located in the background (third layer).

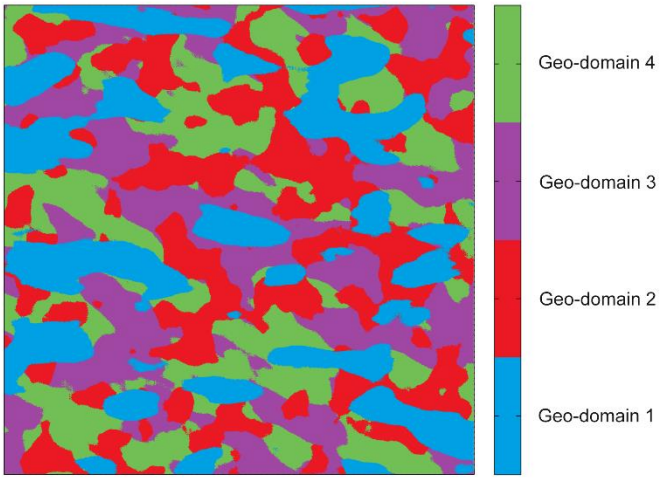

Figure 3.5: Plurigaussian realization with four geological domains distributed in three successive layers

Such a hierarchical approach can easily be generalized to more than four geological domains. An example with seven domains that are numbered chronologically is presented in Figure 3.6 (domain 1 is the youngest and cross-cuts the other ones, while domains 6 and 7 are the oldest). It

is based on a truncation rule that involves six Gaussian random fields $\{Z_1, Z_2, Z_3, Z_4, Z_5, Z_6\}$ and six thresholds $\{t_1, t_2, t_3, t_4, t_5, t_6\}$:

$$\text{Domain at location } \mathbf{x} = \begin{cases} 1 \text{ if } Z_1(\mathbf{x}) \le t_1 \\ 2 \text{ if } Z_1(\mathbf{x}) > t_1 \text{ and } Z_2(\mathbf{x}) \le t_2 \\ 3 \text{ if } Z_1(\mathbf{x}) > t_1, Z_2(\mathbf{x}) > t_2 \text{ and } Z_3(\mathbf{x}) \le t_3 \\ 4 \text{ if } Z_1(\mathbf{x}) > t_1, Z_2(\mathbf{x}) > t_2, Z_3(\mathbf{x}) > t_3 \text{ and } Z_4(\mathbf{x}) \le t_4 \\ 5 \text{ if } Z_1(\mathbf{x}) > t_1, Z_2(\mathbf{x}) > t_2, Z_3(\mathbf{x}) > t_3, Z_4(\mathbf{x}) > t_4 \text{ and } Z_5(\mathbf{x}) \le t_5 \\ 6 \text{ if } Z_1(\mathbf{x}) > t_1, Z_2(\mathbf{x}) > t_2, Z_3(\mathbf{x}) > t_3, Z_4(\mathbf{x}) > t_4, Z_5(\mathbf{x}) > t_5 \text{ and } Z_6(\mathbf{x}) \le t_6 \\ 7 \text{ if } Z_1(\mathbf{x}) > t_1, Z_2(\mathbf{x}) > t_2, Z_3(\mathbf{x}) > t_3, Z_4(\mathbf{x}) > t_4, Z_5(\mathbf{x}) > t_5 \text{ and } Z_6(\mathbf{x}) > t_6 \end{cases} \tag{3.5}$$

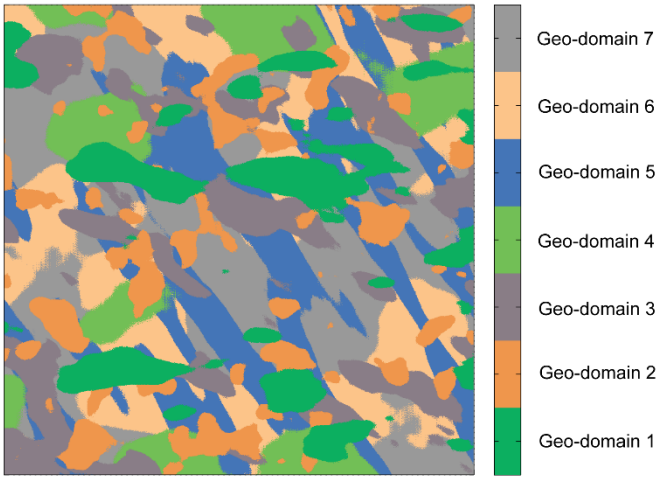

Figure 3.6: Plurigaussian realization with seven geological domains distributed in six successive layers

In practice, the truncation thresholds $\{t_1, t_2, t_3, t_4, t_5, t_6\}$ are defined in order to reproduce the proportions of the different geological domains (Armstrong et al., 2011). For instance, the proportion of the first domain is equal to $G^{-1}(t_1)$, where G stands for the standard Gaussian cumulative distribution function: threshold t_1 can then be defined in order to yield a given proportion for domain 1 (for instance, the proportion inferred from an interpreted geological model). Assuming that Z_1 and Z_2 are independent, the proportion of the second domain is equal to $[1 - G^{-1}(t_1)]\ G^{-1}(t_2)$: as t_1 is already known, threshold t_2 can now be defined in order to yield a given proportion for domain 2. The same procedure can be applied for the remaining thresholds (t_3 to t_6), which relate to the proportions of domains 3 to 7.

1.3.2 Convergence of the Gibbs sampler

Some theoretical criteria have been proposed to study the rate of convergence of Markov chains (Chan, 1993; Tierney, 1994; Roberts and Sahu, 1997; Meyn and Tweedie, 2009). But these criteria are often limited or impractical, insofar as they require determining the spectral radius of the transition kernel of the chain (Arroyo et al., 2012). Instead, an experimental assessment of the convergence is often preferred (Lantuéjoul, 2002; Gelman et al., 2004; Emery, 2007a). The simulated Gaussian values can be checked by their experimental distributions and experimental variograms compared with the theoretical model, either graphically or by statistical testing. For instance, in the case of a Gaussian random field with an exponential variogram model to be generated at a set of 400 data locations, Emery (2008b) shows that the convergence can be practically reached once the Gibbs sampler has visited and updated each data location 25 times, while for a spherical variogram model with 359 data locations, about 100 to 200 updates per data location are sufficient (Emery, 2007a). Armstrong et al. (2011) give similar figures (20 to 100 updates) in other cases.

The Gibbs sampler is also limited concerning the number of data that can participate for solving the kriging system: when the data are numerous, a moving neighborhood implementation is often used, based on the screen-effect approximation (the data located near to the target location screen out the influence of the data located farther away). However, this approximation entails that the Markov chain no longer converges to the desired distribution or does not converge at all (Emery et al., 2014). A dual form of the Gibbs sampler (Lantuéjoul and Desassis, 2012; Arroyo et al., 2012; Emery et al., 2014) has recently been proposed to overcome this difficulty, allowing the Gibbs sampler to be implemented in a unique neighborhood, but, to our best knowledge, this proposal is only applicable in the case of stationary Gaussian random fields.

1.3.3 Domain proportions

As stated above, to determine the truncation thresholds, it is necessary to know the probability of occurrence of each geological domain within the region of interest, which can be estimated by the (declustered) proportion of the available data that belong to the domain under consideration. Two questions arise from this practice:

(1) Are the probabilities of occurrence of the geological domains constant over space?
(2) Can these probabilities be considered as perfectly known?

Concerning the first question, as already mentioned in the introductory chapter, in most cases the distribution of the geological domains is heterogeneous in space. For example, in petroleum reservoirs, the proportions of the lithological domains (lithofacies) vary vertically because of the cyclic changes during deposition. To account for these changes, vertical proportion curves (Matheron et al., 1987; Ravenne et al., 2002) have been designed in order to estimate the domain proportions as a function of depth. These curves can be computed along lines parallel to a chosen

reference level (generally, a chrono-stratigraphic marker), and smoothed to reduce statistical fluctuations and to be representative of genuine geological features in the deposit or reservoir (Roth et al., 1998).

A more general case occurs when the domain proportions vary vertically and laterally. Beucher et al. (2006) constructed a 3D matrix of proportion curves to model the evolution in the proportions both vertically and laterally. The proportions were first calculated locally, in sampled areas, then interpolated (by kriging) over a regular grid covering the region of interest. Inferring regionalized proportions can also account for secondary data, such as geophysical information (Moulière et al., 1997; Moulière, 1998).

Spatially-varying proportions can be associated with spatially-varying thresholds, in accordance with the chosen truncation rule (Eq. 3.1) (the design of the truncation rule is supposed to be the same everywhere). For variogram analysis, it is assumed that the underlying Gaussian random fields are still stationary, i.e., their variograms only depend on the separation vector between data points. Now, because the domain proportions vary in space, the truncation is no longer the same at each location, so that the indicator variograms are no longer stationary. For variogram analysis, one can work with "average variograms". For instance, if the truncation only varies with depth, then the indicator variograms can be calculated in each horizontal plane and then averaged to get a single horizontal variogram on which the model is fitted. However, the theoretical foundation of this practice is not clearly laid out. An alternative is to infer the variograms as if the domain proportions were constant in space (using the global proportions), but this is an approximation as the indicator variograms actually depend on the local domain proportions, through the truncation thresholds.

An additional difficulty in plurigaussian modeling relates to the second question about whether or not the probabilities of occurrence of the geological domains can be known with certainty. In the pure stationary model, where the domain proportions are constant in space, it is reasonable to assume that these proportions are known, provided that enough data are available (declustering techniques can be used when these data are in a non-regular sampling design). Alternatively, an interpreted geological model can be used to calculate the domain proportions. Things get more complicated when the domain proportions are assumed to vary locally: in areas with few data, these proportions cannot be considered as perfectly known any longer, which highlights an internal inconsistency in the model construction. Even in areas with many data, it is problematic to identify the concepts of local proportions (which can be calculated on a single realization by defining a local neighborhood) and local probability of occurrence (which can be calculated at every point-support location based on a large set of realizations). These two concepts only match in the case of the stationary model if one further assumes some ergodicity property.

To sum-up, the use of spatially-varying domain proportions is challenging for both the variogram analysis and the calculation of spatially-varying truncation thresholds. The current practice relies on approximations that are simplistic and may affect the assessment of geological uncertainty.

2 Proposal for non-stationary plurigaussian modeling

The main contribution of this thesis is a generalization of the plurigaussian model to the non-stationary framework. Instead of working with stationary Gaussian random fields and spatially-varying truncation thresholds, the idea is to consider the truncation of intrinsic random fields of order k with generalized Gaussian increments. Hence, the non-stationarity is no longer modeled through the truncation thresholds, but through the underlying random fields to be truncated.

Let us revise the changes that this implies in the inference and simulation stages.

2.1 Truncation rule

Since the truncation rule is aimed at establishing the contact relationships between the simulated geological domains, there is no change in this concept with respect to the stationary model (see Section 1.1.1 of this Chapter).

2.2 Truncation thresholds

According to the second definition of an intrinsic random field of order k (Chapter 2, Section 4.3), an IRF-k is an equivalence class of random fields that differ by a deterministic or random polynomial of degree less than or equal to k. Consider a member (representation) of this class, say Z, and a truncation threshold z. Stating that Z is less than z amounts to stating that $Y = Z - z$ is less than 0, where Y is another representation of the same IRF-k as Z. In other words, regardless the value of the truncation threshold z, the problem can be reformulated in an equivalent way with another representation of the IRF-k and with a zero threshold (Figure 3.7).

This statement can be applied recursively in the hierarchical model presented at Section 1.3.1: in each level or layer, the truncation threshold can be set to zero and does no longer depend on the (estimated) proportions of geological domains. This way, one circumvents the difficulties met when using local domain proportions.

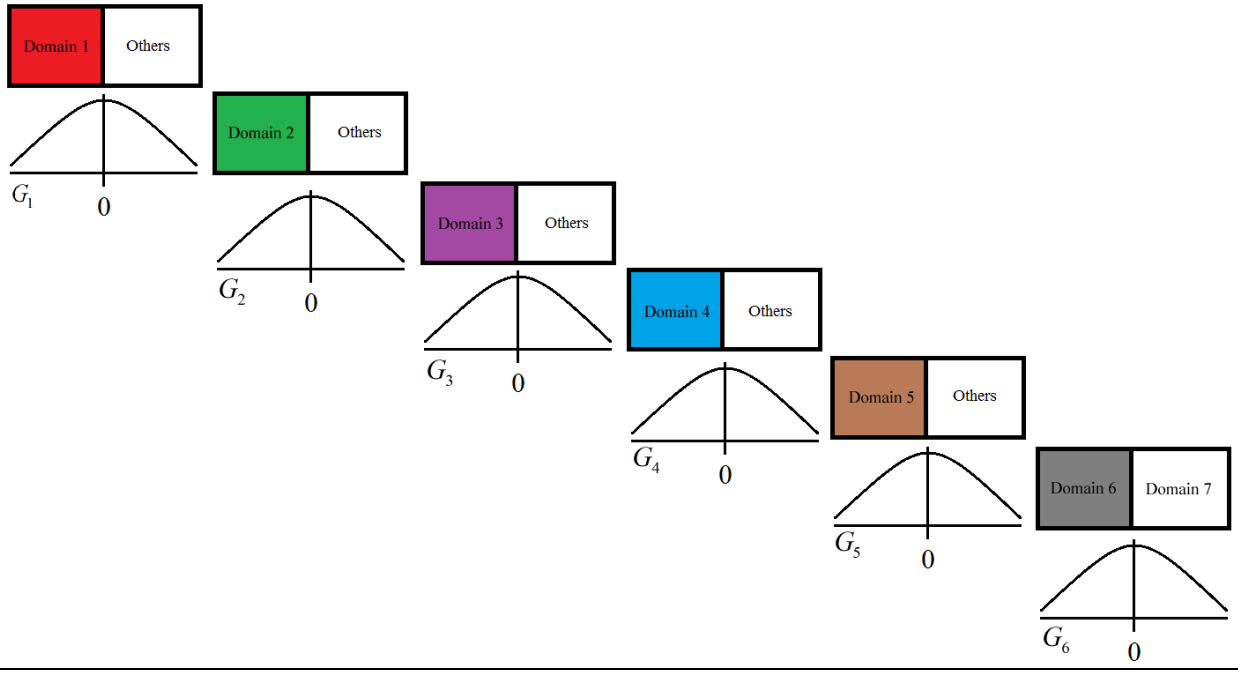

A) Fixing truncation thresholds at zero (hierarchical model)

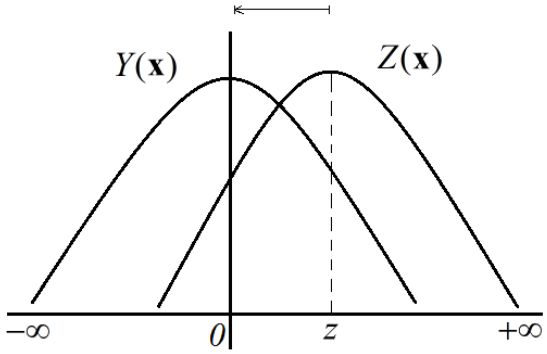

B) Thresholding two representations (Z and Y) of the same IRF-k

Figure 3.7: Threshold analysis in the non-stationary plurigaussian model

2.3 Structural analysis

For ease of presentation, hereunder we will consider the case of a single random field $Z = \{Z(\mathbf{x}): \mathbf{x} \in \mathbb{R}^d\}$ and a single truncation threshold (0). Again, in the case of a hierarchical plurigaussian model, the methodology can be applied recursively, i.e., the structural analysis can be performed separately on each underlying random field.

As mentioned in Section 1.1.3, under the assumption of stationarity, it is possible to establish a relationship between the covariance function of the Gaussian random field and the covariance function (or the variogram) of the indicator random field obtained by truncation. Things get more complicated when the Gaussian random field is no longer stationary, but an intrinsic random field of order k: in this case, the covariance function of Z may not exist, and its spatial correlation structure is described with a generalized covariance $K(\mathbf{h})$, which has no clear interpretation with the indicator random field obtained by truncation.

To break the deadlock, the idea is to choose a specific representation of the desired random field of order *k*, namely an internal representation (see Section 4.6 of Chapter 2), which possesses a covariance function that can be associated with a covariance function of the indicator random field. Let $Z = \{Z(\mathbf{x}): \mathbf{x} \in \mathbb{R}^d\}$ be a representation of an IRF-*k* and define the indicator at threshold 0 by

$$I(\mathbf{x}) = \begin{cases} 1 \text{ if } Z(\mathbf{x}) < 0 \\ 0 \text{ otherwise} \end{cases} \tag{3.6}$$

Consider $n = \frac{(k+d)!}{k!d!}$ data locations $\{\mathbf{x}_1, \ldots \mathbf{x}_n\}$ for which the above indicator is known (Table 3.1). For the sake of simplicity, suppose that the indicator is equal to 1 at all these locations (any other case could be treated similarly). Because an intrinsic random field of order *k* is defined up to a polynomial of degree less than or equal to *k*, one can assume without loss of generality that the random field *Z* is equal to –1 at locations $\mathbf{x}_1, \ldots \mathbf{x}_n$ (indeed, it suffices to choose the *n* coefficients of the polynomial in order to fix the desired values at the selected *n* data locations). If the indicator were equal to 0 at a data location, one can choose *Z* equal to 1 at this location and adapt the following statements accordingly.

	$k = 0$	$k = 1$	$k = 2$
$d = 2$	1	3	6
$d = 3$	1	4	10

Table 3.1. Number *n* of selected data locations as a function of the space dimension (*d*) and order of the intrinsic random field (*k*)

Let us now define an internal representation of the IRF-*k* by putting (Eq. 2.27):

$$Y(\mathbf{x}) = Z(\mathbf{x}) - \sum_{i=1}^{n} \lambda_i \, Z(\mathbf{x}_i) \tag{3.7}$$

with $\lambda = \{\{\lambda_i, \mathbf{x}_i\}_i ; (-1, \mathbf{x})\} \in \Lambda_k$. As the sum of weights of an ALC-*k* is zero, the lambda's add to 1 and one has

$$\sum_{i=1}^{n} \lambda_i \, Z(\mathbf{x}_i) = -1 \tag{3.8}$$

The covariance function of *Y* can be calculated as a function of the generalized covariance of the intrinsic random field (Eq. 2.28):

$$C_Y(\mathbf{x}, \mathbf{x}') = K(\mathbf{x} - \mathbf{x}') - \sum_i \lambda_i \, K(\mathbf{x}_i - \mathbf{x}) - \sum_i \lambda_i \, K(\mathbf{x}_i - \mathbf{x}') + \sum_i \sum_j \lambda_i \, \lambda_j \, K(\mathbf{x}_i - \mathbf{x}_j) \tag{3.9}$$

Based on the previous statements, the indicator can be rewritten in terms of *Y* rather than *Z*:

$$I(\mathbf{x}) = \begin{cases} 1 \text{ if } Y(\mathbf{x}) < 1 \\ 0 \text{ otherwise} \end{cases} \tag{3.10}$$

Because it is an ALC-*k*, $Y(\mathbf{x})$ is normally distributed, with mean value 0 and variance $C_Y(\mathbf{x},\mathbf{x})$ that depends on $\mathbf{x}$. Let us standardize Y to a unit variance by putting

$$\widetilde{Y}(\mathbf{x}) = \frac{Y(\mathbf{x})}{\sqrt{C_Y(\mathbf{x},\mathbf{x})}} \tag{3.11}$$

The covariance of $\widetilde{Y}$ is:

$$\rho(\mathbf{x},\mathbf{x}') = \frac{C_Y(\mathbf{x},\mathbf{x}')}{\sqrt{C_Y(\mathbf{x},\mathbf{x})\,C_Y(\mathbf{x}',\mathbf{x}')}} \tag{3.12}$$

The indicator becomes:

$$I(\mathbf{x}) = \begin{cases} 1 \text{ if } \widetilde{Y}(\mathbf{x}) < y(\mathbf{x}) = 1/\sqrt{C_Y(\mathbf{x},\mathbf{x})} \\ 0 \text{ otherwise} \end{cases} \tag{3.13}$$

One can now express the (non-centered) covariance function of this indicator, by using the relationship between the covariance of a standard Gaussian random field and its indicators. The starting point is the expansion of the indicator into normalized Hermite polynomials $\{H_p: p \in \mathbb{N}\}$ (Rivoirard, 1994; Chilès and Delfiner, 2012):

$$I(\mathbf{x}) = G(y(\mathbf{x})) + \sum_{p=1}^{+\infty} H_{p-1}(y(\mathbf{x}))\, g(y(\mathbf{x}))\, H_p(\widetilde{Y}(\mathbf{x})) \tag{3.14}$$

where g and G stand for the standard Gaussian probability density and cumulative distribution functions, respectively. Because the Hermite polynomials are spatially non-correlated, it comes:

$$\begin{aligned} C_I(\mathbf{x},\mathbf{x}') &:= E\{I(\mathbf{x})I(\mathbf{x}')\} \\ &= G(y(\mathbf{x}))\,G(y(\mathbf{x}')) + \sum_{p=1}^{+\infty} H_{p-1}(y(\mathbf{x}))\,H_{p-1}(y(\mathbf{x}'))\,g(y(\mathbf{x}))\,g(y(\mathbf{x}'))[\rho(\mathbf{x},\mathbf{x}')]^p \end{aligned} \tag{3.15}$$

The left-hand side of this equation can be experimentally calculated for each data pair, as the product of the data indicators. The right-hand side depends on the weights $\{\lambda_1,\ldots,\lambda_n\}$ (known) and the generalized covariance $K(\mathbf{h})$ (unknown). A parametric form can be assumed for the latter, as a positive linear combination of basic nested structures, such as the nugget effect, spherical, exponential or power covariances.

Expression (3.15) is not valid if $\mathbf{x}$ or $\mathbf{x}'$ coincides with one of the first n data locations, at which $\widetilde{Y}$ is undefined. For these data locations ($i = 1\ldots n$, $j = 1\ldots n$), the indicator is equal to 1, so that:

$$C_I(\mathbf{x}_i, \mathbf{x}_j) = 1 \tag{3.16}$$

whereas for any other generic location **x**, one has:

$$C_I(\mathbf{x}, \mathbf{x}_j) = G(y(\mathbf{x})) \tag{3.17}$$

The steps for inferring the spatial correlation structure of the IRF-*k* are therefore the following:

(1) Choose an order *k* for the intrinsic random field to truncate.

(2) Define the basic nested structures that compose the generalized covariance $K(\mathbf{h})$ (nugget, spherical, exponential, power, etc.). The unknowns are the parameters of these structures (scale factors, sills, slopes, shape parameters or exponents).

(3) Calculate the experimental covariance matrix of the indicator data (the matrix entries are 1 or 0).

(4) Calculate the theoretical covariance matrix of the indicator data by using Equations 3.15 to 3.17. The entries of this matrix depend on the parameters to be fitted.

(5) Find the parameters that minimize the squared errors between these experimental and theoretical covariance matrices (sum of squared errors over all the data pairs).

As for the structural analysis of an IRF-*k*, the above procedure is semi-automatic and does not rely on the graphical fitting of some experimental covariance or variogram. This is the price to pay for dealing with non-stationary random fields. A validation of the fitting against a geological interpretation of the region of interest will be suggested in the case study of Chapter 5.

2.4 Conditional simulation

The simulation stage is similar to the stationary case, except for the following:

(1) The non-conditional simulation of an IRF-*k* can be efficiently done with a spectral-turning bands algorithm (Emery and Lantuéjoul, 2006, 2008; Arroyo and Emery, 2016). Most of the other Gaussian simulation algorithms fail or are approximate when they are applied to non-stationary random fields.

(2) In both the Gibbs sampler and the conditioning of the realizations to the data, intrinsic kriging of order *k* has to be used instead of simple kriging (Emery, 2008a; Chilès and Delfiner, 2012).

To assess the convergence of the Gibbs sampler, one can calculate the generalized variogram of the simulated Gaussian values and compare it with the theoretical model (Eq. 2.22). Examples of this procedure applied to synthetic data will be presented in the next chapter, in the case of IRF-0. For orders greater than or equal to 1, one additional difficulty is the calculation of experimental generalized variograms, which is easy only in the case of regularly-spaced data.

When using kriging in a moving neighborhood, the Gibbs sampler is likely not to converge, so a unique neighborhood implementation has to be preferred. This requires solving a kriging system that may be large if many data are available. Unlike the stationary case, to date, no alternative version of the Gibbs sampler has been designed for a unique neighborhood implementation in the presence of large datasets.

Chapter 4: Synthetic case studies

In order to show the applicability of the proposed non-stationary plurigaussian model and to check the correctness of the simulation algorithm, we will develop a proof of concept, consisting of a set of numerical experiments based on synthetic data sets. The following assumptions are made throughout the chapter:

- Simulation will be performed in the 2D space, for ease of visualization.
- The Gibbs sampler and conditioning kriging are obtained with a unique neighborhood implemention.
- The model parameters are perfectly known.
- The case studies are restricted to the truncation of intrinsic random fields of order 0 with Gaussian increments (the extension to IRF-*k* is considered in the real case study presented in the next chapter).

The fundamentals of this approach are threefolds: (i) implementing plurigaussian simulation with intrinsic random fields instead of stationary random fields, (ii) using the variogram instead of the covariance to describe the spatial correlation structure, (iii) using ordinary kriging (equivalent to intrinsic kriging of order 0) instead of simple kriging to determine the conditional distributions; this is useful in both the Gibbs sampler and in the post-processing of the Gaussian realizations in order to make them conditional to data.

1 Step-by-step description of the numerical experiments

The procedure is as follows:

(1) Generate two intrinsic random fields (IRF-0) with power variograms.

(2) Truncate the simulated random fields according to a prespecified rule, giving a reference model of non-stationary geological domains, say, rock types.

(3) Sample the reference model randomly.

(4) Apply the Gibbs sampler to convert the sampled categorical data into data of IRF-0 with power variograms.

(5) Apply the spectral-turning bands algorithm to simulate the IRF-0 conditionally to the data obtained in the previous step.

(6) Truncate according to the specified rule.

(7) Post-process the realizations.

Step 1: Simulation of intrinsic random fields of order 0

Two independent intrinsic random fields with Gaussian increments are simulated by the spectral-turning bands algorithm (Emery and Lantuéjoul, 2006, 2008), with the following specificities:

- Domain: regular grid with 200 × 200 nodes and grid mesh 1 × 1.
- Simulation is performed at a point-support.
- Variogram model: depending on the case under consideration, a linear variogram with slope 0.01, or a power variogram with exponent $\theta = 1.5$ and slope 0.001, is considered.
- Number of realizations: 2 (one for producing each random field)
- No conditioning data.
- Number of turning lines: 1000 (equi-distributed sequence).

Step 2: Reference model

For obtaining realizations of a categorical random field representing the geological domains, one needs to define the truncation rule and thresholds. Concerning the rule, two cases are considered (Figure 4.1) with three and six categories, respectively.

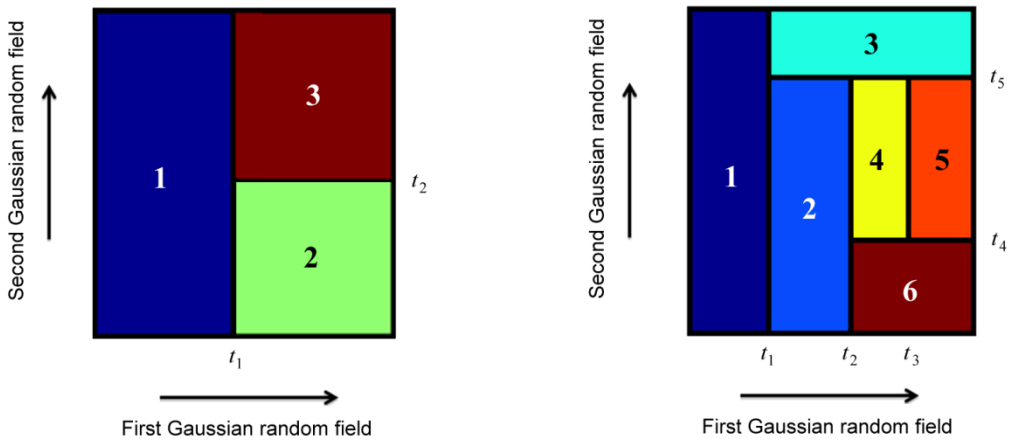

Figure 4.1: Predefined truncation rules

A trial-and-error method has been applied to choose the truncation thresholds, in order to give similar global proportions to the different domains. For example, for the first truncation rule with three domains and two thresholds, threshold t_1 is set as the 33% percentile of the first simulated intrinsic Gaussian random field and threshold t_2 is the 50% percentile (median) of the second simulated intrinsic Gaussian random field (Figure 4.2).

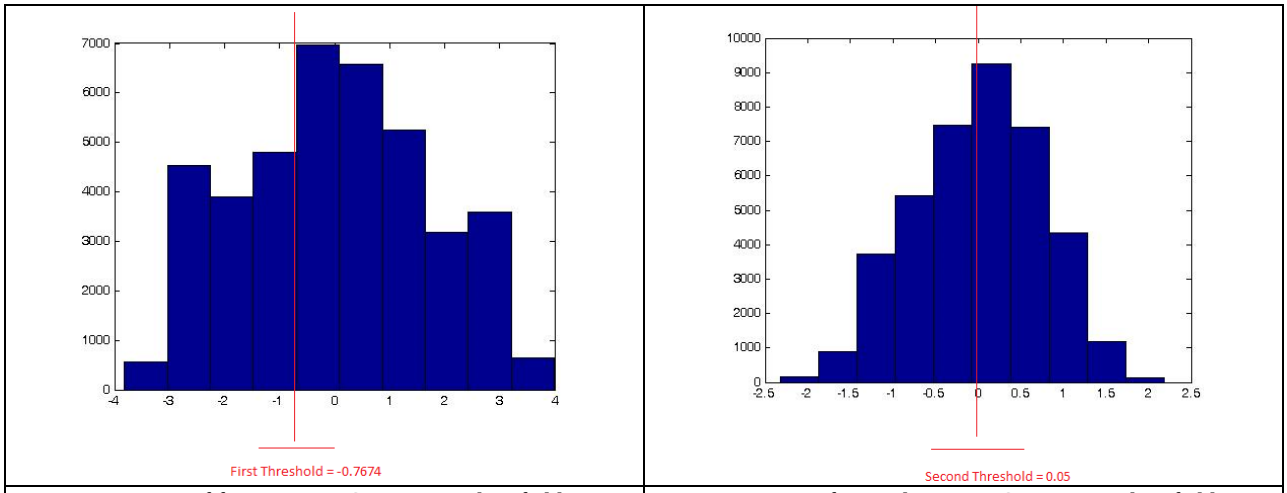

Histogram of first intrinsic Gaussian random field	Histogram of second intrinsic Gaussian random field

Figure 4.2: Threshold definition for the first case (linear variogram with two thresholds)

Step 3: Extract samples

After producing the reference models, one samples these models randomly (uniformly) in order to extract conditioning data. The number of data is set to 10 or 100, depending on the case under consideration, which corresponds to sampling rates of 0.025% and 0.25%, respectively.

Step 4: Gibbs sampling

According to the plurigaussian simulation procedure, first the Gibbs sampler is applied to convert the categorical data into data of the IRF-0. The implementation parameters are as follows:

- The conditional means and variances are determined by intrinsic ordinary kriging
- Kriging is performed in a unique neighborhood
- Number of realizations: 100
- Number of iterations: 200. Each iteration consists of updating all the data values according to a visiting sequence that corresponds to a random permutation of the dataset.

The number of iterations is quite large (200 updates per data). This choice is somehow arbitrary and is aimed at ensuring convergence of the Gibbs sampler to the target distribution. This will be verified experimentally in a next subsection on model validation.

Step 5: Conditional simulation

The spectral-turning bands algorithm of Step 1 is used again to simulate the IRF-0, but, this time, in the scope of conditional simulation over the target grid. The implementation parameters are:

- Number of realizations: 100 for each intrinsic random field
- Conditioning data: output of Gibbs sampler (Step 4)
- Conditioning kriging: ordinary, with a unique neighborhood implementation
- Number of turning lines: 1000 (equi-distributed sequence).

Step 6: Truncation

The truncation rule defined in Step 2 is applied to the simulated IRF-0, to obtain 100 realizations of the geological domains.

Step 7: Post-processing

The realizations are compared with the reference models, in order to check the reproduction of the contact relationships and conditioning data. Also, one is able to determine the uncertainty in the domain proportions and to produce a probability map for each domain.

2 Case 1: linear variograms and truncation rule with three categories

Figure 4.3 shows the maps associated with the reference model (simulated intrinsic random fields and resulting categorical random field), together with the truncation rule. The conditioning data set (100 data) is superimposed on the categorical map.

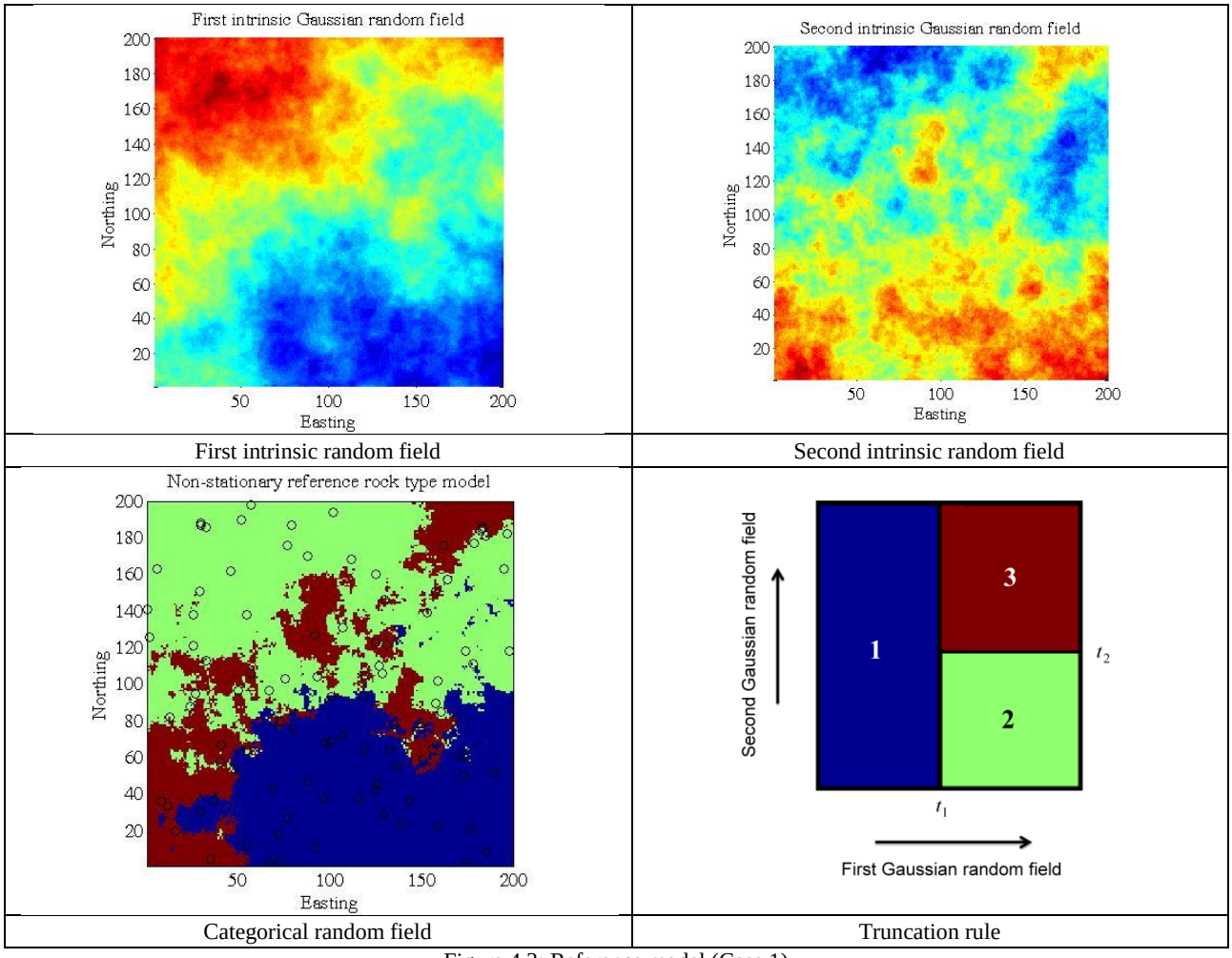

Figure 4.3: Reference model (Case 1)

As can be seen from Figure 4.3, category 1 (blue) is located essentially in the south-eastern part of the map, while category 2 (green) is located in the north-western part of the map and category 3 (red) is situated in the middle with a diagonal position and in some places dominates the green category. In chrono-stratigraphy, it can be interpreted that category 2 (green) is formed firstly, simultaneously with category 3 (red), and category 1 (blue) is dominating these two categories in the post process formation. This event is shown perfectly in the truncation rule at Figure 4.3.

Figure 4.4 presents the locations of the conditioning data extracted from the reference model, as well as five out of the 100 conditional realizations that have been obtained. It is noteworthy that all the realizations reproduce the values of the conditioning data, as well as the global trend and the contacts between categories. From a visual point of view, the applied methodology therefore seems to be successful.

An example of post-processing is shown in Figure 4.5, corresponding to the probability maps of the three categories calculated over the 100 realizations. These maps show a good relation with the reference model and give an insight into the uncertainty in the spatial layout of the boundaries between categories.

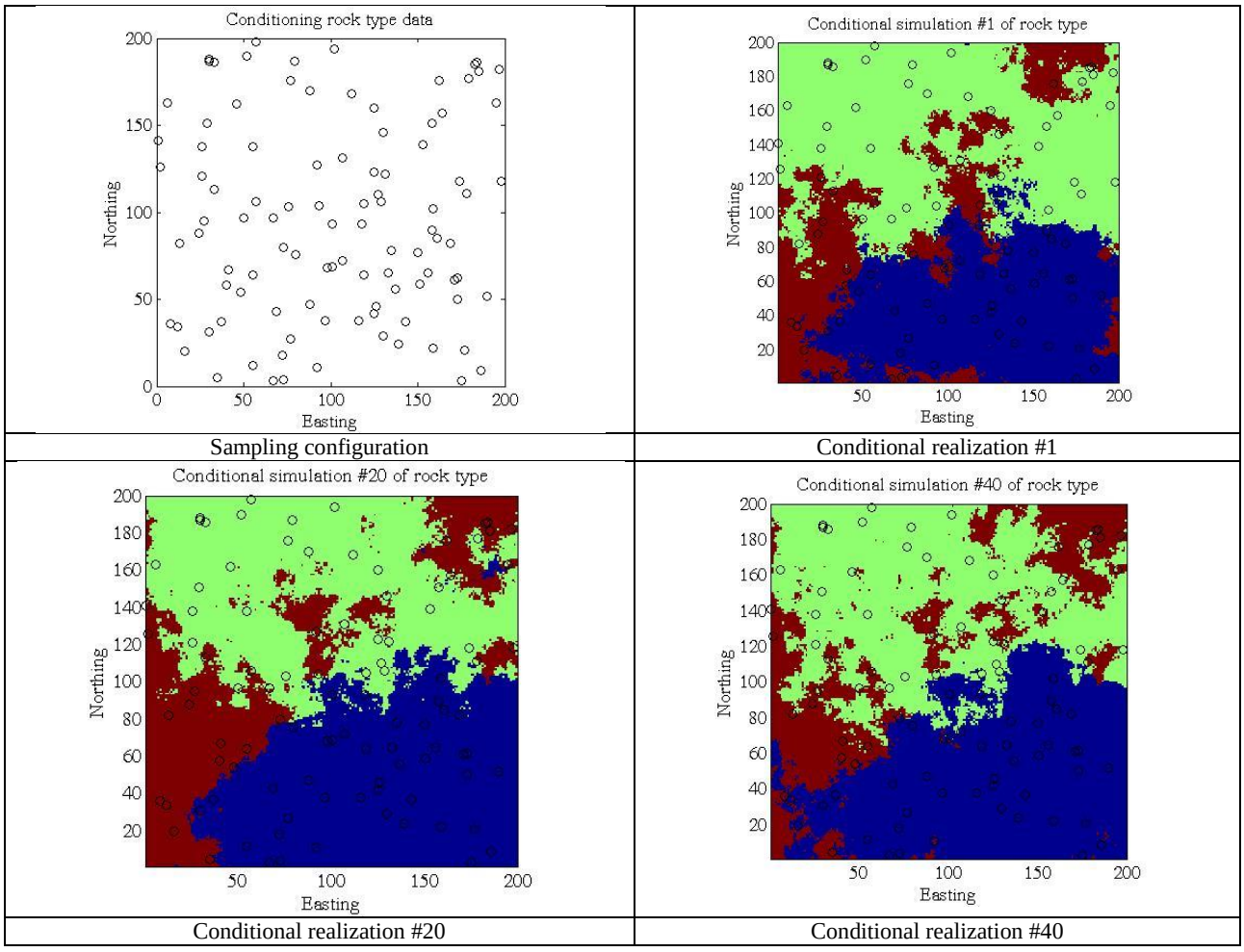

Sampling configuration | Conditional realization #1

Conditional realization #20 | Conditional realization #40

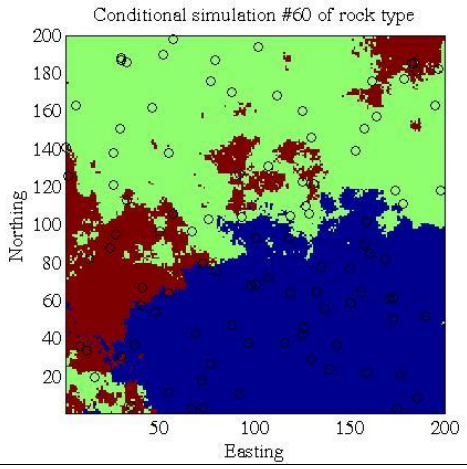

Conditional realization #60

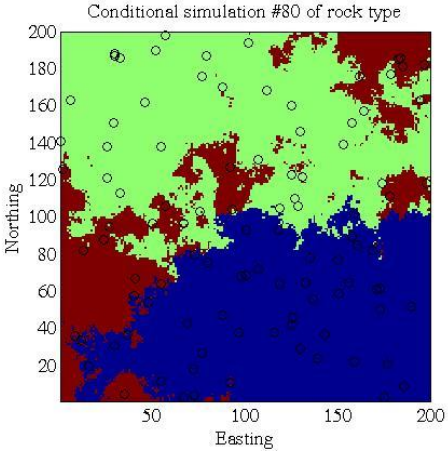

Conditional realization #80

Figure 4.4: Conditioning data locations and examples of conditional realizations (Case 1)

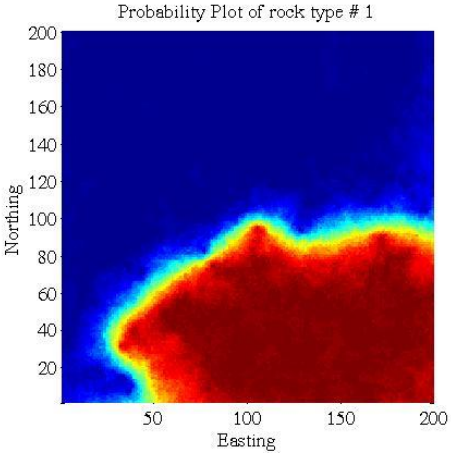

Probability map of category #1

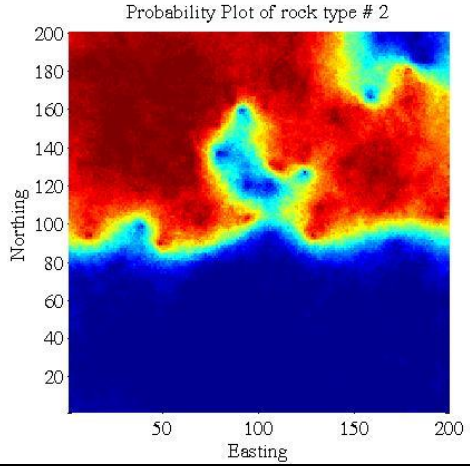

Probability map of category #2

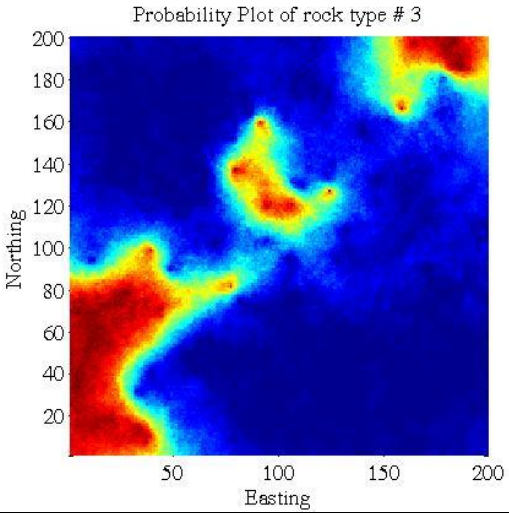

Probability map of category #3

Figure 4.5: Probability maps (Case 1)

3 Case 2: power variograms and truncation rule with three categories

The same exercise is now applied, by changing the linear variogram into a power variogram with exponent 1.5. Because the intrinsic random fields with such a variogram are smoother than that with linear variogram, it is observed that the rock type boundaries are more regular in this case. This is coherent with what is known in the stationary case, in which the behavior of the Gaussian random field variogram near the origin controls the spatial regularity of the domains obtained after truncation (Lantuéjoul, 2002).

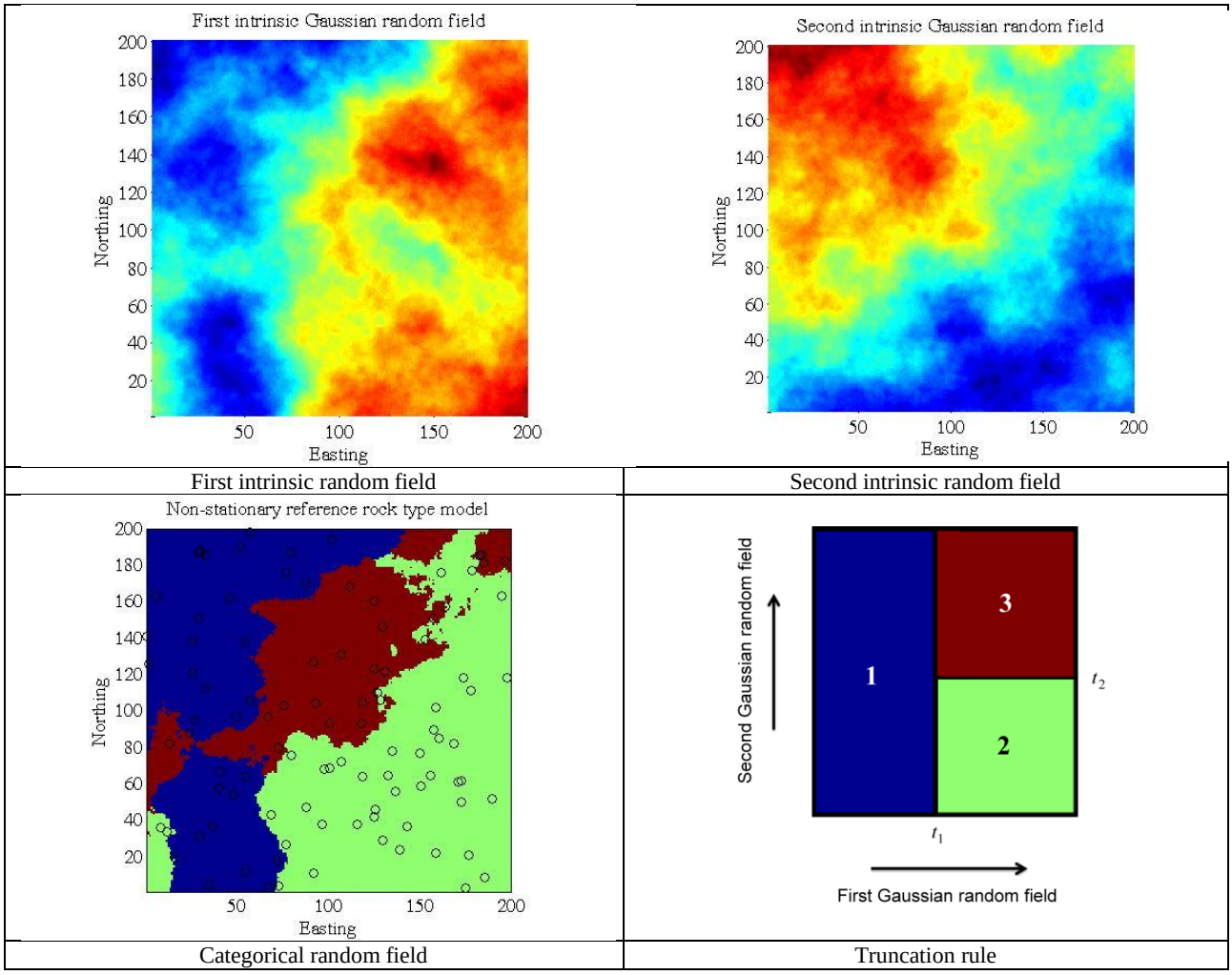

Figure 4.6: Reference model (Case 2)

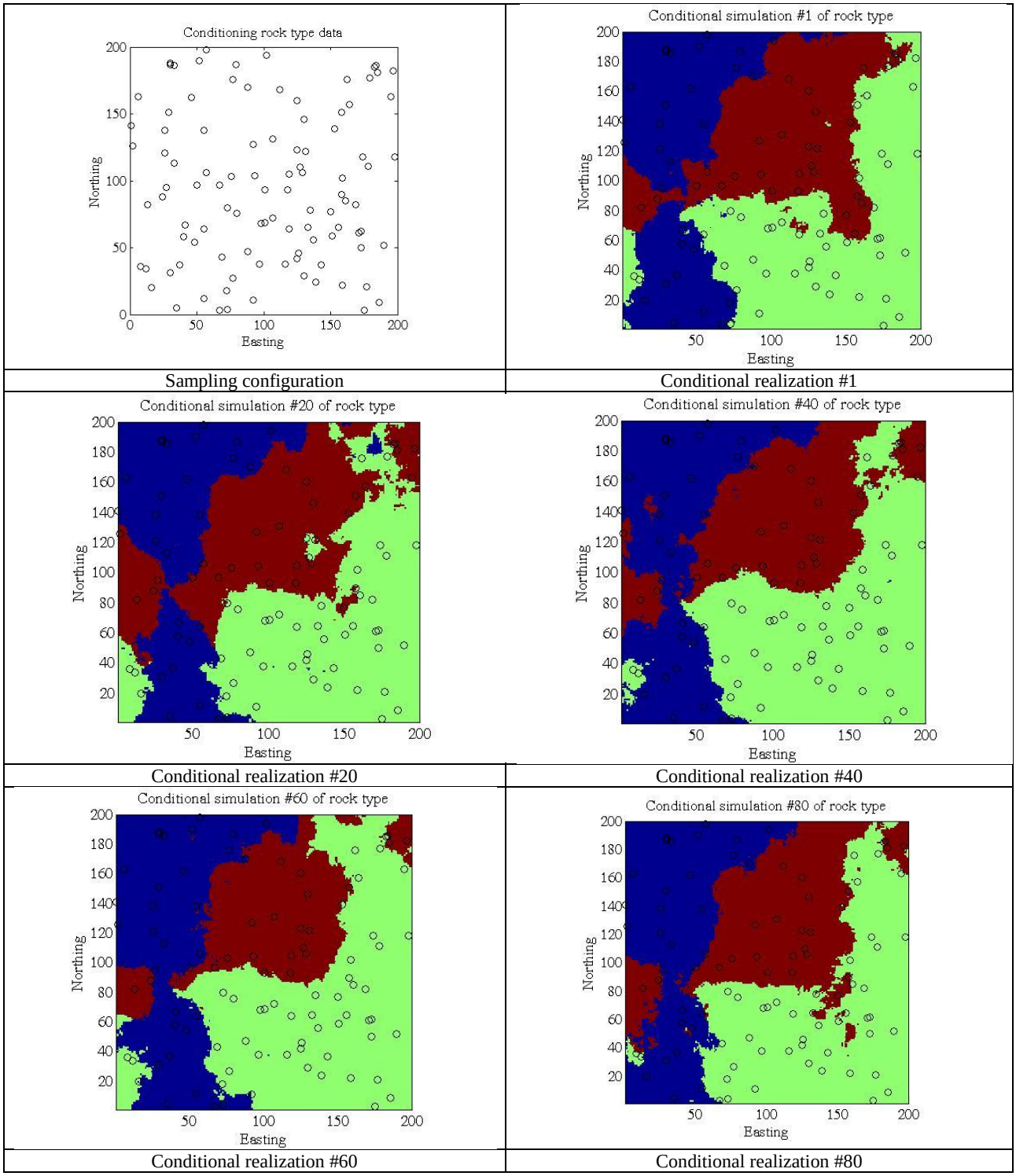

Figure 4.7: Conditioning data locations and examples of conditional realizations (Case 2)

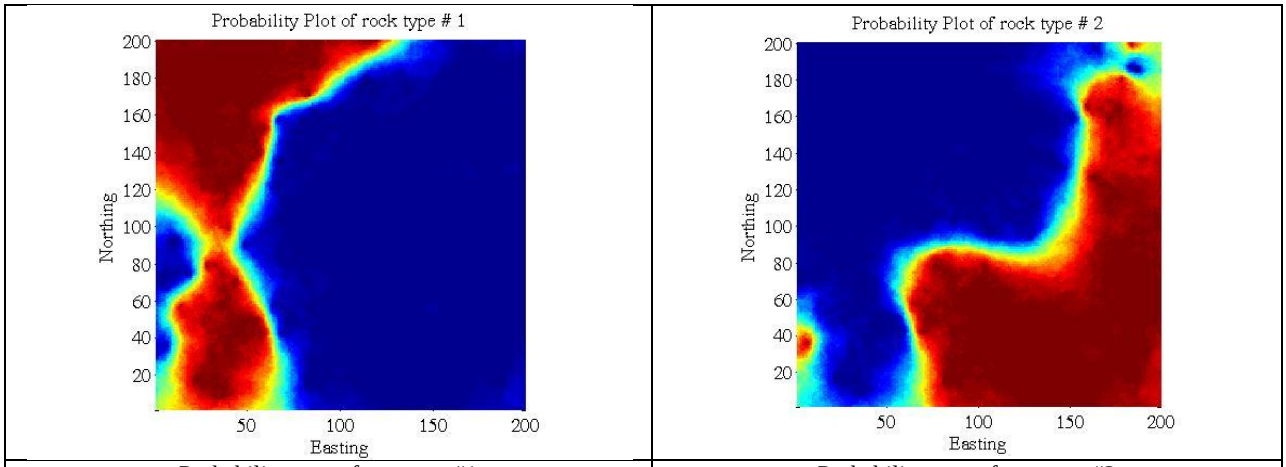

Probability map of category #1

Probability map of category #2

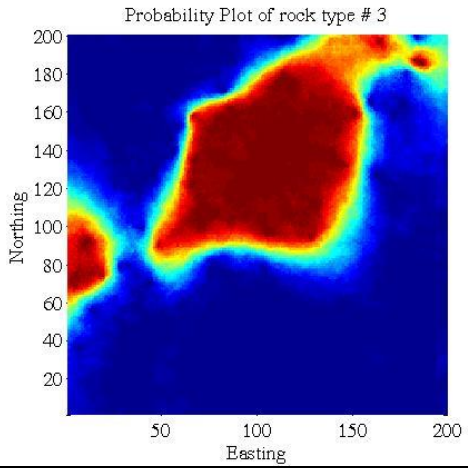

Probability map of category #3

Figure 4.8: Probability maps (Case 2)

4 Case 3: power variograms and truncation rule with six categories

In order to illustrate the versatility of the proposed approach, a third case study is considered, with a more complex truncation rule contemplating six categories. As observed in the following figures, the proposed algorithm is perfectly able to reproduce the conditioning data and the contacts between categories (allowed and forbidden contacts, as indicated in the truncation rule, see Table 4.1).

	Category 1	*Category 2*	*Category 3*	*Category 4*	*Category 5*	*Category 6*
Category 1		allowed	allowed	forbidden	forbidden	forbidden
Category 2	allowed		allowed	allowed	forbidden	allowed
Category 3	allowed	allowed		allowed	allowed	forbidden
Category 4	forbidden	allowed	allowed		allowed	allowed
Category 5	forbidden	forbidden	allowed	allowed		allowed
Category 6	forbidden	allowed	forbidden	allowed	allowed	

Table 4.1: Matrix of contacts between categories

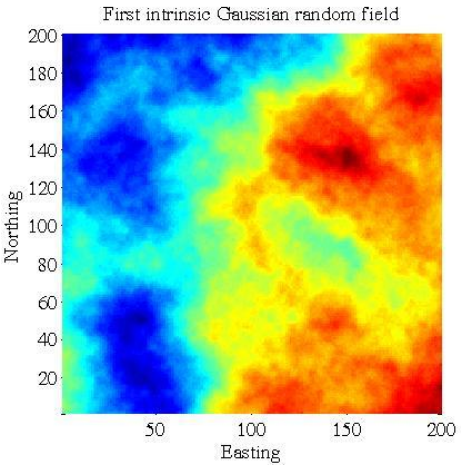

First intrinsic random field

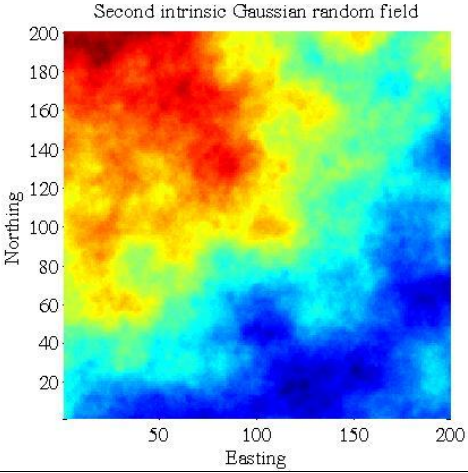

Second intrinsic random field

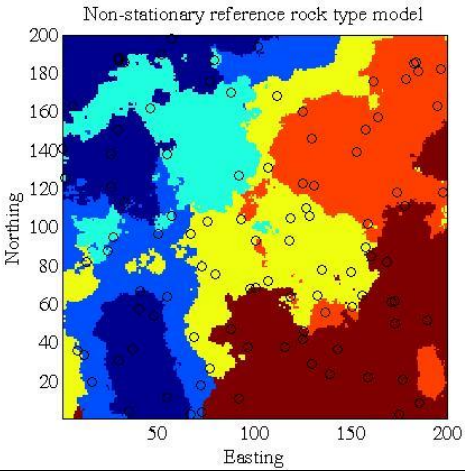

Categorical random field

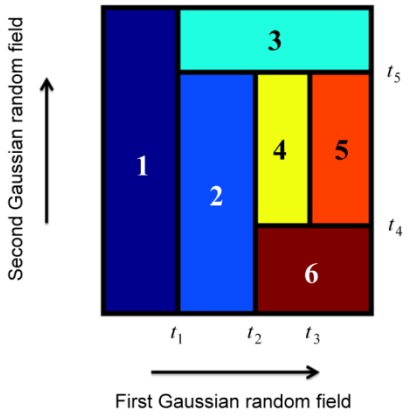

Truncation rule

Figure 4.9: Reference model (Case 3)

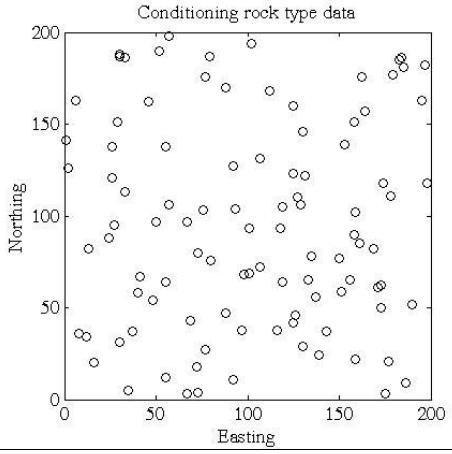

Sampling configuration

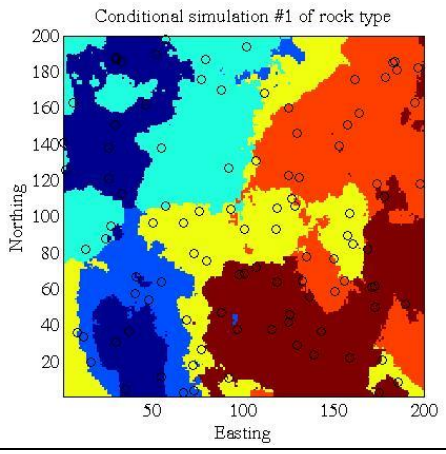

Conditional realization #1

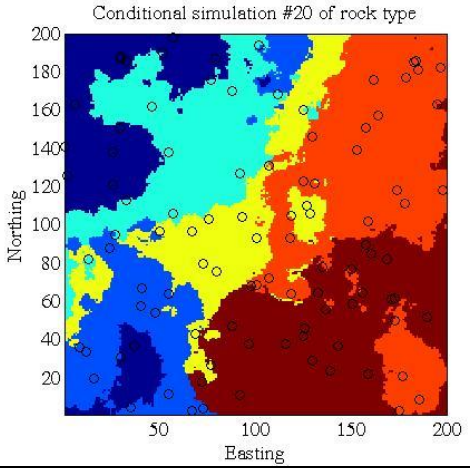

Conditional realization #20

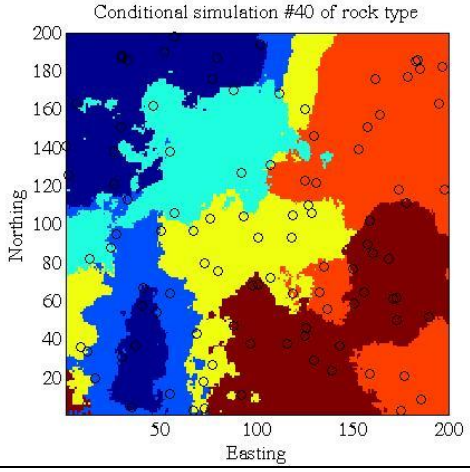

Conditional realization #40

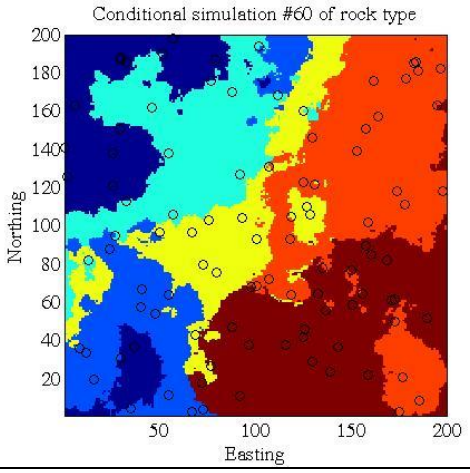

Conditional realization #60

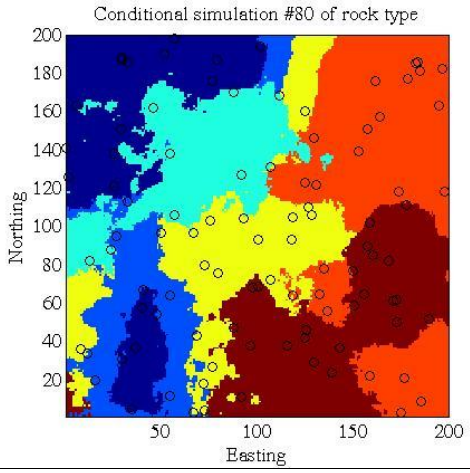

Conditional realization #80

Figure 4.10: Conditioning data locations and examples of conditional realizations (Case 3)

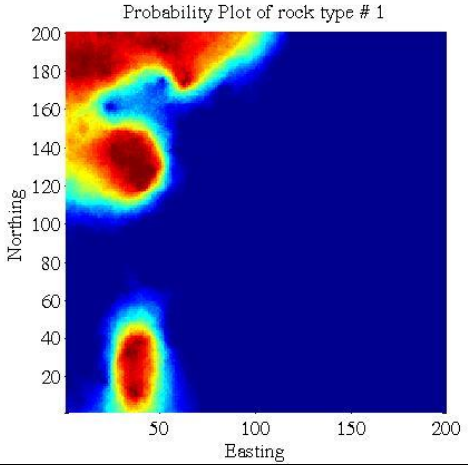

Probability map of category #1

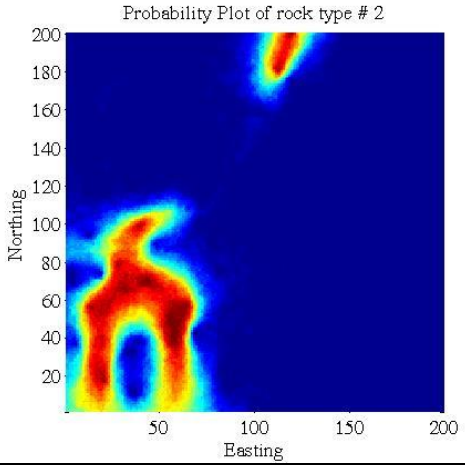

Probability map of category #2

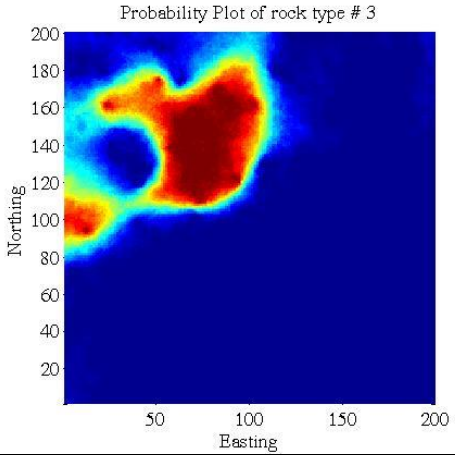

Probability map of category #3

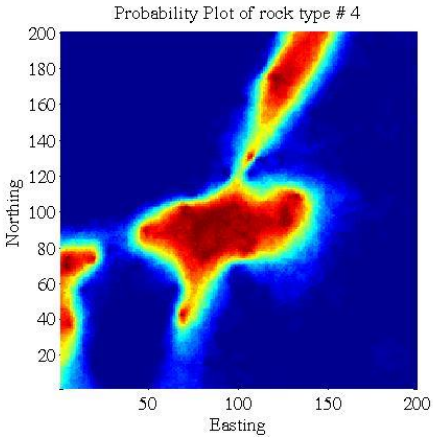

Probability map of category #4

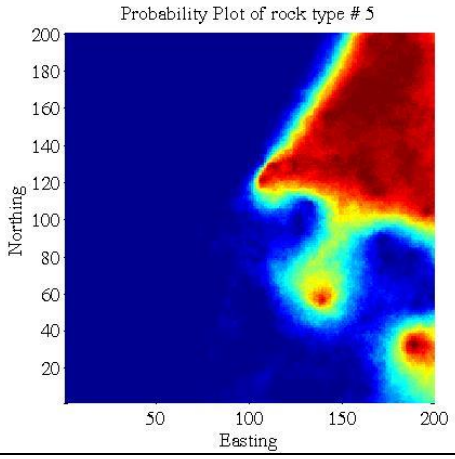

Probability map of category #5

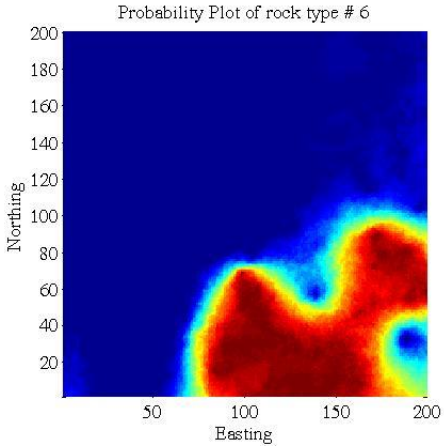

Probability map of category #6

Figure 4.11: Probability maps (Case 3)

5 Sensitivity to the number of conditioning data

The post-processing results are highly sensitive to the number of conditioning data. For instance, let us consider the global proportions of the simulated rock type domains over the region of interest, in Case 1. When 100 data are used, these proportions have a small range of variation when moving from one realization to another (Figure 4.12, left). In contrast, the uncertainty in the proportions considerably increases when only 10 conditioning data are used (Figure 4.12, right).

The uncertainty in the global proportions is higher than what could be obtained in a stationary model because, in the latter, the expected (prior) proportions are fixed by the model parameters (truncation rule and thresholds) and the fluctuations around the expected proportions are bounded since the Gaussian random fields have a finite variance. In contrast, when using intrinsic random fields of order 0, there is no longer any expected proportion, as the intrinsic random fields are defined up to a constant value (so, any domain or category can take any proportion, depending on the realization), and the fluctuations of the intrinsic random fields are potentially infinite since the variograms do not have a finite sill. The proposed model therefore reflects a potentially high uncertainty in the category proportions, bounded only by the presence of the conditioning data.

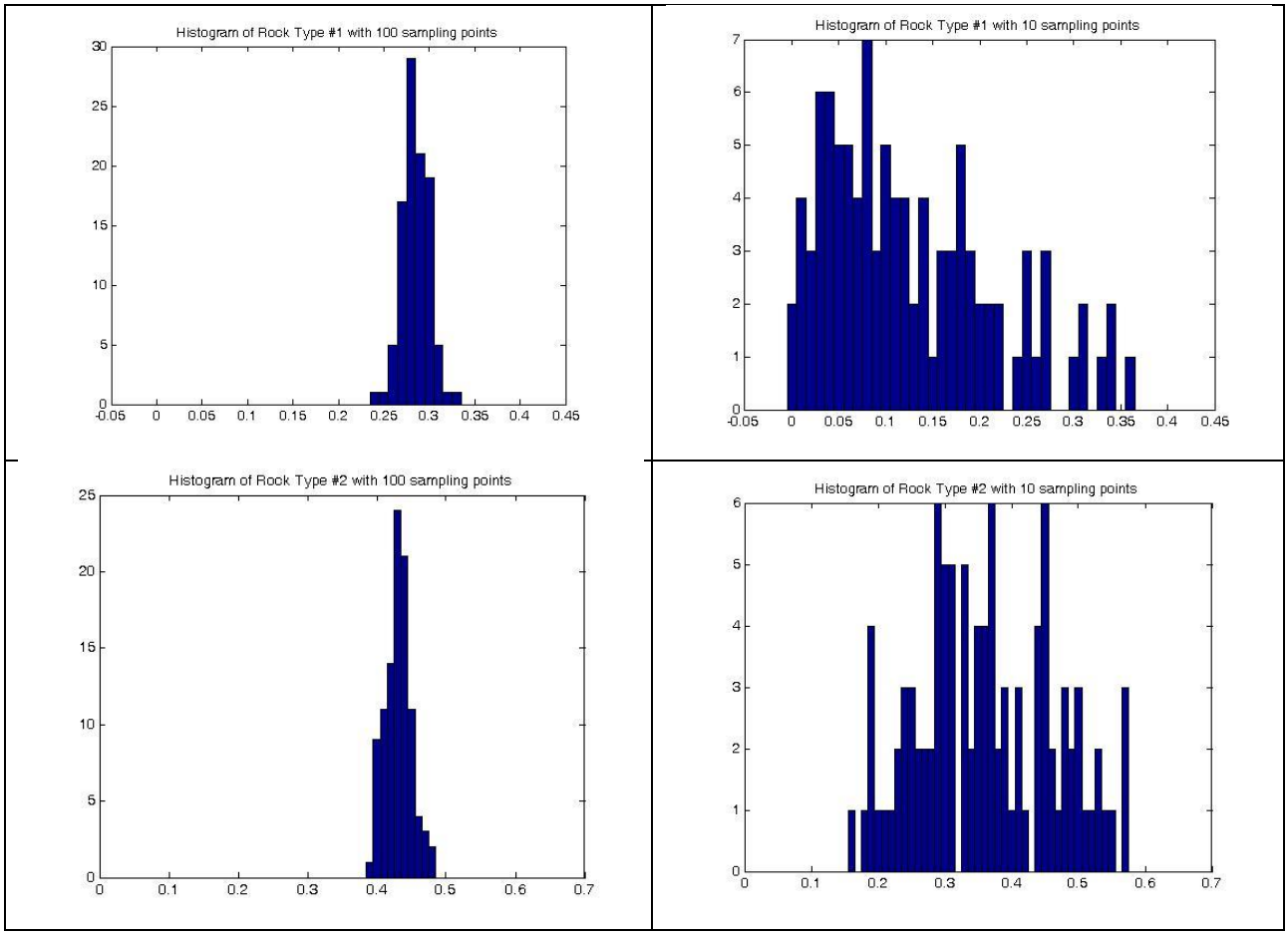

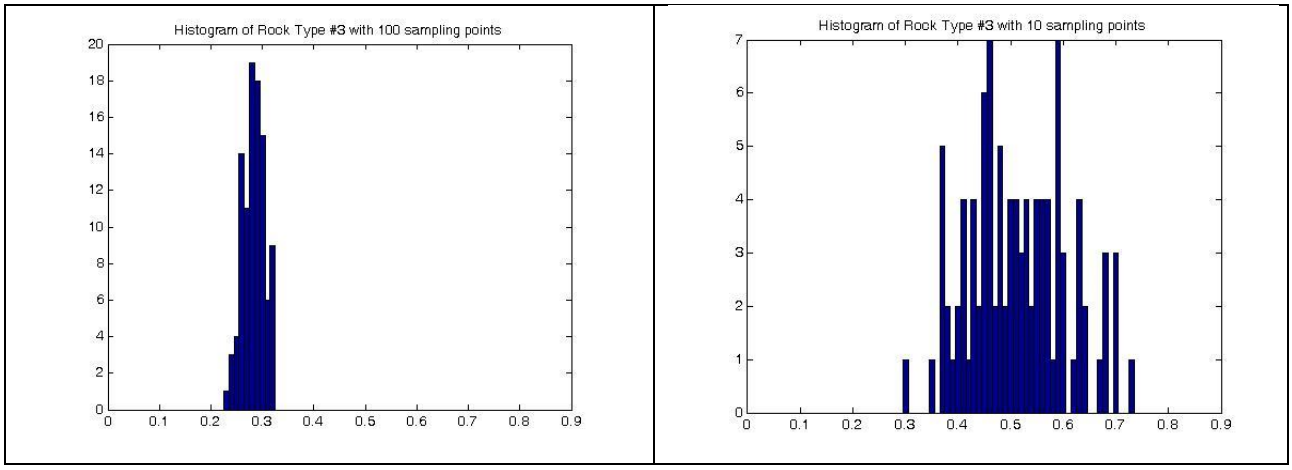

Figure 4.12: Uncertainty in category proportions, depending on the number of conditioning data (100 vs. 10) (Case 1)

6 Model validation

Before concluding, it would be interesting to validate the simulated models beyond the visual inspection of the realizations. To this end, one idea is to check that the realizations reproduce the true spatial continuity. However, because the truncated random fields are not stationary, it is not easy to directly define continuity measures on the simulated category indicators. Instead, it is simpler to check the spatial continuity of the underlying intrinsic random fields of order 0 (before truncation) through their variograms, which is a (linear or power) function of the lag separation vector.

The previous experiments are not perfectly suited to validating the variogram reproduction, as all the realizations are conditioned to the same data set. The variogram of the intrinsic random fields conditioned to some peculiar data set may differ from the prior variogram defined in the model (Emery, 2008b). To avoid distortions due to the conditioning data, a slightly different approach is therefore used for validation purposes:

(1) Generate one hundred realizations of two intrinsic random fields with power variograms.

(2) Truncate the simulated random fields, giving one hundred categorical reference models.

(3) Sample the reference models randomly.

(4) Apply the Gibbs sampler to convert the sampled categorical data into data of IRF-0 with power variograms (one realization per sample).

(5) Apply the spectral-turning bands algorithm to simulate the IRF-0 conditionally to the data obtained in the previous step.

(6) Truncate according to the specified truncation rule.

(7) Check the realizations, by calculating the experimental variograms of the data obtained at Step 4 and of the random fields obtained at Step 5: on average over the 100 realizations, these experimental variograms should coincide, up to small statistical fluctuations, with the prior variograms of the model.

Some examples of realizations are shown in Figure 4.13 for Case 1.

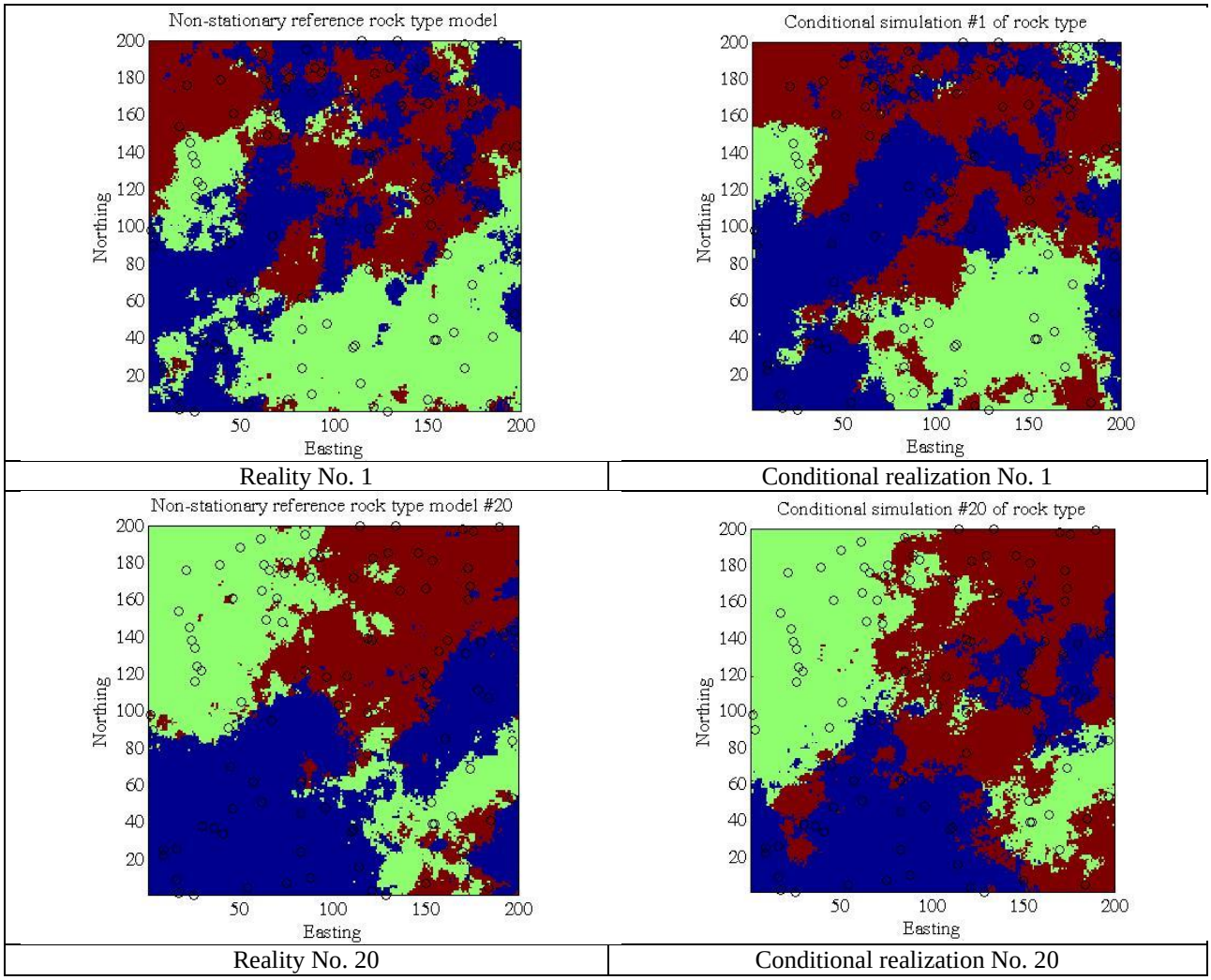

Reality No. 1 | Conditional realization No. 1

Reality No. 20 | Conditional realization No. 20

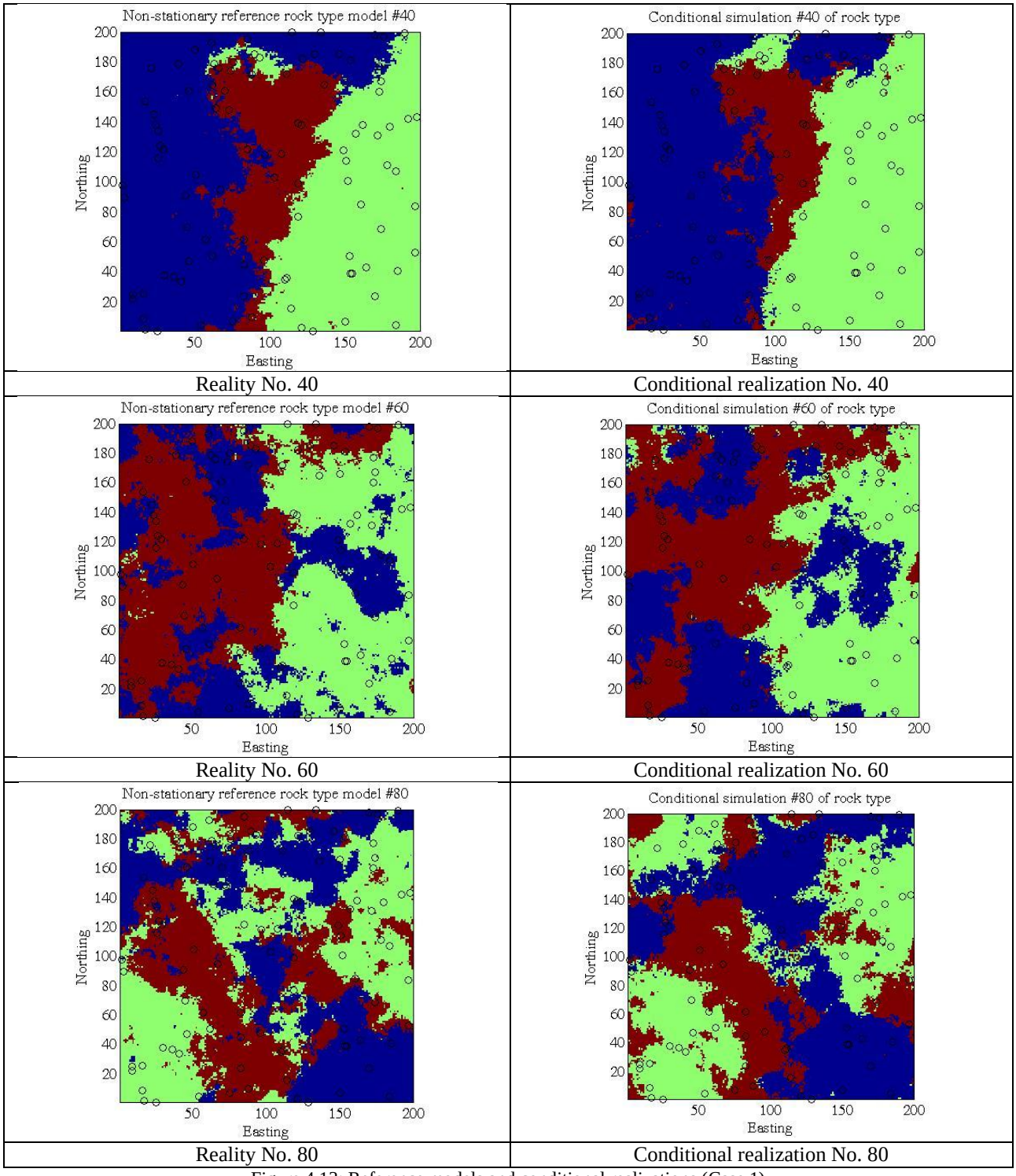

Figure 4.13: Reference models and conditional realizations (Case 1)

The underlying linear variogram (Case 1) is almost perfectly reproduced by the realizations (Figure 4.14): although the experimental variograms of the simulated intrinsic random fields show fluctuations that increase with the lag distance, their average matches the theoretical linear variogram model. The same conclusion prevails for Cases 2 and 3, corresponding to power variograms (Figures 4.15 and 4.16).

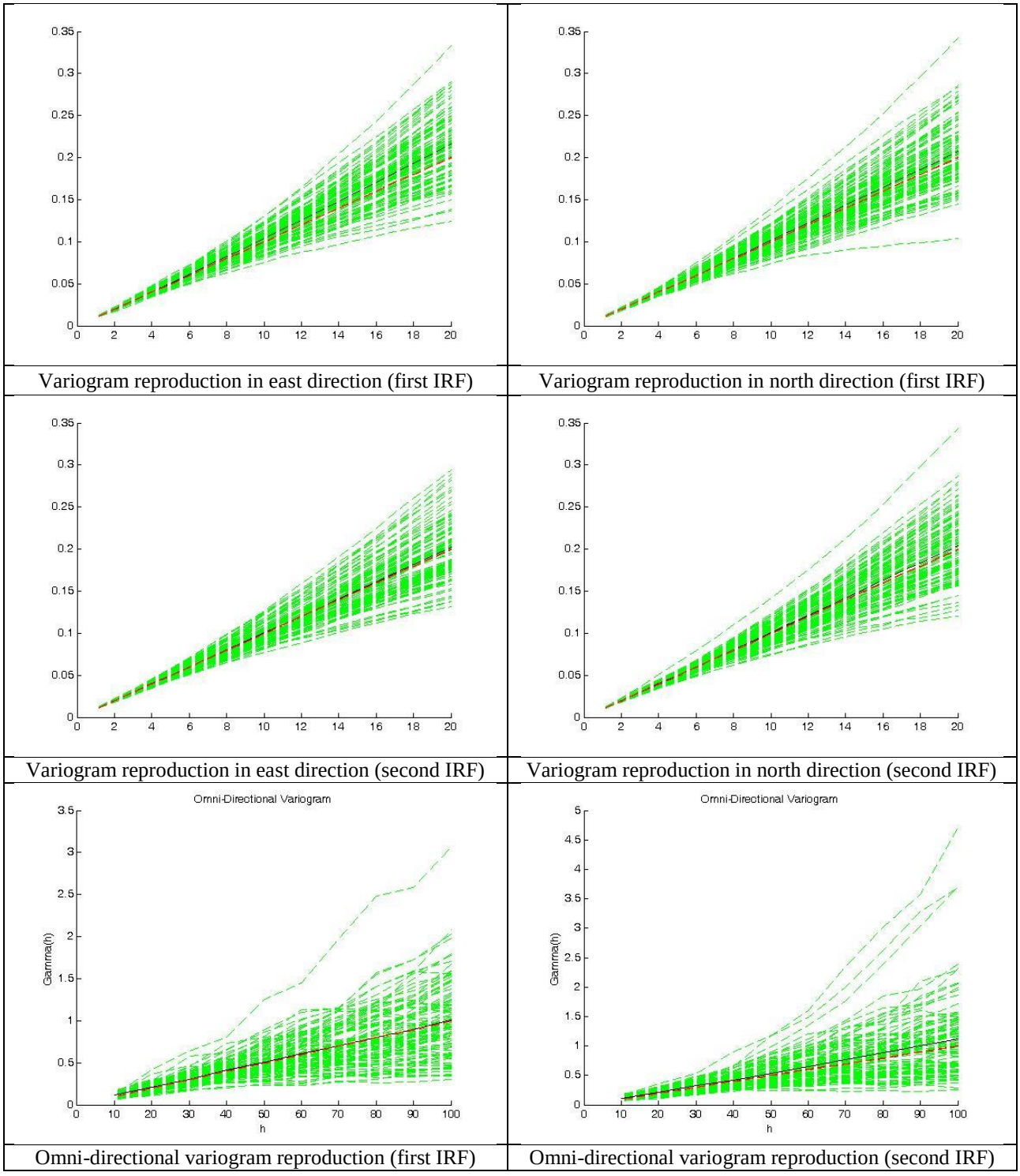

Figure 4.14: Reproduction of variogram for simulated intrinsic random fields (Case 1). Green: experimental variograms calculated for each realization. Red: average of experimental variograms. Black: theoretical variogram model. Top and middle: directional variograms of realizations obtained at Step (5). Bottom: omnidirectional variograms of data obtained at Step (4)

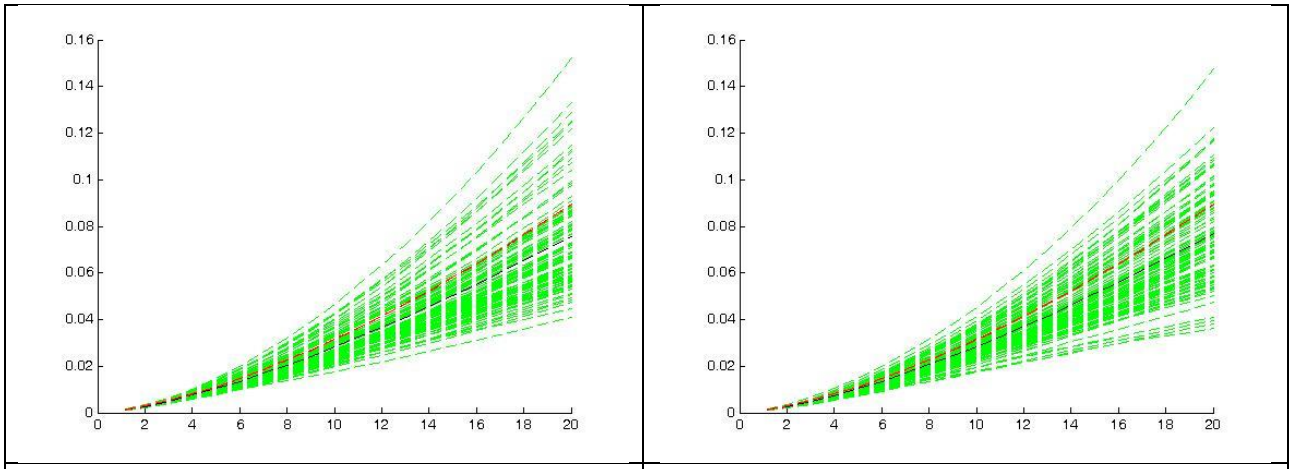

Variogram reproduction in east direction (first IRF) | Variogram reproduction in north direction (first IRF)

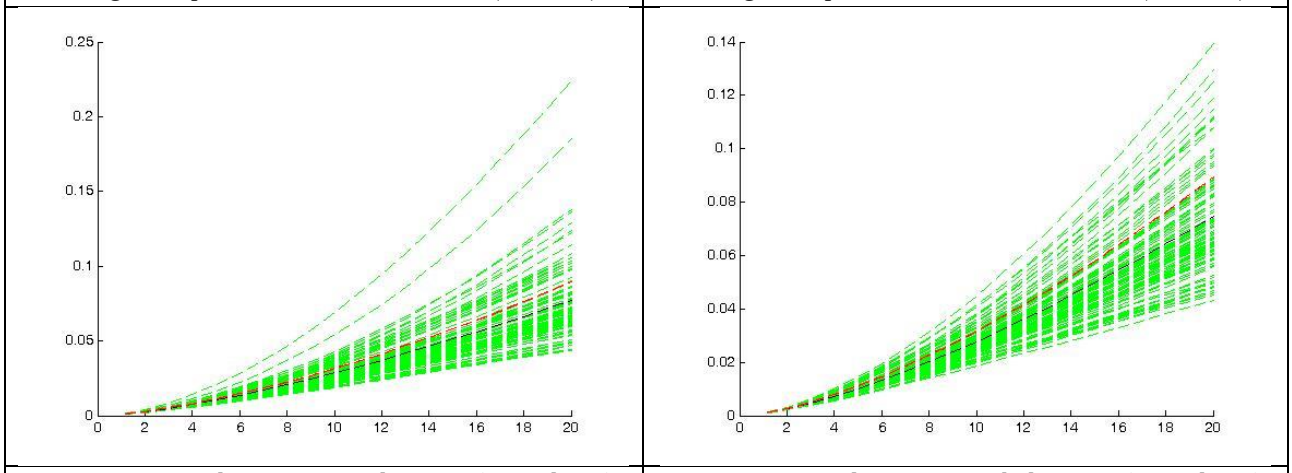

Variogram reproduction in east direction (second IRF) | Variogram reproduction in north direction (second IRF)

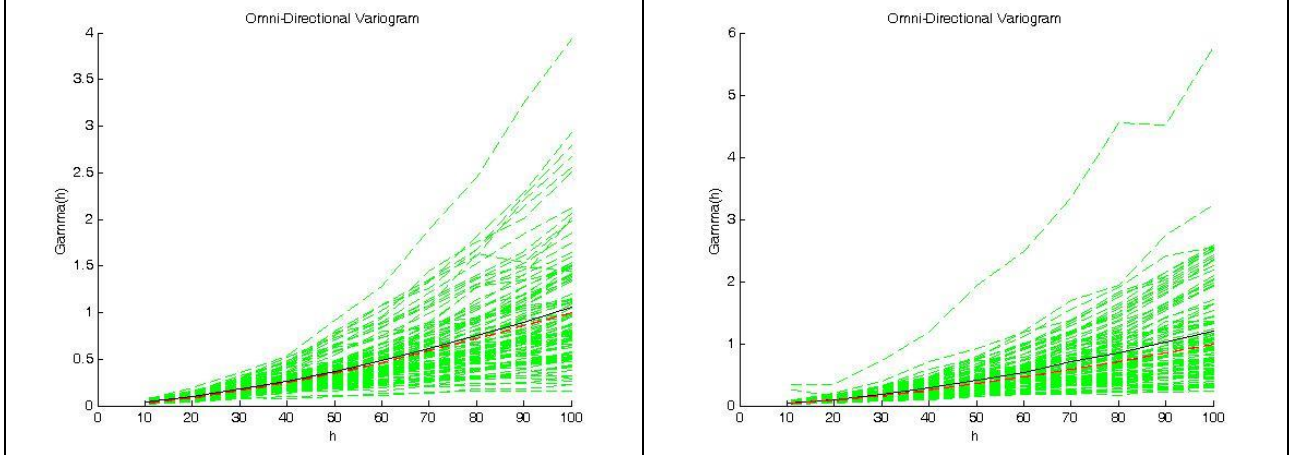

Omni-directional variogram reproduction (first IRF) | Omni-directional variogram reproduction (second IRF)

Figure 4.15: Reproduction of variogram for simulated intrinsic random fields (Case 2). Green: experimental variograms calculated for each realization. Red: average of experimental variograms. Black: theoretical variogram model. Top and middle: directional variograms of realizations obtained at Step (5). Bottom: omnidirectional variograms of data obtained at Step (4)

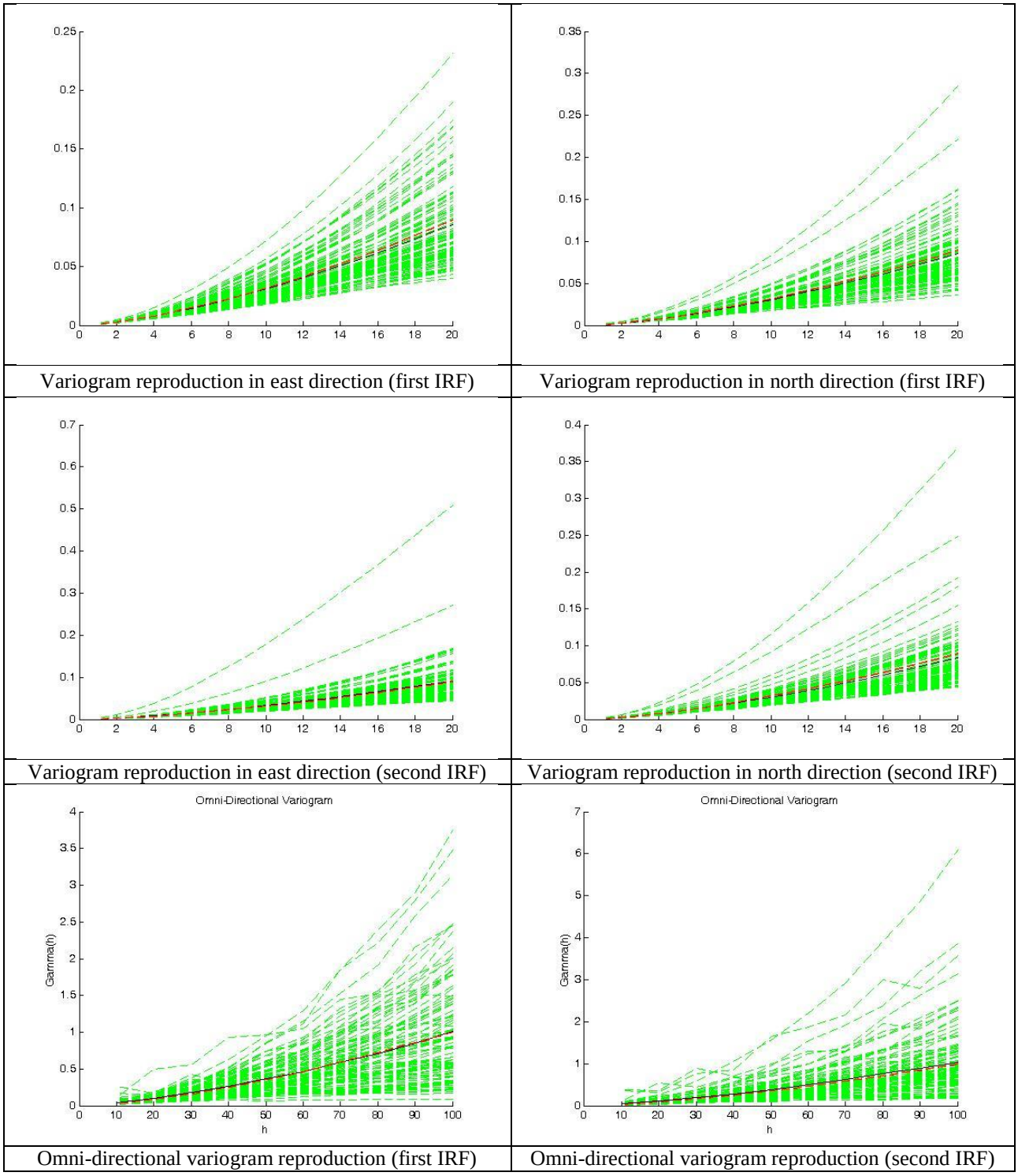

Figure 4.16: Reproduction of variogram for simulated intrinsic random fields (Case 3). Green: experimental variograms calculated for each realization. Red: average of experimental variograms. Black: theoretical variogram model. Top and middle: directional variograms of realizations obtained at Step (5). Bottom: omnidirectional variograms of data obtained at Step (4)

Chapter 5: Real case study: Geological modeling of the Río Blanco – Los Bronces deposit

1 Geological setting

The Río Blanco – Los Bronces ore deposit is a breccia-hosted cogenetic porphyry Cu-Mo deposit located between latitudes 33°07´45" and 33°10´20" in the Central Chilean Andes, about 80 km northeast of Santiago. Los Bronces is emplaced in the western part and is being mined by Anglo American, while the Río Blanco deposit is emplaced in the eastern part, with mineralized bodies (Río Blanco, La Unión, Central, Don Luis, Sur-Sur and La Americana) distributed over an area of six kilometers from north to south and two kilometers from east to west. La Unión, Don Luis and Sur-Sur are mined by Codelco (Andina Division) by open pit and underground operations.

The Río Blanco deposit is partly hosted in the western margin of the San Francisco batholith, a multiphase intrusive containing quartz-diorite, granodiorite, quartz-monzonite, quartz-monzodiorite and granite, and partly in Miocene volcanics of the surrounding Abanico and Farellones formations, which consist of sub-horizontally dipping andesitic lavas (Warnaars et al., 1985; Stambuk et al., 1988).

The earlier alteration phase within the San Francisco batholith is characterized by actinolite ± magnetite ± titanite ± plagioclase disseminations, narrow actinolite ± magnetite veins and magnetite ± clinopyroxene ± actinolite ± plagioclase breccias.

This phase is postdated by an intense potassic alteration of both andesitic lavas and granitoid rocks, centered on the Río Blanco sector and associated with the emplacement of quartz monzonite porphyry intrusions, stockwork veins with biotite ± K feldspar ± quartz ± magnetite ± anhydrite ± sulfides, and multiple mineralized breccias whose matrices are dominated by biotite, tourmaline, quartz, anhydrite and/or specularite with sulfides (chalcopyrite, bornite, molybdenite and minor pyrite).

A second mineralization phase comprises a set of younger, tourmaline rich breccia pipes with varying proportions of quartz, chlorite, sericite, anhydrite, specularite, biotite and sulfides, including chalcopyrite, bornite, molybdenite and minor pyrite. These breccias are dated at between 5.9 and 5.1 Ma and are found to the west of the potassic zone, around the tourmaline-sulfide Donoso breccia, and to the south-east, around the Sur-Sur tourmaline-sulfide-iron oxide breccia.

A detailed geological description of the Río Blanco deposit can be found in the specialized literature (Skewes and Stern, 1995, 1996; Serrano et al., 1996; Kay et al., 1999; Vargas et al., 1999; Kay and Mpodozis, 2001, 2002; Skewes et al., 2003; Frikken, 2003; Frikken et al., 2005; Hollings et al., 2005).

2 Lithology

Seven main rock domains can be recognized within the Río Blanco deposit. These are, from the oldest to the youngest, the following (Table 5.1).

(1) Andesite (AND). The andesite domain consists of volcanic rocks (mainly basaltic andesite, traquiandesite and dacite) of the Abanico and Farellones formations, from late Cretaceous to Oligocene for the Abanico Formation and Miocene for the Farellones Formation. These rocks are affected by quartz-sericitic alteration, biotitization and partial chloritization (Stambuk et al., 1988).

(2) Granitoids (GD). The San Francisco Batholith embraces different types of granitoids, the main ones being the Río Blanco granodiorite in the northern sector, characterized by a coarser grain size and the presence of orthoclase feldspar and plagioclase, and the cascade granodiorite in the southern sector, characterized by a finer grain size and enriched in oligoclase-andesine. Both granitoids mainly correspond to granodiorite, quartz-monzonite, tonalite and diorite (Stambuk et al., 1988; Frikken, 2003).

(3) Tourmaline Breccia (TOB). This rock domain is mainly hosted in granitoids. It outcrops in the Sur-Sur sector over 5 km long striking N10°W to N30°W and presents sharp and steeply dipping contacts with the host rock (Serrano et al., 1996). The matrix is a kind of milled rock flour replaced by secondary tourmaline cement containing specular hematite, sulfide, quartz, magnetite, sulfate (anhydrite, gypsum) and biotite, with open spaces filled by tourmaline-quartz-sulfide. For lower tourmaline contents, the clasts are angular to sub-angular, while they become more rounded for higher tourmaline contents.

(4) Monolithic Breccia (MOB). This rock domain is present in the western sector of Río Blanco and has low copper contents. It was formed after the tourmaline breccia (Frikken, 2003) and is characterized by a chloritic alteration, which appears in both the clasts and the matrix, with a varying intensity (Vargas et al., 1999).

(5) Magmatic Breccia (MAB). This rock domain is characterized by crystalline igneous cement. A heterogeneous brecciation resulted in variable proportions of rock flour matrix and clasts. The clasts are different in size, from 2 mm to more than 5 m wide, and are altered with primary igneous minerals replaced by secondary biotite, magnetite, sulfides and K-feldspar. The matrix is partly substituted for hydrothermal minerals such as biotite, sulfates, quartz, sulfides, magnetite, specularite and tourmaline.

(6) Porphyry (POR). The porphyry domain intruded the magmatic and tourmaline breccias and consists of three main rock types (Serrano et al., 1996): the Don Luis Porphyry, located in the center of the deposit and bounded by the magmatic breccia (this porphyry predominates in the region that will be considered in the next sections); the Quartz Monzonite Porphyry, which cross-cuts the magmatic breccia; and the Feldspar Porphyry, less abundant and presenting a clear-cut contact with the magmatic breccia. These porphyries contain quartz, plagioclase, K-feldspar and biotite phenocrystals.

(7) Pipe (PIP). This domain is composed of two main rock types (Serrano et al., 1996): the Dacitic Pipe, which forms an inverted cone limited by the magmatic breccia, containing

phenocrystals of quartz and plagioclase with minor biotite in a quartz-feldspar matrix; and the Rhyolitic Pipe, which corresponds to the final intrusion in the mineralized sectors, characterized by numerous felsic intrusions.

Code	Rock Domain	Rock Types	Abbreviation	Age
7	Andesite	Andesite	AND	Late Cretaceous to Early Pliocene
6	Granitoids	Río Blanco granodiorite Cascade granodiorite Breccia cascade granodiorite Diorite Granodiorite	GD	Early Pliocene
5	Tourmaline breccia	Andesite tourmaline Río Blanco granodiorite tourmaline Cascade granodiorite tourmaline Tourmaline breccia Tourmaline breccia with andesite Tourmaline breccia with cascade granodiorite Tourmaline breccia with Río Blanco tourmaline Tourmaline breccia with porphyry Tourmaline breccia with abundant tourmaline Quartz sericitic breccia Tourmaline breccia with granodiorite	TOB	Early Pliocene
4	Monolithic Breccia	Breccia porphyry Magmatic breccia of granodiorite Molybdenite breccia Monolithic breccia Tourmaline monolithic breccia Castellana breccia Don Luis porphyry breccia Quartz breccia with Don Luis porphyry Tourmaline breccia of Don Luis porphyry Biotite metasomatic rocks Igneous breccia	MOB	Early Pliocene
3	Magmatic Breccia	Río Blanco granodiorite breccia Anhydrite breccia Hematite breccia Quartz anhydrite breccia	MAB	Late Miocene
2	Porphyry	Quartz monzonite porphyry Feldespathic porphyry Monzonite porphyry Don Luis Porphyry	POR	Middle Miocene
1	Pipe	Dacite contact breccia Rhyolitic pipe Dacitic pipe Rhyolite contact breccia	PIP	Early Miocene

Table 5.1. Main rock domains in the Río Blanco deposit

3 Data and region of interest

In the sequel, we will focus on the northern sector of the Río Blanco deposit, for which two types of data are available: exploration drill holes and an interpreted lithological model. The drill holes are in an irregular design along the northwest-southeast direction; the data consist of information on the prevailing rock types logged at 12,006 drill hole cores and codified into the previously defined rock domains (Table 5.1). As for the lithological model, it consists of a discretization of the sector into blocks with a support of 15 m × 15 m × 16 m, for which the (assumed) prevailing rock domain is assigned to each block. Such a block model has been constructed on the basis of the available drill hole data and of the interpretation of the geological processes, emplacements and alterations.

In the following, to reduce the computation time and to ease visualization, we are interested in simulating the rock domains on a limited region of the interpreted lithological model, consisting of a grid that extends between coordinates 23,237 and 24,242 along the east-west direction, coordinates 25,868 and 27,728 along the north-south direction, and coordinates 3332 and 3348 along the vertical. This grid covers an area of 1.87 km^2 and contains 17,000 nodes with a regular spacing of 15 m × 15 m × 16 m. The number of available drill hole data in this region reduces to 125 (Figure 5.1).

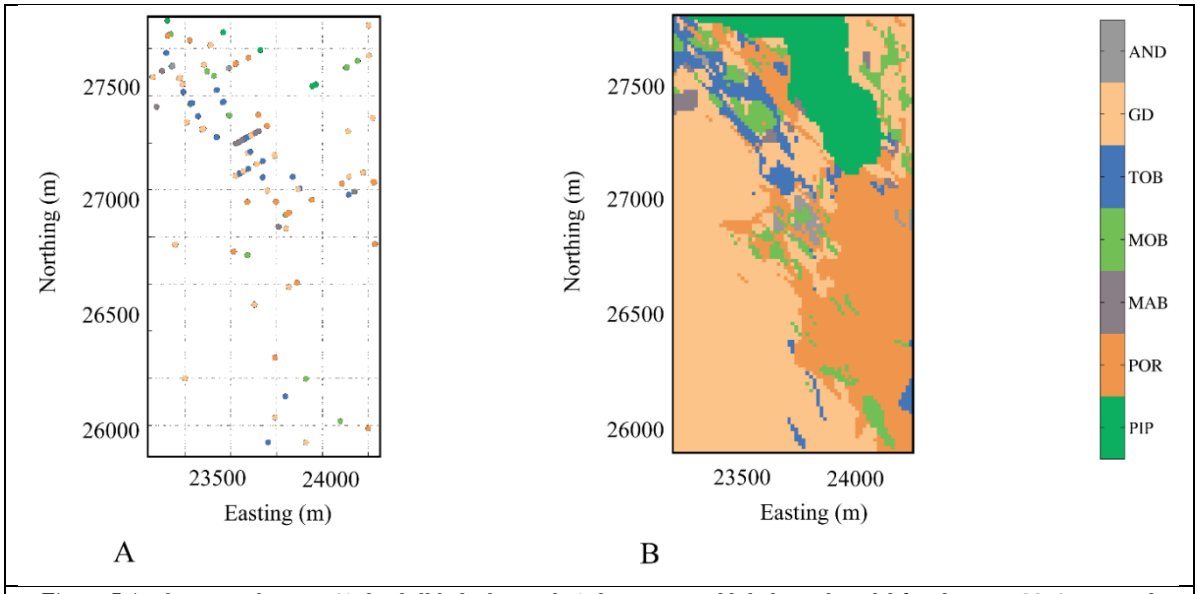

Figure 5.1: Plan view showing A) the drill hole data and B) the interpreted lithological model for elevation 3348 m a.m.s.l

4 Exploratory Data Analysis

In order to present an overview about the exploratory data analysis, it is of interest to consider the proportions of rock domains calculated from the interpreted lithological model and from the 125 drill hole data, before and after declustering (Table 5.2). The declustered proportions are obtained by interpolating the region of interest with the nearest neighbor technique, i.e., by assigning to each grid node the rock domain observed on the closest drill hole data.

Andesite (AND) has the smallest proportion, while granitoids (GD) have the highest proportion in the region in all the three alternatives. The declustered proportions calculated with the drill holes are more in agreement with the proportions calculated on the interpreted lithological model. For instance, the porphyry has a small proportion in the drill holes, however this proportion rises significantly when considering declustering or when using the interpreted lithological model.

Rock domain	Proportion in drill holes data (%)	Declustered proportions in drill hole data (%)	Proportions in interpreted lithological model (%)
PIP	4.8	7.2	10.5
POR	16.8	24.3	26.2
MAB	11.2	3.4	1.2
MOB	11.2	11.9	6.6
TOB	20.0	9.4	5.4
GD	32.8	42.6	49.1
AND	3.2	1.2	1.1

Table 5.2: Estimated proportions of rock domains

The interpreted lithological model suggests that each rock domain may be in contact with each other. Possible forbidden contacts from a geological point of view are somehow ignored. Most of the contacts appear between GD and POR, especially in the central and southern parts of the region under study. Towards to north, PIP is showing contact with POR and GD.

A trend analysis on the declustered drill hole proportions has been implemented to understand the variability of the rock domains along the north-south and east-west directions (Figure 5.2). The most important characteristics obtained from this trend analysis are the following:

(1) PIP: in the east direction, its proportion increases up to coordinate 23,400, then strongly decreases. In the north direction, there is no sign of existing PIP until coordinate 27,250.

(2) POR: from west to east, there is a mild increase in the proportion of porphyry, while in the north direction, it increases up to coordinate 26,800 and decreases afterwards.

(3) MAB: one cannot distinguish any clear trend in this rock domain, yet, there is a very mild tendency to decrease its proportion from west to east.

(4) MOB: from west to east there is an increase of the proportion of this rock domain, but in the north, no trend is distinguishable.

(5) TOB: from west to east, there is an increase up to coordinate 23,500 and a decrease afterwards. In the north direction, it is difficult to interpret a trend.

(6) GD: this rock domain shows a steady decrease in its proportion from west to east, while in the north, this decrease is milder.

(7) AND: due to the low proportion of this rock domain in the region of interest, detecting a trend is somehow unreliable.

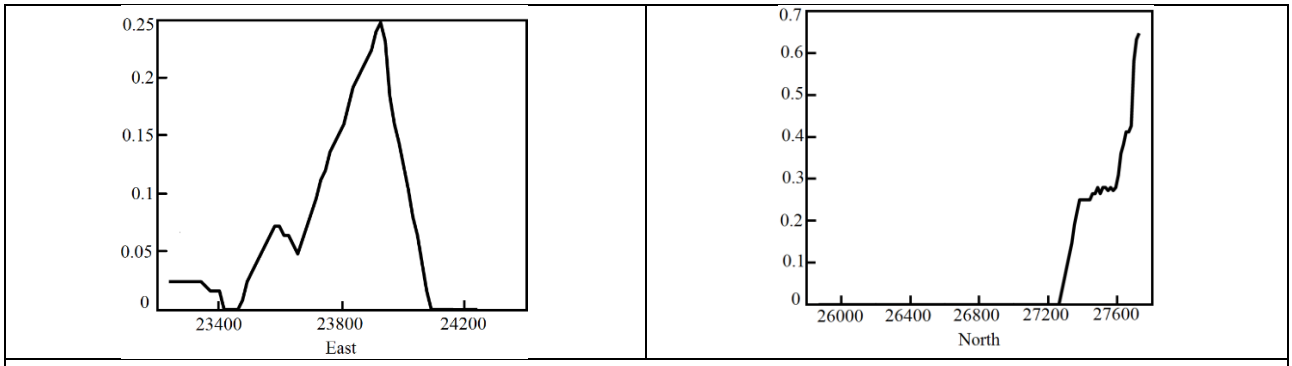

A) PIP

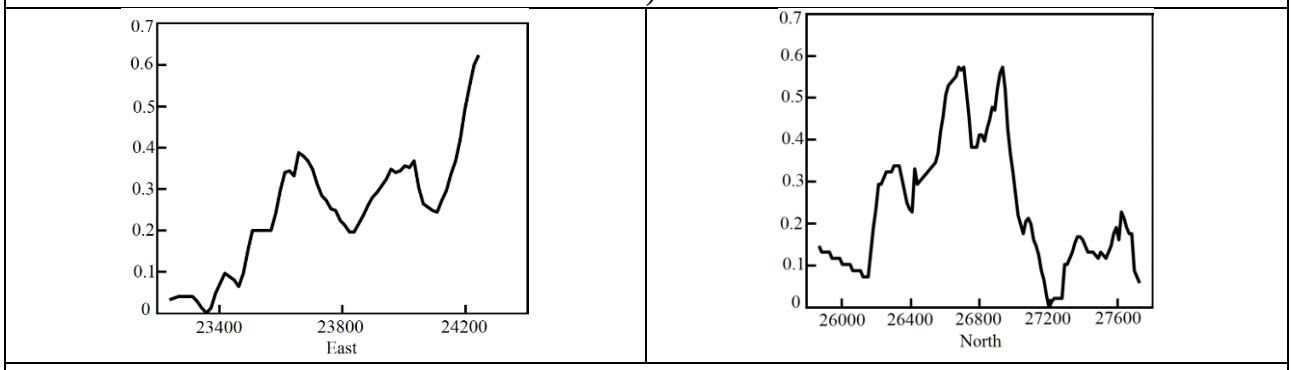

B) POR

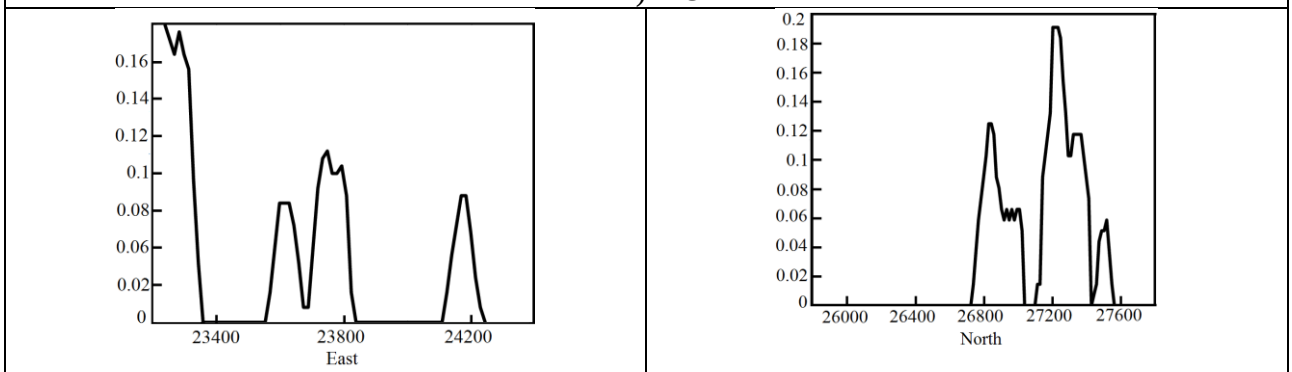

C) MAB

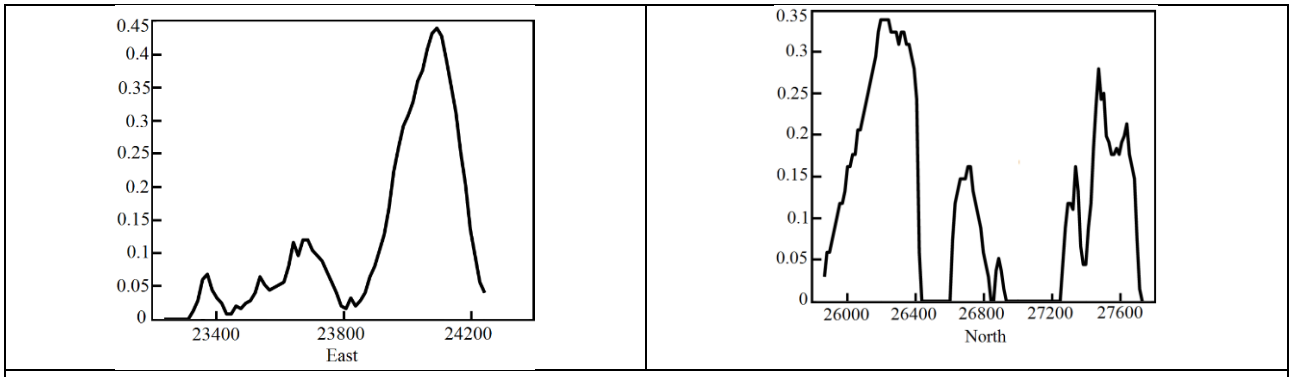

D) MOB

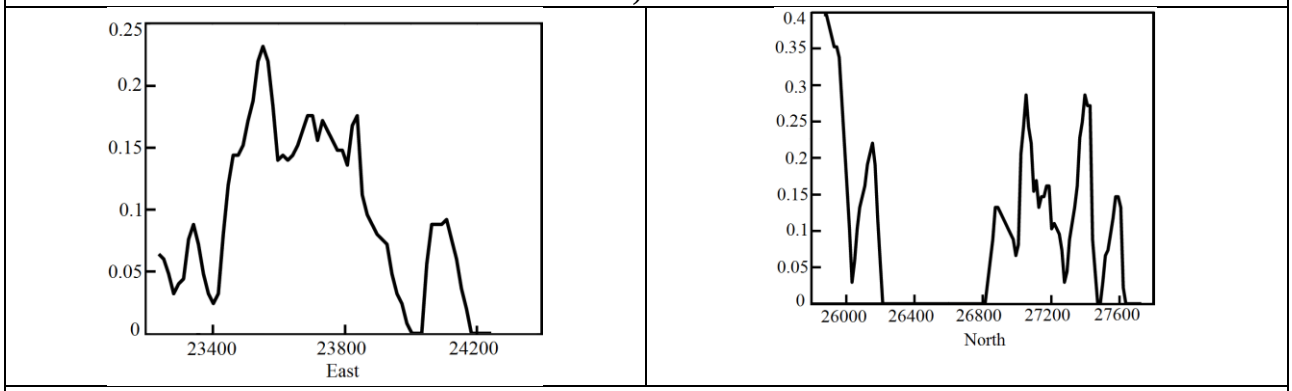

E) TOB

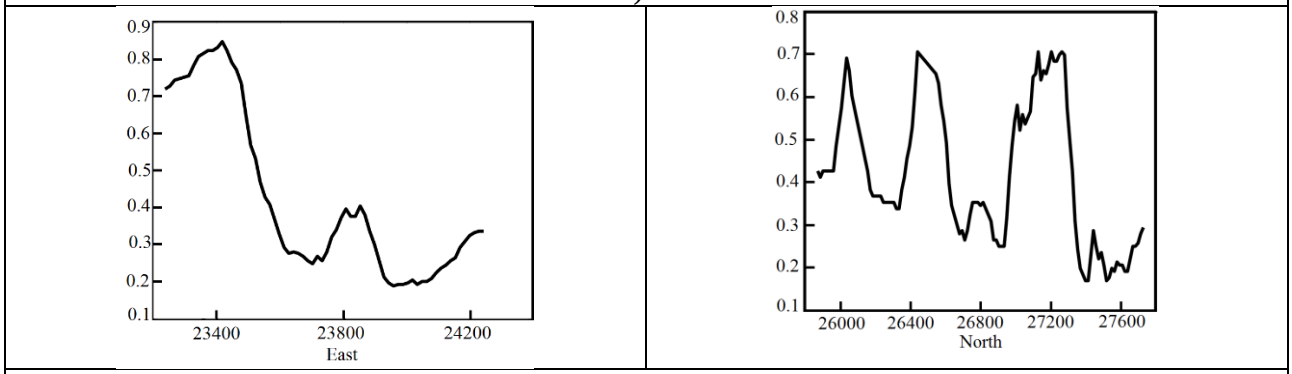

F) GD

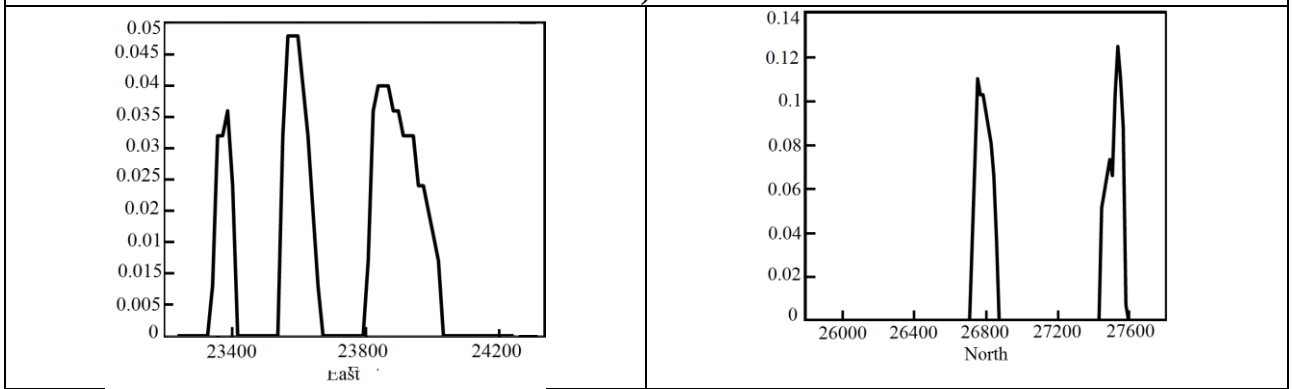

G) AND

Figure 5.2: Proportions of rock domains (ordinate axis) along the east-west and north-south directions (abscissa axis)

5 Stationary plurigaussian model

In this section, two plurigaussian models will be elaborated. The first one (case I) relies on the proportions of rock domains calculated from the interpreted lithological model, while the second one (case II) relies on the declustered proportions calculated from the 125 drill hole data. In each case, the proportions are assumed to be constant in space and perfectly known, which are the assumptions underlying stationary models.

5.1 Definition of the truncation rule

In order to be consistent with the chronology of the rock domains, as per Table 5.1, a hierarchical approach is proposed, as explained in Section 1.3.1 of Chapter 3, based on six Gaussian random fields $\{Z_1, Z_2, Z_3, Z_4, Z_5, Z_6\}$ and six truncation thresholds $\{t_1, t_2, t_3, t_4, t_5, t_6\}$ (Eq. 3.5):

$$\text{Rock domain at location } \mathbf{x} = \begin{cases} 1 \text{ if } Z_1(\mathbf{x}) \le t_1 \\ 2 \text{ if } Z_1(\mathbf{x}) > t_1 \text{ and } Z_2(\mathbf{x}) \le t_2 \\ 3 \text{ if } Z_1(\mathbf{x}) > t_1, Z_2(\mathbf{x}) > t_2 \text{ and } Z_3(\mathbf{x}) \le t_3 \\ 4 \text{ if } Z_1(\mathbf{x}) > t_1, Z_2(\mathbf{x}) > t_2, Z_3(\mathbf{x}) > t_3 \text{ and } Z_4(\mathbf{x}) \le t_4 \\ 5 \text{ if } Z_1(\mathbf{x}) > t_1, Z_2(\mathbf{x}) > t_2, Z_3(\mathbf{x}) > t_3, Z_4(\mathbf{x}) > t_4 \text{ and } Z_5(\mathbf{x}) \le t_5 \\ 6 \text{ if } Z_1(\mathbf{x}) > t_1, Z_2(\mathbf{x}) > t_2, Z_3(\mathbf{x}) > t_3, Z_4(\mathbf{x}) > t_4, Z_5(\mathbf{x}) > t_5 \text{ and } Z_6(\mathbf{x}) \le t_6 \\ 7 \text{ if } Z_1(\mathbf{x}) > t_1, Z_2(\mathbf{x}) > t_2, Z_3(\mathbf{x}) > t_3, Z_4(\mathbf{x}) > t_4, Z_5(\mathbf{x}) > t_5 \text{ and } Z_6(\mathbf{x}) > t_6 \end{cases} \tag{5.1}$$

Such a truncation rule agrees with chronology: rock domain #1 (PIP) appears as the youngest and rock domain #7 (AND) as the oldest. A younger rock domain is likely to cross-cut older ones. At each data location, the information on the prevailing rock domain can be codified into binary indicators, with one indicator associated with each Gaussian random field (Table 5.3). The value of an indicator is 1 when the Gaussian random field is less than the associated threshold, 0 when it is greater than the threshold, or unknown when the Gaussian random field is not involved in the definition of the rock domain.

Rock domain	Rock code	$Z_1 < t_1$?	$Z_2 < t_2$?	$Z_3 < t_3$?	$Z_4 < t_4$?	$Z_5 < t_5$?	$Z_6 < t_6$?
PIP	1	1	unknown	unknown	unknown	unknown	unknown
POR	2	0	1	unknown	unknown	unknown	unknown
MAB	3	0	0	1	unknown	unknown	unknown
MOB	4	0	0	0	1	unknown	unknown
TOB	5	0	0	0	0	1	unknown
GD	6	0	0	0	0	0	1
AND	7	0	0	0	0	0	0

Table 5.3: Codification of rock domains into indicators

5.2 Definition of the truncation thresholds

Accounting for the hierarchical nature of the model, the truncation thresholds $\{t_1, t_2, t_3, t_4, t_5, t_6\}$ are related to the proportions $\{p_1, p_2, p_3, p_4, p_5, p_6, p_7\}$ of the rock domains in the following fashion:

$$
\begin{aligned}
p_1 &= G^{-1}(t_1) \\
p_2 &= [1-G^{-1}(t_1)]G^{-1}(t_2) \\
p_3 &= [1-G^{-1}(t_1)][1-G^{-1}(t_2)]G^{-1}(t_3) \\
p_4 &= [1-G^{-1}(t_1)][1-G^{-1}(t_2)][1-G^{-1}(t_3)]G^{-1}(t_4) \\
p_5 &= [1-G^{-1}(t_1)][1-G^{-1}(t_2)][1-G^{-1}(t_3)][1-G^{-1}(t_4)]G^{-1}(t_5) \\
p_6 &= [1-G^{-1}(t_1)][1-G^{-1}(t_2)][1-G^{-1}(t_3)][1-G^{-1}(t_4)][1-G^{-1}(t_5)]G^{-1}(t_6) \\
p_7 &= [1-G^{-1}(t_1)][1-G^{-1}(t_2)][1-G^{-1}(t_3)][1-G^{-1}(t_4)][1-G^{-1}(t_5)][1-G^{-1}(t_6)]
\end{aligned}
\tag{5.2}
$$

The last equation is redundant with the first six ones and only makes p_7 be the complement of the summed proportions p_1 to p_6. Knowing the rock domain proportions (Table 5.2), one can derive the truncation thresholds to be applied (Table 5.4).

Truncation threshold	Value based on the proportions of interpreted lithological model (Case I)	Value based on the declustered proportions of drill hole data (Case II)
t_1	0.542	0.529
t_2	0.615	0.603
t_3	0.508	0.520
t_4	0.542	0.573
t_5	0.538	0.571
t_6	0.836	0.835

Table 5.4: Calculation of truncation thresholds

5.3 Variogram analysis

Variogram analysis relies on the codification of the drill hole data into indicators (Table 5.3) and on the calculation of their experimental variograms along the three identified main anisotropy directions: N20°W, N70°E and vertical (in this subsection, the entire set of 12,006 drill hole data was used in order to obtain robust directional variograms, as the experimental variograms were not interpretable when considering only the 125 data in the region of interest). This anisotropy is clearly perceptible in the interpreted lithological model, which shows a greater spatial continuity along the direction N20°W in the horizontal plane. For the first two directions, the lag separation distance is set to 15 meters with a tolerance of 7.5 meters, while this distance is set to 10 meters with a tolerance of 5 meters along the vertical direction. From the indicator variograms so obtained, one can derive experimental variograms for the underlying Gaussian random fields (Emery and Cornejo, 2010; Madani and Emery, 2015), see Section 1.1.3 of Chapter 3.

The next step is to fit variogram models (independently) to each experimental variogram. Owing to the fact that the stationary plurigaussian model is based on standard Gaussian random fields, it requires the variogram sills to be equal to 1. In order to ease modeling and to ensure a unit sill value, a semi-automated fitting algorithm has been used (Emery, 2010). The fitting minimizes the mean squared error between experimental and modeled variograms (Figure 5.3).

At this stage, two comments are worth being made. First, the cross-variograms between Gaussian random fields are set to zero, since these random fields are assumed to be independent. Second, the choice of the basic nested structures used for modeling the direct variograms has an impact on the nature of the boundaries between rock domains: structures with a linear behavior near the origin (like the spherical and exponential) lead to irregular boundaries, while structures with a parabolic behavior near the origin (like the cubic and Gaussian) lead to smooth boundaries (Lantuéjoul, 2002). Because this last property is deemed more realistic for the current case study, the experimental variograms are fitted with nested anisotropic cubic models (Table 5.5); the reader is referred to Chilès and Delfiner (2012) for the mathematical expression of the cubic variogram model.

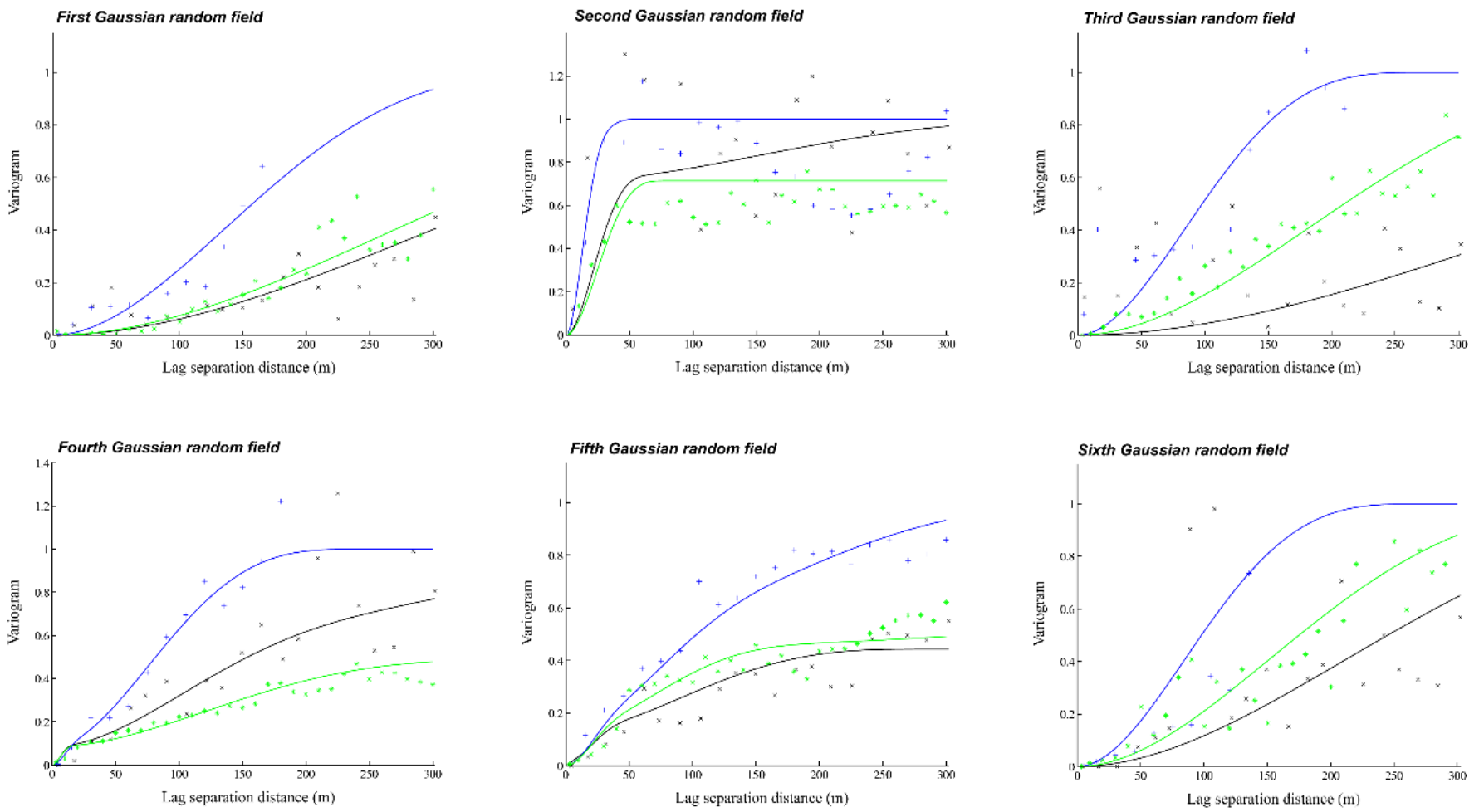

Figure 5.3: Experimental (crosses) and fitted (solid lines) variograms for the six underlying Gaussian random fields, along the anisotropy directions: N20°W (green), N70°E (blue) and vertical (black)

Gaussian random field	Basic nested structure	Sill	Range along N20°W (m)	Range along N70°E (m)	Range along vertical (m)
1	cubic	1.000	1000	450	900
2	cubic	0.713	70	40	80
	cubic	0.287	500	60	infinite
3	cubic	1.000	1200	280	600
4	cubic	0.084	20	30	20
	cubic	0.403	300	250	400
	cubic	0.513	800	250	infinite
5	cubic	0.013	10	60	60
	cubic	0.117	60	60	60
	cubic	0.314	300	200	220
	cubic	0.556	infinite	500	2500
6	cubic	1.000	700	280	500

Table 5.5: Fitted variogram models for the stationary cases

5.4 Construction of realizations of rock domains

Provided with the complete model (truncation rule, truncation thresholds and variograms of the underlying Gaussian random fields), one can simulate the rock domains conditionally to the drill hole data (i.e., forcing the realizations to reproduce the observed rock domains at the drill hole locations) (see Chapter 3, Section 1.2, for details). For the two cases under consideration, a total of one hundred realizations are constructed in the region of interest. Table 5.6 indicates the implementation parameters used for simulation.

Parameter	**Value**
Number of iterations (sweeps over the data set) for Gibbs sampler	30
Number of lines for turning bands simulation	500
Number of neighboring data for conditioning	All the data
Radius (m) of search ellipsoid along direction N20°W	Infinite
Radius (m) of search ellipsoid along direction N70°E	Infinite
Radius (m) of search ellipsoid along vertical direction	Infinite

Table 5.6: Parameters for plurigaussian simulation

In order to test the sensitivity of the results to the number of conditioning drill hole data, the same exercise is repeated by considering subsets of 9 and 43 drill hole data. Therefore, six sub-cases can be distinguished, depending on the input proportions (Case I with proportions calculated from the interpreted lithological model, and Case II with proportions calculated from declustered drill hole data) and on the number of conditioning data (9, 43 and 125) under consideration.

5.5 Post-processing the realizations

The realizations can be used to assess the uncertainty in the volume of each rock domain within the region of interest or, equivalently, in the proportion of the region covered by each domain. This can be done by calculating, for each realization, the proportion of blocks belonging to each domain, then the statistics (minimum, maximum and average) on the proportions so obtained over the 100 realizations. Because the region under study is bounded, the theory of ergodic fluctuations, also known as increasing-domain asymptotics (Cressie, 1993; Chilès and Delfiner, 2012), states that these proportions are likely to deviate from the prior proportions (those used as an input to the model, as per Table 5.2) and vary from one realization to another.

In Tables 5.7 and 5.8, the proportions of magmatic breccia (MAB), tourmaline breccia (TOB) and granitoids (GD) are seen to vary significantly over the realizations and to strongly deviate from the input model proportions calculated from the interpreted lithological model or from the declustered drill hole data. This is a consequence of the under-sampling of these three rock domains, which implies a greater uncertainty in their extent within the region of interest. The ranges of proportions (minimum, maximum and average) calculated over the 100 realizations also differ from one sub-case to another, sometimes significantly. This reflects the importance of correctly choosing the prior proportions of rock domains to input into the plurigaussian model, and the fact that a misspecification of these proportions is likely to provoke biased results. The uncertainty in the model parameters, especially in the prior proportions of the rock domains, is actually ignored by the stationary model.

	Rock domain	Minimum over realizations	Maximum over realizations	Average over realizations	Input model proportions
Case I - 9 conditioning data	**PIP**	0.84%	25.9%	10.37%	10.48%
	POR	19.5%	31.61%	25.94%	26.21%
	MAB	0.14%	10.25%	2.67%	1.15%
	MOB	1.48%	12.45%	6.31%	6.64%
	TOB	0.57%	24.09%	6.33%	5.35%
	GD	36.08%	59.51%	47.50%	49.09%
	AND	0%	3.69%	0.84%	1.08%
Case I - 43 conditioning data	**PIP**	2.25%	17.78%	9.36%	10.48%
	POR	21.57%	31.36%	26.06%	26.21%
	MAB	1.87%	12.67%	5.78%	1.15%
	MOB	3.50%	13.10%	6.92%	6.64%
	TOB	2.35%	15.24%	7.63%	5.35%
	GD	33.45%	53.11%	42.89%	49.09%
	AND	0.07%	7.75%	1.32%	1.08%
Case I - 125 conditioning data	**PIP**	5.28%	21.54%	11.20%	10.48%
	POR	20.65%	29.02%	25.07%	26.21%
	MAB	1.44%	10.15%	5.25%	1.15%
	MOB	4.18%	13.91%	8.15%	6.64%
	TOB	2.84%	17.22%	7.79%	5.35%
	GD	27.77%	47.58%	40.06%	49.09%
	AND	0.58%	5.09%	2.44%	1.08%

Table 5.7: Statistics on the proportions of grid nodes belonging to each rock domain (stationary model, Case I)

	Rock domain	Minimum over realizations	Maximum over realizations	Average over realizations	Input model proportions
Case II - 9 conditioning data	**PIP**	0.41%	21.94%	8.13%	7.20%
	POR	18.13%	28.41%	23.77%	24.27%
	MAB	0.30%	13.82%	4.80%	3.36%
	MOB	4.01%	19.12%	10.79%	11.93%
	TOB	1.01%	27.83%	9.01%	9.44%
	GD	30.52%	54.32%	42.46%	42.56%
	AND	0%	4.40%	1.01%	1.24%
Case II - 43 conditioning data	**PIP**	2.18%	16.72%	8.34%	7.20%
	POR	19.29%	28.34%	23.70%	24.27%
	MAB	2.67%	15.64%	7.45%	3.36%
	MOB	4.90%	17.35%	10.16%	11.93%
	TOB	2.94%	19.17%	9.13%	9.44%
	GD	29.60%	50.11%	39.72%	42.56%
	AND	0.13%	7.63%	1.46%	1.24%
Case II - 125 conditioning data	**PIP**	5.07%	20.21%	10.39%	7.20%
	POR	19.12%	26.44%	22.87%	24.27%
	MAB	2.09%	12.82%	6.74%	3.36%
	MOB	6.75%	18.31%	11.07%	11.93%
	TOB	3.82%	18.64%	9.65%	9.44%
	GD	24.05%	44.45%	36.73%	42.56%
	AND	0.63%	5.02%	2.50%	1.24%

Table 5.8: Statistics on the proportions of grid nodes belonging to each rock domain (stationary model, Case II)

One can also assess the uncertainty in the rock domains at a local (node-by-node) scale, by means of probability maps. The maps are constructed by calculating, for each grid node, the frequency of occurrence of each rock domain over the 100 conditional realizations (Figures 5.5, 5.7 and 5.9). They constitute a complement to the interpreted lithological model, insofar as they show the risk of finding a rock domain different from the expected one. The sectors with little uncertainty are those associated with a high probability for a given rock domain (painted in red in Figures 5.5 to 5.9), indicating that there is little risk of not finding this rock domain, or those associated with a very low probability (painted in dark blue in Figures 5.5 to 5.9), indicating that one is pretty sure of not finding this domain, while the other sectors (painted in light blue, green or yellow in Figures 5.5 to 5.9) are more uncertain.

Compared with the interpreted lithological model (Figures 5.4B, 5.6B and 5.8B), the probability map obtained for the first rock domain (PIP) is somehow acceptable. In contrast, the probability map obtained for the sixth rock domain (GD) bears little resemblance to the interpreted model, while that of the second rock domain (POR) is patchy and does not match at all, irrespective of the number of conditioning data (9, 43 or 125) under consideration. For these two rock domains, the probability is close to zero or to one near the conditioning data locations, but intermediate over the rest of the region, which means that the layout of the rock domain boundaries is highly uncertain.

These features were foreseeable as the result of assuming a stationary model, in which the prior probability of occurrence of each rock domain is constant in space, which reflects a phenomenon that tends to repeat itself in space without any trend. The conditioning to the drill hole data improves the results only locally, but their effect is modest due to the small number of such data.

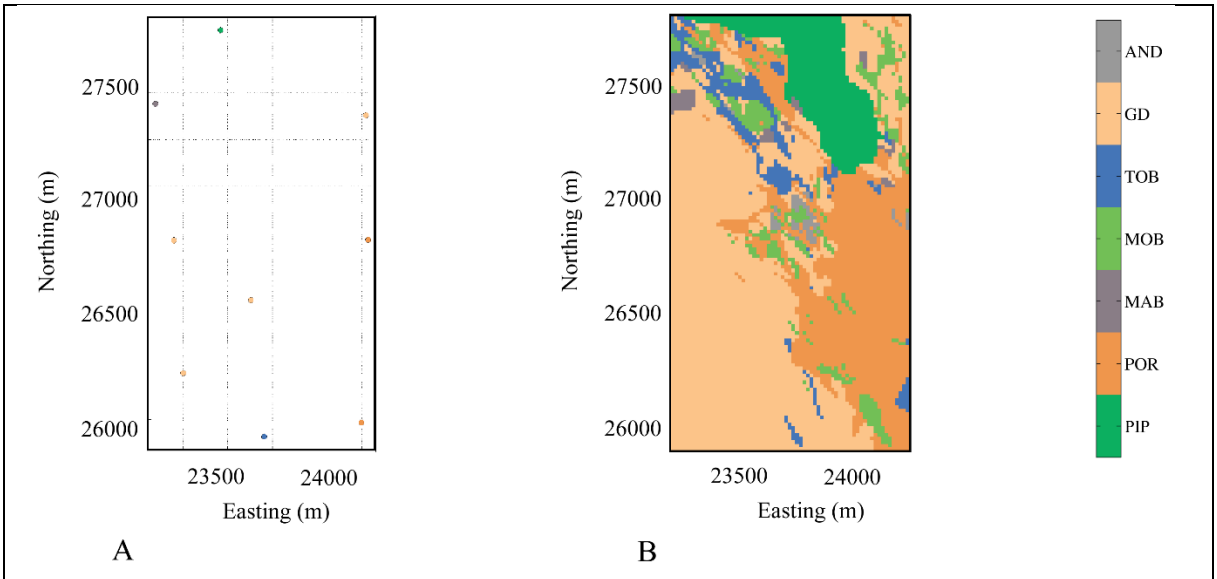

Figure 5.4: Location map of 9 conditioning data (left) and interpreted lithological model (right)

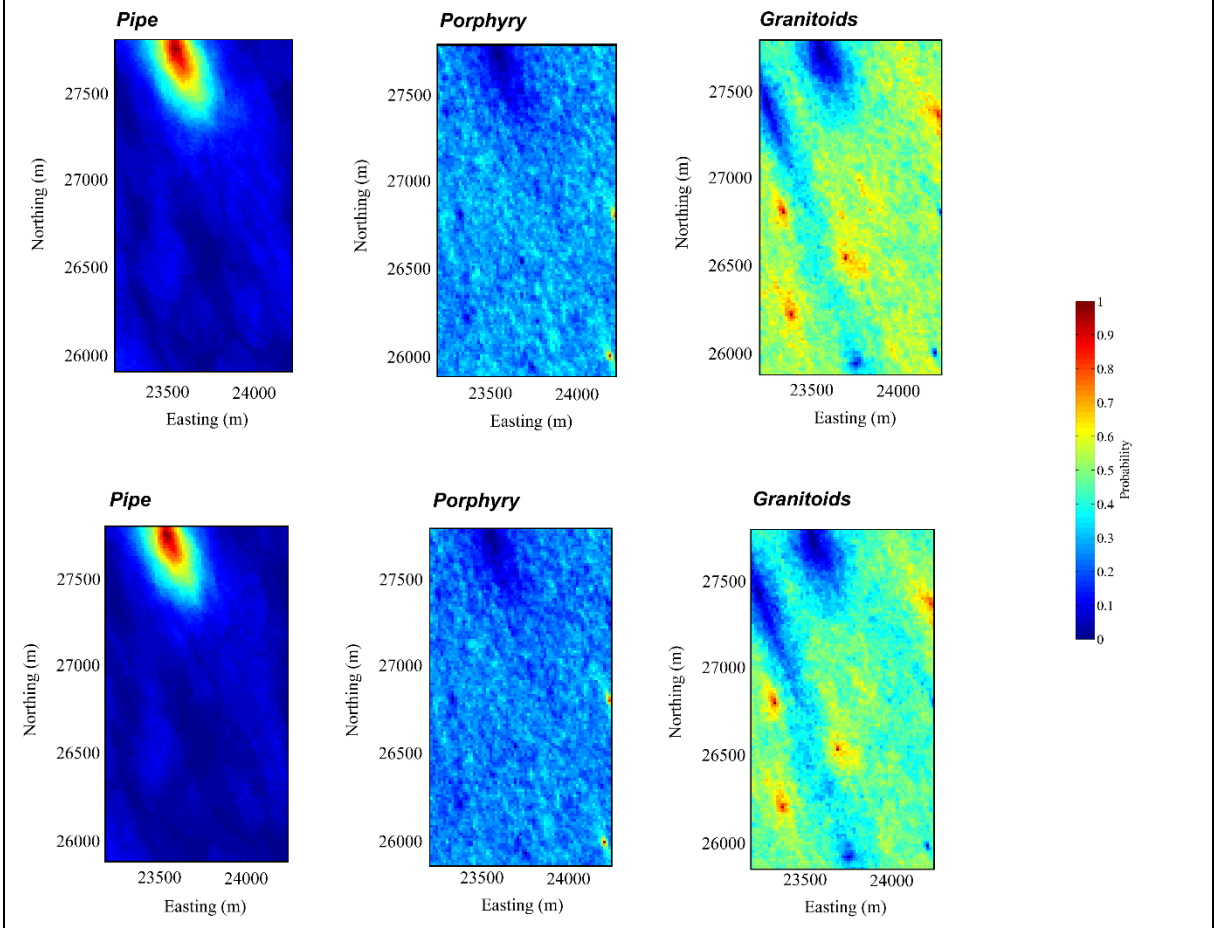

Figure 5.5: Plan views showing the probabilities of occurrence of three rock domains at elevation 3348 m a.m.s.l, calculated using 100 realizations. Top row: case I and bottom row: case II (9 conditioning data)

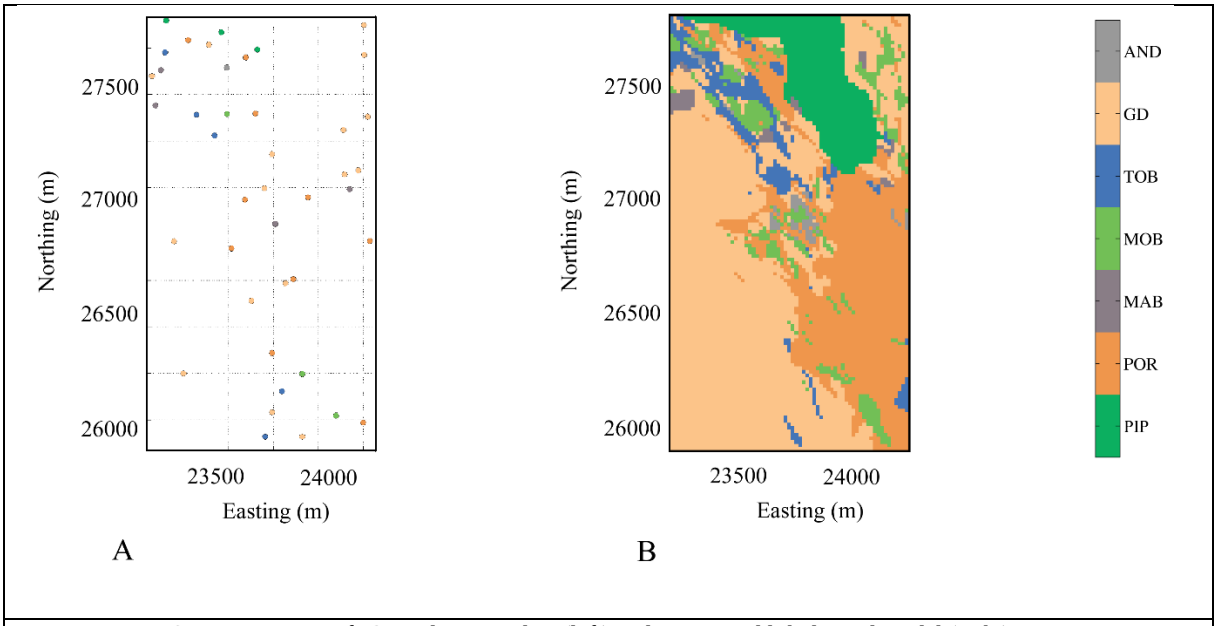

Figure 5.6: Location map of 43 conditioning data (left) and interpreted lithological model (right)

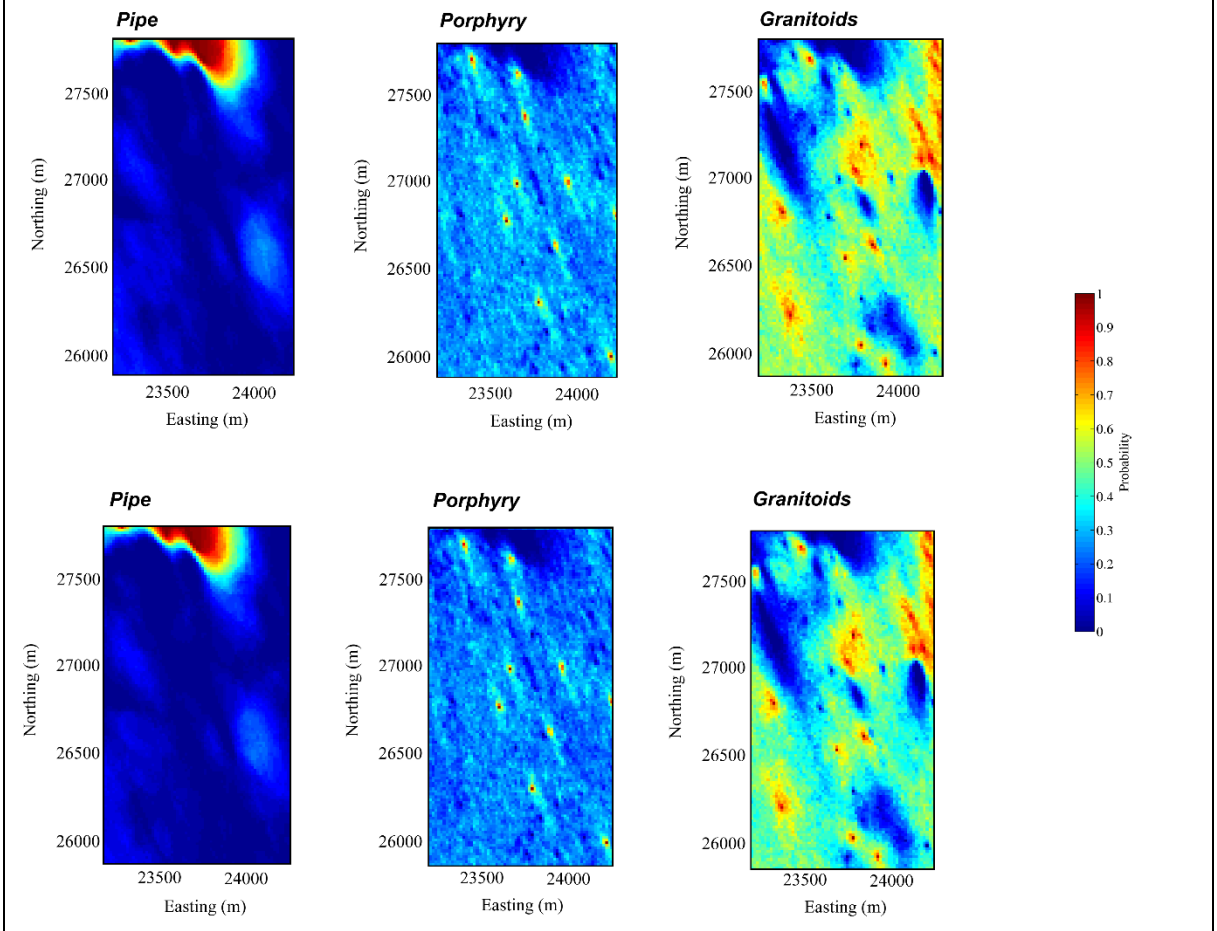

Figure 5.7: Plan views showing the probabilities of occurrence of three rock domains at elevation 3348 m a.m.s.l, calculated using 100 realizations. Top row: case I and bottom row: case II (43 conditioning data).

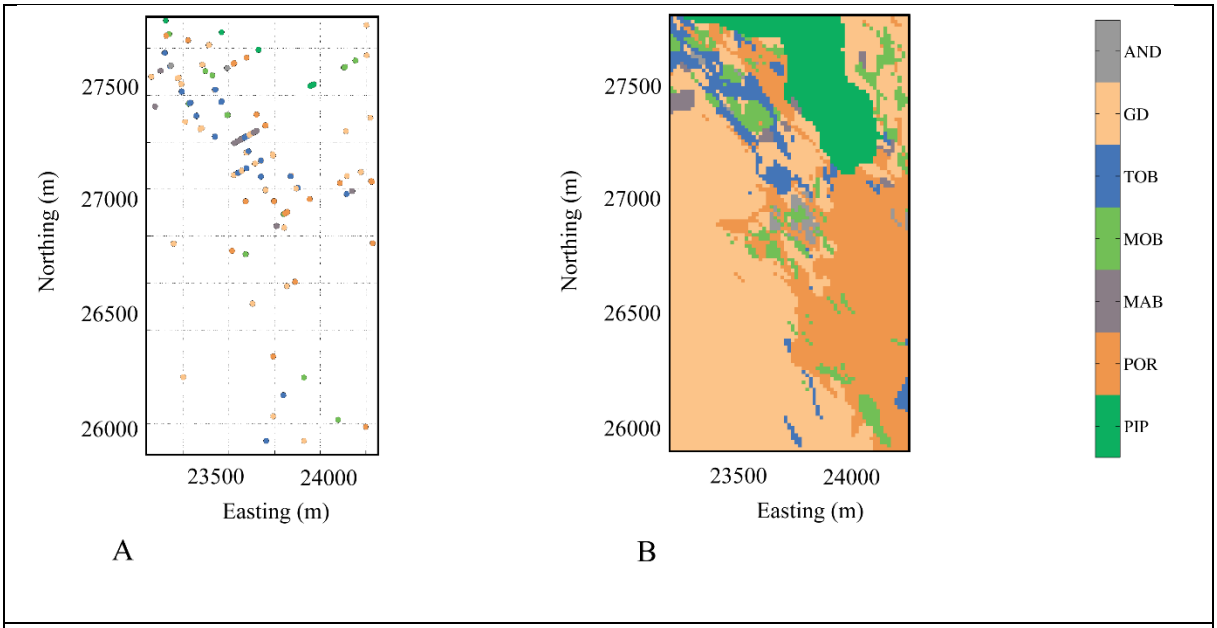

Figure 5.8: Location map of 125 conditioning data (left) and interpreted lithological model (right)

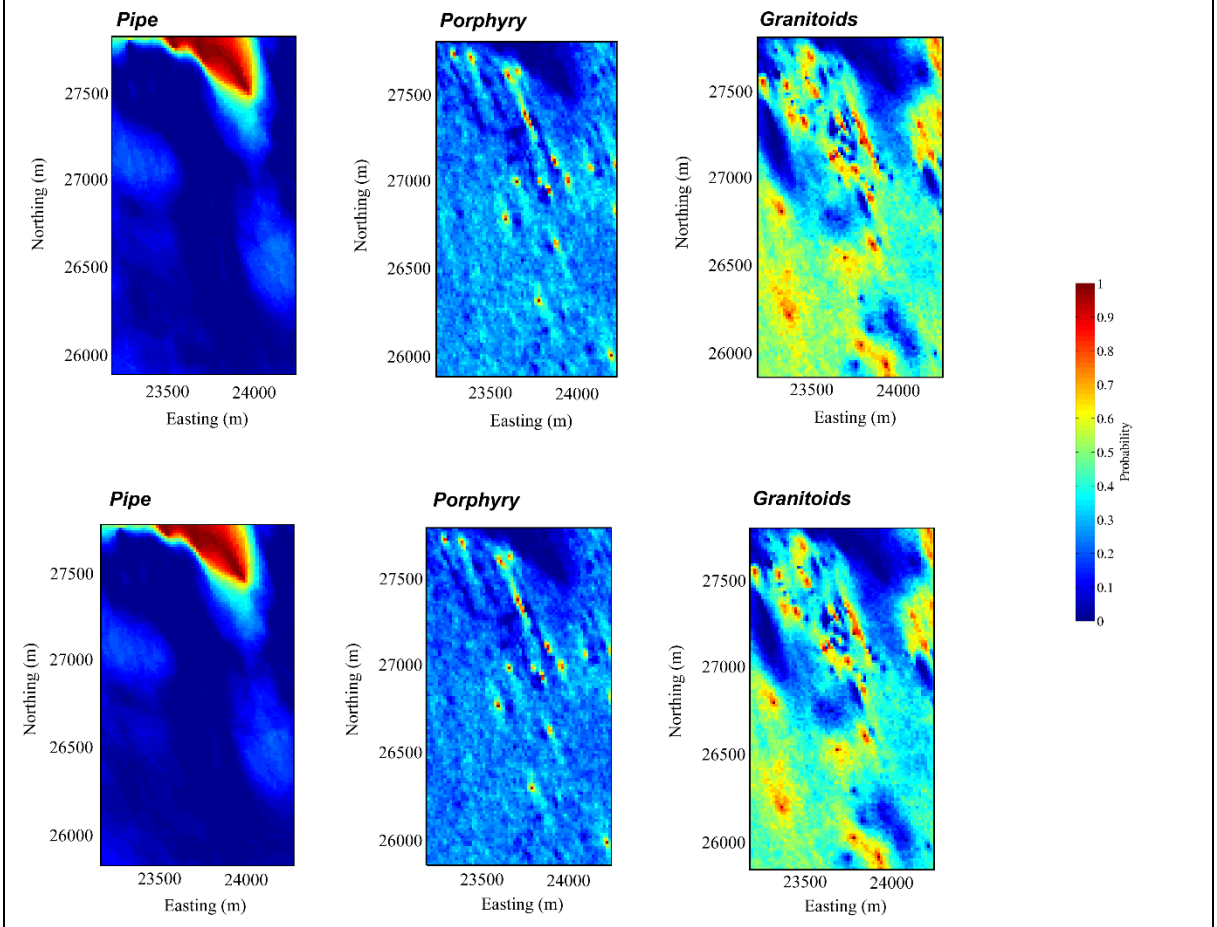

Figure 5.9: Plan views showing the probabilities of occurrence of three rock domains at elevation 3348 m a.m.s.l, calculated using 100 realizations. Top row: case I and bottom row: case II (125 conditioning data).

6 Non-stationary plurigaussian model

6.1 Model presentation

The stationary model developed in the previous subsection faces two limitations:

(1) The inability to reproduce spatial trends in the distribution of rock domains.

(2) Possible misspecifications in the proportions of rock domains, which may bias the results.

A non-stationary model may be able to overcome these limitations. One option is to assume that the proportions of rock domains vary locally and to infer the truncation thresholds accordingly, while considering that the underlying Gaussian random fields remain stationary. The calculation of local proportions of rock domains can be done on the basis of the drill hole data or of the interpreted lithological model, by means of moving windows statistics or geographically-weighted statistics (Armstrong et al. 2011). A challenge is the choice of the moving window size, or of the kernel function in the case of geographically weighted statistics, which greatly influences the results. This choice is actually a trade-off between our uncertainty and our reliance on the interpreted model. With a very large window, the calculated proportions will tend to the global proportions, meaning that the spatial variations of rock domain proportions that are seen in the interpreted lithological model tend to be ignored. On the contrary, with a very small window, the local proportions will tend to 0 or 1, depending on whether or not the rock domain is present in the interpreted model at the target location; in such a case, one is extremely confident in the interpreted lithological model and the simulated rock domains will not depart from this model too much. An application of this approach to the Río Blanco case study is presented in Madani and Emery (2015) and reproduced in Appendix. However, even if it solves the first abovementioned limitation, the use of spatially-varying proportions makes the second limitation more critical, as misspecifications in the domain proportions may be more severe locally than globally.

A second option, which will be presented in this section, is the use of intrinsic random fields of order k instead of stationary random fields. This idea makes sense not only to reproduce spatial trends or zonal features in the distribution of rock domains, but also to avoid misspecifying the truncation thresholds, since these thresholds may be set to zero as explained in Section 2.2 of Chapter 3. Therefore, the two abovementioned limitations can be addressed in this IRF-k model.

Concerning the Río Blanco case study, the truncation rule remains the same as that presented in the stationary model (Section 5.1) and the truncation thresholds are set to zero. To complete the determination of the model parameters, it remains to infer the spatial correlation structure (i.e., the generalized covariance functions) of the underlying intrinsic random fields of order k.

6.2 Generalized covariance analysis

The semi-automatic fitting procedure presented in Section 2.3 of Chapter 3 requires choosing a set of basic nested structures for each underlying random field to be truncated. By default, the structures fitted in the stationary model (Table 5.5) are considered, together with power models whose exponents are determined by trial and error. As the fit relies on a least-square approach, one criterion for choosing the exponents of the power models is to minimize the total sum of squares of errors. Another criterion is to calculate the probability maps with the fitted models and compare these maps with the interpreted lithological model: the closer, the better.

The final results of this trial-and-error process are presented in Table 5.9.

Intrinsic Gaussian random field	Basic nested structure	Sill or slope	Scale factor along N20°W (m)	Scale factor along N70°E (m)	Scale factor along vertical (m)	Exponent
1	Cubic	0.075	1000	450	900	
	Power	0.040	2000	1000	2000	0.5
2	Cubic	2.3×10^{-9}	70	40	80	
	Cubic	1.9×10^{-10}	500	60	infinite	
	Power	0.001	15000	10000	17500	3.0
3	Cubic	1.4×10^{-7}	1200	280	600	
	Power	0.367	4500	1000	2000	0.5
4	Cubic	0.130	20	30	20	
	Cubic	0.104	300	250	400	
	Cubic	1.2×10^{-6}	800	250	infinite	
	Power	0.386	1800	1000	3000	0.5
5	Cubic	8.4×10^{-7}	10	60	60	
	Cubic	3.0×10^{-7}	60	60	60	
	Cubic	5.3×10^{-6}	300	200	220	
	Cubic	4.3×10^{-5}	infinite	500	2500	
	Power	0.596	1.80	1.00	1.30	1.0
6	Cubic	7.99	700	280	500	
	Power	19.99	0.25	0.10	0.20	3.0

Table 5.9: Fitted generalized covariance models for the non-stationary case

6.3 Conditional simulation and post-processing of the realizations

Having completed the specification of the model parameters, one can simulate the rock domains in the region of interest, conditionally to the drill hole data. This is very similar to the stationary case, except for the use of intrinsic kriging of order *k* instead of simple kriging in both the Gibbs sampler and conditioning process. One hundred realizations are constructed for each conditioning subset (with 9, 43 and 125 data, respectively), with the same implementation parameters as in Table 5.6.

Figure 5.10 shows a plan view of three realizations for each case. The conditioning data here play a central role, as in the first case with very few data (9), the pattern of simulated rock domains is largely controlled by the drifts produced by chance fluctuations. In the case with 125 data, it is noticeable that the realizations bear resemblance to the interpreted lithological model, although the latter only plays a role in the inference and validation of the model parameters, but is not used as an input in the simulation process. In particular, the layouts of porphyry (POR) and granitoids (GD) are much more realistic than with the stationary model.

As before, the realizations can be used to assess the uncertainty in the proportion of each rock domain within the region of interest (Table 5.10), or locally at each target grid node, through probability maps (Figures 5.11 to 5.16). Despite the fluctuations on each individual realization, these maps, which are calculated by processing all the realizations, are strikingly similar to the interpreted lithological model for pipe (PIP), porphyry (POR) and granitoids (GD).

	Rock domain	Minimum over realizations	Maximum over realizations	Average over realizations	Interpreted lithological model
IRF-*k* - 9 conditioning data	**PIP**	0.15%	42.75%	11.77%	10.48%
	POR	4.06%	48.42%	23.05%	26.21%
	MAB	0.01%	40.77%	10.15%	1.15%
	MOB	0.00%	23.57%	1.18%	6.64%
	TOB	0.11%	38.49%	7.10%	5.35%
	GD	6.30%	70.77%	37.31%	49.09%
	AND	0.00%	34.83%	9.41%	1.08%
IRF-*k* - 43 conditioning data	**PIP**	1.32%	14.14%	5.75%	10.48%
	POR	15.51%	60.21%	29.56%	26.21%
	MAB	1.65%	19.55%	7.80%	1.15%
	MOB	0.87%	21.26%	6.87%	6.64%
	TOB	3.81%	20.92%	11.32%	5.35%
	GD	13.16%	49.71%	33.47%	49.09%
	AND	1.43%	15.91%	5.18%	1.08%
IRF-*k* - 125 conditioning data	**PIP**	4.28%	23.72%	10.70%	10.48%
	POR	18.02%	51.20%	27.25%	26.21%
	MAB	1.29%	20.33%	5.90%	1.15%
	MOB	3.70%	22.75%	11.02%	6.64%
	TOB	3.95%	22.95%	11.17%	5.35%
	GD	17.80%	44.79%	29.23%	49.09%
	AND	1.54%	12.22%	4.69%	1.08%

Table 5.10: Statistics on the proportions of grid nodes belonging to each rock domain (non-stationary model)

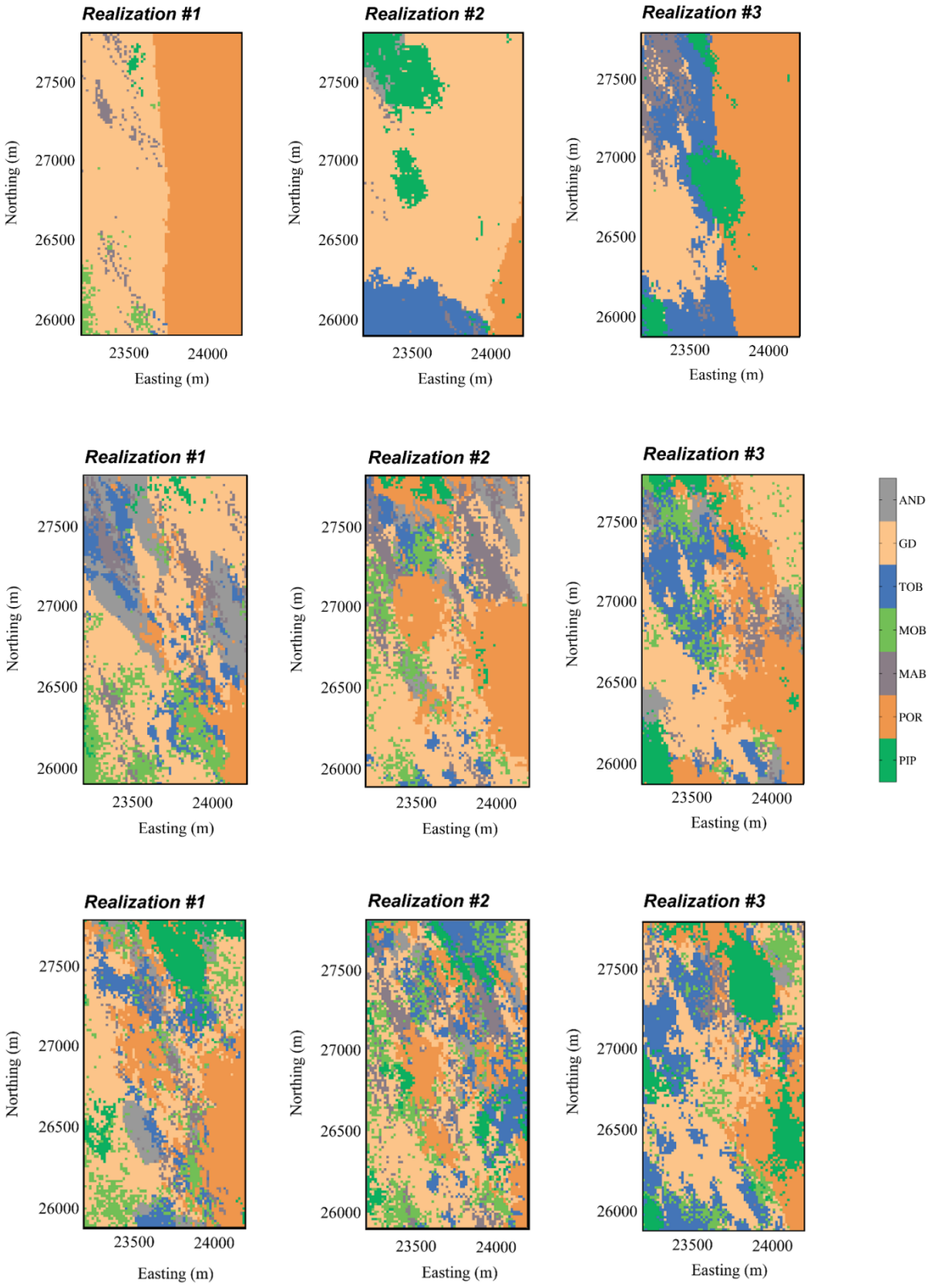

Figure 5.10: Plan views of three realizations of the rock domains for elevation 3348 m a.m.s.l, conditioned to 9 drill hole data (top), 43 drill hole data (middle) or 125 drill hole data (bottom)

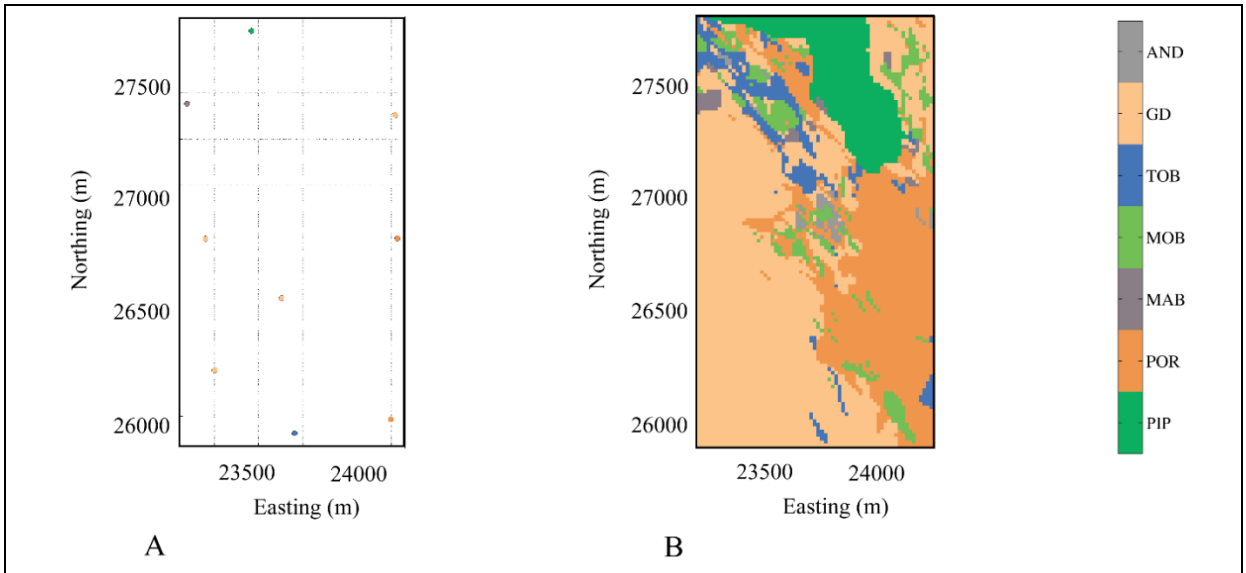

Figure 5.11: Location map of 9 conditioning data (left) and interpreted lithological model (right)

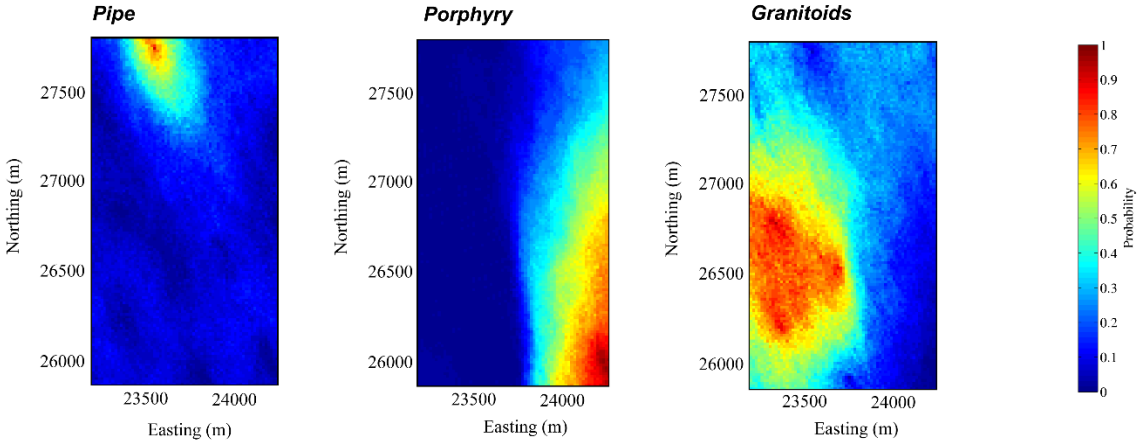

Figure 5.12: Plan views showing the probabilities of occurrence of three rock domains at elevation 3348 m a.m.s.l, calculated using 100 realizations (9 conditioning data)

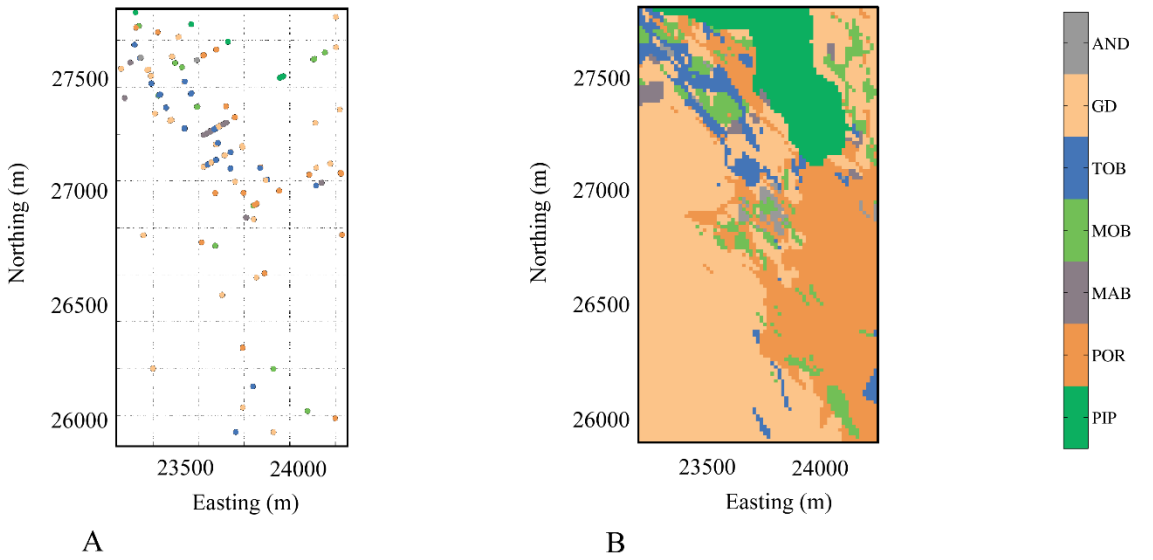

Figure 5.13: Location map of 43 conditioning data (left) and interpreted lithological model (right)

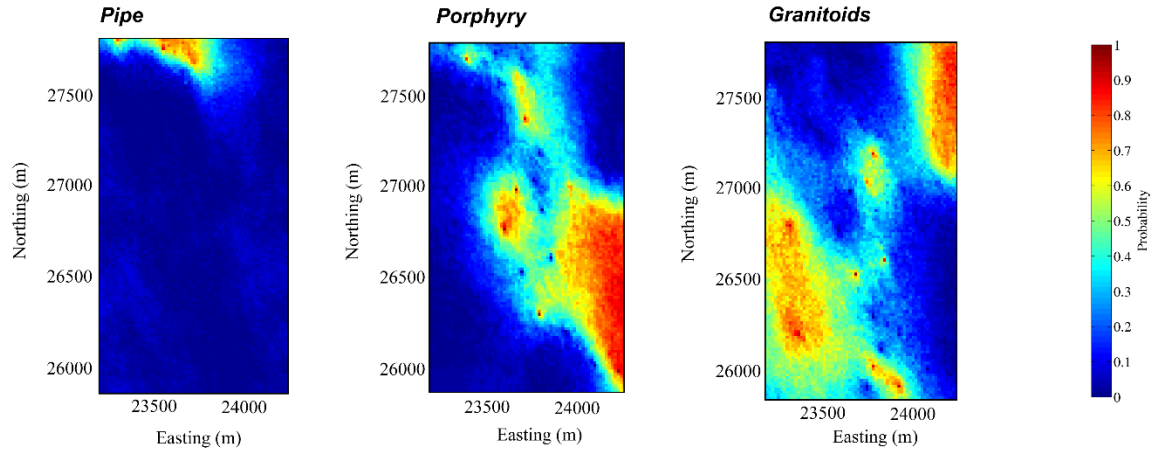

Figure 5.14: Plan views showing the probabilities of occurrence of three rock domains at elevation 3348 m a.m.s.l, calculated using 100 realizations (43 conditioning data)

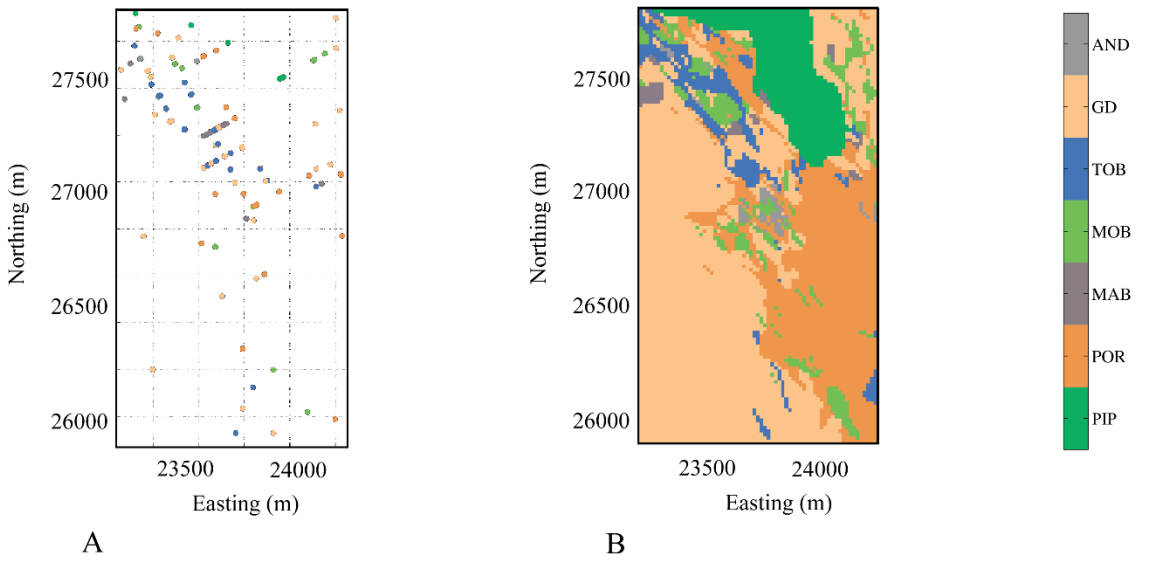

Figure 5.15: Location map of 125 conditioning data (left) and interpreted lithological model (right)

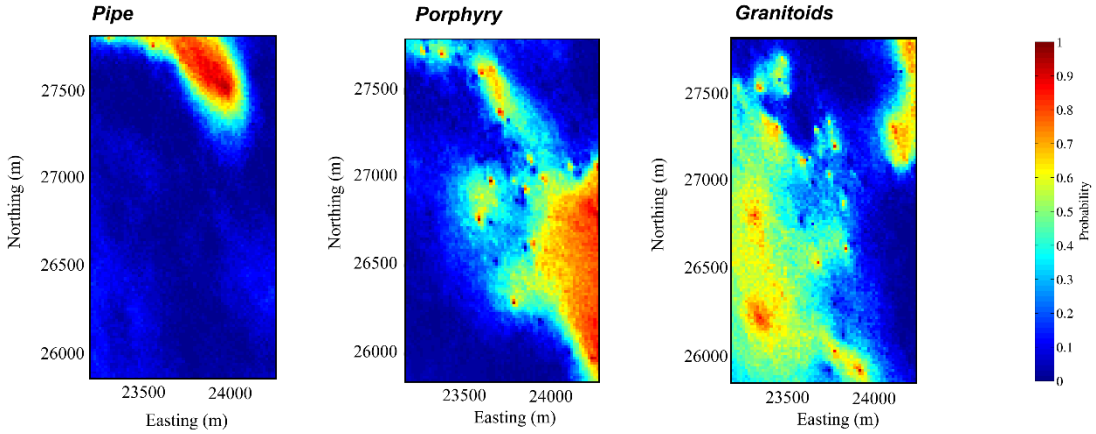

Figure 5.16: Plan views showing the probabilities of occurrence of three rock domains at elevation 3348 m a.m.s.l, calculated using 100 realizations (125 conditioning data)

From the probability maps, one can construct a lithological model by selecting, for each grid node, the most probable rock domain. This model can be compared to the interpreted lithological model in order to identify the grid nodes for which the interpreted rock domain matches the most probable one, and the grid nodes for which there is a mismatch and the interpreted model may be revised or additional drill holes should be taken to reduce uncertainty (Figures 5.17 to 5.19). The latter nodes, mostly located near the boundaries of pipe, porphyry and granitoids, correspond to nodes with a moderate probability (0.3 to 0.6) for the most probable rock domain (in other words, none of the rock domains has a high probability of occurrence). The numbers of matches and mismatches for the target grid nodes are indicated in Tables 5.11 to 5.13: depending on the sub-case (with 9, 43 and 125 conditioning data), one obtains 10,507, 11,116 and 12,425 matches over a total of 17,000 grid nodes, i.e., the interpreted rock domain corresponds to the most probable domain for 61.8%, 65.4% and 73.1% of the grid nodes, respectively. These results are highly satisfactory, given the low number of conditioning data. For comparison, in the stationary model presented in Section 5 of this chapter, these percentages of matches vary between 47.2% and 54.4%, which demonstrate the significant improvement of the proposed non-stationary model over the stationary one.

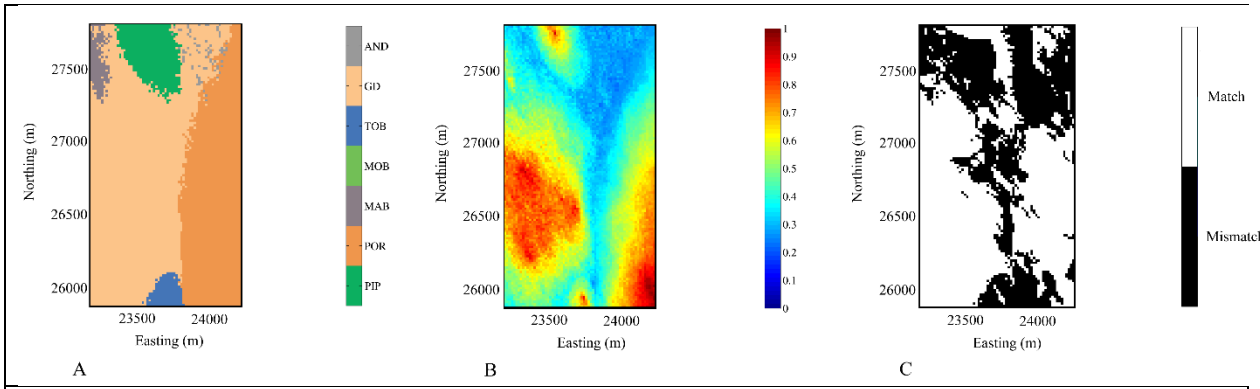

Figure 5.17: Plan views showing A) the most probable rock domain at elevation 3348 m, B) the probability of occurrence of the most probable domain, and C) the matches and mismatches with respect to the interpreted lithological model (9 conditioning data)

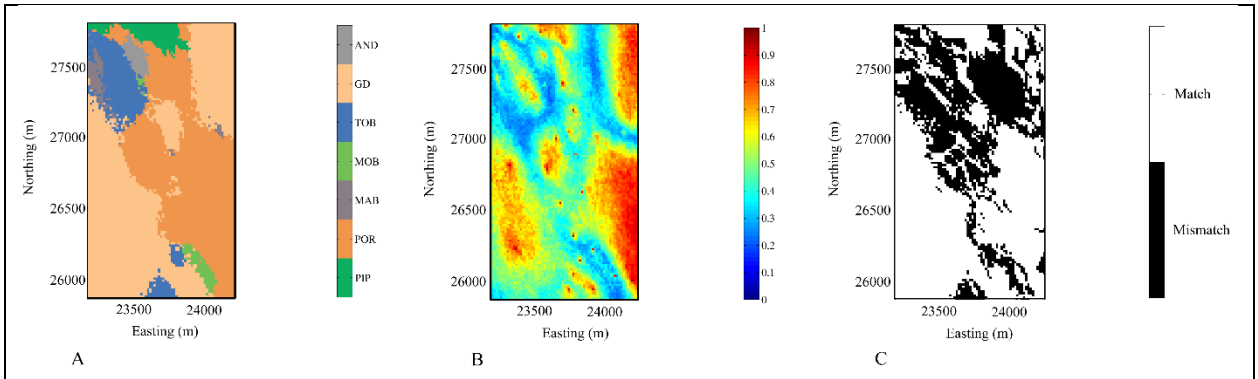

Figure 5.18: Plan views showing A) the most probable rock domain at elevation 3348 m, B) the probability of occurrence of the most probable domain, and C) the matches and mismatches with respect to the interpreted lithological model (43 conditioning data)

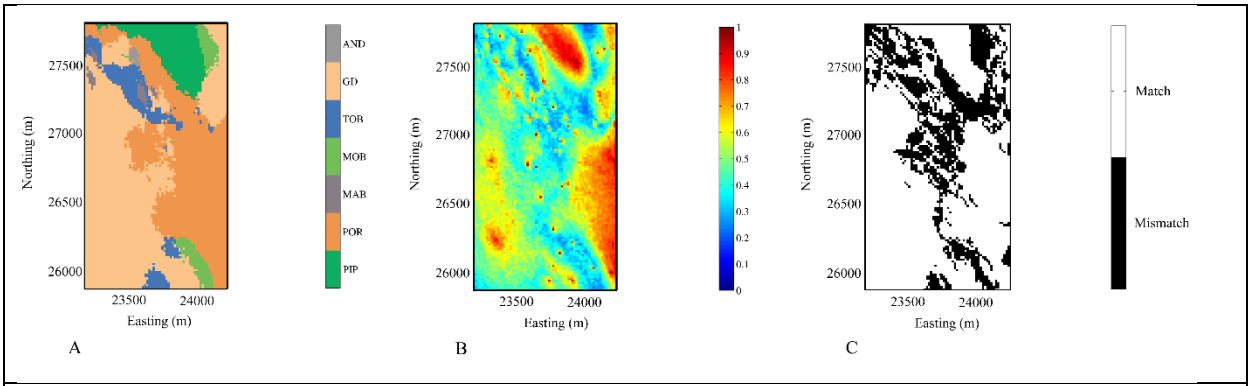

Figure 5.19: Plan views showing A) the most probable rock domain at elevation 3348 m, B) the probability of occurrence of the most probable domain, and C) the matches and mismatches with respect to the interpreted lithological model (125 conditioning data)

		Most probable rock domain							
		PIP	**POR**	**MAB**	**MOB**	**TOB**	**GD**	**AND**	TOTAL
Interpreted model	**PIP**	432	175	5	0	0	1128	42	1782
	POR	325	3290	7	0	0	834	0	4,456
	MAB	15	31	60	0	0	88	2	196
	MOB	84	353	41	0	0	637	14	1129
	TOB	105	141	66	0	26	571	0	909
	GD	132	1109	133	0	236	6709	26	8,345
	AND	5	44	1	0	0	133	0	183
	TOTAL	1,098	5,143	313	0	262	10,100	84	17,000

Table 5.11: Numbers of grid nodes per rock domain, according to the interpreted lithological model and to the model based on the most probable rock domain (9 conditioning data)

		Most probable rock domain							
		PIP	**POR**	**MAB**	**MOB**	**TOB**	**GD**	**AND**	TOTAL
Interpreted model	**PIP**	533	703	0	0	0	545	1	1782
	POR	17	3898	11	62	42	375	51	4,456
	MAB	0	56	73	0	18	49	0	196
	MOB	18	474	13	74	191	344	15	1129
	TOB	26	335	9	0	381	120	38	909
	GD	48	1155	169	47	755	6147	24	8,345
	AND	0	126	3	0	21	29	4	183
	TOTAL	642	6,747	278	183	1408	7,609	133	17,000

Table 5.12: Numbers of grid nodes per rock domain, according to the interpreted lithological model and to the model based on the most probable rock domain (43 conditioning data)

		Most probable rock domain							
		PIP	**POR**	**MAB**	**MOB**	**TOB**	**GD**	**AND**	TOTAL
Interpreted model	**PIP**	1259	391	0	0	5	127	0	1782
	POR	6	3909	4	121	50	335	31	4,456
	MAB	19	35	64	2	4	72	0	196
	MOB	34	416	31	192	176	266	14	1129
	TOB	5	310	13	3	403	159	16	909
	GD	234	751	50	300	410	6587	13	8,345
	AND	0	129	3	1	9	30	11	183
	TOTAL	1,557	5,941	165	619	1057	7,576	85	17,000

Table 5.13: Numbers of grid nodes per rock domain, according to the interpreted lithological model and to the model based on the most probable rock domain (125 conditioning data)

Chapter 6: Discussion and conclusions

1 General discussion

The synthetic and real case studies demonstrate that the truncated Gaussian and plurigaussian models can be extended to the non-stationary framework, by considering intrinsic random fields of order *k* with Gaussian generalized increments instead of stationary Gaussian random fields. The simulation of geological domains is performed similarly to the stationary case, except for the type of kriging used in the Gibbs sampler and in the conditioning stage, where intrinsic kriging of order *k* replaces simple kriging. Regarding the simulation of an intrinsic random field of order *k* with Gaussian generalized increments, it can be performed efficiently with a spectral - turning bands algorithm and only requires the knowledge of the generalized covariance of the random field.

The benefits of the proposed non-stationary plurigaussian model are twofold. First and foremost, it allows reproducing spatial trends and zonal patterns in the distribution of geological domains. This is a very common feature in the modeling of lithological, mineralogical and / or alteration domains due to the parameters that affect the ore body formation, such as genesis, paragenesis and regional structures. The current implementation of the plurigaussian model, based on the truncation of stationary Gaussian random fields, is not able to reproduce these trends and zonal patterns, unless spatially-varying truncation thresholds are defined, which amounts to specifying spatially-varying proportions of the geological domains under study. However, such an approach suffers from two important limitations in the inference of the model parameters: (i) it assumes a perfect knowledge of the local domain proportions, which is unrealistic in practice, and (ii) the theoretical background for variogram analysis is not clearly laid out. Here lies the second benefit of our proposal, insofar as the simulation process does not rely on local domain proportions, thus it is not affected by a possible misspecification of these proportions when the available data are scarce or the geology is not well known; also, a procedure has been designed to infer the spatial correlation structure on a sound basis. In the case of spatial prediction, a similar problem occurs with simple kriging when a locally-varying mean value has to be defined: this kriging type is often replaced by ordinary kriging, with an unknown mean value at the scale of the kriging neighborhood, or with universal or intrinsic kriging of order *k*, which assumes a spatially-varying and, at the same time, unknown mean value. The proposed plurigaussian model goes in the same line, in the context of simulation rather than prediction.

The real case study has proven the applicability of this model to simulate multiple rock domains, using a hierarchical approach to define the truncation rule in accordance with the chronology of the domains, whereas the conventional stationary model produces realizations of the domains that do not bear resemblance with the lithological model interpreted by geologists.

In practice, the main difficulty of the proposed plurigaussian model stems from the inference of the generalized covariances of the underlying intrinsic random fields. Indeed, one does not have access to an experimental variogram on which to fit a variogram model, as in the stationary case. Instead, a semi-automated fitting procedure has been designed, based on the calculation of the indicator covariances between all the pairs of data locations, followed by a least-square optimization to determine the parameters of the generalized covariance functions to be modeled. Some tips can however help for the fitting, such as considering the stationary fit as an initial stage and adding non-stationary structures (e.g., power generalized covariances with exponents chosen by trial and error), and comparing the probability maps derived from a set of realizations with a prior geological model in order to make sure that the fitted model agrees with the geological interpretation of the deposit.

Other difficulties that have been met relate to the Gibbs sampler and the truncation rule. About the former, the convergence of the Gibbs sampler is not guaranteed if one works with a moving neighborhood implementation. Some solutions exist in the case of stationary models (Lantuéjoul and Desassis, 2012; Arroyo et al., 2012; Emery et al., 2014) and their extension to the conditional simulation of intrinsic random fields of order k is a topic of further research. With respect to the truncation rule, the use of a hierarchical model only requires a single truncation threshold for each underlying intrinsic random field, which can be set to zero. However, the extension to the multiple truncation of the same random field is not straightforward, as it would require the definition of several thresholds for the same random field, only one of which could be set to zero. Again, additional research is needed to extend the proposed formalism to such complex truncation rules involving multiple truncations.

2 Conclusions

The spatial modeling of geological domains is critical to characterize geological heterogeneities in ore bodies and to further quantify the chemical, physical, mineralogical and geo-metallurgical properties of the material to be mined. As the boundaries of the geological domains are generally uncertain, stochastic spatial models are increasingly used in place of, or in complement to, deterministic models. To date, a variety of stochastic simulation approaches have been developed to model the spatial layout of geological domains. Among them, plurigaussian simulation offers a flexible framework, as it allows reproducing (i) the topological constraints (contact relationships) on the domains, (ii) the domain proportions, (iii) the spatial correlation structure of these domains and (iv) the available conditioning data.

However, in most of the case studies developed to date (Skvortsova et al. 2001, 2002; Fontaine and Beucher, 2006; Carrasco et al., 2007; Emery and González 2007a, 2007b; Deutsch and Deutsch, 2014), it calls the attention that plurigaussian simulation is restricted to a few geological domains (no more than five), which can be explained because of the difficulty in imposing given contact relationships with a higher number of domains. Another restriction, more fundamental, relates to the definition of the domain proportions, for which the plurigaussian model is caught in

a dilemma: if these proportions are assumed constant in space (stationary model), then the simulation is unable to reproduce spatial trends and zonal patterns; but if the proportions are assumed to vary in space, their inference is likely to be locally inaccurate and the model becomes sensitive to a misspecification of these proportions.

In this context, the objective of this thesis was twofold. First, from a methodological point of view, it was of interest to extend the currently used plurigaussian model in order to increase its versatility, by allowing modeling more geological domains with possibly complex contact relationships and reproducing trends on the domain distribution in space. From a practical point of view, it was of interest to validate the proposal through synthetic and real case studies in order to determine its applicability.

Both objectives have been achieved. Concerning the methodology, a non-stationary plurigaussian model based on the truncation of intrinsic random fields of order *k* instead of stationary random fields has been proposed, together with tools and algorithms for inferring the model parameters and for constructing realizations conditioned to existing data. As for the practice, the Río Blanco case study demonstrated that, even with few conditioning data (only 125 over a geographical area of 1.87 km^2), it is possible to construct simulated models of rock domains that have an acceptable coincidence with the interpretation made by geologists, in a much more successful way than does the conventional stationary plurigaussian model. The proposed model therefore allows a more realistic assessment of the geological uncertainty, with its subsequent gains in the evaluation of mineral resources and ore reserves. This model combines, on the one hand, a sound theoretical framework (in particular, concerning the design of algorithms for fitting the underlying generalized covariance functions or for simulating intrinsic random fields of order *k*) and, on the other hand, the consideration of qualitative geological knowledge, such as the chronology, contact relationships or spatial trends of the domains to be simulated, for guiding the modeling process and validating it.

3 Perspectives

The proposal has brought up several issues that might be considered as future research directions, in particular: (i) the search for improvements in the structure identification, (ii) the extension of the Gibbs sampler applied to intrinsic random fields in the presence of large datasets, and (iii) the threshold analysis when the truncation rule gets complex and the proposed hierarchical approach is no longer applicable.

Another research direction that would deserve being explored relates to the extension of the plurigaussian model to the description of geological domains that are likely to overlap, such as hydrothermal alteration domains that overprint each other in time, or of geological domains that exhibit transitional boundaries governed by hydrothermal or supergene alteration gradients (e.g., temperature, pH, Eh or chemical gradients) rather than clear-cut boundaries. Such features could be reproduced by using multiple truncation thresholds for each underlying Gaussian random field.

Bibliography

[1] Alabert, F.G. (1987): Stochastic imaging of spatial distributions using hard and soft information. Master's Thesis, Stanford University, Stanford, CA.

[2] Alfaro, M. (1994): Control geológico en la estimación de reservas. Minerales 49: 25-32

[3] Allard, D., D'Or, D., Biver, P., Froidevaux, R. (2012): Non-parametric diagrams for plurigaussian simulation of lithologies. In: Ninth International Geostatistics Congress, Oslo

[4] Almeida, J. (2010): Stochastic simulation methods for characterization of lithoclasses in carbonate reservoirs. Earth-Science Reviews 101: 250–270

[5] Armstrong, M., Galli, A., Beucher, H., Le Loc'h, G., Renard, D., Doligez, B., Eschard, R., Geffroy, F. (2011): Plurigaussian Simulations in Geosciences. Springer, Berlin

[6] Arroyo, D., Emery, X. (2015): Simulation of intrinsic random fields of order k with Gaussian generalized increments by Gibbs sampling. Mathematical Geosciences 47(8): 955-974

[7] Arroyo, D., Emery, X. (2016): Spectral simulation of vector random fields with stationary Gaussian increments in d-dimensional Euclidean spaces. Stochastic Environmental Research and Risk Assessment, in press.

[8] Arroyo, D., Emery, X., Peláez, M. (2012): An enhanced Gibbs sampler algorithm for non-conditional simulation of Gaussian random vectors. Computers & Geosciences 46:138–148

[9] Besag, J. (1986): On the statistical analysis of dirty pictures. Journal of the Royal Statistical Society B 48: 259–302

[10] Beucher, H., Galli, A., Le Loc'h, G., Ravenne, C. (1993): Including a regional trend in reservoir modeling using the truncated Gaussian method. In: Soares, A. (ed.) Geostatistics Tróia'92. Kluwer Academic, Dordrecht, 555-566

[11] Beucher, H., Doligez, B., Yarus, J.M. (2006): Modeling complex reservoirs with multiple conditional techniques: a practical approach to reservoir characterization. In: Coburn, T.C., Yarus, J.M., Chambers, R.L. (eds.) Stochastic modeling and Geostatistics: Principles, Methods, and Case Studies, volume II: AAPG Computer Applications in Geology 5, pp. 289-299

[12] Biver, P., Haas, A., Bacquet, C. (2002): Uncertainties in facies proportion estimation II: application to geostatistical simulation of facies and assessment of volumetric uncertainties. Mathematical Geology 34(6): 703-714

[13] Boisvert, J.B., Deutsch, C.V. (2011): Programs for kriging and sequential Gaussian simulation with locally varying anisotropy using non-Euclidean distances. Computers & Geosciences 37(4): 495-510

[14] Boisvert, J.B., Manchuk, J.G., Deutsch, C.V. (2009): Kriging in the presence of locally varying anisotropy using non-Euclidean distances. Mathematical Geosciences 41(5): 585-601

[15] Box, G.E.P., Jenkins, G.M. (1970): Time Series Analysis: Forecasting and Control. Holden-Day, San Francisco

[16] Bruno, R., Raspa, G. (1993): Towards a direct structural analysis of an IRF-k. In: Soares, A. (ed.) Geostatistics Tróia'92. Kluwer, Dordrecht, 49-59

[17] Brunsdon, C., Fotheringham, A., Charlton, M. (2002): Geographically weighted summary statistics – a framework for localized exploratory data analysis. Computers, Environment and Urban Systems 26(6): 501-524

[18] Buttafuoco, G., Castrignano, A. (2005): Study of the spatio-temporal variation of soil moisture under forest using intrinsic random functions of order k. Geoderma 128 (3–4): 208–220

[19] Cáceres, A., Emery, X., Aedo, L., Gálvez, O. (2011): Stochastic geological modeling using implicit boundary simulation. In: Beniscelli, J., Kuyvenhoven, R., Hoal, K.O. (eds.), Proceedings of the 2nd International Seminar on Geology for the Mining Industry GEOMIN 2011. Gecamin Ltda, Santiago, Chile, 10 p.

[20] Carle, S.F., Fogg, G.E (1996): Transition probability-based indicator geostatistics. Mathematical Geology 28(4): 453–476

[21] Carr, J.C., Beatson, R.K., Cherrie, J.B., Mitchell, T.J., Fright W.R., McCallum, B.C., Evans, T.R. (2001): Reconstruction and representation of 3D objects with radial basis functions. In: Proceedings of the 2001 SIGGRAPH Conference, Los Angeles, California, USA, pp. 67-76.

[22] Carrasco, P., Ibarra, F., Rojas, R., Le Loc'h, G., Séguret, S. (2007): Application of the truncated Gaussian simulation method to a porphyry copper deposit. In: Magri, E. (ed.) Proceedings of the 33rd International Symposium on Application of Computers and Operations research in the Mineral Industry APCOM 2007, pp. 31-39

[23] Casella, G., George, E.I. (1992): Explaining the Gibbs sampler. American Statistician 46(3): 167–174.

[24] Cassiani, G., Christakos, G. (1998): Analysis and estimation of natural processes with nonhomogeneous spatial variation using secondary information. Mathematical Geology 30(1): 57-76

[25] Chan, K.S. (1993): Asymptotic behavior of the Gibbs sampler. Journal of the American Statistical Association 88(421): 320–326.

[26] Chauvet, P. (1993): Processing data with a spatial support: geostatistics and its methods. In: Cahiers de Géostatistique, Fasc. 4, Ecole des Mines de Paris

[27] Chauvet, P. (1999): Aide-mémoire de géostatistique linéaire. Les Presses de l'Ecole des Mines, Paris.

[28] Chessa, A.G., Martinius, A.W. (1992): Object-based modelling of the spatial distribution of fluvial sandstone deposits. In: Christie, M.A., Da Silva, F.V., Farmer, C.L., Guillon, O., Heinemann, Z.E., Lemonnier, P., Regtien J.M.M., van Spronsen, E. (eds.) Proceedings of the 3rd European Conference on the Mathematics of Oil Recovery, Delft University Press, pp. 5–14

[29] Chiasson, P., Soulie, M. (1997): Nonparametric estimation of generalized covariances by modeling on-line data. Mathematical Geology 29(1): 153-172

[30] Chilès, J.P., (1977): Géostatistique des phénomènes non stationnaires (dans le plan). Doctoral Thesis, Université de Nancy I, Nancy, 152 pp.

[31] Chilès, J.P., Delfiner, P. (1997): discrete exact simulation by the Fourier method. In: Baafi, E.Y., Schofield, N.A. (eds.) Geostatistics Wollongong' 96, pp. 258-269. Kluwer, Dordrecht

[32] Chilès, J.P., Delfiner, P. (2012): Geostatistics: Modeling Spatial Uncertainty. Wiley, New York

[33] Chilès, J.P., Gable, R. (1984): Three-dimensional modelling of a geothermal field. In: Verly, G., David, M., Journel, A.G., Maréchal, A. (eds.) Geostatistics for Natural Resources Characterization, pp. 587–598. Reidel, Dordrecht

[34] Chilès J.P., Gentier, S. (1993): Geostatistical modelling of a single fracture. In: Soares, A. (ed.) Geostatistics Tróia'92. Kluwer, Dordrecht, 95-108

[35] Chugunova, T.L., Hu, L.Y. (2008): Multiple-point simulations constrained by continuous auxiliary data. Mathematical Geosciences 40(2): 133-146

[36] Costa, J.F. (2009): Interpolating datasets with trends: a modified median polish approach. Computers & Geosciences 35(11): 2222-2230

[37] Cox, D.R., Miller, H.D. (1977): The theory of Stochastic Processes. Chapman and Hall / CRC

[38] Cressie, N. (1987): A nonparametric view of generalized covariances for kriging. Mathematical Geology 19(5): 563-586

[39] Cressie, N.A.C. (1993): Statistics for Spatial Data. Wiley, New York

[40] Daly, C., Caers, J. (2010): Multi-point geostatistics - an introductory overview. First Break 28(9): 39-47

[41] Damian, D., Sampson, P.D., Guttorp, P. (2000): Bayesian estimation of semi-parametric nonstationary spatial covariance structure. Environmetrics 12: 161-176

[42] David, M. (1988): Handbook of Applied Advanced Geostatistical Ore Reserve Estimation. Elsevier, Amsterdam

[43] David, M., Crozel, D., Robb, J.M. (1986): Automated mapping of the ocean floor using the theory of intrinsic random functions of order k. Marine Geophysical Researches 8(1): 49–74

[44] Davis, M. (1987): Production of conditional simulations via the LU triangular decomposition of the covariance matrix. Mathematical Geology 19(2): 91–98

[45] De Marsily, G. (1986): Quantitative Hydrogeology: Groundwater Hydrology for Engineers. Academic, San Diego

[46] Delfiner, P. (1976): Linear estimation of nonstationary spatial phenomena. In: Guarascio, M., David, M., Huijbregts, C.J. (eds.) Advanced Geostatistics in the Mining Industry. Reidel, Dordrecht, 49-68

[47] Delfiner, P., Chilès, J.P. (1977): Conditional simulations: A new Monte-Carlo approach to probabilistic evaluation of hydrocarbon in place. SPE paper 6985, pp. 32

[48] Deraisme, J., Field, M. (2006): Geostatistical simulations of kimberlite orebodies: application to sampling optimization. Proceedings of the 6th international mining geology conference, Darwin, NT, Australia, 21-23 Aug 2006, pp. 193-203

[49] Deutsch, C.V. (2002): Geostatistical Reservoir Modeling. Oxford University Press

[50] Deutsch, C.V. (2006): A sequential indicator simulation program for categorical variables with point and block data: BlockSIS, Computers & Geosciences 32: 1669–1681

[51] Deutsch JL, Deutsch CV (2014): A multidimensional scaling approach to enforce reproduction of transition probabilities in truncated plurigaussian simulation. Stochastic Environmental Research and Risk Assessment 28(3): 707–716

[52] Deutsch, C.V., Journel, A.G. (1992): GSLIB: Geostatistical software library and user's guide. Oxford University Press, New York, pp. 340

[53] Dimitrakopoulos, R. (1990): Conditional simulation of intrinsic random functions of order k. Mathematical Geology 22(3): 361-380

[54] Dong, A. (1990): Estimation géostatistique des phénomènes régis par des équations aux dérivées partielles. Doctoral dissertation, Ecole des Mines de Paris, Paris

[55] Dowd, P.A. (1994): Geological controls in the geostatistical simulation of hydrocarbon reservoirs. Arabian Journal for Science and Engineering 19(2B): 237–247

[56] Dowd, P.A., Pardo-Iguzquiza, E., Xu, C. (2003): Plurigau: a computer program for simulating spatial facies using the truncated plurigaussian method. Computers & Geosciences 29(2): 123–141

[57] Dubrule, O. (1993): Introducing more geology in stochastic reservoir modelling. In: Soares, A. (ed.) Geostatistics Troia'92. Kluwer Academic, Dordrecht, pp. 351–369

[58] Emery, X. (2004): Properties and limitations of sequential indicator simulation. Stochastic Environmental Research and Risk Assessment 18(6): 414-424

[59] Emery, X. (2007a): Using the Gibbs sampler for conditional simulation of Gaussian-based random fields. Computers & Geosciences 33(4): 522-537

[60] Emery, X. (2007b): Simulation of geological domains using the plurigaussian model: New developments and computer programs. Computers & Geosciences 33(9): 1189–1201

[61] Emery, X. (2008a): Uncertainty modeling and spatial prediction by multi-Gaussian kriging: accounting for an unknown mean value. Computers & Geosciences 34(11): 1431–1442

[62] Emery, X. (2008b): Statistical tests for validating geostatistical simulation algorithms. Computers & Geosciences 34(11): 1610–1620

[63] Emery, X. (2010): Iterative algorithms for fitting a linear model of coregionalization. Computers & Geosciences 36(9): 1150-1160

[64] Emery, X., Arroyo, D., Peláez, M. (2014): Simulating large Gaussian vectors subject to inequality constraints by Gibbs sampling. Mathematical Geosciences 46: 265-283

[65] Emery, X., Cornejo, J. (2010): Truncated Gaussian simulation of discrete-valued, ordinal coregionalized variables. Computers & Geosciences 36(10): 1325-1338

[66] Emery, X., González, K.E. (2007a): Incorporating the uncertainty in geological boundaries into mineral resources evaluation. Journal of the Geological Society of India 69 (1): 29–38

[67] Emery, X., González, K.E. (2007b): Probabilistic modeling of mineralogical domains and its application to resources evaluation. The Journal of the Southern African Institute of Mining and Metallurgy 107(12): 803-809

[68] Emery, X., Lantuéjoul, C. (2006): TBSIM: A computer program for conditional simulation of three-dimensional Gaussian random fields via the turning bands method. Computers & Geosciences 32(10): 1615–1628

[69] Emery, X., Lantuéjoul, C. (2008): A spectral approach to simulating intrinsic random fields with power and spline generalized covariances. Computational Geosciences 12(1): 121-132

[70] Emery, X., Ortiz, J.M, Cáceres, A.M. (2008): Geostatistical modeling of rock type domains with spatially varying proportions: application to a porphyry copper deposit. The Journal of the Southern African Institute of Mining and Metallurgy 108(5): 285-292

[71] Emery, X., Robles, L.N. (2009): Simulation of mineral grades with hard and soft conditioning data: application to a porphyry copper deposit. Computational Geosciences 13(1): 79-89

[72] Farmer, C.L. (1992): Numerical rocks. In: King, P.R. (Ed.), The Mathematics of Oil Recovery. Clarendon Press, Oxford, pp. 437–447

[73] Flandrin, P. (1992): Wavelet analysis and synthesis of fractional Brownian motion. IEEE Trans. Inf. Theory 38(2): 910–917

[74] Fontaine, L., Beucher, H. (2006): Simulation of the Muyumkum uranium roll front deposit by using truncated plurigaussian method. In: Proceedings of the 6th international mining geology conference, Darwin, NT Australia, 21-23 Aug 2006

[75] Fossen, H., Teyssier, C., Whitney, D.L. (2013): Transtensional folding. Journal of Structural Geology 56: 89-102

[76] Fournier, A., Fussell, D., Carpenter, R.L. (1982): Computer rendering of stochastic models. Commun. ACM 25(6): 371–384

[77] Freulon, X., de Fouquet, C. (1991): Remarques sur la pratique des bandes tournantes à 3D. In: de Fouquet, C. (ed.) Compte Rendu des Journées de Géostatistique, Cahiers de Géostatistique, Fasc. 1, Ecole des Mines de Paris, pp. 101-117.

[78] Frikken, P.H. (2003): Breccia-hosted copper-molybdenum mineralization at Río Blanco, Chile. Ph.D. Dissertation, University of Tasmania, Australia

[79] Frikken, P.H., Cooke, D.R., Walshe, J.L., Archibald, D., Skarmeta, J., Serrano, L., Vargas, R. (2005): Mineralogical and isotopic zonation in the Sur-Sur tourmaline breccia, Río Blanco-Los Bronces Cu-Mo deposit, Chile: implications for ore genesis. Economic Geology 100: 935–961

[80] Fuentes, M. (2001): A high frequency kriging approach for non-stationary environmental processes. Environmetrics 12(5): 469-483

[81] Fuentes, M. (2002): Spectral methods for nonstationary spatial processes. Biometrika 89: 197- 210

[82] Galli, A., Beucher, H., Le Loc'h, G., Doligez, B. (1994): The pros and cons of the truncated Gaussian method. In: Armstrong, M., Dowd, P.A. (eds.) Geostatistical simulations. Kluwer, Dordrecht, pp. 217-233.

[83] Galli, A., Gao, H. (2001): Rate of convergence of the Gibbs sampler in the Gaussian case. Mathematical Geology 33(6): 653–677.

[84] Gelman, A., Carlin, J.B., Stern, H.S., Rubin, D.B., (2004): Bayesian Data Analysis. Chapman & Hall/CRC, Boca Raton

[85] Geman, S., Geman, D. (1984): Stochastic relaxation, Gibbs distributions, and the Bayesian restoration of images. IEEE Transactions on Pattern Analysis and Machine Intelligence 6: 721–741

[86] Gentle, J.E. (2009): Computational statistics. Springer, New York

[87] Gneiting, T. (1999): The correlation bias for two-dimensional simulations by turning bands. Mathematical Geology 31(2): 195–211.

[88] Gneiting, T., Sasvári, Z., Schlather, M. (2001): Analogies and correspondences between variograms and covariance functions. Advances in Applied Probability 33(3): 617–630

[89] Gómez–Hernández, J., Journel, A.G. (1993): Joint sequential simulation of multigaussian fields. In: Soares, A. (ed.) Geostatistics Troia'92. Kluwer Academic, Dordrecht, pp. 85–94

[90] Goovaerts, P. (1997): Geostatistics for Natural Resources Evaluation. Oxford University Press, New York

[91] Guardiano, F., Srivastava, M. (1993): Multivariate geostatistics: beyond bivariate moments. In: Soares, A. (ed.) Geostatistics Tróia '92. Kluwer Academic, Dordrecht, pp. 133–144

[92] Guilbert, J.M., Park, C.F. (1986) The Geology of Ore Deposits. W.H. Freeman, New York

[93] Guttorp, P., Sampson, P.D. (1994): Methods for estimating heterogeneous spatial covariance functions with environmental applications. In: Patil, G.P., Rao, C.R. (eds.) Handbook of Statistics XII: Environmental Statistics. Elsevier, New York, 663-690

[94] Haas, T. (1990): Kriging and automated variogram modeling within a moving window. Atmospheric Environment, Part A: General Topics 24(7): 1759-1769

[95] Haas, T.C. (1995): Local prediction of a spatio-temporal process with an application to wet sulfate deposition. Journal of the American Statistical Association 90: 1189-1199

[96] Higdon, D. (2002): Space and space-time modeling using process convolutions. In: Anderson, C.W., Barnett, V., Chatwin, P.C., El-Shaarawi, A.H. (eds.) Quantitative Methods for Current Environmental Issues. Springer, London, 37-54

[97] Higdon, D., Swall, J., Kern, J. (1999): Non-stationary spatial modeling. In: Bernardo, J.M., Berger, J.O., Dawid, A.P., Smith, A.F.M. (eds.) Bayesian Statistics 6, Oxford University Press, Oxford, 761-768

[98] Hollings, P., Cooke, D., Clark, A. (2005): Regional geochemistry of tertiary igneous rocks in Central Chile: implications for the geodynamic environment of giant porphyry copper and epithermal gold mineralization. Economic Geology 100: 887–904

[99] Houlding, S.W. (1994): 3D Geoscience Modeling, Computer Techniques for Geological Characterization. Springer, New York, p. 321

[100] Huang, C.F., Yao, Y.G., Cressie, N., Hsing, T.L. (2009): Multivariate intrinsic random functions for cokriging. Mathematical Geosciences 41(8): 887-904

[101] Hudson, G., Wackernagel, H. (1994): Mapping temperature using kriging with external drift: theory and an example from Scotland. International Journal of Climatology 14(1): 77-91

[102] Journel, A.G. (1983): Nonparametric estimation of spatial distribution. Mathematical Geology 15 (3): 445–468

[103] Journel, A.G. (1989): Fundamentals of geostatistics in five lessons. Short Course in Geology, vol. 8. American Geophysical Union

[104] Journel, A.G., Alabert, F.G. (1988): Focusing on spatial connectivity of extreme valued attributes: stochastic indicator models of reservoir heterogeneities, SPE Paper 18324

[105] Journel, A.G., Huijbregts, C.J. (1978): Mining Geostatistics. Academic Press, London

[106] Journel, A.G., Isaaks, E.H. (1984): Conditional indicator simulation: application to a Saskatchewan uranium deposit. Mathematical Geology 16(7): 685–718

[107] Journel, A.G., Rossi, M.E. (1989): When do we need a trend model in kriging? Mathematical Geology 21(7): 715-739

[108] Kay, S.M., Mpodozis, C. (2001): Central Andes ore deposits linked to evolving shallow subduction systems and thickening crust. GSA Today 11:4–9

[109] Kay, S.M., Mpodozis, C. (2002): Magmatism as a probe to the Neogene shallowing of the Nazca plate beneath the modern Chilean flat-slab. Journal of South American Earth Sciences 15(1): 39–57

[110] Kay, S.M., Mpodozis, C., Coira, B. (1999): Neogene magmatism, tectonism and mineral deposits of the central Andes. In: Skinner, B.J. (ed.) Geology and ore deposits of the Central Andes. Special Publication No. 7. Society of Economic Geologists, Littleton, pp. 7–59

[111] Kim, H.M., Mallick, B.K., Holmes, C.C. (2005): Analyzing nonstationary spatial data using piecewise Gaussian processes. Journal of the American Statistical Association 100(470): 653-668

[112] Kirkpatrick, S., Gelatt, C.D., Vecchi, M.P. (1983): Optimization by simulated annealing. Science 220(4598): 671–680.

[113] Kitanidis, P.K. (1983): Statistical estimation of polynomial generalized covariance functions and hydrologic applications. Water Resources Research 19(4): 909-921

[114] Kitanidis, P.K. (1985): Minimum-variance unbiased quadratic estimation of covariances of regionalized variables. Mathematical Geology 17(2): 195-208

[115] Kitanidis, P.K. (1999): Generalized covariance functions associated with the Laplace equation and their use in interpolation and inverse problems. Water Resources Research 35(5): 1361–1367

[116] Krige, D.G. (1997): A practical analysis of the effects of spatial structure and of data available and accessed, on conditional biases in ordinary kriging. In: Baafi, E.Y., Schofield, N.A. (eds.) Geostatistics Wollongong 96. Kluwer Academic, Dordrecht, pp. 799-810

[117] Kunsch, H.R., Papritz, A., Bassi, F. (1997): Generalized cross-covariances and their estimation. Mathematical Geology 29(6): 779-799

[118] Lantuéjoul, C. (1994): Non conditional simulation of stationary isotropic multigaussian random functions. In: Armstrong, M., Dowd, P.A. (eds.) Geostatistical Simulations, pp. 147–177. Kluwer, Dordrecht

[119] Lantuéjoul, C. (2002): Geostatistical Simulation, Models and Algorithms. Springer, Berlin

[120] Lantuéjoul, C., Desassis, N. (2012): Simulation of a Gaussian random vector: a propagative version of the Gibbs sampler. In: Ninth International Geostatistics Congress, Oslo.

[121] Larrondo, P., Leuangthong, O., Deutsch, C.V. (2004): Grade estimation in multiple rock types using a linear model of coregionalization for soft boundaries. In: Magri, E., Ortiz, J., Knights, P., Henríquez, F., Vera, M., Barahona, C. (eds.) International Conference on Mining Innovation MININ 2004. Gecamin Ltda, Santiago, pp. 187-196

[122] Le Cointe, P. (2006): Kriging with partial differential equations in hydrogeology. Master's thesis, Université Pierre et Marie Curie, Ecole des Mines de Paris & Ecole Nationale du Génie Rural des Eaux et Forêts, Paris

[123] Le Loc'h, G., Beucher, H., Galli, A., Doligez, B. (1994): Improvement in the truncated Gaussian method: combining several Gaussian functions. In: ECMOR IV, Fourth European Conference on the Mathematics of Oil Recovery. Røros, Norway

[124] Le Loc'h, G., Galli, A. (1997): Truncated plurigaussian method: theoretical and practical points of view. In: Baafi, E.Y., Schofield, N.A. (Eds.), Geostatistics Wollongong'96. Kluwer Academic, Dordrecht, pp. 211–222.

[125] Lowell, J.D., Guilbert, J.M. (1970) Lateral and vertical alteration-mineralization zoning in porphyry ore deposits. Economic Geology 65: 373-408

[126] Machuca-Mory, D., Deutsch, C.V. (2008): Location dependent variograms. In: Ortiz, J.M., Emery, X. (eds.) Proceedings of the Eighth International Geostatistics Congress. Gecamin Ltda, Santiago, 497-506

[127] Machuca-Mory, D.F., Deutsch, C.V. (2013): Non-stationary geostatistical modeling based on distance weighted statistics and distributions. Mathematical Geosciences 45(1): 31-48

[128] Madani, N., Emery, X. (2015): Simulation of geo-domains accounting for chronology and contact relationships: application to the Río Blanco copper deposit. Stochastic Environmental Research and Risk Assessment 29: 2173–2191

[129] Mallet, J.L. (1992): Discrete smooth interpolation. Computer Aided Design 24(4): 263–270.

[130] Mallet, J.L. (2002): Geomodeling. Oxford University Press, New York, pp. 624

[131] Mantoglou, A., Wilson, J.L. (1982): The turning bands method for simulation of random fields using line generation by a spectral method. Water Resources Research 18(5): 1379–1394.

[132] Mardia, K.V., Goodall, C.R. (1993): Spatial-temporal analysis of multivariate environmental monitoring data. In: Patil, G.P., Rao, C.R. (eds.) Multivariate Environmental Statistics. Elsevier, Amsterdam, 347-385

[133] Mariethoz, G., Caers, J. (2014): Multiple-point Geostatistics: Stochastic Modeling with Training Images. Wiley, New York

[134] Mariethoz, G., Renard, P., Cornaton, F., Jaquet, O. (2009): Truncated plurigaussian simulations to characterize aquifer heterogeneity. Ground Water 47(1): 13-24

[135] Marshall, R.J., Mardia, K.V. (1985): Minimum norm quadratic estimation of components of spatial covariance. Mathematical Geology 17(5): 517-525

[136] Matheron, G. (1968): Modèle séquentiel de partition aléatoire. Technical Report, Centre de Morphologie Mathématique, Ecole des Mines de Paris

[137] Matheron, G. (1969): Le krigeage universel. Cahiers du Centre de Morphologie Mathématique de Fontainebleau, Fasc. 1, Ecole Nationale Supérieure des Mines de Paris

[138] Matheron, G. (1971): The Theory of Regionalized Variables and its Applications, Ecole Nationale Supérieure des Mines de Paris, Fontainebleau, 212 p

[139] Matheron, G. (1973): The intrinsic random functions and their applications. Advances in Applied Probability 5(3): 439-468

[140] Matheron, G. (1975): Random sets and Integral Geometry. John Wiley & sons, New York.

[141] Matheron, G., Beucher, H., de Fouquet, C., Galli, A., Guerillot, D., Ravenne, C. (1987): Conditional simulation of the geometry of fluvio deltaic reservoirs. SPE 1987 Annual technical conference and exhibition, Dallas, Texas, pp 591-599. SPE

[142] Matheron, G., Beucher, H., de Fouquet, C., Galli, A., Ravenne, C. (1988): Simulation conditionnelle à trois facies d'une falaise de la formation du Brent. Sciences de la Terre, Série Informatique Géologique 28: 213–249.

[143] McLennan, J., Deutsch, C.V. (2007): BOUNDSIM: Implicit boundary modeling. In: Magri, E. (ed.) Proceedings of the 33rd International Symposium on Applications of Computers and Operations Research in the Mineral Industry APCOM 2007, Santiago, Chile, pp. 41-48

[144] Mejia, J.M., Rodríguez-Iturbe, I. (1974): On the synthesis of random field sampling from the spectrum: An application to the generation of hydrologic spatial processes. Water Resources Research 10(4): 705-711

[145] Meyn, S., Tweedie, R.L. (2009): Markov Chains and Stochastic Stability, second edition. Cambridge University Press, Cambridge

[146] Monestiez, P., Switzer, P. (1991): Semiparametric estimation of nonstationary spatial covariance models by metric multidimensional scaling. Technical Report, Department of Statistics, Stanford University, Stanford

[147] Moulière, D. (1998): Intégration d'information sismiques pour la simulation de reservoirs. Thèse de Docteur de l'Ecole des Mines de Paris, pp. 182

[148] Moulière, D., Beucher, H., Hu, LY., Fournier, F., Terdich, P., Melchiori, F., Griffi, G. (1997): Integration of seismic derived information in reservoir stochastic modeling using the truncated Gaussian approach. In: Baafi, E., Schofield, N.A. (eds.) Geostatistics Wollongong '96. Kluwer Academic, Dordrecht, pp. 374-385

[149] Myers, D.E. (1989): To be or not to be... stationary? That is the question. Mathematical Geology 21(3): 347–362.

[150] Nychka, D., Wikle, C., Royle, A. (2002): Multiresolution models for nonstationary spatial covariance functions. Statistical Modeling 2: 299-314

[151] Ortiz, J.M. (2003): Characterization of high order correlation for enhanced indicator simulation. Ph.D. Dissertation, University of Alberta

[152] Ortiz, J.M., Deutsch, C.V. (2004): Indicator simulation accounting for multiple-point statistics. Mathematical Geology 36(5): 545–565

[153] Ortiz, J.M., Emery, X. (2006): Geostatistical estimation of mineral resources with soft geological boundaries: a comparative study. Journal of the South African Institute of Mining and Metallurgy 106(8): 577-584

[154] Pardo-Igúzquiza, E. (1997): GCINFE: A computer program for inference of polynomial generalized covariance functions. Computers & Geosciences 23(2): 163-174

[155] Pintore, A., Holmes, C.C. (2005): A dimension-reduction approach for spectral tempering using empirical orthogonal functions. In: Leuangthong, O., Deutsch, C.V. (eds.) Geostatistics Banff 2004. Springer, Dordrecht, pp. 1007-1015

[156] Ravenne, C., Galli, A., Doligez, B., Beucher, H., Eschard, R. (2002): Quantification of facies relationships via proportion curves. In: Armstrong, M., Bettini, C., Champigny, N., Galli, A., Remacre, A. (eds.) Geostatistics Rio 2000. Kluwer Academic, Dordrecht, pp. 19-40

[157] Renard, D. (1989): Automatic structure recognition. In: Armstrong, M. (ed.) Geostatistics. Kluwer, Dordrecht, 579-590

[158] Ripley, B.D. (1987): Stochastic Simulation. John Wiley & Sons, New York.

[159] Rivest, M., Marcotte, D., Pasquier, P. (2008): Hydraulic head field estimation using kriging with an external drift: a way to consider conceptual model information. Journal of Hydrology 361(3-4): 349-361

[160] Rivoirard, J. (1994): Introduction to Disjunctive Kriging and Non-Linear Geostatistics. Oxford University Press, New York.

[161] Rivoirard, J. (2002): On the structural link between variables in kriging with external drift. Mathematical Geology 34(7): 797-808

[162] Roberts, G.O., Sahu, S.K. (1997): Updating schemes, correlation structure, blocking and parameterization for the Gibbs sampler. Journal of the Royal Statistical Society B59(2): 291–317

[163] Robles, L., Emery, X., Ortiz, J.M. (2007): Geostatistical simulation of mineral grades in the presence of spatial trends. In: Magri, E.J. (ed.) Proceedings of the 33rd International Symposium on Applications of Computers and Operations Research in the Mineral Industry APCOM 2007, Santiago, Chile

[164] Rondon, O. (2009): A look at the Plurigaussian simulation for a nickel laterite deposit. Presented at the 7th international mining & geology conference, Perth

[165] Roth, C., Armstrong, M., Galli, A., Le Loc'h, G. (1998) Using plurigaussian simulation to reproduce lithofacies with contrasting anisotropies. In: Proceedings of the International

Symposium on the Application of Computers and Operations Research in the Mineral Industry APCOM' 98, Institution of Mining and Metallurgy, London.

[166] Rothman, D.H. (1985): Nonlinear inversion, statistical mechanics and residual statics estimation. Geophysics 50: 2784–2796.

[167] Sampson, P.D., Damian, D., Guttorp, P. (2001): Advances in modeling and inference for environmental processes with nonstationary spatial covariance. In: Monestiez, P., Allard, D., Froidevaux, R. (eds.) GeoENV 2000: Geostatistics for Environmental Applications. Kluwer, Dordrecht, pp. 17-32

[168] Sampson, P.D., Guttorp, P.T. (1992): Nonparametric estimation of nonstationary spatial covariance structure. Journal of the American Statistical Association 87: 108-119

[169] Séguret, S., Huchon, P. (1990): Trigonometric kriging: a new method for removing the diurnal variation from geomagnetic data. Journal of Geophysical Research 95(B13): 21383-21397

[170] Sellan, F. (1995): Wavelet transform based fractional Brownian-motion synthesis. Compte Rendu de l'Académie des Sciences, Série I Mathématique 321(3): 351–358

[171] Serra, J. (1982): Image analysis and mathematical morphology. Academic Press, London

[172] Serrano, L., Vargas, R., Stambuk, V., Aguilar, C., Galeb, M., Holmgren, C., Contreras, A., Godoy, S., Vela, I., Skewes, M.A., Stern, C.R. (1996): The late Miocene to early Pliocene Río Blanco-Los Bronces copper deposit, Central Chilean Andes. In: Camus, F., Sillitoe, R.H., Petersen, R. (eds.) Andean copper deposits: new discoveries, mineralization, styles and metallogeny. Special Publication No. 5. Society of Economic Geologists, Littleton, pp. 119–130

[173] Shinozuka, M. (1971): Simulation of multivariate and multidimensional random processes. The Journal of the Acoustical Society of America, 49(1B): 357-367.

[174] Skewes, M.A., Holmgren, C., Stern, C.R. (2003): The Donoso copper-rich, tourmaline-bearing breccia pipe in central Chile: petrologic, fluid inclusion and stable isotope evidence for an origin from magmatic fluids. Miner Deposita 38(1): 2–21

[175] Skewes, M.A., Stern, C.R. (1995): Genesis of the late Miocene to Pliocene copper deposits of central Chile in the context of Andean magmatic and tectonic evolution. International Geology Review 37(10): 893–909

[176] Skewes, M.A., Stern, C.R. (1996): Late Miocene mineralized breccias in the Andes of central Chile: Sr and Nd isotopic evidence for multiple magmatic sources. In: Camus, F., Sillitoe, R.H., Petersen, R. (eds.) Andean copper deposits: new discoveries, mineralization, styles and metallogeny. Special Publication No. 5. Society of Economic Geologists, Littleton, pp. 119–130

[177] Skvortsova, T., Armstrong, M., Beucher, H., Forkes, J., Thwaites, A., Turner, R. (2001): Applying plurigaussian simulations to a granite hosted orebody. In: Kleingeld, W.J., Krige, D.G. (eds.) Geostats 2000 Cape Town. Geostatistical Association of Southern Africa, Johannesburg, pp. 904–911

[178] Skvortsova, T., Beucher, H., Armstrong, M., Forkes, J., Thwaites, A., Turner, R. (2002): Simulating the geometry of a granite-hosted uranium orebody. In: Armstrong, M., Bettini, C., Champigny, N., Galli, A., Remacre, A. (eds.) Geostatistics Rio 2000. Kluwer, Dordrecht, pp. 85–99

[179] Smith, R.L. (1996): Estimating nonstationary spatial correlations. University of North Carolina.

[180] Stambuk, V., Aguilar, C., Blondel, J., Galeb, M., Serrano, L., Vargas, R. (1988): Geología del yacimiento Río Blanco. Technical Report. Codelco-Chile, División Andina

[181] Stein, M.L. (1986): A modification of minimum norm quadratic estimation of a generalized covariance function for use with large data sets. Mathematical Geology 18(7): 625-633

[182] Stein, M.L. (2001): Local stationarity and simulation of self-affine intrinsic random functions. IEEE Trans. Inf. Theory 47(4): 1385–1390

[183] Stein, M.L. (2002): Fast and exact simulation of fractional Brownian surfaces. Journal of Computational and Graphical Statistics 11(3): 587–599

[184] Stephenson, J., Holmes, C., Gallagher, K., Pintore, A. (2005): A statistical technique for modeling non-stationary spatial processes. In: Leuangthong, O., Deutsch, C.V. (eds.) Geostatistics Banff 2004. Springer, Dordrecht, pp. 125-134

[185] Stoyan, D., Kendall, W.S., Mecke, J. (1996): Stochastic Geometry and Its Applications, second ed. Wiley, New York

[186] Strebelle, S., Journel, A.G. (2000): Sequential simulation drawing structures from training images. In: Kleingeld, W.J., Krige, D.G. (eds.) Geostats 2000 Cape Town. Geostatistical Association of Southern Africa, Johannesburg

[187] Stroet, C., Snepvangers, J. (2005): Mapping curvilinear structures with local anisotropy kriging. Mathematical Geology 37(6): 635-649

[188] Suárez-Arriaga, M.C., Samaniego, F. (1998): Intrinsic random functions of high order and their application to the modeling of non-stationary geothermal parameters. In: Proceedings of the Twenty-third Workshop on Geothermal Reservoir Engineering, pp. 169–175. Technical report SGP-TR-158, Stanford University, Stanford

[189] Sullivan, J., Satchwell, S., Ferraz, G. (2007): Grade estimation in the presence of trends – the adaptive search approach applied to the Andina Copper Deposit, Chile. In: Magri, E.J.

(ed.) Proceedings of the 33rd International Symposium on the Application of Computers and Operations Research in the Mineral Industry. Gecamin Ltda, Santiago, pp. 35-143

[190] Tierney, L. (1994): Markov chains for exploring posterior distributions. The Annals of Statistics 22(4): 1701–1762

[191] Tompson, A.F.B., Ababou, R., Gelhar, L.W. (1989): Implementation of the three-dimensional turning bands random field generator. Water Resources Research 25(8): 2227–2243

[192] Vargas, R., Gustafson, L.B., Vukasovic, M., Tidy, E., Skewes, M.A. (1999): Ore breccias in the Río Blanco-Los Bronces copper deposit, Chile. In: Skinner, B.J. (ed.) Geology and ore deposits of the Central Andes. Special Publication No. 7. Society of Economic Geologists, Littleton, pp. 281–297

[193] Vargas-Guzman, J.A. (2008): Transitive geostatistics for stepwise modeling across boundaries between rock regions. Mathematical Geology 40(8): 861-873

[194] Viseur, S. (1999): Stochastic Boolean simulation of fluvial deposits: a new approach combining accuracy with efficiency. In: Proceedings of the 1999 SPE Annual Technical Conference and Exhibition, Houston. Society of Petroleum Engineers, SPE 56688

[195] Vistelius, A.B. (1989): Principles of Mathematical Geology. Kluwer Academic Publishers, Dordrecht, p. 500

[196] Voss, R.F. (1985): Random fractal forgeries. In: Earnshaw, R.A. (ed.) Fundamental Algorithms for Computer Graphics, pp. 805–835. Springer, Berlin

[197] Wackernagel, H. (2003): Multivariate Geostatistics: An Introduction with Applications. Springer-Verlag, Berlin

[198] Warnaars, F., Holgrem, C., Barassi, S. (1985): Porphyry copper and tourmaline breccias at Los Bronces-Río Blanco, Chile. Economic Geology 80: 1544–1565

[199] Xu, C., Dowd, P.A., Mardia, K.V., Fowell, R.J. (2006): A flexible true plurigaussian code for spatial facies simulations. Computers & Geosciences 32(10): 1629-1645

[200] Xu, W. (1996): Conditional curvilinear stochastic simulation using pixel-based algorithms. Mathematical Geology 28(7): 937-949

[201] Yin, Z.M. (1996): New methods for simulation of fractional Brownian motion. Journal of Computational Physics 127(1): 66–72

[202] Yunsel, T., Ersoy, A. (2011): Geological modeling of gold deposit based on grade domaining using plurigaussian simulation technique. Natural Resources Research 20(4): 1-19

[203] Yunsel, T., Ersoy, A. (2013): Geological modeling of rock type domains in the Balya (Turkey) lead-zinc deposit using plurigaussian simulation. Central European Journal of Geosciences 5(1): 77-89

[204] Zeldin, B.A., Spanos, P.D. (1996): Random field representation and synthesis using wavelet bases. J. Appl. Mech.—Trans ASME 63(4): 946–952

[205] Zimmerman, D.L. (1989): Computationally efficient restricted maximum likelihood estimation of generalized covariance functions. Mathematical Geology 21(7): 655-672

Appendix

This appendix reproduces a paper that has been published in Stochastic Environmental Research and Risk Assessment, which presents an application of a non-stationary plurigaussian model to the Río Blanco case study. Contrary to the proposal of this thesis, non-stationarity is obtained by using spatially-varying truncation thresholds, which are determined by inferring the local domain proportions on the basis of the interpreted geological model. The similarity between this model and the realizations of the rock domains is largely explained because the former is used to define the input local proportions of the plurigaussian model.

The information of the paper is the following.

Title

Simulation of geo-domains accounting for chronology and contact relationships: application to the Río Blanco copper deposit

Authors

Nasser Madani, Xavier Emery

Journal

Stochastic Environmental Research and Risk Assessment

Publication date

December 2015, Volume 29, Issue 8, pp. 2173-2191

Simulation of geo-domains accounting for chronology and contact relationships: Application to the Río Blanco copper deposit

Nasser Madani[1] and Xavier Emery[2]

Abstract

The plurigaussian model is increasingly used for simulating geo-domains and quantifying geological uncertainty in the subsurface. However, because they rely on the truncation of only two Gaussian random fields, the current implementations of this model are often restricted in the number of geo-domains that can be simulated and in their contact relationships. A solution to overcome these restrictions is to increase the number of underlying Gaussian random fields. Such an approach yields a very flexible model, able to reproduce the contact relationships between geo-domains in agreement with their chronology (i.e., such that younger geo-domains cross-cut the older ones), as well as the geo-domain proportions and spatial correlation structure.

The proposed approach is applied to a dataset from the Río Blanco copper deposit in the Chilean Central Andes, in which it is of interest to simulate the layout of seven rock units (andesite, granitoid, tourmaline breccia, monolithic breccia, magmatic breccia, porphyry and pipe). The results are used to map the probabilities of occurrence of the rock units and to identify the sectors where the interpreted rock model is uncertain.

Keywords: Geological uncertainty; geological heterogeneity; domaining; plurigaussian simulation; hierarchical modeling

[1] Department of Mining Engineering, University of Chile;
Advanced Mining Technology Center, University of Chile;
CSIRO-Chile International Center of Excellence in Mining and Mineral Processing;
E-mail address: nasser.madani@ing.uchile.cl

[2] Corresponding author
Department of Mining Engineering, University of Chile;
Advanced Mining Technology Center, University of Chile;
Postal address: Avenida Tupper 2069, Santiago 8370451, Chile
Phone: +56-2-29780650
E-mail address: xemery@ing.uchile.cl

1. Introduction

The spatial modeling of geological domains (hereafter named geo-domains) is important to characterize rock properties and geological heterogeneities in the subsurface. Examples of applications include groundwater hydrology, mining and petroleum exploration, in which it is of interest to describe heterogeneous aquifers, deposits and reservoirs at multiple scales, in order to predict the distribution of in-situ resources and to manage subsurface activities (e.g., forecast of production performance and remediation procedures) (De Marsily et al., 2005; Journel and Huijbregts, 1978; Deutsch, 2002).

Since the boundaries of the geo-domains are generally uncertain, stochastic spatial models are increasingly used in place of, or in complement to, deterministic models. They rely on the use of simulation techniques that no longer provide a unique layout of the geo-domains, but a set of alternative scenarios that mimic the actual distribution of the geo-domains in space (Chilès and Delfiner, 2012).

To date, a variety of simulation approaches have been developed for modeling spatial geo-domains, including object-based models (Lantuéjoul, 2002), sequential indicator simulation (Journel and Alabert, 1990), simulation based on multiple-point statistics (Strebelle, 2002; Rezaee et al., 2014), truncated Gaussian simulation (Matheron et al., 1987, 1988) and plurigaussian simulation (Armstrong et al., 2011). The latter offers a flexible framework, as it allows incorporating topological constraints (contact relationships) on the simulated geo-domains, in addition to reproducing the proportions and the spatial correlation structure of these domains. In the past decade, it has found wide acceptance in the field of natural resources evaluation, in particular, for modeling aquifers, petroleum reservoirs and ore bodies of varied natures such as porphyry, epithermal, granite-hosted, carbonate hosted, roll front and lateritic deposits (Skvortsova et al., 2001, 2002; Deraisme and Field, 2006; Fontaine and Beucher, 2006; Carrasco et al., 2007; Emery and González, 2007a, 2007b; Emery et al., 2008; Mariethoz el al., 2009; Rondon, 2009; Yunsel and Ersoy, 2011, 2013; Jeannée et al., 2013; Talebi et al., 2013, 2014; Deutsch and Deutsch, 2014). In most of these studies, if not all, it calls the attention that the simulation is restricted to a few geo-domains (no more than five), which can be explained because of the difficulty in imposing specific contact relationships with a higher number of geo-domains.

The aim of this paper is twofold. First, from a methodological point of view, it is of interest to present an extension of the currently used plurigaussian model, in order to increase its versatility and to allow modeling numerous geo-domains with possible complex contact relationships. Second, our aim is to apply this model to the simulation of seven rock type domains in the Río Blanco deposit, a giant porphyry copper deposit located in the Central Andes of Chile.

2. Methodology

2.1. Truncated Gaussian simulation

The truncated Gaussian model was coined in the late 1980s (Matheron et al., 1987, 1988) for simulating geo-domains (lithofacies) in oil reservoirs. It relies on a Gaussian random field (usually assumed to be second-order stationary, with zero mean and unit variance) and a set of truncation thresholds, defining each geo-domain as the set of points in space where the value of the Gaussian random field belongs to an interval defined with these thresholds. For example, to simulate two geo-domains D_1 and D_2, one would define a unique threshold t and associate D_1 with the points of space where the Gaussian random field is below t, and D_2 with the points where this field is above t (Fig. 1). Likewise, to simulate N geo-domains, one has to define N–1 thresholds. Once the ordering of the geo-domains has been chosen, there is a one-to-one relationship between the thresholds and the proportion of space covered by each geo-domain (Armstrong et al., 2011).

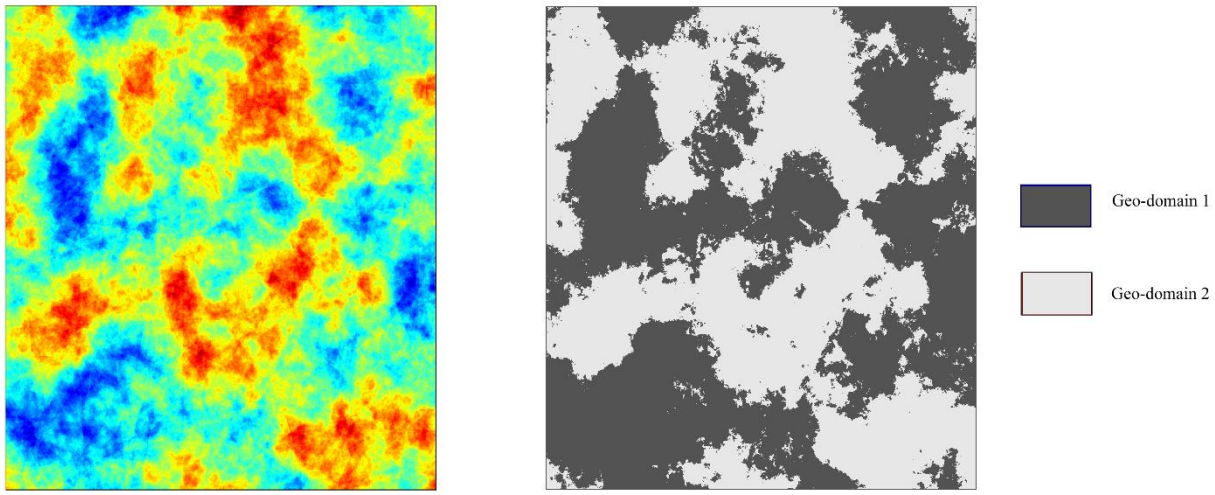

Figure 1. Simulated Gaussian random field (left) and associated geo-domains (right)

The auto-covariance function $C(\mathbf{h})$ of the underlying Gaussian random field is related to the spatial correlation structure of the geo-domains, which can be represented by the variogram of the geo-domain indicators (Armstrong et al., 2011; Chilès and Delfiner, 2012). For example, in the case of two geo-domains defined by a single truncation threshold t, one has:

$$\gamma_t(\mathbf{h}) = G(t)[1-G(t)] - \frac{1}{2\pi}\int_0^{\arcsin[C(\mathbf{h})]} \exp\left[-\frac{t^2}{1+\sin\theta}\right] d\theta \qquad (1)$$

where $C(\mathbf{h})$ is the auto-covariance function of the standard Gaussian random field, G is the standard normal cumulative distribution function, and $\gamma_t(\mathbf{h})$ is the variogram of the indicator

obtained by truncating the Gaussian random field at threshold *t*. The calculation of the integral in Eq. (1) can be performed by numerical integration or by using expansions into series (Kyriakidis et al., 1999; Emery, 2007). In practice, there is information about the geo-domain indicators (0 or 1) at sampling locations, which allows calculating the indicator variograms and fitting a suitable model for the covariance function of the Gaussian random field.

Once the model is specified, the simulation conditional to the sampling information can be performed through the following steps (Lantuéjoul, 2002):

1) Simulation of the Gaussian random field at the locations where the geo-domains are known. To this end, an iterative procedure (Gibbs sampler) is used, which allows converting the indicator data (0 or 1) into Gaussian data.

2) Simulation of the Gaussian random field at the target locations. At this stage, many algorithms can be used: turning bands, sequential, spectral, etc. (Lantuéjoul, 2002; Chilès and Delfiner, 2012).

3) Truncation in order to obtain a simulation of the two geo-domains (geo-domain 1 when the simulated Gaussian random field is smaller than the truncation threshold *t*, geo-domain 2 otherwise).

2.2. Plurigaussian simulation

The plurigaussian model (Galli et al., 1994; Le Loc'h and Galli, 1997) is a generalization of the truncated Gaussian model, aimed at producing a wider range of patterns and allowing for more complicated types of contacts between geo-domains. The basic idea is to use several Gaussian random fields and to define the geo-domains by a multivariate truncation rule. For instance, a three-domain truncation rule can be defined on the basis of two Gaussian random fields and two thresholds: if the first Gaussian random field is less than the first threshold, then one finds the first geo-domain; otherwise, if the second Gaussian random field is less than the second threshold, one finds the second geo-domain; otherwise, one finds the third geo-domain. Such a truncation rule can be represented through a two-dimensional flag, in which each axis represents one Gaussian random field (Fig. 2C). In practice, to restrict the number of parameters and to ease their inference, one usually works with two Gaussian random fields, which are furthermore assumed to be independent (such an independence assumption is sometimes not made, e.g., Dowd et al., 2003; Armstrong et al., 2011). With this simplification, the plurigaussian model requires defining:

- the truncation rule: it has an impact on the contact relationships between geo-domains (which domains can be in contact and which domains cannot);

- the truncation thresholds: they have an impact on the geo-domain proportions;

- the auto-covariance functions of the Gaussian random fields: they have an impact on the variograms of the geo-domain indicators.

One of the current limitations of the plurigaussian model is the design of a two-dimensional flag representing the truncation rule. The choice of this rule has implications on the spatial relationships between geo-domains, in particular, with respect to permissible and forbidden contacts. For instance, Fig. 2C shows that the three geo-domains can touch each other, whereas Fig. 2D shows two geo-domains that cannot have contact together. Most often, the flag consists of a partition of the two-dimensional space into rectangles (Armstrong et al., 2011) or unions of rectangles (Emery, 2007), although more general designs can be considered (Allard et al., 2012; Deutsch and Deutsch, 2014).

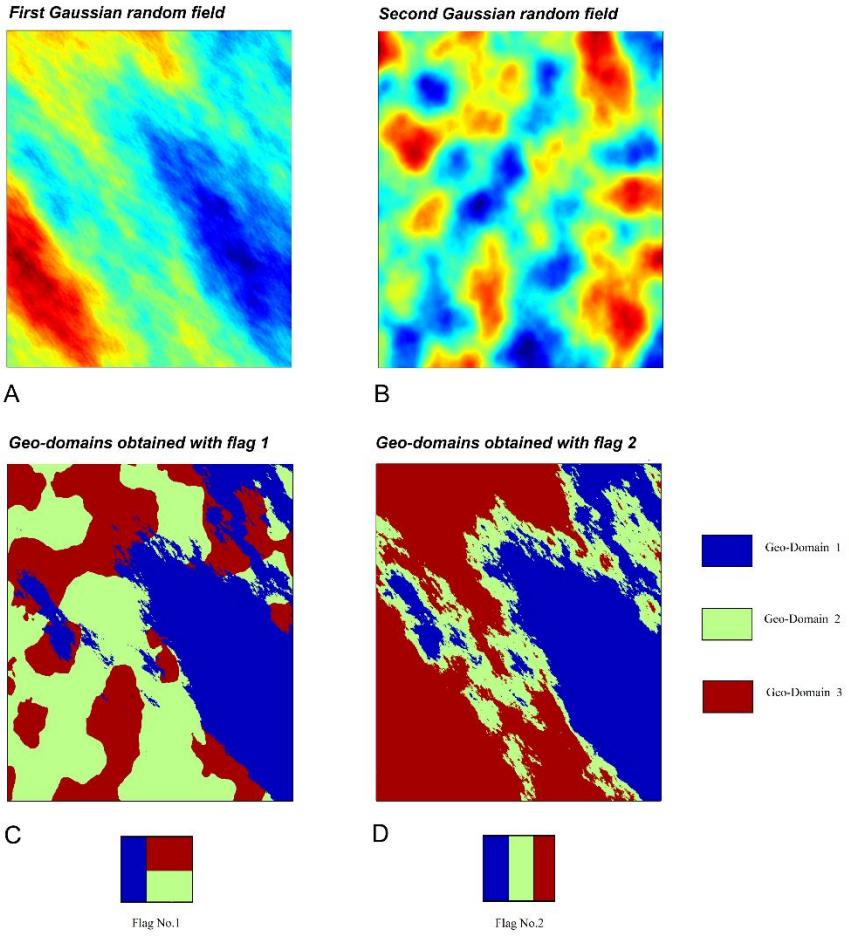

Figure 2. Simulated Gaussian random fields (top)
and associated geo-domains (bottom)

2.3. Proposal: hierarchical approach

2.3.1. Principle

Defining a truncation rule through a two-dimensional flag offers the following advantages:

1) One can visually control the contact relationships between geo-domains: two geo-domains are in contact in space if they are in contact on the flag representing the truncation rule.

2) One can also control the chronology relationships between geo-domains. For instance, in Fig. 2C, the first geo-domain (1) appears in the foreground (first layer) and can then be interpreted as a younger domain that cross-cuts the other two older geo-domains (2 and 3), which appear in the background (last layer).

However, by restricting to a two-dimensional flag (as in most applications), one is often limited in the number of geo-domains that can be modeled, especially when all these geo-domains are mutually in contact, a situation that often arises in practice. For instance, Fig. 3 presents a few examples of flags with four geo-domains (modified from Armstrong et al., 2011): none of them allows each geo-domain to be in contact with each other, as there is always some prohibited contact between geo-domains.

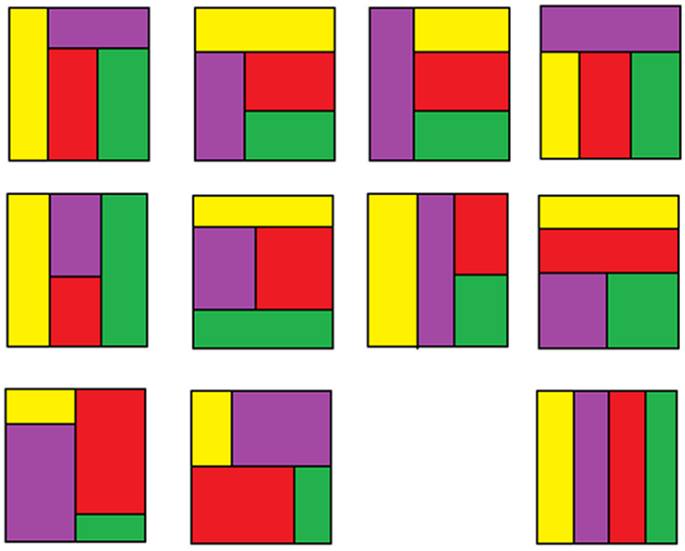

Figure 3. Examples of truncation rules with four geo-domains (modified from Armstrong et al., 2011). The geo-domains represented in yellow and green are never in contact

To overcome this limitation, following Xu et al. (2006) and Emery (2007), the key idea of this work is to increase the number of underlying Gaussian random fields, so as to increase the dimensionality of the flag used to represent the truncation rule and to allow the geo-domains to be in contact altogether. As an example, consider the following four-domain truncation rule, based on three underlying Gaussian random fields $\{Y_1, Y_2, Y_3\}$ and three truncation thresholds $\{t_1, t_2, t_3\}$, which can be represented by a three-dimensional flag (Fig. 4):

$$\text{Geo}-\text{domain at location } \mathbf{x} = \begin{cases} 1 \text{ if } Y_1(\mathbf{x}) \le t_1 \\ 2 \text{ if } Y_1(\mathbf{x}) > t_1 \text{ and } Y_2(\mathbf{x}) \le t_2 \\ 3 \text{ if } Y_1(\mathbf{x}) > t_1, Y_2(\mathbf{x}) > t_2 \text{ and } Y_3(\mathbf{x}) \le t_3 \\ 4 \text{ if } Y_1(\mathbf{x}) > t_1, Y_2(\mathbf{x}) > t_2 \text{ and } Y_3(\mathbf{x}) > t_3 \end{cases} \quad (2)$$

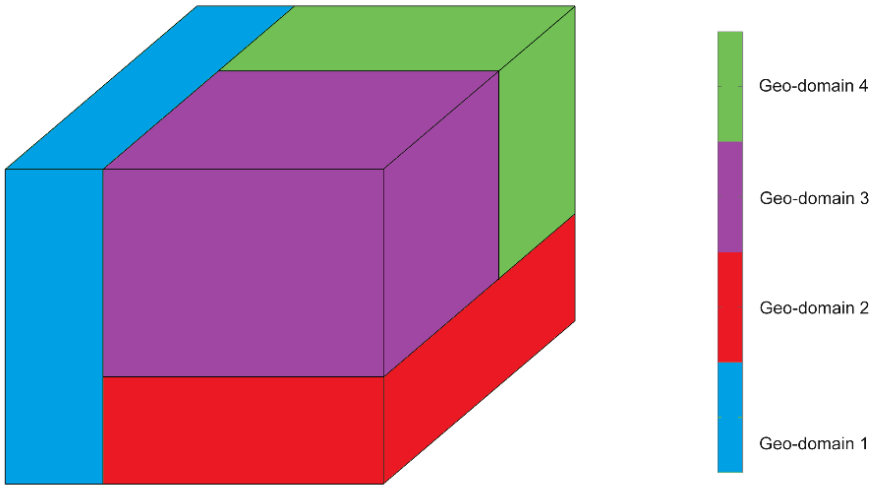

Figure 4. Three-dimensional flag representing a truncation rule with four geo-domains that are mutually in contact. Each axis of this flag corresponds to an underlying Gaussian random field

A realization of this model is shown in Fig. 5. The first geo-domain (painted in blue) appears in the foreground or first "layer" (it may represent a younger domain that cross-cuts the other ones). The second geo-domain (red) is in a second layer, while geo-domains 3 and 4 (purple and green) are located in the background (third layer).

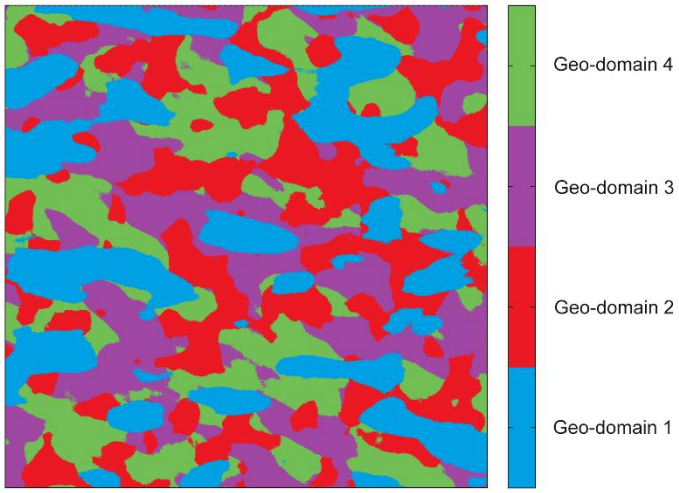

Figure 5. Plurigaussian realization with four geo-domains distributed in three successive layers

Such a hierarchical approach can easily be generalized to more than four geo-domains. An example with seven geo-domains that are numbered chronologically is presented in Fig. 6 (geo-domain 1 is the youngest and cross-cuts the other ones, while geo-domains 6 and 7 are the oldest). It is based on a truncation rule that involves six Gaussian random fields $\{Y_1, Y_2, Y_3, Y_4, Y_5, Y_6\}$ and six thresholds $\{t_1, t_2, t_3, t_4, t_5, t_6\}$:

$$\text{Geo}-\text{domain at location } \mathbf{x} = \begin{cases} 1 \text{ if } Y_1(\mathbf{x}) \le t_1 \\ 2 \text{ if } Y_1(\mathbf{x}) > t_1 \text{ and } Y_2(\mathbf{x}) \le t_2 \\ 3 \text{ if } Y_1(\mathbf{x}) > t_1, Y_2(\mathbf{x}) > t_2 \text{ and } Y_3(\mathbf{x}) \le t_3 \\ 4 \text{ if } Y_1(\mathbf{x}) > t_1, Y_2(\mathbf{x}) > t_2, Y_3(\mathbf{x}) > t_3 \text{ and } Y_4(\mathbf{x}) \le t_4 \\ 5 \text{ if } Y_1(\mathbf{x}) > t_1, Y_2(\mathbf{x}) > t_2, Y_3(\mathbf{x}) > t_3, Y_4(\mathbf{x}) > t_4 \text{ and } Y_5(\mathbf{x}) \le t_5 \\ 6 \text{ if } Y_1(\mathbf{x}) > t_1, Y_2(\mathbf{x}) > t_2, Y_3(\mathbf{x}) > t_3, Y_4(\mathbf{x}) > t_4, Y_5(\mathbf{x}) > t_5 \text{ and } Y_6(\mathbf{x}) \le t_6 \\ 7 \text{ if } Y_1(\mathbf{x}) > t_1, Y_2(\mathbf{x}) > t_2, Y_3(\mathbf{x}) > t_3, Y_4(\mathbf{x}) > t_4, Y_5(\mathbf{x}) > t_5 \text{ and } Y_6(\mathbf{x}) > t_6 \end{cases} \quad (3)$$

To ease inference, in the following, the Gaussian random fields are assumed to be mutually independent and second-order stationary, with zero mean and unit variance.

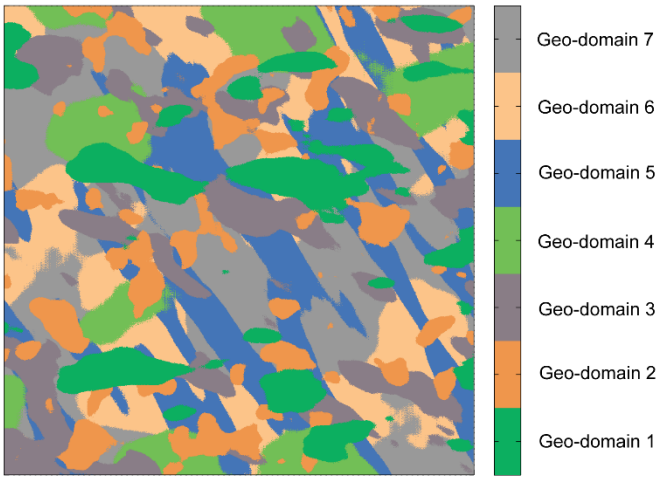

Figure 6. Plurigaussian realization with seven geo-domains distributed in six successive layers

2.3.2. Inference of truncation thresholds

The previous truncation rule depends on six scalar thresholds $\{t_1, t_2, t_3, t_4, t_5, t_6\}$, which can be defined in order to reproduce the proportions of the different geo-domains (Armstrong et al., 2011). For instance, the proportion of the first geo-domain is equal to $G^{-1}(t_1)$, where G stands for the standard Gaussian cumulative distribution function: threshold t_1 can then be defined in order to yield a given proportion for geo-domain 1 (for instance, the proportion inferred from an interpreted geological model). Likewise, since Y_1 and Y_2 are independent, the proportion of the second geo-domain is equal to $[1 - G^{-1}(t_1)]\ G^{-1}(t_2)$: as t_1 is already known, threshold t_2 can now be defined in order to yield a given proportion for geo-domain 2. The same procedure can be applied for the remaining thresholds (t_3 to t_6), which relate to the proportions of geo-domains 3 to 7. Spatial variations in the geo-domain proportions can be imposed by using spatially varying thresholds, i.e., by considering that $t_1, t_2, t_3, t_4, t_5, t_6$ depend on the location under consideration, while the design of the truncation rule is the same at every location. An example of such a spatially-varying proportion model will be presented in Section 3.

2.3.3. Variogram analysis

As mentioned in Section 2.1, the auto-covariance functions (equivalently, the variograms) of the underlying Gaussian random fields are related to the indicator variograms associated with the geo-domains (Eq. (1)). In Eq. (1), it is seen that, when the value of $C(\mathbf{h})$ increases from -1 to 1, the value of the integral increases, insofar as the integrand is positive and the upper bound of the integral increases, so that the value of the indicator variogram $\gamma_t(\mathbf{h})$ decreases. Accordingly, there exists a one-to-one relationship between $C(\mathbf{h})$ and $\gamma_t(\mathbf{h})$, and one can express the former as a function of the latter (Kyriakidis et al., 1999):

$$C(\mathbf{h}) = \phi_t(\gamma_t(\mathbf{h})), \quad (4)$$

with ϕ a function that depends on the chosen truncation threshold t.

In the proposed hierarchical model, the geo-domain data can be converted into indicator data (0, 1, or unknown value) on whether or not the Gaussian random fields are below their respective thresholds (see Table 1 for an illustration to the truncation rule presented in Eq. (3)). The indicator variograms can therefore be experimentally calculated and, using Eq. (4), converted into covariance values (equivalently, into variograms) for the underlying Gaussian random fields. These experimental Gaussian covariances / variograms can finally be fitted by theoretical covariance / variogram models.

Geo-domain	$Y_1 < t_1$?	$Y_2 < t_2$?	$Y_3 < t_3$?	$Y_4 < t_4$?	$Y_5 < t_5$?	$Y_6 < t_6$?
1	1	unknown	unknown	unknown	unknown	unknown
2	0	1	unknown	unknown	unknown	unknown
3	0	0	1	unknown	unknown	unknown
4	0	0	0	1	unknown	unknown
5	0	0	0	0	1	unknown
6	0	0	0	0	0	1
7	0	0	0	0	0	0

Table 1. Codification of geo-domain data into indicator data

2.3.4. Comments on the modeling process

Although the use of more than two Gaussian random fields for plurigaussian modeling has already been proposed by several authors (Xu et al., 2006; Emery, 2007, Deutsch and Deutsch, 2014), the hierarchical approach presented in Sections 2.3.1 to 2.3.3 improves these proposals in two aspects. The first one is the definition of spatially varying truncation thresholds in order to account for spatially varying proportions of the geo-domains. The second one relates to variogram analysis. In former proposals (except for the simple case of truncated Gaussian simulation, based on a single Gaussian random field), the variograms of the underlying Gaussian random fields are fitted indirectly, on the basis of the experimental indicator variograms: accordingly, the user is not aware of which basic nested structures are the most appropriate and a trial-and-error process is often used (Armstrong et al., 2011). In our proposal, the experimental indicator variograms are transformed into experimental variograms for the Gaussian random fields, allowing a direct and more accurate fitting of these variograms.

3. Case study: Río Blanco ore deposit

3.1. Geographical and geological settings

The Río Blanco – Los Bronces ore deposit is a breccia-hosted cogenetic porphyry Cu-Mo deposit located between latitudes 33°07´45" and 33°10´20" in the Central Chilean Andes, about 80 km northeast of Santiago. Los Bronces is emplaced in the western part and is being mined by Anglo American, while the Río Blanco deposit is emplaced in the eastern part, with mineralized bodies (Río Blanco, La Unión, Central, Don Luis, Sur-Sur and La Americana) distributed over an area of six kilometers from north to south and two kilometers from east to west. La Unión, Don Luis and Sur-Sur are mined by Codelco (Andina Division) by open pit and underground operations.

The Río Blanco deposit is partly hosted in the western margin of the San Francisco batholith, a multiphase intrusive containing quartz-diorite, granodiorite, quartz-monzonite, quartz-monzodiorite and granite, and partly in Miocene volcanics of the surrounding Abanico and Farellones formations, which consist of sub-horizontally dipping andesitic lavas (Warnaars et al., 1985; Stambuk et al., 1988).

The earlier alteration phase within the San Francisco batholith is characterized by actinolite ± magnetite ± titanite ± plagioclase disseminations, narrow actinolite ± magnetite veins and magnetite ± clinopyroxene ± actinolite ± plagioclase breccias.

This phase is postdated by an intense potassic alteration of both andesitic lavas and granitoid rocks, centered on the Río Blanco sector and associated with the emplacement of quartz monzonite porphyry intrusions, stockwork veins with biotite ± K feldspar ± quartz ± magnetite ± anhydrite ± sulfides, and multiple mineralized breccias whose matrices are dominated by biotite, tourmaline, quartz, anhydrite and/or specularite with sulfides (chalcopyrite, bornite, molybdenite and minor pyrite).

A second mineralization phase comprises a set of younger, tourmaline rich breccia pipes with varying proportions of quartz, chlorite, sericite, anhydrite, specularite, biotite and sulfides, including chalcopyrite, bornite, molybdenite and minor pyrite. These breccias are dated at between 5.9 and 5.1 Ma and are found to the west of the potassic zone, around the tourmaline-sulfide Donoso breccia, and to the south-east, around the Sur-Sur tourmaline-sulfide-iron oxide breccia.

A detailed geological description of the Río Blanco deposit can be found in the specialized literature (Skewes and Stern, 1995, 1996; Serrano et al., 1996; Kay et al., 1999; Vargas et al., 1999; Kay and Mpodozis, 2001, 2002; Skewes et al., 2003; Frikken, 2003; Frikken et al., 2005; Hollings et al., 2005).

3.2. Lithology

Seven main rock units can be recognized within the Río Blanco deposit. These are, from the oldest to the youngest, the following (Table 2).

1) **Andesite (AND)**. The andesite unit consists of volcanic rocks (mainly basaltic andesite, traquiandesite and dacite) of the Abanico and Farellones formations, from late Cretaceous to Oligocene for the Abanico Formation and Miocene for the Farellones Formation. These rocks are affected by quartz-sericitic alteration, biotitization and partial chloritization (Stambuk et al., 1988).

2) **Granitoids (GD)**. The San Francisco Batholith embraces different types of granitoids, the main ones being the Río Blanco granodiorite in the northern sector, characterized by a coarser grain size and the presence of orthoclase feldspar and plagioclase, and the cascade granodiorite in the southern sector, characterized by a finer grain size and enriched in oligoclase-andesine. Both granitoids mainly correspond to granodiorite, quartz-monzonite, tonalite and diorite (Stambuk et al., 1988; Frikken, 2003).

3) **Tourmaline Breccia (TOB)**. This rock unit is mainly hosted in granitoids. It outcrops in the Sur-Sur sector over 5 km long striking N10°W to N30°W and presents sharp and steeply dipping contacts with the host rock (Serrano et al., 1996). The matrix is a kind of milled rock flour replaced by secondary tourmaline cement containing specular hematite, sulfide, quartz, magnetite, sulfate (anhydrite, gypsum) and biotite, with open spaces filled by tourmaline-quartz-sulfide. For lower tourmaline contents, the clasts are angular to sub-angular, while they become more rounded for higher tourmaline contents.

4) **Monolithic Breccia (MOB)**. This rock unit is present in the western sector of Río Blanco and has low copper contents. It was formed after the tourmaline breccia (Frikken, 2003) and is characterized by a chloritic alteration, which appears in both the clasts and the matrix, with a varying intensity (Vargas et al., 1999).

5) **Magmatic Breccia (MAB)**. This rock unit is characterized by crystalline igneous cement. A heterogeneous brecciation resulted in variable proportions of rock flour matrix and clasts. The clasts are different in size, from 2 mm to more than 5 m wide, and are altered with primary igneous minerals replaced by secondary biotite, magnetite, sulfides and K-feldspar. The matrix is partly substituted for hydrothermal minerals such as biotite, sulfates, quartz, sulfides, magnetite, specularite and tourmaline.

6) **Porphyry (POR)**. The porphyry unit intruded the magmatic and tourmaline breccias and consists of three main rock types (Serrano et al., 1996): the Don Luis Porphyry, located in the center of the deposit and bounded by the magmatic breccia (this porphyry

predominates in the region that will be considered in the next sections); the Quartz Monzonite Porphyry, which cross-cuts the magmatic breccia; and the Feldspar Porphyry, less abundant and presenting a clear-cut contact with the magmatic breccia. These porphyries contain quartz, plagioclase, K-feldspar and biotite phenocrystals.

7) **Pipe (PIP)**. This unit is composed of two main rock types (Serrano et al., 1996): the Dacitic Pipe, which forms an inverted cone limited by the magmatic breccia, containing phenocrystals of quartz and plagioclase with minor biotite in a quartz-feldspar matrix; and the Rhyolitic Pipe, which corresponds to the final intrusion in the mineralized sectors, characterized by numerous felsic intrusions.

3.3.Data presentation

In the following, we will focus on the northern sector of the Río Blanco deposit, for which two types of data are available: exploration drill holes and an interpreted lithological model. The drill holes are in an irregular design along the northwest-southeast direction (Fig. 7A); the data consist of information on the prevailing rock types logged at drill hole cores and codified into the previously defined rock units (Table 2). As for the lithological model, it consists of a discretization of the region of interest into blocks with a support of 15m × 15m × 16 m, for which the (assumed) prevailing rock unit is assigned to each block (Fig. 7B). Such a block model has been constructed on the basis of the available drill hole data, as well as on the interpretation of the geological processes, emplacements and alterations.

Code	Rock Unit	Rock Types	Abbreviation	Age
7	Andesite	Andesite	AND	Late Cretaceous to Early Pliocene
6	Granitoids	Río Blanco granodiorite Cascade granodiorite Breccia cascade granodiorite Diorite Granodiorite	GD	Early Pliocene
5	Tourmaline breccia	Andesite tourmaline Río Blanco granodiorite tourmaline Cascade granodiorite tourmaline Tourmaline breccia Tourmaline breccia with andesite Tourmaline breccia with cascade granodiorite Tourmaline breccia with Río Blanco tourmaline Tourmaline breccia with porphyry Tourmaline breccia with abundant tourmaline Quartz sericitic breccia Tourmaline breccia with granodiorite	TOB	Early Pliocene
4	Monolithic Breccia	Breccia porphyry Magmatic breccia of granodiorite Molybdenite breccia Monolithic breccia Tourmaline monolithic breccia Castellana breccia Don Luis porphyry breccia Quartz breccia with Don Luis porphyry Tourmaline breccia of Don Luis porphyry Biotite metasomatic rocks Igneous breccia	MOB	Early Pliocene
3	Magmatic Breccia	Río Blanco granodiorite breccia Anhydrite breccia Hematite breccia Quartz anhydrite breccia	MAB	Late Miocene
2	Porphyry	Quartz monzonite porphyry Feldespathic porphyry Monzonite porphyry Don Luis Porphyry	POR	Middle Miocene
1	Pipe	Dacite contact breccia Rhyolitic pipe Dacitic pipe Rhyolite contact breccia	PIP	Early Miocene

Table 2. Main rock units in the Río Blanco deposit

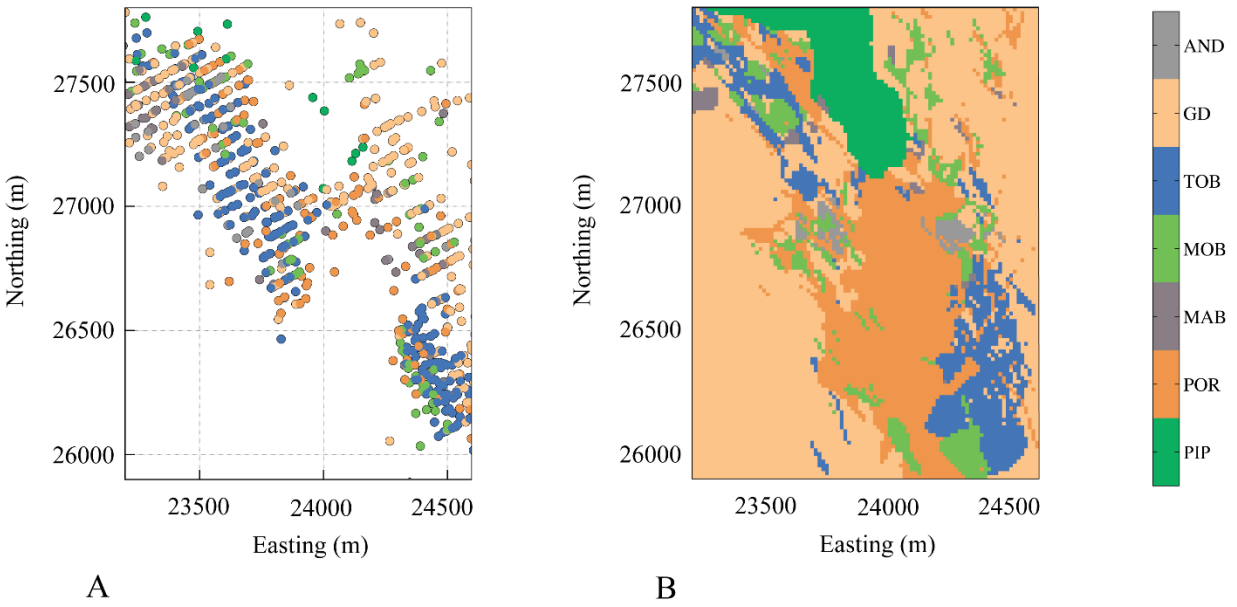

Figure 7. Plan view showing A) the drill hole data and B) the interpreted lithological model for elevation 3348 m a.m.s.l.

3.4. Plurigaussian modeling

3.4.1. Truncation rule

The rock units will be simulated by using the plurigaussian model presented in Section 2.2, with the hierarchical approach defined in Section 2.3. To allow every unit to be in contact with any other unit, six independent Gaussian random fields $\{Y_1, Y_2, Y_3, Y_4, Y_5, Y_6\}$ will be considered, with the same truncation rule as that defined in Fig. 6 and Eq. (3). Such a truncation rule agrees with the rock unit chronology: rock unit 1 (PIP) appears as the youngest and rock unit 7 (AND) as the oldest. A younger rock unit is likely to cross-cut older ones.

3.4.2. Truncation thresholds

As explained in Section 2.3.2, the truncation thresholds $\{t_1, t_2, t_3, t_4, t_5, t_6\}$ are defined in order to reproduce the rock unit proportions. For a greater realism of the realizations, local proportions (consequently, local thresholds) can be used at this stage. For instance, from the interpreted lithological model (Fig. 7B), it is seen that pipe (PIP) is more frequent in the northern part of the region under study, while tourmaline breccia (TOB) and porphyry (POR) are more frequent in the southern part. To determine the local proportions and local thresholds, the following procedure is proposed:

1) Based on the interpreted lithological model (Fig. 7B), for each block and each drill hole sample, calculate the local proportion of each rock unit (proportion of the rock unit observed in a moving window centered at the target block or target drill hole sample). The use of moving windows to infer spatially varying proportions is not novel (Armstrong et al., 2011), although this approach is often applied to the sole drill hole data and the resulting proportions are further interpolated to regions without data. Here, there is no need for such an interpolation, insofar as the local proportions of rock units are derived from the interpreted lithological model, which covers the entire region of interest.

2) Convert the local proportions into thresholds, leaving unchanged the design of the truncation rule.

The size of the moving window used in step 1) depends on how much the interpreted model can be trusted. With a very large window, the calculated proportions will tend to the global proportions, meaning that the spatial variations of rock unit proportions that are perceptible in the interpreted model tend to be ignored. On the contrary, with a very small window, the local proportions will tend to 0 or 1, depending on whether or not the rock unit is present in the interpreted model at the target block or sample; in such a case, one is extremely confident in the interpreted model and the simulated rock units will not depart from this model too much. In the present study, a rectangular moving window of 135m × 135m × 144m (i.e., 9 blocks along each direction) has been chosen for the calculation of the local proportions of rock units; this size is a trade-off between our uncertainty and our reliance on the interpreted model. Such a choice can be validated by checking the ability of the plurigaussian model to accurately measure the geological uncertainty, see Section 3.6 on the split-sample method.

3.4.3. Variogram analysis

The drill hole data on the prevailing rock units are codified into indicators (Table 1) and the experimental indicator variograms are calculated along the three identified main anisotropy directions: N20°W, N70°E and vertical. For the first two directions, the lag separation distance is set to 15 meters with a tolerance of 7.5 meters, while this distance is set to 10 meters with a tolerance of 5 meters along the vertical. From the indicator variograms so obtained, one can derive variograms for the underlying Gaussian random fields (Eq. (4)).

The next step is to fit variogram models (independently) to each experimental variogram. Owing to the fact that the plurigaussian model is based on standard Gaussian random fields, it requires the variogram sills to be equal to 1. In order to ease modeling and to ensure a unit sill value, a semi-automated fitting algorithm has been used (Emery, 2010). The fitting minimizes the mean squared error between experimental and modeled variograms (Fig. 8). At this stage, two comments are worth being made. First, the cross-variograms between Gaussian random fields are

set to zero, since these random fields are assumed to be independent. Second, the choice of the basic nested structures used for modeling the direct variograms has an impact on the nature of the boundaries between rock units: structures with a linear behavior near the origin (like the spherical and exponential) lead to irregular boundaries, while structures with a parabolic behavior near the origin (like the cubic and Gaussian) lead to smooth boundaries (Lantuéjoul, 2002). Because this last property is deemed more realistic for the current case study, the sample variograms are fitted with nested anisotropic cubic models (Table 3).

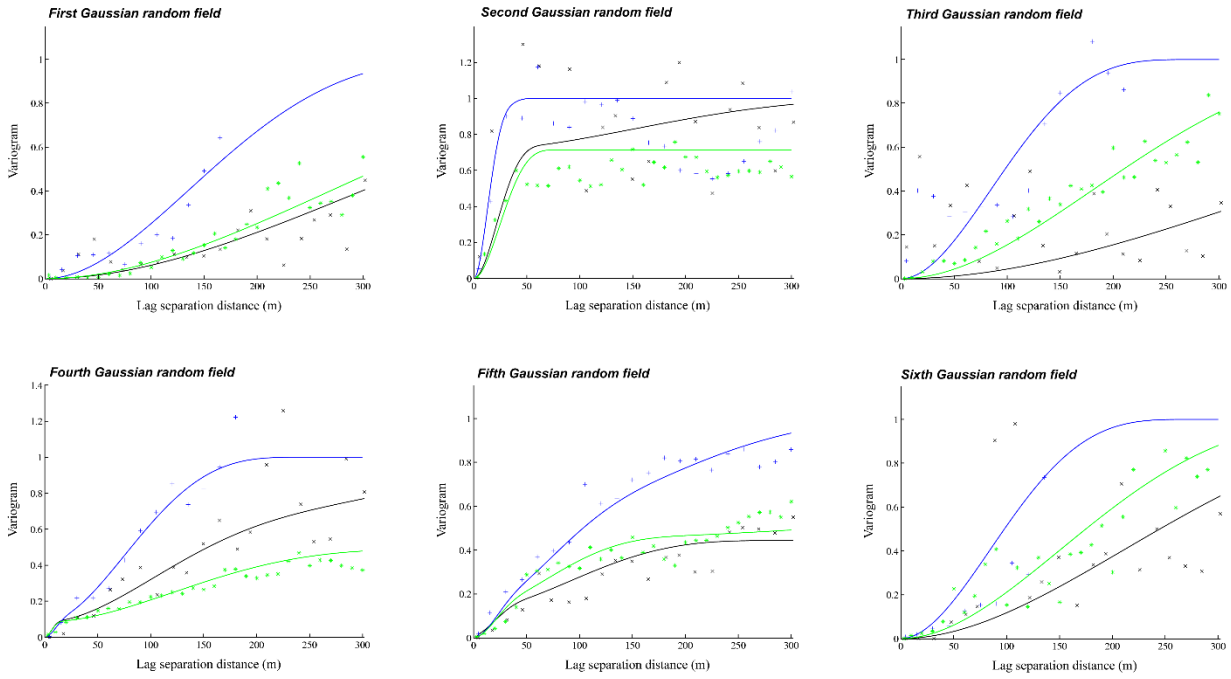

Figure 8. Experimental (crosses) and fitted (solid lines) variograms for the six underlying Gaussian random fields, along the main anisotropy directions: N20°W (green), N70°E (blue) and vertical (black)

Gaussian random field	Basic nested structure	Sill	Range along N20°W (m)	Range along N70°E (m)	Range along vertical (m)
1	Cubic	1.000	1000	450	900
2	Cubic	0.713	70	40	80
	Cubic	0.287	500	60	infinite
3	Cubic	1.000	1200	280	600
4	Cubic	0.084	20	30	20
	Cubic	0.403	300	250	400
	Cubic	0.513	800	250	infinite
5	Cubic	0.013	10	60	60
	Cubic	0.117	60	60	60
	Cubic	0.314	300	200	220
	Cubic	0.556	infinite	500	2500
6	cubic	1.000	700	280	500

Table 3. Specification of fitted variogram models

3.5.Plurigaussian simulation

3.5.1. Construction of realizations of rock units

Provided with the complete model (truncation rule, local truncation thresholds and variograms of underlying Gaussian random fields), one can simulate the rock units over the domain of interest, conditionally to the drill hole data (i.e., restricting the realizations to reproduce the observed rock units at the drill hole locations). A total of one hundred realizations have been constructed, using an adaptation of a program published by Emery (2007). Table 4 indicates the main implementation parameters used for simulation.

Parameter	**Value**
Number of iterations (sweeps over the data set) for Gibbs sampler	30
Number of lines for turning bands simulation	500
Number of neighboring data for conditioning	40
Radius (m) of search ellipsoid along direction N20°W	200
Radius (m) of search ellipsoid along direction N70°E	120
Radius (m) of search ellipsoid along vertical direction	120

Table 4. Parameters for plurigaussian simulation

Figure 9 shows a plan view of four realizations, which globally agree with the interpreted model depicted in Figure 7B. Each realization gives an alternative scenario of what could be the distribution of rock units, as it reproduces the geostatistical properties of the actual rock units (chronology and contact relationships controlled by the truncation rule; local proportions controlled by the truncation thresholds; spatial continuity controlled by the fitted variograms) and, furthermore, is consistent with the drill hole conditioning data. The set of realizations additionally provides an insight into geological uncertainty, as one can appreciate whether or not the rock units change from one scenario to another.

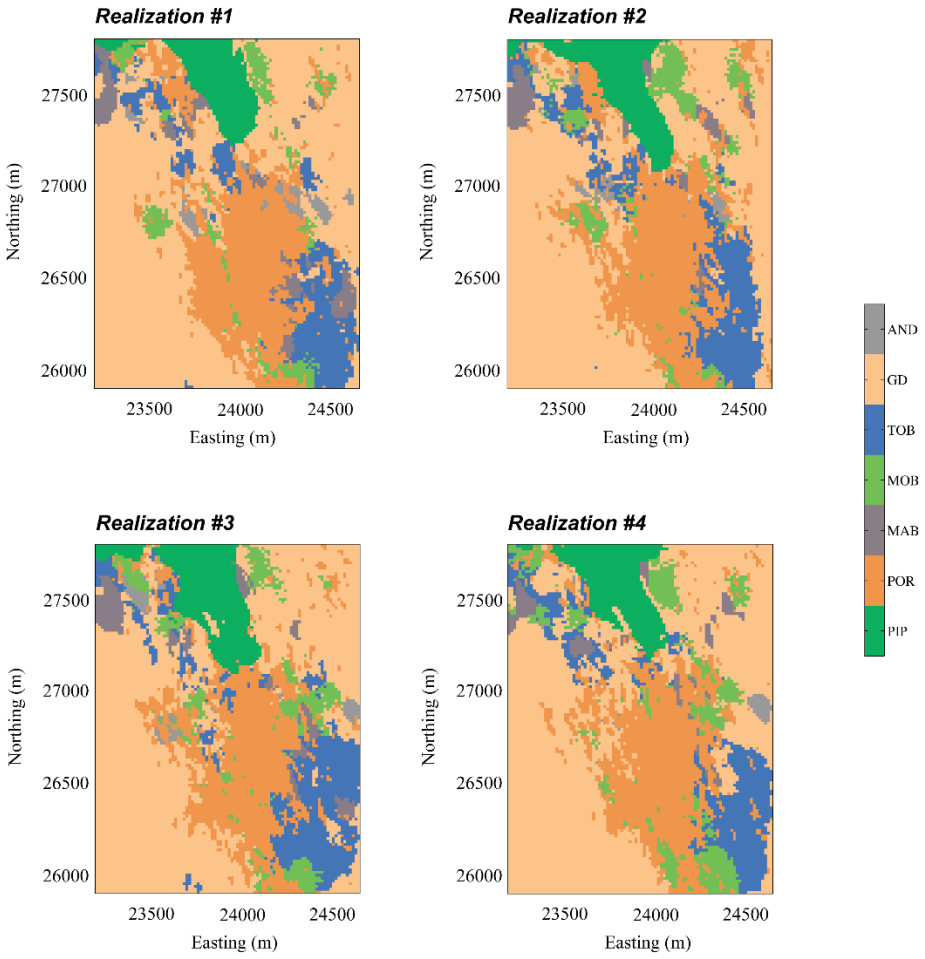

Figure 9. Plan views of four realizations of the rock units for elevation 3348 m a.m.s.l, conditioned to the drill hole data of Fig. 7A

3.5.2. Post-processing the realizations

The realizations can be used to assess the uncertainty in the volume of each rock unit within the simulation domain or, equivalently, in the proportion of the simulation domain covered by each rock unit. This can be done by calculating, for each realization, the proportion of blocks belonging to each rock unit, then the statistics on the proportions so obtained over the realizations. As the simulation domain is bounded, the theory of ergodic fluctuations or increasing-domain asymptotics (Cressie, 1993; Chilès and Delfiner, 2012) states that these proportions are likely to deviate from the expected proportions (those corresponding to the lithological model) and vary from one realization to another. In particular, one observes a greater uncertainty in the proportion of granitoids, which varies between 46.1 and 53.7% (Table 5). This can be explained because this rock unit is under-sampled with respect to the other ones (Fig. 7), so that the layout of its boundaries is more uncertain. The range of uncertainty (7.6%) lies in-between what would be obtained in the following two extreme cases:

- No spatial correlation (pure nugget variograms): in this case, the proportion of granitoids would be the average of 23,750 independent Bernoulli variables (one variable per block) with mean equal to 0.509 (expected proportion of granitoids, as per the interpreted lithological model). As the standard deviation of such an average is very small (0.0032), the variation in the proportion of granitoids over the realizations would be close to zero.

- Perfect spatial correlation (variograms increasing infinitely slowly along all the directions): in this case, the proportion of granitoids would be the result of a single Bernoulli variable with mean 0.509, identical for all the blocks. Over 100 realizations, the expected variation in this proportion would be 100%.

Rock unit	Minimum over realizations	Maximum over realizations	Average over realizations	Interpreted model
PIP	5.1%	9.2%	7.3%	7.5%
POR	20.1%	24.5%	22.6%	22.2%
MAB	1.6%	4.5%	2.8%	1.1%
MOB	3.7%	8.0%	5.7%	6.9%
TOB	8.1%	14.0%	10.3%	10.2%
GD	46.1%	53.7%	50.3%	50.9%
AND	0.2%	2.2%	1.1%	1.2%

Table 5. Statistics on the proportions of blocks belonging to each rock unit

One can also assess the uncertainty in the rock units at a local (block-by-block) scale, by means of probability maps. The maps are constructed by calculating, for each block, the frequency of occurrence of each rock unit over the 100 conditional realizations (Fig. 10). They constitute a complement to the interpreted lithological model, insofar as they show the risk of finding a rock unit different from the one that has been scheduled. The sectors with little uncertainty are those associated with a high probability for a given rock unit (painted in red in Fig. 10), indicating that there is little risk of not finding this rock unit, or those associated with a very low probability (painted in dark blue in Fig. 10), indicating that one is pretty sure of not finding this unit, while the other sectors (painted in light blue, green or yellow in Figure 10) are more uncertain.

From these probability maps, one can construct a lithological model by selecting, for each block, the most probable rock unit (Fig. 11A). This model can then be compared to the interpreted lithological model (Fig 7B) in order to identify the blocks for which the interpreted rock unit matches the most probable one, and the blocks for which there is a mismatch and the interpreted model may be revised (Fig 11C). The latter blocks are mostly located near the boundaries of pipe, porphyry and granitoids, and correspond to the blocks with a moderate probability (0.3 to 0.6) for the most probable rock unit (in other words, none of the units has a high probability of occurrence) (Fig. 11B). The numbers of matches and mismatches for the blocks at elevation 3348 m a.m.s.l are indicated in Table 6: one obtains 19,199 matches over a total of 23,750 blocks, i.e., the interpreted rock unit corresponds to the most probable unit for 81% of the blocks.

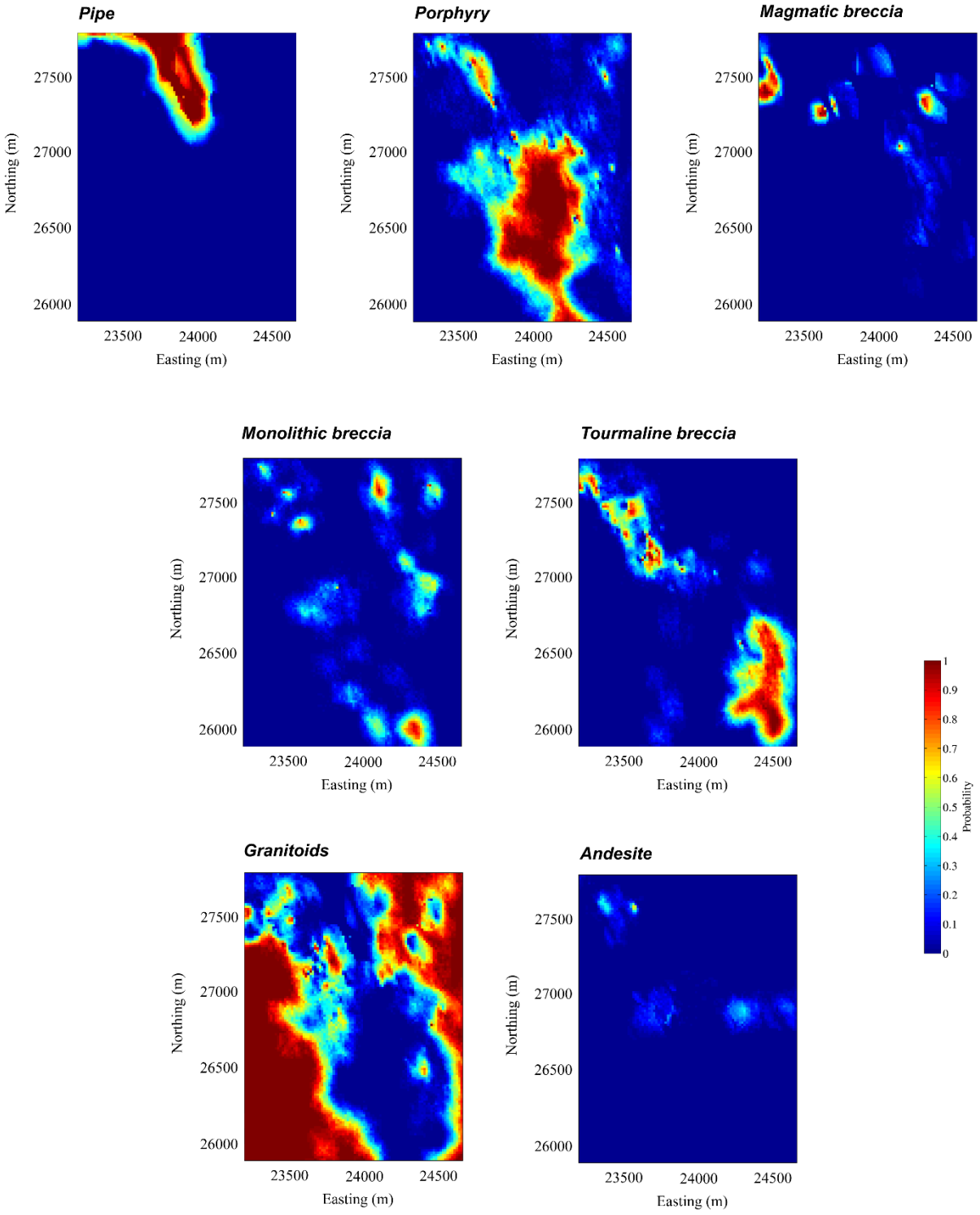

Figure 10. Plan views showing the probabilities of occurrence of each rock unit at elevation 3348 m a.m.s.l, calculated using 100 realizations

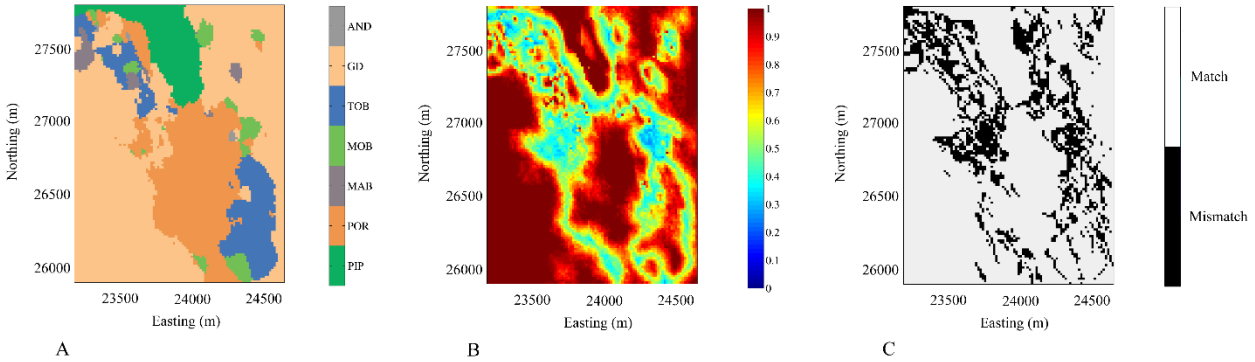

Figure 11. Plan views showing A) the most probable rock unit at elevation 3348 m a.m.s.l, B) the probability of occurrence of the most probable unit, and C) the matches and mismatches with respect to the interpreted model (Fig. 7B)

Other useful information that can be obtained from the realizations relates to the so-called transition probabilities, which give the frequencies of simulated rock units at two adjacent blocks, on average over the simulation domain and over the realizations (Table 7). In particular, one observes that every rock unit is likely to be in contact with every other, except the youngest and oldest ones, namely pipe (PIP) and andesite (AND). Also, around 8% to 14% of the porphyry (POR), breccia (TOB, MOB, MAB) and andesite (AND) blocks are in contact with granitoid (GD), and 9% to 15% of breccia (TOB, MOB, MAB) blocks are in contact with porphyry (POR).

		Most probable unit							
		PIP	**POR**	**MAB**	**MOB**	**TOB**	**GD**	**AND**	TOTAL
Interpreted model	**PIP**	1699	26	0	0	0	57	0	1782
	POR	33	4182	29	59	206	752	6	5267
	MAB	17	27	142	3	11	52	0	252
	MOB	31	443	39	511	181	424	17	1646
	TOB	43	179	28	42	1679	431	13	2415
	GD	191	285	170	205	307	10,938	0	12,096
	AND	0	135	1	24	12	72	48	292
	TOTAL	2014	5277	409	844	2396	12,726	84	23,750

Table 6. Numbers of blocks per rock unit, according to interpreted model and to model based on the most probable rock unit

		one finds a block belonging to rock unit…						
		PIP	**POR**	**MAB**	**MOB**	**TOB**	**GD**	**AND**
When leaving a block of rock unit…	**PIP**	0.9315	0.0180	0.0057	0.0056	0.0045	0.0345	0.0000
	POR	0.0057	0.7930	0.0114	0.0385	0.0439	0.0997	0.0078
	MAB	0.0142	0.0924	0.7125	0.0207	0.0403	0.1152	0.0046
	MOB	0.0072	0.1532	0.0102	0.6290	0.0513	0.1385	0.0106
	TOB	0.0032	0.0960	0.0109	0.0280	0.7703	0.0874	0.0043
	GD	0.0050	0.0452	0.0064	0.0157	0.0181	0.9068	0.0028
	AND	0.0012	0.1673	0.0130	0.0582	0.0449	0.1362	0.5791

Table 7. Transition probabilities calculated by considering the simulated rock units on adjacent blocks (average statistics over 100 realizations)

3.6. Model validation

In order to make sure that plurigaussian simulation provides accurate results, a split-sample validation exercise is carried out. It consists in partitioning the drill hole dataset into two subsets and simulating the rock units at the locations of one of these subsets (referred to as the testing subset), using as conditioning information the data of the other subset (training subset). In the present case, the drill hole data belonging to the testing and training subsets have been chosen at random, with half of the data in each subset.

Using the realizations so obtained, the probability of occurrence of each rock unit can be calculated at each data of the testing subset. Then, for each rock unit, the data of the testing subset are sorted by increasing probability of occurrence of this unit: for a given probability p (up to some calculation tolerances), one expects that a proportion p of the testing data actually match this rock unit. The match or mismatch can be visualized in a calibration plot, as shown in Fig. 12.

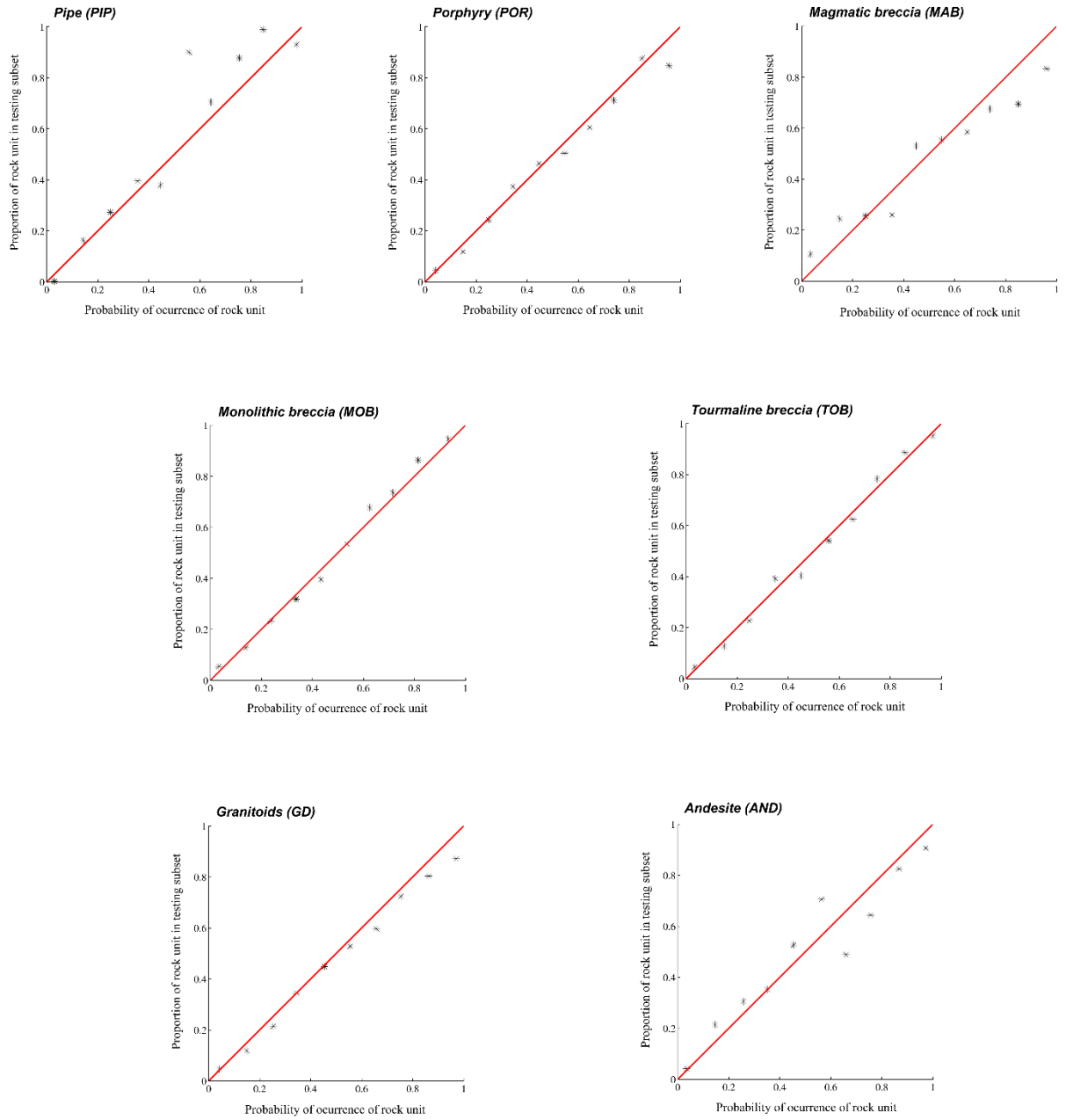

Figure 12. Split-sample validation: calibration plot comparing the probability of occurrence of a rock unit (abscissa) and the proportion of rock unit actually observed at the testing subset (ordinate). The red line corresponds to the identity

Arguably, this validation exercise makes use of the interpreted lithological model (through the calculation of local rock unit proportions and local thresholds, see Section 3.4.2), which is constructed on the basis of the entire drill hole dataset, and not only the training subset. The testing data are thus indirectly accounted for, which may lead to an overly optimistic assessment of the ability of the plurigaussian model to quantify uncertainty. For instance, if the local proportions are calculated within a small moving window, then these proportions will be either 0 or 1, depending on whether the rock unit at the block under consideration is absent or present in

the interpreted lithological model. In such a case, the simulated rock units always match the interpreted rock units and the testing data are perfectly reproduced, insofar as these data agree with the interpreted lithological model, giving the impression that the model is validated. In such a case, the calibration plot consists of only two points, corresponding to probabilities 0 and 1 (see Figs. 13A and 14A for an illustration to two rock units).

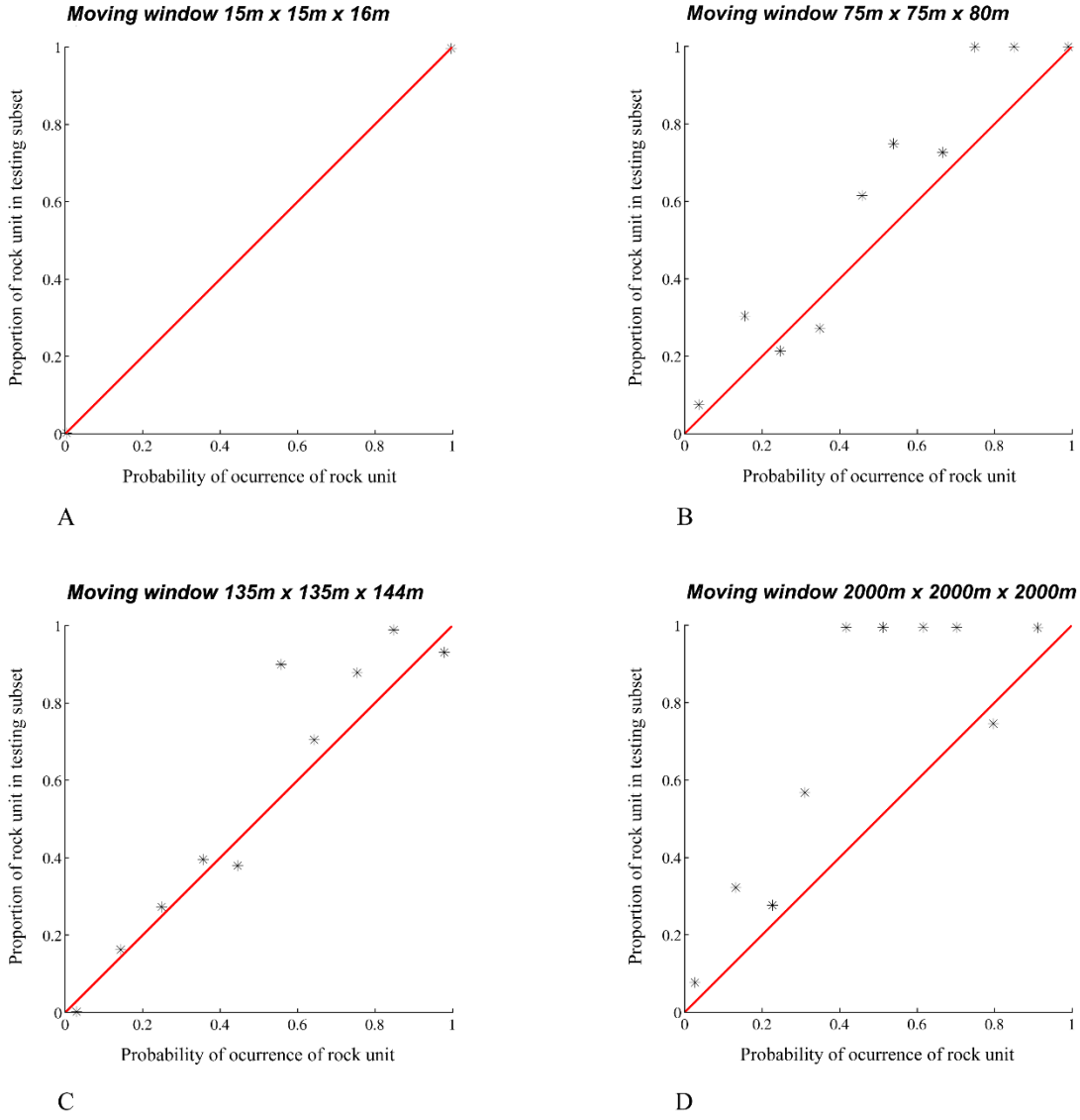

Figure 13. Calibration plots associated with pipe (PIP) for different window sizes used for calculating the local rock unit proportions

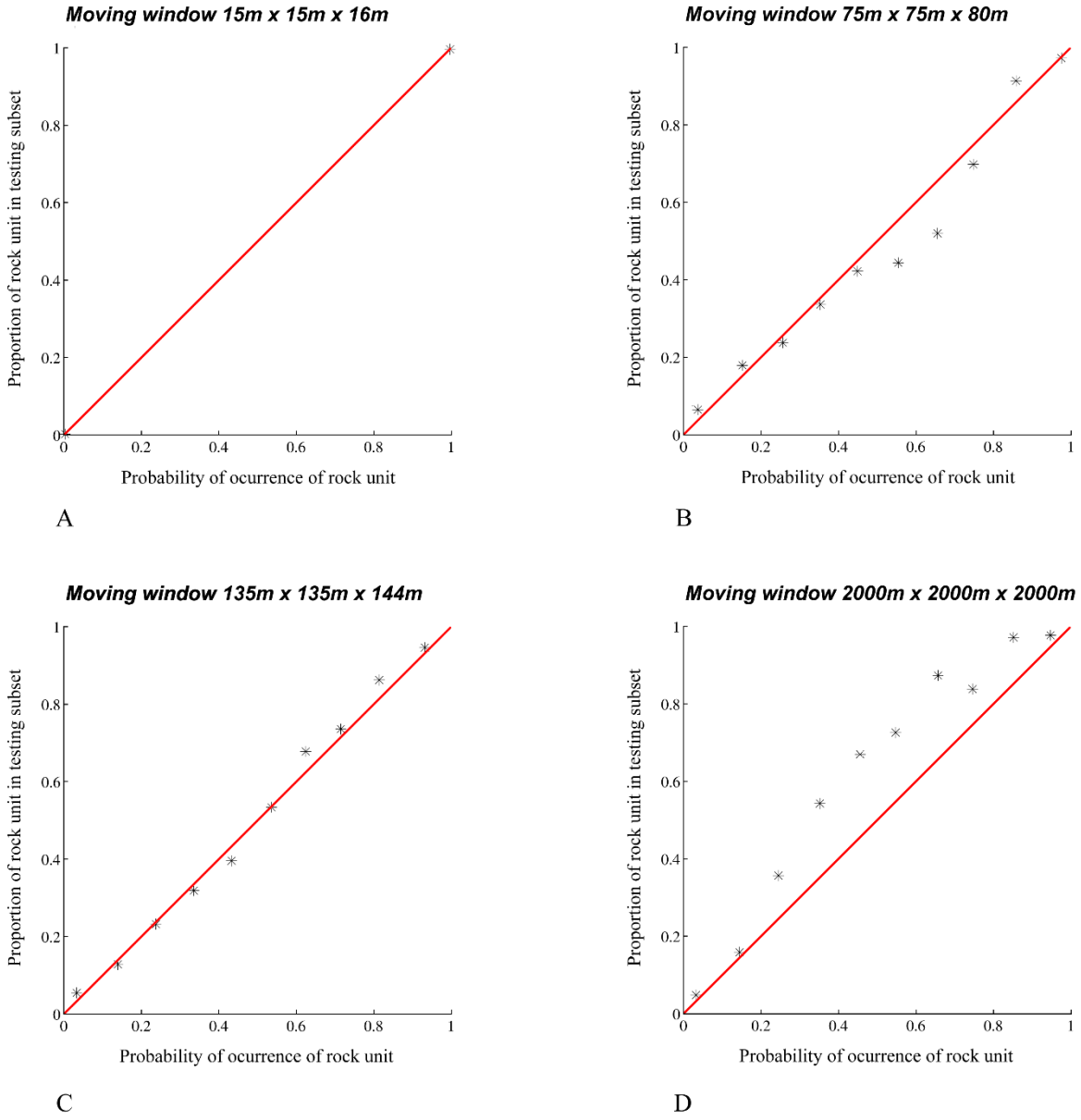

Figure 14. Calibration plots associated with monolithic breccia (MOB) for different window sizes used for calculating the local rock unit proportions

Such a drawback is mitigated when the local rock unit proportions are calculated using a large moving window, in which case the value of any particular testing data is not influential any more in the local proportion model. Based on this premise, to avoid the validation results being misleading, the size of the moving window should be the largest one that yields calibration plots close to the diagonal line. In particular, if a stationary model were adequate, the moving window should be infinitely large and the global rock unit proportions should be used. In the present case study however, a stationary model is questionable and the use of global proportions does not yield a fully satisfactory validation (Figs. 13D, 14D). When decreasing the window size, the

validation results improve, becoming acceptable with a size of 135m × 135m × 144m (Figs. 13C, 14C) or smaller (Figs. 13B, 14B). This is the reason why a moving window of size 135m × 135m × 144m has been used in the Section 3.4.2, as this option fulfills the trade-off between the ability to adequately quantify uncertainty and the request of an as large as possible moving window. The window size could be reduced if our confidence in the interpreted lithological model increases, but this would be a somewhat subjective decision.

4. Conclusions

The plurigaussian model offers a simple framework for simulating geo-domains, but the current implementations are often restricted in the number of geo-domains and in their contact relationships. The proposed hierarchical approach overcomes these limitations and increases the model versatility, providing a set of realistic models that constitute alternative representations of the true (unknown) distribution of geo-domains in space:

- Each realization reproduces the contact relationships between geo-domains. These relationships can be designed in order to agree with chronology, so that younger geo-domains appear in the foreground and are likely to cross-cut older geo-domains, which appear in the background.

- Each realization also reproduces the local geo-domain proportions, via the choice of local truncation thresholds, and the spatial correlation of the geo-domain indicators, via the choice of the variograms of the underlying Gaussian random fields.

- Finally, each realization is consistent with the data used as conditioning information in the simulation process.

In addition to these properties, the construction of multiple realizations (as opposed to a single interpreted model) allows assessing geological uncertainty, through the calculation of probability maps and transition probability matrices, and identifying sectors for which the actual geo-domains are more uncertain. These outputs are helpful for decision-making related to the valorization, planning and operation of the mining project.

Acknowledgements
This research was funded by the Chilean Commission for Scientific and Technological Research, through Project CONICYT/FONDECYT/REGULAR/N°1130085. The authors acknowledge the support from Claudio Martínez from Codelco-Chile (Andina Division), who provided the dataset used in this work, as well as the comments by Grégoire Mariethoz and another anonymous reviewer, who helped to improve the manuscript.

5. References

Allard, D., D'Or, D., Biver, P., Froidevaux, R., 2012. Non-parametric diagrams for plurigaussian simulations of lithologies. In: Ninth International Geostatistics Congress, Oslo. http://geostats2012.nr.no/pdfs/1746887.pdf. Accessed 23 November 2014

Armstrong, M., Galli, A., Beucher, H., Le Loc'h, G., Renard, D., Doligez, B., Eschard, R., Geffroy, F., 2011. Plurigaussian Simulations in Geosciences. Springer, Berlin.

Carrasco, P., Ibarra, F., Rojas, R., Le Loc'h, G., Séguret, S., 2007. Application of the truncated Gaussian simulation method to a porphyry copper deposit. In: Magri, E. (ed.), 33rd International Symposium on Applications of Computers and Operations Research in the Mineral Industry. Gecamin, Santiago, pp. 31-39.

Chilès JP, Delfiner P, 2012. Geostatistics: Modeling Spatial Uncertainty, 2th edition. Wiley, New York.

Cressie NAC, 1993. Statistics for Spatial Data, rev. edition. Wiley, New York.

De Marsily, G., Delay, F., Gonçalves, J., Renard, P., Teles, V., Violette, S., 2005. Dealing with spatial heterogeneity. Hydrogeology Journal 13(1): 161-183.

Deraisme, J., Field, M., 2006. Geostatistical simulations of kimberlite orebodies: application to sampling optimization. In: Dominy, S. (ed.), 6th International Mining Geology Conference, Darwin. Australasian Institute of Mining and Metallurgy, Melbourne, pp 193-203.

Deutsch, C.V., 2002. Geostatistical Reservoir Modeling. Oxford University Press, New York.

Deutsch, J.L., Deutsch, C.V., 2014. A multidimensional scaling approach to enforce reproduction of transition probabilities in truncated plurigaussian simulation. Stochastic Environmental Research and Risk Assessment 28(3): 707-716.

Dowd, P.A., Pardo-Igúzquiza, E., Xu, C., 2003. Plurigau: a computer program for simulating spatial facies using the truncated plurigaussian method. Computers & Geosciences 29(2): 123-141.

Emery, X., 2007. Simulation of geological domains using the plurigaussian model: new developments and computer programs. Computers & Geosciences 32(9): 1189-1201.

Emery, X., 2010. Iterative algorithms for fitting a linear model of coregionalization. Computers & Geosciences 36(9): 1150-1160.

Emery, X., González, K.E., 2007a. Incorporating the uncertainty in geological boundaries into mineral resources evaluation. Journal of the Geological Society of India 69(1): 29-38.

Emery, X., González, K.E., 2007b. Probabilistic modelling of lithological domains and its application to resources evaluation. Journal of the South African Institute of Mining and Metallurgy 107(12): 803-809.

Emery, X., Ortiz, J.M., Cáceres, A.M., 2008. Geostatistical modelling of rock type domains with spatially varying proportions: Application to a porphyry copper deposit. Journal of the South African Institute of Mining and Metallurgy 108(5): 285-292.

Fontaine, L., Beucher, H., 2006. Simulation of the Muyumkum uranium roll front deposit by using truncated plurigaussian method. In: Dominy, S. (ed.), 6th International Mining

Geology Conference, Darwin. Australasian Institute of Mining and Metallurgy, Melbourne, pp. 205-215.

Frikken, P.H., 2003. Breccia-hosted copper-molybdenum mineralization at Río Blanco, Chile. PhD dissertation. University of Tasmania, Australia.

Frikken, P.H., Cooke, D.R., Walshe, J.L., Archibald, D., Skarmeta, J., Serrano, L., Vargas, R., 2005. Mineralogical and isotopic zonation in the Sur-Sur tourmaline breccia, Río Blanco-Los Bronces Cu-Mo deposit, Chile: implications for ore genesis. Economic Geology 100: 935-961.

Galli, A., Beucher, H., Le Loc'h, G., Doligez, B., and Heresim Group., 1994. The pros and cons of the truncated Gaussian method. In: Armstrong, M., Dowd, P.A. (eds.) Geostatistical Simulations. Kluwer, Dordrecht, pp. 217-233.

Hollings, P., Cooke, D., Clark, A., 2005. Regional geochemistry of Tertiary igneous rocks in Central Chile: implications for the geodynamic environment of giant porphyry copper and epithermal gold mineralization. Economic Geology 100: 887-904.

Jeannée, N., Bardou, E., Faucheux, C., Ornstein, P., 2013. Geostatistical assessment of ice content distribution within the Glacier Bonnard. Mathematical Geosciences 45: 591-599.

Journel, A.G., Alabert, F.G., (1990) New method for reservoir mapping. Journal of Petroleum Technology 42(2): 212-218

Journel, A.G., Huijbregts, C.J., 1978. Mining Geostatistics. Academic Press, London.

Kay, S.M., Mpodozis, C., 2001. Central Andes ore deposits linked to evolving shallow subduction systems and thickening crust. GSA Today 11: 4-9.

Kay, S.M., Mpodozis, C., 2002. Magmatism as a probe to the Neogene shallowing of the Nazca plate beneath the modern Chilean flat-slab. Journal of South American Earth Sciences 15: 39-57.

Kay, S.M., Mpodozis, C., Coira, B., 1999. Neogene magmatism, tectonism and mineral deposits of the central Andes. In: Skinner, B.J. (ed.) Geology and Ore Deposits of the Central Andes. Special Publication no. 7, Society of Economic Geologists, Littleton, Colorado, pp. 7-59.

Kyriakidis, P.C., Deutsch, C.V., Grant, M.L., 1999. Calculation of the normal scores variogram used for truncated Gaussian lithofacies simulation: theory and Fortran code. Computers & Geosciences 25(2): 161-169.

Lantuéjoul, C., 2002. Geostatistical Simulation: Models and Algorithms. Springer, Berlin.

Le Loc'h, G., Galli, A., 1997. Truncated plurigaussian method: theoretical and practical points of view. In: Baafi, E.Y., Schofield, N.A. (eds.) Geostatistics Wollongong' 96. Kluwer, Dordrecht, pp. 211-222.

Mariethoz, G., Renard, P., Cornaton, F., Jaquet, O., 2009. Truncated plurigaussian simulations to characterize aquifer heterogeneity. Ground Water 47(1): 13-24.

Matheron, G., Beucher, H., de Fouquet, C., Galli, A., Guerillot, D., Ravenne, C., 1987. Conditional simulation of the geometry of fluvio-deltaic reservoirs. In: 62nd Annual Technical Conference and Exhibition of the Society of Petroleum Engineers, pp. 591-599. SPE technical paper 16753.

Matheron, G., Beucher, H., de Fouquet, C., Galli, A., Ravenne, C., 1988. Simulation conditionelle à trois facies d'une falaise de la formation du Brent. Sciences de la Terre, Série Informatique Géologique, 28: 213-249.

Rezaee, H., Asghari, O., Koneshloo, M., Ortiz, J.M., 2014. Multiple-point geostatistical simulation of dykes: application at Sungun porphyry copper system, Iran. Stochastic Environmental Research and Risk Assessment, in press.

Rondon, O., 2009. A look at the plurigaussian simulation for a nickel laterite deposit. In: Dominy, S. (ed.), 7th International Mining & Geology Conference. The Australasian Institute of Mining and Metallurgy, Melbourne.

Serrano, L., Vargas, R., Stambuk, V., Aguilar, C., Galeb, M., Holmgren, C., Contreras, A., Godoy, S., Vela, I., Skewes, M.A., Stern, C.R., 1996. The late Miocene to early Pliocene Río Blanco-Los Bronces copper deposit, Central Chilean Andes. In: Camus, F., Sillitoe, R.H., Petersen, R. (eds.) Andean Copper Deposits: New Discoveries, Mineralization, Styles and Metallogeny. Special Publication no. 5, Society of Economic Geologists, Littleton, Colorado, pp. 119-130.

Skewes, M.A., Holmgren, C., Stern, C.R., 2003. The Donoso copper-rich, tourmaline-bearing breccia pipe in central Chile: petrologic, fluid inclusion and stable isotope evidence for an origin from magmatic fluids. Mineralium Deposita 38(1): 2-21.

Skewes, M.A., Stern, C.R., 1995. Genesis of the Late Miocene to Pliocene copper deposits of central Chile in the context of Andean magmatic and tectonic evolution. International Geology Review 37: 893-909.

Skewes, M.A., Stern, C.R., 1996. Late Miocene mineralized breccias in the Andes of central Chile: Sr and Nd isotopic evidence for multiple magmatic sources. In: Camus, F., Sillitoe, R.H., Petersen, R. (eds.) Andean Copper Deposits: New Discoveries, Mineralization, Styles and Metallogeny. Special Publication no. 5, Society of Economic Geologists, Littleton, Colorado, pp. 119-130.

Skvortsova, T., Armstrong, M., Beucher, H., Forkes, J., Thwaites, A., Turner, R., 2001. Applying plurigaussian simulations to a granite-hosted orebody. In: Kleingeld, W.J., Krige, D.G. (eds.) Geostats 200 Cape Town. Geostatistical Association of Southern Africa, Johannesburg, pp. 904-911.

Skvortsova, T., Beucher, H., Armstrong, M., Forkes, J., Thwaites, A., Turner, R., 2002. Simulating the geometry of a granite-hosted uranium orebody. In: Armstrong, M., Bettini, C., Champigny, N., Galli, A., Remacre, A. (eds.) Geostatistics Rio 2000. Kluwer Academic, Dordrecht, pp. 85-99.

Stambuk, V., Aguilar, C., Blondel, J., Galeb, M., Serrano, L., Vargas, R., 1988. Geología del yacimiento Río Blanco. Technical Report, Codelco-Chile, División Andina.

Strebelle, S., 2002. Conditional simulation of complex geological structures using multiple-point statistics. Mathematical Geology 34(1): 1-22.

Talebi, H., Asghari, O., Emery, X., 2013. Application of plurigaussian simulation to delineate the layout of alteration domains in Sungun copper deposit. Central European Journal of Geosciences 5(4): 514-522.

Talebi, H., Asghari, O., Emery X., 2014. Simulation of the lately injected dykes in an Iranian porphyry copper deposit using the plurigaussian model. Arabian Journal of Geosciences 7(7): 2771-2780.

Vargas, R., Gustafson, L.B., Vukasovic, M., Tidy, E., Skewes, M.A., 1999. Ore breccias in the Río Blanco-Los Bronces copper deposit, Chile. In: Skinner, B.J. (ed.) Geology and Ore Deposits of the Central Andes. Special Publication no. 7, Society of Economic Geologists, Littleton, Colorado, pp. 281-297.

Warnaars, F., Holgrem, C., Barassi, S., 1985. Porphyry copper and tourmaline breccias at Los Bronces – Río Blanco, Chile. Economic Geology 80: 1544-1565.

Xu, C., Dowd, P.A., Mardia, K.V., Fowell, R.J., 2006. A flexible true plurigaussian code for spatial facies simulations. Computers & Geosciences 32(10): 1629-1645.

Yunsel, T., Ersoy, A., 2011. Geological modeling of gold deposit based on grade domaining using plurigaussian simulation technique. Natural Resources Research 20(4): 1-19.

Yunsel, T., Ersoy, A., 2013. Geological modeling of rock type domains in the Balya (Turkey) lead-zinc deposit using plurigaussian simulation. Central European Journal of Geosciences 5(1): 77-89.